



# iPSC-DERIVED MICROGLIA AS A MODEL OF IMMUNE DYSFUNCTION IN NEURODEGENERATIVE DISEASES

A thesis submitted for the degree of

**Doctor of Philosophy (PhD)**

by

**Aurelien Bunga**

2018

# ACKNOWLEDGEMENTS

*“Ndenge nini na zongisela Mokonzi Nzambe wa nga malamumanso asali na ngai, Nazali na nyongo ya bolingo bwa ye, Bolingo bwa ye ezali bolingo bwa seko.”*

I would like to sincerely thank my supervisors Nick and Julie for their invaluable guidance, and support throughout my time at Cardiff. I am lucky to have worked with them and learned a huge amount under their mentorship and I am very grateful for the opportunities that I have had over the last few years. I'd also like to thank the Wellcome Trust for funding my PhD studentship.

I really appreciate all the help and encouragement along the way from many colleagues and friends – a conversation here, a piece of advice there. Thank you. Thanks also to Robert Andrews and Katherine Tansey for their vital help and support with RNA-sequencing analysis. Thank you to everyone in the lab for putting up with me and my funny ways: Beth, Elisa and Jincy; Kimmy J and Jasmine; Emma and her funny Welsh accent for teaching me the ropes. Thanks to Oly, Lee, Kira, Ellen, Rae, Rachael and Jon – this experience would have been a lot less enjoyable without you!

A special thank you to my sisters Youssillya, Aurore and Jenny, and my parents Julien and Jeanette, who are my biggest inspiration and without whom this would not have been possible. I'll be eternally grateful for their faith in me and their many sacrifices and for everything that they do for us.

*Nzambe azwa lokumu mpe nkembo.*

# ABSTRACT

It is now increasingly evident that neurodegenerative diseases such as Alzheimer's disease (AD) and Huntington's disease (HD) trigger immune activation within the CNS and activate innate immune responses, which are primarily driven by microglia.

HD is caused by a CAG repeat expansion in the huntingtin gene (HTT), leading to translation of an aberrant and pathogenic mutant HTT. Studies in mouse models have shown that HD microglia acquire a hyper-reactive inflammatory phenotype, mediated by a gain of toxicity of mutant HTT. Using a HD induced pluripotent stem cell (iPSC) line containing 109 CAG repeats in the HTT gene, microglia-like cells were generated with the aim of characterising their phenotype. RNA sequencing was used to explore the microglial-specific transcriptional changes associated with mutant HTT and pathway analysis carried out to predict any downstream processes affected in the HD109 microglia. Several immune-related functions including chemotaxis and phagocytosis were subsequently identified as dysregulated or impaired. However, upon functional assay validation, no phenotypic abnormalities were manifest in the HD109 microglia, with comparisons made against WT Kolf2 and isogenic HD109 corrected iPSC-derived microglia. Similarly, the in vitro microglia did not exhibit the inflammatory phenotype characteristic of diseased HD microglia and other immune cells.

Loss-of-function variants in the microglia-enriched gene encoding ATP-binding cassette transporter A7 (ABCA7) increase Alzheimer's disease risk. Although it has been suggested to play a role in amyloid beta phagocytosis, the precise role of ABCA7 in AD pathogenesis remains unknown. To that end, ABCA7 knockout iPSCs were generated using CRISPR/Cas9 and in preliminary results, loss-of-function mutations in ABCA7 were found to impair phagocytosis of *E. coli* bioparticles and regulate in vitro microglial inflammatory responses.

This thesis demonstrates that iPSC-derived microglia can serve as a platform for exploring the inflammatory pathways mediating microglial involvement in AD and HD pathogenesis, thus enabling in-depth mechanistic studies that bridge the gap between clinical and animal models.

# ABBREVIATIONS

A $\beta$	Amyloid $\beta$
ABCA7	ATP-binding cassette transporter A7
ABI3	ABI family member 3
A $\beta$ O	Amyloid $\beta$ oligomers
AD	Alzheimer's disease
ADF	Advanced DMEM F12
ADGC	Alzheimer's Disease Genetic Consortium
ADORA3	Adenosine A3 receptor
ADP	Adenosine diphosphate
AGM	Aorta-gonad mesonephros
ANOVA	Analysis of variance
APC	Antigen presenting cell
ApoE	Apolipoprotein E
APP	Amyloid precursor protein
ATP	Adenosine triphosphate
BBB	Blood brain barrier
BIN1	Bridging Integrator-1
BMP4	Bone morphogenetic protein 4
C1QA	Complement C1q subcomponent subunit A
CABLES1	Cdk5 and ABL1 enzyme substrate 1
CAMP	Cathelin-related antimicrobial peptide
CCL	Chemokine (C-C motif) ligand
CD	Cluster of differentiation
CD2AP	CD1-associated protein
CLU	Clusterin
CNS	Central nervous system
CORO1A	Coronin-1A
COX	Cyclooxygenase
CR1	Complement receptor 1

CRISPR	Clustered Regularly Interspaced Short Palindromic Repeats
CSF	Cerebrospinal fluid
CSF1R	Colony stimulating factor 1 receptor
CXCL	Chemokine (C-X-C motif) ligand
CX3CL1	Chemokine (C-X3-C motif) ligand 1 (or fractalkine ligand)
CX3CR1	CX3C chemokine receptor 1 (or fractalkine receptor)
CYBB	Cytochrome b-245 heavy chain (or NADPH oxidase 2)
DAMP	Damage-associated molecular pattern
DAVID	Database for Annotation, Visualization and Integrated Discovery
DE	Differentially expressed
DMEM	Dulbecco's Modified Eagle Media
EAAT	Excitatory amino acid transporter
EB	Embryoid body
ECM	Extracellular matrix
EMP	Erythro-myeloid progenitors
EPHA-1	Ephrin type-A receptor 1
ERK	Extracellular signal-regulated kinase
FACS	Fluorescence-activated cell sorting
FABP4	Fatty acid binding protein 4
FASN	Fatty acid synthase
FCCP	Carbonyl cyanide-4-(trifluoromethoxy)phenylhydrazone
FCGR	Fc gamma receptor
FDR	False discovery rate
FITC	Fluorescein Isothiocyanate
FLK1	Fetal Liver Kinase 1 (also VEGF Receptor)
GABA	Gamma-aminobutyric acid
GAS6	Growth arrest-specific 6
GERAD	Genetic and Environmental Risk in Alzheimer's Disease Consortium
GFP	Green fluorescent protein
GM-CSF	Granulocyte Macrophage Colony Stimulating Factor
GO	Gene Ontology
GPR34	G protein-coupled receptor 34

GSEA	Gene set enrichment analysis
GWAS	Genome-wide association studies
HD	Huntington's disease
HEXB	Beta-hexosaminidase subunit beta
HMG-coA	$\beta$ -Hydroxy $\beta$ -methylglutaryl-CoA
HSC	Haematopoietic stem cell
HTT	Huntingtin
IBA1	Ionised Calcium-Binding Adapter Molecule 1
ICAM1	Intracellular Adhesion Molecule 1
IFITM	Interferon-induced transmembrane protein
IFN	Interferon
IL	Interleukin
INPP5D	Inositol polyphosphate-5-phosphatase D
iPSC	Induced Pluripotent Stem Cell
IRF	Interferon regulatory factor
KEGG	Kyoto Encyclopaedia of Genes and Genomes
KO	Knockout
LD	Linkage disequilibrium
LDLR	Low-density lipoprotein receptor
LGMN	Legumain
LOAD	Late-onset Alzheimer's disease
LPS	Lipopolysaccharide
LRP1	Low density lipoprotein receptor-related protein 1
MAPK	Mitogen-activated protein kinase
MAO-B	Monoamine oxidase B
MARCO	Macrophage receptor with collagenous structure
M-CSF	Macrophage Colony Stimulating Factor
Macpre	Macrophage precursor
MCI	Mild Cognitive Impairment
MCP-1	Monocyte chemoattractant protein 1 (or CCL2)
MEF2C	Monocyte-specific enhancer factor 2C
MERTK	MER proto-oncogene Tyrosine Kinase

MG	Microglia
MHC	Major Histocompatibility complex
mHTT	Mutant HTT
MMP	Matrix metalloproteinase
mRNA	Messenger RNA
MS4A	Membrane-spanning 4-domain family, subfamily A
MSN	Medium spiny neuron
NADPH	Nicotinamide adenine dinucleotide phosphate
NBD	Nucleotide binding domain
NF $\kappa$ B	Nuclear factor kappa-light-chain-enhancer of activated B cells
NLRC5	NLR family CARD domain containing 5
NLRP3	NOD-Like Receptor family Pyrin domain 3
NSAID	Non-steroidal anti-inflammatory drug
OCR	Oxygen consumption rate
OLFML3	Olfactomedin-3 like protein 3
PAMP	Pathogen-associated molecular pattern
PCA	Principal component analysis
PE	Phycoerythrin
PET	Positron emission tomography
PICALM	Phosphatidylinositol binding clathrin assembly protein
PLCG2	Phospholipase C Gamma 2
PPAR $\gamma$	Peroxisome proliferator-activated receptor gamma
PROS1	Protein S
PRR	Pattern recognition receptor
PC	Phosphatidylcholine
PS	Phosphatidylserine
PSEN	Presenilin
P2RX	Purinergic receptor P2X
P2RY	Purinergic receptor P2Y
ROS	Reactive oxygen species
RUNX1	Runt Related Transcription Factor 1
SERPINB2	Serpin family B member 2

SCF	Stem Cell Factor
SIGLEC	Sialic acid-binding immunoglobulin-like lectin
SLCO2B1	solute carrier organic anion transporter family member 2B1
SNP	Single nucleotide polymorphism
SORL1	Sortilin-related receptor 1
SPI1	Transcription factor PU.1
SREBF2	Sterol regulatory element-binding protein 2
STAT	Signal Transducer and Activator of Transcription
SYK	Spleen tyrosine kinase
TCA	Tricarboxylic acid
TGF- $\beta$	Transforming Growth Factor $\beta$
TGFBR1	Transforming Growth Factor $\beta$ receptor 1
TLR	Toll Like Receptor
TMD	Transmembrane domain
TMEM119	Transmembrane protein 119
TNF	Tumour necrosis factor
TREM2	Triggering Receptor Expressed on Myeloid Cells 2
tSNE	t-distributed stochastic neighbour embedding
TSPO	Translocator Protein
TYROBP	TYRO protein tyrosine Kinase-binding protein (or DAP12)
VEGF	Vascular Endothelial Growth Factor
WT	Wild-type
YS	Yolk sac

# TABLE OF CONTENTS

<b>1. INTRODUCTION</b>	<b>12</b>
<b>1.1 NEUROINFLAMMATION IN ALZHEIMER'S AND HUNTINGTON'S DISEASE</b>	<b>12</b>
1.1.1 <i>Neuroinflammation in Alzheimer's and Huntington's disease</i>	12
1.1.2 <i>Immune system and microglial dysfunction in Huntington's disease</i>	18
1.1.3 <i>Genetics of Alzheimer's disease implicate microglia dysfunction in Alzheimer's disease</i>	20
<b>1.2 MICROGLIA</b>	<b>26</b>
1.2.1 <i>Origins of microglia</i>	26
1.2.2 <i>Microglia arise from precursors formed during embryonic haematopoiesis</i>	27
1.2.3 <i>Microglia physiology and functional diversity</i>	30
1.2.4 <i>Microglia phenotypes and activity states</i>	35
<b>1.3 ASSOCIATION OF ABCA7 WITH ALZHEIMER'S DISEASE</b>	<b>38</b>
1.3.1 <i>Expression profile and structure of ABCA7</i>	40
1.3.2 <i>Function and physiological properties of ABCA7</i>	42
1.3.3 <i>ABCA7 function in Alzheimer's disease</i>	44
<b>1.4 PROJECT AIMS</b>	<b>47</b>
<b>2. MATERIAL AND METHODS</b>	<b>12</b>
<b>2.1 MATERIALS</b>	<b>12</b>
2.1.1 <i>Cell culture reagents</i>	12
2.1.4 <i>Buffers, consumables and kits</i>	13
<b>2.2 MAINTENANCE AND CULTURE OF HUMAN INDUCED PLURIPOTENT STEM CELLS</b>	<b>14</b>
2.2.1 <i>Maintenance of human iPSC lines</i>	14
2.2.2 <i>Maintenance of THP-1 monocytes</i>	14
<b>2.3 DIRECTED DIFFERENTIATION OF iPSCS INTO MICROGLIA-LIKE CELLS</b>	<b>15</b>
2.3.1 <i>Differentiation of human iPSCs into embryoid bodies (EBs)</i>	15
2.3.2 <i>Differentiation of EBs into monocyte-like macrophage precursor cells</i>	15
2.3.3 <i>Induction of microglia-like phenotype</i>	15
<b>2.4 FUNCTIONAL ASSAYS</b>	<b>16</b>
2.4.1 <i>Stimulation with amyloid beta oligomers and reverse amyloid beta</i>	16
2.4.2 <i>Phagocytic uptake of pHrodo red E. coli bioparticles</i>	17
2.4.3 <i>IncuCyte S3 chemotaxis assay</i>	18
2.4.4 <i>Seahorse XFe96 assays for mitochondrial bioenergetics and glycolytic flux</i>	18
2.4.5 <i>Cholesterol staining</i>	20
2.4.6 <i>Sphingomyelin staining</i>	20
2.4.7 <i>Phospholipid staining</i>	20
<b>2.5 FLOW CYTOMETRY</b>	<b>21</b>
<b>2.6 IMMUNOCYTOCHEMISTRY</b>	<b>21</b>
2.6.1 <i>Immunocytochemistry</i>	21
2.6.2 <i>Cytocentrifugation</i>	22
<b>2.7 RNA EXTRACTION AND qRT-PCR</b>	<b>23</b>
2.7.1 <i>PowerUp SYBR Green qRT-PCR</i>	23
2.7.2 <i>Fluidigm High Throughput qRT-PCR</i>	24
2.7.3 <i>qRT-PCR primers</i>	27
<b>2.8 CRISPR/Cas9-MEDIATED MUTATION OF ABCA7 GENE</b>	<b>28</b>
2.8.1 <i>CRISPR guide RNAs design and preparation</i>	28
2.8.2 <i>Cell culture, transfection and selection of targeted clones</i>	29
<b>2.9 RNA SEQUENCING AND ANALYSES</b>	<b>31</b>
2.9.1 <i>RNA Sequencing library construction and sequencing</i>	31
2.9.2 <i>RNA-seq read mapping, gene counts estimation and differential gene expression analysis</i>	31
2.9.3 <i>Comparative Gene Set Enrichment Analysis of iPSC-derived microglia</i>	32
2.9.4 <i>iPathwayGuide Impact Analysis</i>	32
2.9.5 <i>Upstream regulator analysis</i>	33

2.10 STATISTICAL ANALYSIS.....	33
<b>3. TRANSCRIPTOMIC AND FUNCTIONAL VALIDATION OF HUMAN iPSC-DERIVED MICROGLIA.....</b>	<b>34</b>
3.1 INTRODUCTION .....	34
3.2 AIMS .....	35
3.3 RESULTS.....	36
3.2.1 Human iPSC-derived microglia cells express characteristic microglial markers.....	36
3.2.2 Transcriptomic profiling of human iPSC-derived microglia reveals a microglial signature.....	42
3.2.3 Functional analysis and validation of Kolf2 iPSC-derived microglia.....	53
3.3 SUMMARY AND DISCUSSION.....	58
<b>4. CHARACTERISATION OF THE CELL-AUTONOMOUS EFFECTS OF THE HTT GENE CAG EXPANSION ON iPSC-DERIVED MICROGLIA.....</b>	<b>63</b>
4.1 INTRODUCTION .....	63
4.2 AIMS .....	65
4.3 RESULTS.....	66
4.3.1 Transcriptomic analysis of HD109 iPSC-derived microglia .....	66
4.3.2 Functional validation of HD109 of iPSC-derived microglia.....	81
4.4 SUMMARY AND DISCUSSION.....	88
<b>5. EXPLORING THE EFFECTS OF CORRECTING THE HD MUTATION ON IMMUNE DYSFUNCTION IN iPSC-DERIVED HD MICROGLIA .....</b>	<b>92</b>
5.1 INTRODUCTION .....	92
5.2 AIMS .....	94
5.3 RESULTS.....	95
5.3.1 Does correcting the HTT CAG expansion reverse the gene expression changes observed in HD109 iPSC-derived microglia?.....	95
5.3.2 Effects of correcting the HD mutation on the microglial inflammatory response under stimulatory conditions .....	99
5.3.3 HD109 microglia do not manifest transcriptome-associated functional deficits in phagocytosis and chemotaxis.....	103
5.3.4 HD109 microglia do not exhibit deficits in mitochondrial respiration associated with other HD cell types .....	108
5.4 SUMMARY AND DISCUSSION.....	114
<b>6. INVESTIGATION OF THE EFFECTS OF ABCA7 LOSS-OF-FUNCTION IN HUMAN iPSC-DERIVED MICROGLIA. 119</b>	<b>119</b>
6.1 INTRODUCTION .....	119
6.2 AIMS .....	121
6.3 RESULTS.....	122
6.3.1 Generation of ABCA7 KO iPSC lines by CRISPR-Cas9.....	122
6.3.2 Validation of ABCA7-edited iPSC-derived microglial cells.....	127
6.3.3 ABCA7 loss of function impairs phagocytosis in iPSC-derived microglia.....	132
6.3.4 Is ABCA7 involved in intracellular lipid trafficking?.....	136
6.3 SUMMARY AND DISCUSSION.....	137
<b>7. GENERAL DISCUSSION .....</b>	<b>141</b>
7.1 GENERAL DISCUSSION AND FUTURE PERSPECTIVES.....	141
7.1.1 Characterisation of the phenotype of HD109 iPSC-derived microglia.....	141
7.1.2 The effects of correcting the HD CAG mutation on the microglial phenotype.....	143
7.1.3 Modelling neuroinflammation with iPSC-derived microglia .....	145
7.2 CONCLUDING REMARKS .....	147
<b>8. REFERENCES.....</b>	<b>148</b>
<b>9. APPENDICES.....</b>	<b>173</b>
Appendix 1. Top 50 differentially expressed genes in HD109 iPSC-derived microglia. ....	173

*Appendix 2. IPA output of upstream transcriptional regulators inhibited in HD109 iPSC-derived microglia.*  
..... 174

*Appendix 3. IPA output of upstream transcriptional regulators activated in HD109 iPSC-derived microglia.*  
..... 175

*Appendix 4. IPA output of inhibited upstream transcriptional regulators specific to HD109 iPSC-derived  
macrophage precursors..... 175*

*Appendix 5. Microglia response to cholesterol depletion ..... 176*

*Appendix 6. List of qRT-PCR primers used in this project (continued)..... 176*

## 2. MATERIAL AND METHODS

### 2.1 Materials

#### 2.1.1 Cell culture reagents

Cell culture reagent	Supplier	Catalogue number
RPMI 1640	Gibco	1185093
Fetal Bovine Serum	Gibco	10439024
Glutamax	Thermo Fisher	35050-038
Penicillin/Streptomycin (5000U/5000µg)	Gibco	15070063
BMP-4	PeptoTech	120-05ET
SCF	Miltenyi Biotec	130-093-991
VEGF	PeptoTech	100-20
E8 Flex Medium	Life Technologies	A2858501
X-VIVO15	Scientific Laboratory Supplies	LZBE02-060Q
M-CSF	BioLegend	574806
IL-3	BioLegend	578006
β-mercaptoethanol	Life Technologies	31350
IL-34	BioLegend	577906
GM-CSF	BioLegend	572902
Fibronectin	Merck Millipore	FC010-10MG
PBS pH 7.4	Gibco	10010015
Vitronectin	Gibco	A31804
ReLeSR	Stem Cell Technologies	05872
Y-27632 dihydrochloride (ROCK inhibitor)	Tocris	1254
40 µm cell strainers	Scientific Laboratory Supplies	431750
D-PBS	Life Technologies	14190250
Trypan Blue solution	Sigma Aldrich	T8154
DMEM-F12, no phenol red	Thermo Fisher	11039021

**Table 2.1** List of reagents used for cell culture and differentiation.

Cell culture media	Composition
THP-1 maintenance media	RPMI 1640 + 10% FBS + 2 mM Glutamax + Penicillin/Streptomycin 50U/50µg
E8-3G (EB differentiation medium)	E8 + 50 ng/ml BMP4 + 50 ng/ml VEGF + 20 ng/ml SCF

X-VIVO factory medium	X-VIVO15 + 2 mM Glutamax + 50U/50µg Penicillin/Streptomycin + 50 µM β-mercaptoethanol + 50 ng/ml M-CSF + 25 ng/ml IL-3
Microglia differentiation medium	X-VIVO15 + 100 ng/ml IL-34 + 10 ng/ml GM-CSF

**Table 2.2 List of media used for cell culture and microglial differentiation**

#### 2.1.4 Buffers, consumables and kits

	Composition
DNA lysis buffer	1 M Tris pH 8.0 (2.5 ml), 0.5 M EDTA (1 ml) , 10% SDS (155 µl), 5 M NaCl (200 µl), Deionised water (46 ml)
ICC Blocking buffer (external markers)	3% Bovine Serum Albumin (BSA), 2% Normal Serum (Goat/Chicken), PBS pH 7.4 (up to 50 ml)
ICC Blocking buffer (internal markers)	3% BSA, 2% Normal Serum (Goat/Chicken), 0.1% Triton X-100, PBS pH 7.4 (up to 50 ml)
FACS buffer	0.1% BSA, PBS pH 7.4

**Table 2.3 List of buffers.**

Consumable	Supplier	Catalogue number
Superscript II Reverse Transcriptase kit	Invitrogen	18064014
RNEasy Mini kit	Qiagen	74104
PowerUp SYBR Green Master Mix	Applied Biosystems	A25778
P3 Primary Cell 4D-Nucleofector Kit	Lonza	V4XP-3032
Bovine Serum Albumin (BSA)	Sigma Aldrich	A7906
Normal Goat/Chicken Serum	Dako	X0907/X0903
Triton X-100	Sigma Aldrich	T8787
Formalin (4% FPA)	Sigma Aldrich	HT5011
Poly-D-Lysine	Poly-D-Lysine	Poly-D-Lysine
Sigma Aldrich	Sigma Aldrich	Sigma Aldrich
Cytospin funnels	Fisher Scientific	11972345

**Table 2.4 List of consumables and kits used.**

## 2.2 Maintenance and culture of human induced pluripotent stem cells

### 2.2.1 Maintenance of human iPSC lines

Studies were performed using two feeder-free human iPSC lines: Kolf2-C1 and HD109. Kolf2-C1 iPSC lines were generated from fibroblasts collected from a healthy 55-59-year-old male and reprogramming carried out by non-integrating Sendai virus transduction of Oct4, Sox2, Klf4 and cMyc. HD109 iPSC lines were derived from fibroblasts collected from a 9-year-old female with juvenile onset HD from the age of 4, with severe bradykinesia, rigidity and dystonia at time of biopsy (HD iPSC Consortium 2012). Reprogramming was conducted by lentiviral transduction of Oct4, Sox2, Klf4 and cMyc. For both cell lines, normal karyotypes and expression of pluripotent stem cell markers were confirmed. All cell cultures were maintained in a humidified incubator (37°C, 5% CO<sub>2</sub>).

iPSCs were cultured in feeder-free conditions on 6-well plates (Corning) coated in vitronectin (0.5 µg/cm<sup>2</sup>; Gibco, Life Technologies) and fed with E8 Flex medium. Medium was changed daily, and cells were passaged using ReLeSR every 3-5 days (or at 80% confluence). For passaging, cells were washed once with PBS pH 7.4 and the ReLeSR added before incubation at 37°C for 5 minutes. The dissociation reagent was removed by aspiration and fresh E8 Flex medium added to gently detach the colonies by homogenisation with a pipette. The mixture was transferred to a 15 ml Falcon tube and centrifuged for 3 minutes at 1000 rpm. The supernatant was aspirated, and cell pellet re-suspended in warm E8 Flex for plating.

### 2.2.2 Maintenance of THP-1 monocytes

THP-1 monocytes were a kind gift from Dr Shane Wainwright (Cardiff University). The cells were cultured with monocyte maintenance medium (see section 2.1.1) in non-adherent T75 flasks. The cells were seeded at a density of 2x10<sup>5</sup> cells per ml and re-suspended in 19 ml of media. Once concentration exceeded 1x10<sup>6</sup> cells per ml, they were collected by centrifugation (1000 rpm for 3 minutes) and split in a 1:5 ratio into T75 flasks.

## 2.3 Directed differentiation of iPSCs into microglia-like cells

### 2.3.1 Differentiation of human iPSCs into embryoid bodies (EBs)

Day 0: iPSC colonies grown to confluence on 6-well plates were washed with 1x PBS pH 7.4 at room temperature, ReLeSR was added (1 ml per well) and the cells placed in incubator. After 2-3 minutes, the dissociation reagent was aspirated, and the side of the plate was lightly tapped for 1-2 minutes to allow colonies to dislodge. Following this step, 2ml of warm E8 medium was gently added to each well to allow the aggregated cells to form floating EBs and the plate returned to the incubator for one day.

Day 1: EBs were carefully transferred to a 15-ml tube and allowed to settle by gravity. The supernatant medium was removed and replaced with E8 + 50 ng/ml BMP-4, 50 ng/ml VEGF and 20 ng/ml SCF. EBs were cultured in E8-3G media for 7 days, with a 50% media change every two days.

### 2.3.2 Differentiation of EBs into monocyte-like macrophage precursor cells

E8-3G- cultured EBs were collected and further differentiated to make 'factories' by seeding 15 EBs into one well of a 6-well plate in X-VIVO15 media supplemented with 50 ng/ml M-CSF and 25 ng/ml IL-3. The culture media from the factories was changed weekly. After approximately 2 weeks, non-adherent (monocyte-like) myeloid cells would become visible in the supernatant media of the factories, were harvested weekly and the culture media replenished. For harvesting, the supernatant was passed through a 40  $\mu\text{m}$  cell strainer, centrifuged for 3 minutes at 1000 rpm and the resulting pellet gently re-suspended for use in assays described below or plated onto glass coverslips or tissue-culture plates.

### 2.3.3 Induction of microglia-like phenotype

Non-adherent myeloid cells harvested from the factories were plated at a density of  $2-3 \times 10^5$  cells per well and 10,000 onto PDL-treated (100  $\mu\text{g}/\text{ml}$  in borate buffer) tissue culture 6-well plates and glass coverslips respectively, pre-coated with 5  $\mu\text{g}/\text{cm}^2$  fibronectin. The cells were cultured in XVIVO15 medium supplemented with 10ng/ml GM-CSF and 100 ng/ml IL-34. The medium was changed after 7 days and cells incubated in standard culture conditions for 14 days, prior to being used for experiments.

## 2.4 Functional assays

Name	Supplier	Catalogue number
A $\beta$ <sub>1-42</sub> peptide	California Peptide Research	641-15
Reverse A $\beta$ <sub>42-1</sub>	Tocris	3391
HFIP	Sigma Aldrich	H-8508
Bafilomycin A1	Sigma Aldrich	B1793-10UG
Cytochalasin D	Sigma Aldrich	C8273-1MG
pHrodo red E. coli bioparticles	Life Technologies	P35361
Live Cell Imaging Solution	Life Technologies	A14291DJ
96-well black-walled $\mu$ -clear microplates	Greiner Bio-One	655097
ClearView 96-well Migration plates	Essen BioScience	4582
ClearView 96-well reservoir plates	Essen BioScience	4600
Seahorse XF Cell Mito Stress Test	Agilent Technologies	103015-100
Seahorse XF96 V3 PS cell culture microplates	Agilent Technologies	101085-004
Seahorse XF calibrant	Agilent Technologies	100840
Seahorse XF 1.0 M Glucose solution	Agilent Technologies	103577-100
Seahorse XF RPMI Medium pH 7.4	Agilent Technologies	103576-100
Seahorse XF96 sensor cartridge	Agilent Technologies	102601-100
Filipin	Sigma Aldrich	F9765
Ibidi 8-well $\mu$ -slides	Thistle Scientific	80826
Lysenin Antiserum	Peptide International	NLY-14802-v
LipidTOX Red Phospholipidosis Detection Reagent	Invitrogen	H34351
Complement C1q	Merck Millipore	204876-1MG
Lipopolysaccharide	Sigma Aldrich	L2654-1MG
IL-4	PeptoTech	200-04
ADP	Sigma Aldrich	A2754-500MG
CX3CL1	BioLegend	583404

**Table 2.5 List of material, media and consumables used for functional assays.**

### 2.4.1 Stimulation with amyloid beta oligomers and reverse amyloid beta

Synthetic A $\beta$ <sub>1-42</sub> peptides were resuspended in ice-cold HFIP (or 1,1,1,3,3,3,-hexafluoropropan-2-ol), by adding 222  $\mu$ l to 1mg and aliquoted into microcentrifuge tubes

(100  $\mu$ l = 0.45 mg). Each aliquot was dried overnight under a stream of N<sub>2</sub> gas to allow HFIP evaporation (and stored long term at -80°C). The resulting peptide films were dissolved to 5 mM A $\beta$  stock by adding 20  $\mu$ l DMSO to 0.45 mg peptide. The peptide stock was further diluted to 100  $\mu$ M in phenol red-free F-12 medium and the suspension incubated at 4°C for 24 hours to allow oligomerisation. Following incubation, the A $\beta$  mixture was centrifuged in the cold for 10 min at 14,000 rpm to pellet out any fibrils. The supernatant was collected as A $\beta$  oligomeric preparation, diluted in phenol red-free medium before use.

#### 2.4.2 Phagocytic uptake of pHrodo red E. coli bioparticles

This assay was used to measure the formation of acidified phagosomes: as the pHrodo red E. coli bioparticles reach the acidic environment of the phagosome (pH 4.5-5.5), the intensity of the fluorescence is greatly enhanced, enabling direct quantification of phagocytosis in real-time. First, pHrodo red E. coli bioparticles were resuspended to 1mg/ml in Live Cell Imaging Solution. The mixture was homogenised, transferred to glass vial and sonicated for 5 min prior to each experiment.

Precursor cells collected from differentiation factories were plated onto 96-well PDL-treated, black walled  $\mu$ -clear flat bottom microplates at a density of 20,000 cells/well in a 100  $\mu$ l suspension and differentiated to microglia for 14 days. Before the assay, the growth medium was removed and replaced with 75  $\mu$ l of live cell imaging solution. After 10  $\mu$ g per well of pHrodo E. coli was added, the microplates were transferred into the IncuCyte S3 live-cell imaging system (Essen BioScience), housed inside a 37°C/5% CO<sub>2</sub> incubator. The microplates were imaged in the IncuCyte for 4-6 hours with a 20x objective. At least four images per well were taken every 15 or 20 min and analysis carried out using the IncuCyte S3 Base software. Red channel acquisition was 400 ms and phase contrast masking and cell segmentation was applied to exclude cells from background, with an area filter of 50  $\mu$ m<sup>2</sup> to exclude objects. Background red channel noise was subtracted using Top-Hat correction with a radius of 20  $\mu$ m and a threshold of 2 red corrected units (Kapellos et al. 2016). As a positive control for inhibited phagocytosis, cells were pre-treated for 1 hour with 10  $\mu$ M of the actin polymerisation inhibitor cytochalasin D or bafilomycin A1, an inhibitor of the phagolysosome V-ATPase.

#### 2.4.3 IncuCyte S3 chemotaxis assay

The chemotaxis assays were conducted with IncuCyte ClearView 96-well Migration plates, featuring a low pore density membrane that separates an upper and lower chamber and requires cells to migrate across the membrane surface to reach a pore. Prior to cell plating, both sides of the IncuCyte ClearView plate membrane were coated with fibronectin: 150  $\mu\text{l}$  per well was added to an IncuCyte ClearView 96-well reservoir plate and 20  $\mu\text{l}$  was added to the insert wells, before the insert wells were gently placed onto the reservoir plate. The migration plate was then incubated at 37°C for 30 min before being allowed to cool down to room temperature for another 30 min. The fibronectin was then aspirated from both the reservoir plate and insert and replaced with 200  $\mu\text{l}$  of D-PBS to the reservoir plate. Microglia precursor cells were then seeded into each well of the insert plate in 60  $\mu\text{l}$  at 3000 cells per well and allowed to settle on the membrane at room temperature for 15-30 min. The cells were differentiated to microglia within the plate for 14 days, with a media change after 7 days.

On the day of the assay, chemoattractants were made to desired concentrations in XVIVO medium, with 200  $\mu\text{l}$  added to the appropriate wells of a reservoir plate and the insert plate carefully placed onto the chemoattractant-containing reservoir plate. The migration plate was transferred to the IncuCyte S3 system for scanning. 10x objective, phase channel scans of both the top and bottom sides of the insert were scheduled every 30 min for 24 hours. Migration was quantified by the IncuCyte analysis software as the appearance of in focus cells on the bottom of the well and the surface area they occupied (total phase object area in  $\mu\text{m}^2$  /well).

#### 2.4.4 Seahorse XFe96 assays for mitochondrial bioenergetics and glycolytic flux

The Seahorse XFe96 Analyser measures oxygen consumption rate (OCR) and extracellular acidification rate (ECAR) over a specified time period and at particular time intervals as a way of assessing mitochondrial respiration (via cellular oxygen consumption) and glycolytic proton efflux. Using the manufacturer's standardised protocol for the Seahorse XF Cell Mito Stress Test, cell respiration can be measured under basal conditions and subsequent exposures to the ATP coupler oligomycin, the uncoupler carbonyl cyanide-*p*-trifluoromethoxyphenylhydrazone (FCCP), and the complex I inhibitor Rotenone. Oligomycin,

which acts by inhibiting the proton channel of the ATP synthase (complex V), is used in this protocol to calculate the percentage of oxygen consumption allocated to ATP synthesis. Treatment with FCCP, which disturbs the transport of hydrogen ions across the mitochondrial membrane, affects the mitochondrial membrane potential and results in a rapid increase in OCR. Lastly, rotenone injection leads to a shutdown of mitochondrial respiration. Therefore, each administered compound allows the assessment of different aspects of mitochondrial respiration, including basal respiration, maximal respiration, spare respiratory capacity, proton leak and ATP production.

The optimal seeding density and test compound concentrations were determined during preliminary experiments to identify the optimal number of cells required to detect a sufficient shift in OCR and ECAR. The Seahorse XF Cell Mito Stress test, which assays mitochondrial respiration, generates a bioenergetics profile, whereby each injected drug allows different properties of mitochondrial respiration to be measured.

20,000 microglia precursor cells per well were seeded onto PDL-coated Seahorse XF96 V3 PS cell culture microplates and differentiated for 14 days in XVIVO with IL-34 and GM-CSF. Prior to plating, the plates were coated with fibronectin. Cells were seeded in a 80  $\mu$ l suspension of Seahorse XF RPMI media pH 7.4 supplemented with 10 mM glucose, 1 mM sodium pyruvate and 2 mM L-glutamine and allowed to adhere to the plate for 1 hour at room temperature to allow for even distribution across the well before being moved to a humidified 5% CO<sub>2</sub> incubator at 37°C. Four wells were kept empty to serve as background control.

The day prior to the experiment, the Seahorse XFe96 Analyser was turned on to allow the temperature to stabilise. 200  $\mu$ l of Seahorse XF calibrant was added to the Seahorse XF96 sensor cartridge and kept in a non-CO<sub>2</sub> incubator overnight. The day of the experiment, the hydrated cartridge was loaded with the test compounds oligomycin (2 $\mu$ M, 25  $\mu$ l), FCCP (2.5 $\mu$ M, 25  $\mu$ l) and antimycin A/rotenone (0.5 $\mu$ M, 25  $\mu$ l) diluted in pre-warmed Seahorse XF RPMI media at a 10x concentration to dose delivered to cells. The cartridge was then inserted into the Seahorse XFe96 machine and the Seahorse XF Cell Mito Stress test protocol set up for calibration according to the manufacturer's instructions. While the machine was calibrating, the cell culture microplate was removed from the 37°C CO<sub>2</sub> incubator, the XVIVO growth medium removed, the cells washed once with Seahorse XF calibrant and incubated with 175  $\mu$ l per well of Seahorse XF RPMI assay medium for 45-60 min at 37°C in a non-CO<sub>2</sub>

incubator. Following calibration and assay medium incubation, the cell culture microplate was inserted into the analyser and the Seahorse XF Cell Mito Stress test protocol was run: 3 successive readings (every 5 min) of basal respiration, followed by a drug injection sequence of oligomycin, FCCP and rotenone/antimycin A with 3 sequential readings every 5 min under condition.

#### 2.4.5 Cholesterol staining

Cholesterol staining was performed using filipin, a cytochemical cholesterol-specific probe (Te Vruchte et al. 2004). 14-day differentiated microglia on PDL-treated and fibronectin-coated 8-well  $\mu$ -slides were washed once with PBS and fixed in 4% PFA for 15 min followed by three PBS washes. Cells were incubated with 125  $\mu$ g/ml filipin (diluted in XVIVO medium) for 30 min in the dark at room temperature, after which the filipin-containing media was removed, and cells washed in PBS. Imaging was performed using a Zeiss Axio Imager A1 microscope in conjunction with an AxioCam High-Resolution Camera and Axiovision software v4.8.

#### 2.4.6 Sphingomyelin staining

The sphingomyelin-specific stain used for these experiments was lysenin (0.1  $\mu$ g/ml; Peptide International). Microglia cells plated on Ibidi chamber slides were washed with PBS once, fixed with 4% PFA and then stained with the sphingomyelin stain lysenin overnight (diluted in PBS + 1% BSA + 0.1% saponin). Following overnight incubation, cells were washed with PBS three times, incubated with lysenin anti-serum (1:500 dilution in PBS) at room temperature for 1 hour before incubation with a fluorescent secondary antibody (1:500 dilution in PBS) at room temperature for 30 min. Incubation medium was removed, Hoechst nuclear staining was applied followed by two PBS washes. Cells were imaged with a Zeiss Axio Imager A1 microscope and High-Resolution Camera and Axiovision software v4.8.

#### 2.4.7 Phospholipid staining

Phospholipidosis was analysed using LipidTOX Red Phospholipidosis Detection Reagent (Nioi et al. 2007). Microglia differentiated on Ibidi chamber slides were washed once with PBS and incubated with LipidTOX (1:1000 dilution in X-VIVO medium) for 4h to detect

phospholipidosis. Subsequently, the media was removed, and nuclei were stained with Hoechst before images were obtained with Zeiss Axio Imager A1 microscope and High-Resolution Camera and Axiovision software v4.8. LipidTOX was excited at 543 nm and its emission was detected at 594 nm.

## 2.5 Flow Cytometry

Fluorescence-activated cell sorting (FACS) was carried out for the analysis of cell surface molecules on the non-adherent cells collected from supernatant of differentiated factories as described above. Cells were washed in 0.1% BSA in PBS, centrifuged at 1000 rpm for 3 minutes and the resulting pellet was re-suspended in 200 µl of 0.1% BSA in PBS. For single-colour staining, 5 µl of the conjugated antibody or isotype-matching control (with the same fluorophore, from the same manufacturer) was added to the suspension and the mixture incubated at room temperature in the dark for one hour. For two-colour staining, two antibodies or two isotype controls (attached to different fluorophores) were added together. Following primary staining, the cells were washed twice with 0.1% BSA in PBS and centrifuged, before being transferred to 5 ml round bottom tubes (BD Falcon) in 200 µl of 0.1% BSA in PBS. Fluorescence was measured using a BD LSR Fortessa and data analysed using FlowJo software. The following antibodies and isotype controls were used.

Antibody	Clone	Supplier	Catalogue number
CD14-APC	61D3	eBioscience	17-0149-41
CD11b-APC	ICRF44	eBioscience	17-0118-42
CD45-FITC	2D1	eBioscience	11-9459-42
CD34-PECy7	4H11	eBioscience	25-0349-42
IgG1k-APC	APC isotype control	eBioscience	17-4714-81
IgG1k-FITC	FITC isotype control	eBioscience	11-4714-81
IgG1k-PECy7	PE-Cy7 isotype control	eBioscience	25-4714-80

**Table 2.6** List of conjugated antibodies used for flow cytometry analysis experiments.

## 2.6 Immunocytochemistry

### 2.6.1 Immunocytochemistry

Non-adherent myeloid cells were collected from the differentiated factories and plated onto glass coverslips. Cultured cells were washed in 1xPBS pH7.4, fixed with 4% paraformaldehyde (PFA) for 15 min at room temperature and washed 3 times with PBS. Fixed cells were

incubated with blocking buffer (3% goat/chicken/donkey serum, 0.1% Triton-X in PBS) for 1 hour at room temperature before overnight incubation at 4°C with primary antibodies (see list below) diluted in blocking buffer. Following overnight incubation, cells were subjected to 3 washes of 5 min, followed by a 1-hour incubation at room temperature, protected from light, with fluorescent secondary antibodies diluted in blocking solution. Coverslips were subsequently incubated with Hoechst at 1:5000 in blocking buffer and mounted on microscope slides. Images were taken using an Olympus BX61 fluorescent microscope.

The ICC primary and secondary antibodies used were as follows:

1° antibody	Host	Dilution	Supplier
CD34	Mouse anti-human	1:100	Abcam AB6330
CD45	Mouse anti-human	1:100	R&D Systems MAB1430
P2RY12	Rabbit anti-human	1:100	Abcam AB188968
IBA-1	Goat anti-human	1:100	Abcam AB5076
TGFBR1	Rabbit anti-human	1:50	Abcam AB31013
TMEM119	Rabbit anti-human	1:100	Abcam AB185333
CX3CR1	Rabbit anti-human	1:100	Bio-Rad AHP1589

**Table 2.7 List of primary antibodies used for immunocytochemistry.**

2° antibody	Dilution	Supplier
Alexa Fluor goat anti-mouse IgG 488	1:400	Invitrogen A11001
Alexa Fluor goat anti-mouse IgG 594	1:400	Invitrogen A11032
Alexa Fluor goat anti-rabbit IgG 594	1:400	Invitrogen A11037
Alexa Fluor goat anti-rabbit IgG 488	1:400	Invitrogen A11034
Alexa Fluor chicken anti-goat IgG 594	1:400	Invitrogen A21468
Alexa Fluor chicken anti-rabbit IgG 488	1:400	Invitrogen A21441
Alexa Fluor chicken anti-mouse IgG 594	1:400	Invitrogen A21201

**Table 2.8 List of secondary antibodies used for immunocytochemistry.**

### 2.6.2 Cytocentrifugation

Cells were washed and fixed as described. To make cytopins,  $1 \times 10^5$  cells were spun at 800 rpm for 1 min through pre-wet filters onto glass slides using a Centurion CYT04 centrifuge before staining as described in section 2.6.1.

## 2.7 RNA extraction and qRT-PCR

For RNA extraction, samples were harvested and lysed in RLT buffer (RNEasy Mini kit, Qiagen) containing 10 µl/ml β-mercaptoethanol. Total RNA was extracted according to the manufacturer's protocols. The concentration and purity of the extracted RNA samples were measured by spectrophotometry (Nanodrop).

### 2.7.1 PowerUp SYBR Green qRT-PCR

Reverse transcription was carried out using Superscript II kit, with 1 µg template RNA in a 20 µl reaction volume. The resulting cDNA samples were diluted 1:5 by adding 80 µl of deionised water and readied for qRT-PCR. Each qRT-PCR reaction, comprising 1 µl of the diluted cDNA product in a 20 µl volume, was placed in a thermocycler set up with the cycling parameters: 25°C for 10 min, 42°C for 50 min and 70°C for 15 min.

RT-qPCR was carried out on a CFX Connect Real Time System (Bio-Rad) using PowerUp SYBR Green Master Mix (Applied Biosystems). Quantification of target gene transcripts was carried out using primers designed and validated with established efficiencies between 90 and 105%. Primers were specifically designed following these parameters: T<sub>m</sub> close to 60°C and qPCR product between 80 and 120 bp.

qPCR component	Volume
10 µM Primer mix	1 µl
PowerUp SYBR Green Master Mix	10 µl
RNAse-free deionised water	8 µl
cDNA	1 µl

The qPCR reaction mix was added to a 96-well plate, which was centrifuged for 1 minute at 1500 rpm and put through the cycling program described below.

Step	Temperature	Time	Cycle	
UDG activation	50°C	2 min	Hold	
Polymerase activation	95°C	2 min	Hold	
Denaturation	95°C	15 sec	40	
Annealing/extension	60°C	1 min		
Stage	Step	Ramp rate	Temp	Time
	Step 1	1.6°C/sec	95°C	15 sec

Melt curve stage	Step 2	1.6°C/sec	60°C	1 min
	Step 3 (dissociation)	0.15°C/sec	95°C	15 sec

For analysis, the delta-delta CT method was used to determine relative gene expression values, with 3 biological replicates. Each biological replicate was analysed in triplicate.

### 2.7.2 Fluidigm High Throughput qRT-PCR

Reagent	Catalogue number	Supplier
Random hexamers	C1181	Promega
Fluidigm Reverse Transcription Master Mix kit	100-6300	Fluidigm
Preamp Master Mix kit	100-5580	Fluidigm
Exonuclease I	M0293S	New England BioLabs
TE buffer	12090015	Invitrogen
Fluidigm 96.96 Dynamic Array IFC chip	BMK-M-96.96	Fluidigm
96.96 Dynamic Array DNA Binding Dye and Assay loading reagent kits	100-3400	Fluidigm
SsoFast EvaGreen Supermix with low ROX	172-5211	BioRad
20X DNA Binding Dye Sample Loading Reagent	100-3400	Fluidigm
Control line fluid	89000021	Fluidigm

**Table 2.8 List of consumables used for Fluidigm qRT-PCR.**

Samples were harvested and RNA extraction carried out as described above. cDNA synthesis was performed using 100 ng of total RNA and random hexamers with the Fluidigm Reverse Transcription Master Mix kit. According to the manufacturer's instructions, samples had to undergo a round of preamplification prior to use with the high throughput array. 1.25 µl of each cDNA sample was pre-amplified using the Preamp Master Mix along with 0.5 µl of the pooled gene primers (500 nM per primer). The preamplification reactions (see table 2.8) was carried out using a 2 min 95°C denaturation step and 10 cycles of 15s at 95°C and 4 min at

60°C. The pre-amplified samples then underwent a clean-up step with Exonuclease I, where 2 µl of diluted Exo I at 4U/µl was added to each 5-µl preamplified reaction. The mixtures were put on a cycling program of digestion at 37°C for 30 min and inactivation at 80°C for 15 min. Following this treatment, the pre-amplified reactions were diluted 5 times using TE buffer.

Component	Vol per reaction (µl)	Vol for 96 reactions + 20% overage* (µl)
PREAMPLIFICATION PRE-MIX		
Preamp Master Mix	1.00	115.2
Pooled Gene primers	0.50	57.6
DNase-free H <sub>2</sub> O	2.25	259.2
cDNA	1.25	-
<b>Total</b>	<b>5.00</b>	-

**Table 2.8** Preamplification reaction using Fluidigm Preamp Master Mix. \*20% overage for ease of pipetting.

For the high throughput qPCR, a Fluidigm 96.96 Dynamic Array IFC chip, which is formatted to run reactions for 96 samples and 96 genes, was used (Spurgeon et al. 2008). The primer reaction or assay mixes (see table 2.9) were prepared on a 96-well PCR plate using the 96.96 Dynamic Array DNA Binding Dye and Assay loading reagent kits. The forward and reverse primers were first combined in microcentrifuge tubes before being added to loading reagent and TE DNA suspension buffer in individual wells of a 96-well plate. The plate was later vortexed for 30 sec and centrifuged at 1000 g for 1 min before pipetting into the IFC inlets.

Component	Vol per inlet (µl)	Vol for 50 µl stock
2x Assay Loading Reagent	2.5	25
1X TE buffer	2.25	22.5
100 µM Forward + Reverse primers	0.25	2.5
<b>Total</b>	<b>5</b>	<b>50</b>

**Table 2.9** Fluidigm 96.96 IFC primer reaction mix preparation. Final concentration of each primer is 5 µM in the inlet and 500 nM in the final reaction. For ease of pipetting, mixtures were made up as 50 µl stocks.

The sample reaction mixtures containing preamplified and Exo I-treated cDNA were prepared as shown in table 10 using SsoFast EvaGreen Supermix with low ROX and 20X DNA Binding Dye Sample Loading Reagent. The sample pre-mix was made up in a microcentrifuge tube being aliquoted as 3.3 µl per well of a 96-well plate, to which each preamplified cDNA sample was added. The cDNA sample mixture plate was vortexed and centrifuged as above before loading onto the IFC inlets.

Component	Vol per inlet + 20% overage (µl)	Vol for 96.96 IFC for 60 samples (µl)
SAMPLE PRE-MIX		
2X Sso fast EvaGreen	3.0	360
20X DNA Binding Dye	0.3	36
Preamplified & Exo I-treated cDNA	2.7	-
<b>Total</b>	<b>6.00</b>	-

**Table 2.10 Fluidigm 96.96 IFC sample reaction mixture preparation.**

Having prepared the sample and assay mixes, the chip was first primed after control line fluid was injected into each accumulator on the IFC. Following the priming script, 5 µl of primer assay mix and 5 µl of sample were loaded into their respective inlets of the 96.96 IFC chip and the chip placed in the HX controller for automatic loading and mixing. After loading, the chip was moved to the BioMark HD Real-Time PCR System (Fluidigm). The cycling program was GE Fast 96x96 PCR+Melt v2.

Segment	Type	Temp (°C)	Duration (sec)	BioMark HD Ramp rate (°C/s)
1	Thermal mix	70	2400	5.5
		60	30	5.5
2	Hot Start	95	60	5.5
3	PCR (30 cycles)	96	5	5.5
		60	20	5.5
4	Melting curve	60	3	1
		60-95		1°C/3s

**Table 2.11 Cycling parameters for BioMark HD Real-Time PCR platform for use with 96.96 IFC chip.**

Post chip run qPCR data analysis was initially done using the BioMark Gene Expression Data Analysis software, which analyses individual data points and generates Ct values using “pass” and “fail” scores. Fail data points, which feature melting curves with aberrant T<sub>m</sub> or from non-specific amplification, were removed after this initial analysis. Raw Ct values were then downloaded from the software as a data frame, and subsequently processed using Singular Analysis Toolset (Fluidigm), which runs the R script “fluidigmSC”. This script performs a series of differential gene expression analysis such as ANOVA, PCA, tSNE and hierarchical clustering to identify differentially expressed genes of interest. Gene expression values are generated as log<sub>2</sub> expression counts, converted from Ct values above the recommended background default of 24 (Livak et al. 2013).

### 2.7.3 qRT-PCR primers

Gene	Forward	Reverse
Nestin	GTTCCAGCTGGCTGTGGAGGC	GCTGCTGCCGACCTTCCAGG
Brachyury	TCAGCAAAGTCAAGCTCACCA	CCCCAACTCTCACTATGTGGATT
Flk1	GGCCAATAATCAGAGTGGCA	CCAGTGTCATTTCCGATCACTTT
RUNX1	CTGCCCATCGCTTTCAAGGT	GCCGAGTAGTTTTTCATCATTGCC
CD34	TGGACCGCGGCTTTGCT	CCCTGGGTAGGTAACCTCTGGG
CD45	CATTTGGCTTTGCCTTTCTG	TTCTCTTTCAAAGGTGCTTGC
IBA1	GCTGAGCTATGAGCCAAACC	TCATCCAGCCTCTCTTCTG
Kir2.1	GGTTTGCTTTGGCTCAGTCG	GAACATGTCCTGTTGCTGGC
Nav1.6	GGCAATGTTTCAGCTCTACGC	ATTGTCTTCAGGCCTGGGATT
TREM2	CTGGAGATCTCTGTTCCCC	AGAAGGATGGAAGTGGGTGG
CSF1R	TATGTCAAAGACCCTGCCCCG	GTGAGCAGACAGGGCAGTAG
CD11b	GAAAGGCAAGGAAGCCGGAG	TGGATCTGTCCTTCTTTAGCCG
TMEM119	CTTCTGGATGGGATAGTGGAC	GCACAGACGATGAACATCAGC
ABCA7	GCTGAGGAACTTGACCAAGGTAT	CCTGCTCCATTCACACCCAG
PLCG2	AACTGCAGACTTCGAGGAGC	AGGGGCTTTCACGACGTTAT
INPP5D	CTGCGTGCTGTATCGGAATTG	AAGAACCTCATGGAGACGCC
SREBF2	AGGCAGGCTTTGAAGACGAA	AGCTTCCCTGTGATGTGCAG
IL-1 $\beta$	TTCGAGGCACAAGGCACAA	TGGCTGCTTCAGACACTTGAG
TNF $\alpha$	GCCCATGTTGTAGCAAACCC	TATCTCTCAGCTCCACGACA
IL-6	ACCCCCAATAAATATAGGACTGGA	TTCTCTTTCGTTCCCGGTGG
TGF $\beta$ <sub>1</sub>	GGCTGTATTTAAGGACACCCGT	GACACAGAGATCCGCAGTCC
IL-10	AAGACCCAGACATCAAGGCG	AATCGATGACAGCGCCGTAG
P2RY12	GGAGCTGCAGAACAGAACT	AGTTGCCAAACCTCTTTGTGATA
GAS6	ACC TGACCGTGGGAGGTATT	GTGTCTTCTCCGTTCCAGCCA
ABCA1	ACTGGTTTGGCGAGGAAAGT	CAGCTTCAAGTGGGTGGGTT
LRP1	CTCGGATGAGCCCAAGGAAG	TCACCGCAATCGTTGTCGTA
FASN	GTGCCCTGAGCTGGACTACT	AAGCCGTAGTTGCTCTGTCC
HMGCS1	GACTGTCCTTTCGTGGCTCA	GAAAGAGCTGTGTGAAGGATAGA
HMGCR	TCGGTGGCCTCTAGTGAGAT	ACAAAGAGGCCATGCATTGCG
PPARG	ACAAGGCCATTTTCTCAAACGAG	CAAAGTTGGTGGGCCAGAATG
LDLR	ACCACAGAGGATGAGGTCCA	GTCATCCTCCAGACTGACCATC
CX3CR1	TGGGGCCTTACCATGGAT	GCCAATGGCAAAGATGACGGAG

**Table 2.12** List of primers used for Fluidigm qRT-PCR. For rest of the list, see appendix 6.

## 2.8 CRISPR/Cas9-mediated mutation of ABCA7 gene

### 2.8.1 CRISPR guide RNAs design and preparation

Single guide RNAs (gRNA) targeting the ABCA7 gene were designed using the Wellcome Sanger Institute and Deskgen CRISPR design tools, with focus on reducing off target effects such as modification of unintended genomic sites. The Alt-R CRISPR-Cas9 system (Integrated DNA Technologies or IDT) was used because of its high editing efficiency compared to vector constructs (Kim et al. 2014; Zuris et al. 2015). This method forms a ribonucleoprotein (RNP) complex by combining a *S.p.* Cas9 Nuclease (1081058 – IDT) with a target crRNA and a fluorescently labelled ATTO 550 tracrRNA (1075928 – IDT). Delivery of the activated RNP complex causes double-stranded DNA cleavage of the target DNA by Cas9, activating the non-homologous end joining system (NHEJ). The gRNAs chosen for the study were mapped onto coding exons 2 (Ex2P1) and 8 (Ex8P1) of the ABCA7 gene and were predicted to have minimal off-target effects in the genome.

gRNA name	Target region	Sequence
Ex2P1	Exon 2	GGAAGAATTTTCATGTATCGCCGG
Ex8P1	Exon 8	CACTGCTGCAGAGACCCCGAGGG

To generate the RNP complex, each crRNA oligo and tracrRNA was resuspended to 200  $\mu$ M in nuclease-free duplex buffer (IDT). Then, a crRNA:tracrRNA duplex was formed by combining each oligo with a tracrRNA in equimolar concentration: 1.7  $\mu$ l crRNA + 1.7  $\mu$ l tracrRNA + 1.7  $\mu$ l of nuclease-free duplex buffer. The reaction mixture was heated at 95°C for 5 min and allowed to cool at room temperature. To assemble the RNP complex for each oligo, the reaction mixture below was set up and incubated for 20 min at room temperature prior to transfection. The Cas9 nuclease was made up by diluting 3.1  $\mu$ l of 10  $\mu$ g/ $\mu$ l Cas9 stock with 1.9  $\mu$ l Cas9 storage buffer (10 mM tris-HCl pH 7.4, 300 mM NaCl, 0.1 mM EDTA, 1mM DTT).

Component	Volume ( $\mu$ l)
cRNA:tracrRNA complex (1 $\mu$ M)	2.5
Cas9 nuclease (6.2 $\mu$ g/ $\mu$ l)	2.5
Total volume	5

### 2.8.2 Cell culture, transfection and selection of targeted clones

Kolf2 iPS cells were grown to 70-80% confluence and maintained in E8 medium, as described before. On the day of transfection, media was removed and replaced with E8 media containing 10  $\mu$ M ROCK inhibitor for 1-2 hours before transfection. Cells were washed once with PBS pH 7.4 and dissociated with pre-warmed accutase for approximately 5 min (Life Technologies). E8 media containing ROCK inhibitor was added to inactivate the accutase, the mixture homogenised, centrifuged at 1500 rpm for 3 min and counted with 1 million cells being used. Cells were then resuspended in 100  $\mu$ l of nucleofection buffer, made up of 78  $\mu$ l P3 buffer and 22  $\mu$ l supplement from the P3 Primary Cell 4D-Nucleofector Kit. 5  $\mu$ l of each assembled RNP was added to the suspension, which was then transferred to an Amaxa cuvette. The cuvette was gently tapped onto a flat surface to eliminate bubbles. Cells were transfected with RNP complexes by electroporation using the Amaxa 4D Nucleofector system (program CA137). Following nucleofection, the cells were allowed to recover for  $\sim$  10 min at 37°C, before addition of pre-warmed E8 + ROCK inhibitor media and plating onto a culture dish pre-coated with vitronectin. 24 hours post nucleofection, the transfected cells were FACS sorted to select for the top 10% of the most fluorescent cells, for increased editing efficiency. Briefly, the transfected cells were washed in PBS and dissociated as single cells with accutase, as above. The cells were then centrifuged and resuspended in 500  $\mu$ l in E8 media + ROCK inhibitor into FACS tubes for sorting in a FACS ARIA Fusion (BD Biosciences) using the tracrRNA ATTO550. The sorted cells were collected in a FACS tube containing 1 ml of E8 + ROCK inhibitor, replated onto a 10 cm tissue culture dish pre-coated with vitronectin in order to obtain single cell clones. The following day, the culture media was changed to E8 medium and thereafter the cells were fed every other day, being monitored daily for the formation of colonies. Around 7 days after transfection, single colonies were cut in half and picked onto two separate 96-well plates by using a P20 pipette set at 10  $\mu$ l – cells grown one plate were used for genomic DNA extraction and PCR screening to detect successful excision of the target region (see table 2.13 below). The corresponding 96-well plate was used for clonal expansion.

PCR primer	Target region	Sequence
Ex2F	Exon 2	ATTGGTTTACTCCACCCCTGGG
Ex2R	Exon 2	GAGTCGTTGAAGTTGCTCAGGC
Ex8F	Exon 8	ctttgcctctcagagcctcagt
Ex8R	Exon 8	GGAAACCGAGGTCAGTCACTCA

PCR component	Volume ( $\mu$ l)
5x colourless GoTaq Flexi buffer	10
25 mM MgCl <sub>2</sub> solution	5
10 $\mu$ M dNTPs	1
Ex2F2 Primer	1
Ex8R6 Primer	1
Extracted DNA with DNA lysis buffer	1
GoTaq DNA polymerase	0.25
<b>Nuclease-free water to</b>	<b>50</b>

**Table 2.13 ABCA7 KO PCR screening reaction.**

For genomic DNA extraction, cells in 96-well plates were washed once with PBS before addition of DNA lysis buffer (see section 2.1.4) supplemented with 2% proteinase K. 50  $\mu$ l of DNA lysis buffer was added per well and the mixture incubated at 55°C for 4 hours or overnight. This was followed by inactivation at 95°C for 30 minutes, where each extracted DNA sample was diluted 1 in 10 in 10 mM Tris pH 8.0. The diluted and inactivated DNA sample was then used for PCR assay outlined below. The PCR cycling parameters were set up as follows:

Step	Temperature	Time	Cycle
Initial denaturation	95°C	2 min	1
Denaturation	95°C	15 secs	30
Annealing	60°C	45 secs	
Extension	72°C	1 min	
Final extension	72°C	5 min	1

96-well plate clones found to carry the successful mutation after PCR screening were subjected to sub-cloning. To do this, the cells were washed with PBS and incubated with accutase for 5 min to ensure a single cell suspension. Pre-warmed E8 media was added to the cell suspension to inactivate the accutase and the mixture centrifuged at 1000rpm for 3 min. The cells were then re-suspended in E8 + ROCK inhibitor media before plating at very low density in a vitronectin-coated 10 cm culture dish. This allowed the cells to expand from single cells, before individual colonies from the dish were picked, grown and expanded in 24-well plates before another round of PCR screening. All expanded sub-clones were also kept as

frozen pellets. The PCR-amplified DNA were separated by agarose gel electrophoresis using 2% gels.

## 2.9 RNA Sequencing and Analyses

### 2.9.1 RNA Sequencing library construction and sequencing

Samples used for RNA sequencing (RNA-seq) were harvested using RLT buffer from RNeasy Mini Kit before total RNA was extracted from lysates following the protocols of the manufacturer. RNA-seq was performed at the Genomics Research Hub of Cardiff University School of Biosciences by Angela Marchbank. RNA integrity was measured for all samples with the Agilent Bioanalyser 2100 (Agilent Technologies) and samples with RNA integrity number above 8 were retained for library construction. The Illumina TruSeq mRNA stranded protocol was used to perform cDNA synthesis from all samples and generate poly-A mRNA libraries. 1 µg of RNA was used to construct RNA-seq libraries. Libraries were then assessed for their quality with the Agilent 4200 TapeStation (Agilent Technologies) and sequenced as single-end 75 bp reads on the Illumina NextSeq500 sequencer, generating 40 million reads per sample.

### 2.9.2 RNA-seq read mapping, gene counts estimation and differential gene expression analysis

RNA-seq reads (fastq files) were first trimmed using Trimmomatic (version 0.35) (Bolger et al. 2014) and then mapped to the GRCh38.89 reference human genome using STAR (version 2.5.1b) (Dobin et al. 2013). Transcripts were assembled before raw read counts per gene were generated using the software FeatureCounts (Liao et al. 2014). Transcripts with at least 1 count per million in at least one sample were considered to represent expressed genes and retained for further downstream analysis, otherwise removed. Differential gene expression analysis was carried out with the Bioconductor package DESeq2 (release 3.6) to generate gene expression values as FPKM (Fragments per Kilobase of transcript per Million mapped reads) (Love et al. 2014). The Benjamini-Hochberg (BH) multiple testing correction procedure, which decreases false discovery rate, was employed to compute adjusted p-values. Principal component analysis of the normalised expression counts was performed using the R function “prcomp” and plotted with “ggplot”. Hierarchical clustering heatmap based on normalised gene expression counts was conducted using the R function “pheatmap”.

### 2.9.3 Comparative Gene Set Enrichment Analysis of iPSC-derived microglia

Single-ended RNA-seq data for human cortical neurons, astrocytes and myeloid cells (Zhang et al., 2016) was retrieved from Gene Expression Omnibus (accession GSE73721). The downloaded raw fastq files were processed along the same pipeline as described above to produce raw gene counts. These were combined with values from our data to estimate normalised gene expression counts with corresponding adjusted p-values. Genes with p-adjusted < 0.05 were chosen to carry out a comprehensive Gene Set Enrichment Analysis (GSEA) of the stem cell-derived microglia datasets. GSEA analyses whether enrichment of differential expression among gene sets relates to biological hypotheses and pathways (Subramanian et al. 2005). GSEA orders all genes according to their differential expression statistic, and tests whether genes in a specific gene set have a higher overall rank than would be expected by chance. A pathway set was chosen consisting of Gene Ontology (GO) (Harris et al. 2004), Kyoto Encyclopaedia of Genes and Genomes (KEGG) (Kanehisa et al. 2012), Reactome (Croft et al. 2014), BioCarta and NCI pathway interaction database (Schaefer et al. 2009). Upregulated and downregulated genes in iPSC-derived microglia were assessed separately.

### 2.9.4 iPathwayGuide Impact Analysis

Pathway Impact Analysis was run using AdvaitaBio iPathwayGuide (<https://www.advaitabio.com/ipathwayguide.html>) to identify significantly impacted pathways. This method utilises a systems biology approach and incorporates the classical probabilistic aspects of analysis (e.g. GSEA) with important biological factors: “the magnitude of the expression changes of each gene, the position of the differentially expressed genes on the given pathways, the topology of the pathway that describes how these genes interact, and the type of signalling interactions between them” (Draghici et al. 2007; Donato et al. 2013).

This method analyses DE gene datasets in the context of pathways from the KEGG database (Kanehisa et al., 2012), gene ontologies from Gene Ontology consortium database (Ashburner et al. 2000) and miRNAs from the miRBase (Release 21). The pathways are then scored according to two criteria: (i) the over-representation of DE genes in a given pathway and (ii) the perturbation of that pathway computed by propagating the measured expression

changes across the pathway topology. These criteria are taken account to calculate two probability values: pORA and pAcc. pORA expresses the probability of observing the number of DE genes in a given pathway that is greater than or equal to the probability by random chance. The second probability pAcc is calculated based on the amount of total accumulation measured in each pathway and the sum of all of all absolute accumulations of the genes in a given pathway. The probability values are then combined into one final pathway score by calculating a p value using Fisher's method, corrected for multiple comparisons by False discovery rate (FDR).

### 2.9.5 Upstream regulator analysis

Upstream regulator analysis was performed using the Ingenuity Pathway Analysis (Ingenuity Systems, Qiagen). This program predicts potential upstream regulators and mechanistic networks that explain the gene expression changes observed in a dataset, by calculating P-values of overlap and activation z-score statistics. The P-value of overlap establishes whether there is a statistically significant overlap between gene expression changes in a dataset and the genes affected by an upstream regulator (regulators with p value of < 0.01 qualified). The activation z-score considers the direction of gene expression changes and is used to predict whether regulators are activated or inhibited in the dataset. Generally, a z-score of > 2 or < -2 is regarded as significant. A cut-off of 0.01 was used to decide which genes were included in this analysis.

### 2.10 Statistical analysis

Statistical analysis of Fluidigm qRT-PCR data was carried out using GraphPad Prism 7.0 software. Data were represented as average  $\log_2$  expression values generated by Fluidigm analysis R package (see section 2.7.1). When comparing the  $\log_2$  expression from multiple conditions against a control group, one-way ANOVA with Dunnett's post hoc comparison was used. For assessing data from experiments with independent variables and one continuous dependent variable, a two-way ANOVA with Tukey's post hoc multiple comparisons test was carried out. Asterisks representing significance are defined as follows: ns – not significant; P > 0.05; \*\* P < 0.01; \*\*\* P < 0.001; \*\*\*\* P < 0.0001.

# 3. TRANSCRIPTOMIC AND FUNCTIONAL VALIDATION OF HUMAN IPSC-DERIVED MICROGLIA

## 3.1 Introduction

Animal models have been invaluable in advancing our understanding of neurodegenerative diseases such as Alzheimer's and Huntington's disease (Götz & Ittner 2008; Laferla & Green 2012). Much has been gained from animal studies, including the now recognised importance of research focusing on the role of neuroinflammation, and specifically microglia in those disorders (see section 1.1). Nonetheless, the emphasis needs to shift towards elucidating the phenotypic characteristics of diseased microglia, as well as how they can be harnessed to treat disease. Indeed, it can be argued that the failure of several clinical trials and paucity of new therapies (Cummings et al. 2014) highlight a necessity for improved disease models that bridge the gap between the clinic and animal models.

In that respect, advances in stem cell technology since the advent of induced pluripotent stem cells (iPSCs) (Takahashi & Yamanaka 2006; Okita et al. 2007; Takahashi et al. 2007) have revolutionised in vitro disease modelling, leading to the development of several reliable protocols for differentiation of iPSCs into neurons and astrocytes (Krencik et al. 2011; Serio et al. 2013; Shaltouki et al. 2013). Prior to the beginning of this study, there were no published protocols for in vitro differentiation of microglia. As established through lineage tracing studies, microglia arise from primitive yolk-sac derived haematopoietic precursors during embryonic development that colonise the developing brain (Ginhoux et al. 2010). Therefore, any strategy for microglial differentiation would require mimicking the steps leading to yolk sac haematopoiesis (Ginhoux et al. 2013). Based on this rationale, a number of microglia differentiation protocols have since been reported (Muffat et al. 2016; Abud et al. 2017; Haenseler et al. 2017; Pandya et al. 2017). The protocol used in this study (see

section 2.3) was adapted from work by (Karlsson et al. 2008; van Wilgenburg et al. 2013), who showed that monocyte-like primitive macrophage precursors can be derived from human stem cells. The differentiation method involves culturing embryoid bodies (EBs) in serum-free and feeder-free medium containing the cytokines IL-3 and macrophage colony-stimulating factor (M-CSF) to promote the formation of the non-adherent myeloid cells in the culture supernatants. These macrophage precursors are then harvested from the culture medium and differentiated to a microglial phenotype by the addition of two growth factors: the astrocyte-derived granulocyte M-CSF (GM-CSF) and IL-34, which have been shown to induce a ramified microglia phenotype from human monocytes (Ohigdani et al. 2014). In the CNS, IL-34 is produced by neurons and is required to maintain microglial survival (Wang et al. 2012; Greter et al. 2012). This protocol compares favourably to the others mentioned in its simplicity and straightforwardness, while it involves little manipulation other than a simple weekly harvest of the macrophage precursors, compared to a trituration-based method (Muffat et al. 2016) and rounds of FACS-sorting (Pandya et al. 2017).

### 3.2 Aims

This chapter set out to characterise microglia differentiated from iPSCs using the protocol described in section 2.3. Two cell lines of different genetic backgrounds Kolf2 and HD109 were used, enabling an appraisal of the efficacy and reproducibility of the differentiation protocol. Using RNA sequencing, the transcriptome profile of the differentiated microglia was investigated, with emphasis on the differences between macrophage precursors and microglia highlighted here.

### 3.3 Results

#### 3.2.1 Human iPSC-derived microglia cells express characteristic microglial markers

Figure 3.1 displays a schematic of the differentiation process, including the time course and changes in culture conditions through the early parts of the protocol. Split into three parts, the early stages of the protocol involve the formation of EBs and culture in E8-3G medium to induce mesoderm layer differentiation. Preliminary experiments indicated that E8-3G-treated EBs were committed to the mesoderm lineage, increasing expression of Brachyury, a transcription factor required for mesoderm layer formation and haematopoietic stem cell differentiation. Similarly, this treatment was found to increase expression of the haematopoietic stem cell marker CD34 and of RUNX1, a transcription factor that regulates haematopoietic stem cell differentiation (data not shown). Taken together, these results indicated a definite switch upon EB formation and culture with VEGF, BMP4 and SCF.

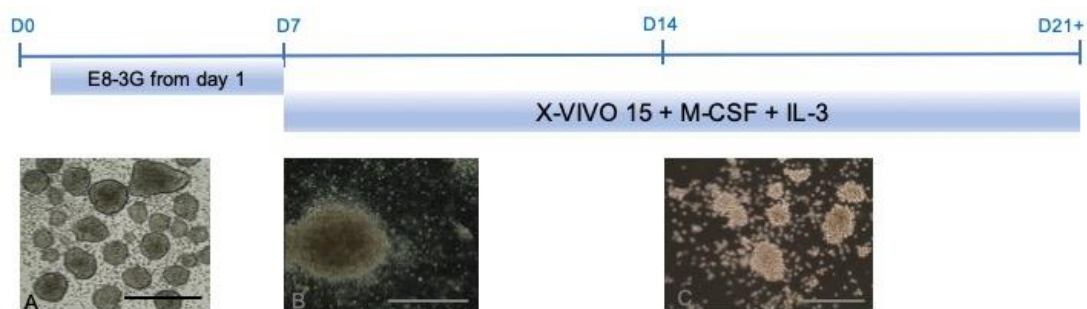


**Figure 3.1 Schematic representation of the protocol for the differentiation of human iPSCs into macrophage precursor cells.**

Feeder-free iPSCs were enzymatically dissociated using ReLeSR to form embryoid bodies (A), which were subsequently cultured in E8 medium with 50 ng/ml BMP-4, 50 ng/ml VEGF and 20 ng/ml SCF (or E8-3G) for 7-10 days to allow the EBs to form cystic structures. EBs were further differentiated by seeding 6-8 EBs into a well of 6-well plate cultured in X-VIVO15 media supplemented with M-CSF and IL-3. Under these conditions, EBs adhere to the culture surface and begin to spread, forming factories (B). As the factories continue to differentiate, there is formation of phase bright cells, which increase in number and are shed from their factory colonies, allowing them to be harvested from the supernatant weekly (C). Scale bars represent 50  $\mu$ m.

In the second stage of differentiation, non-adherent cells produced in the supernatant of differentiation factories were harvested and assayed for expression of various myeloid-specific markers by immunocytochemistry (Figure 3.2). Cytocentrifugation and immunostaining of the cells revealed a highly homogeneous population of cells where typical myeloid surface antigens CD45 and CD11b were expressed. Interestingly, the supernatant cells were also positive for CD34, suggesting that they

were still undergoing maturation. This trend was similar in both the HD109 and Kolf2 differentiated cells (Figure 3.2).

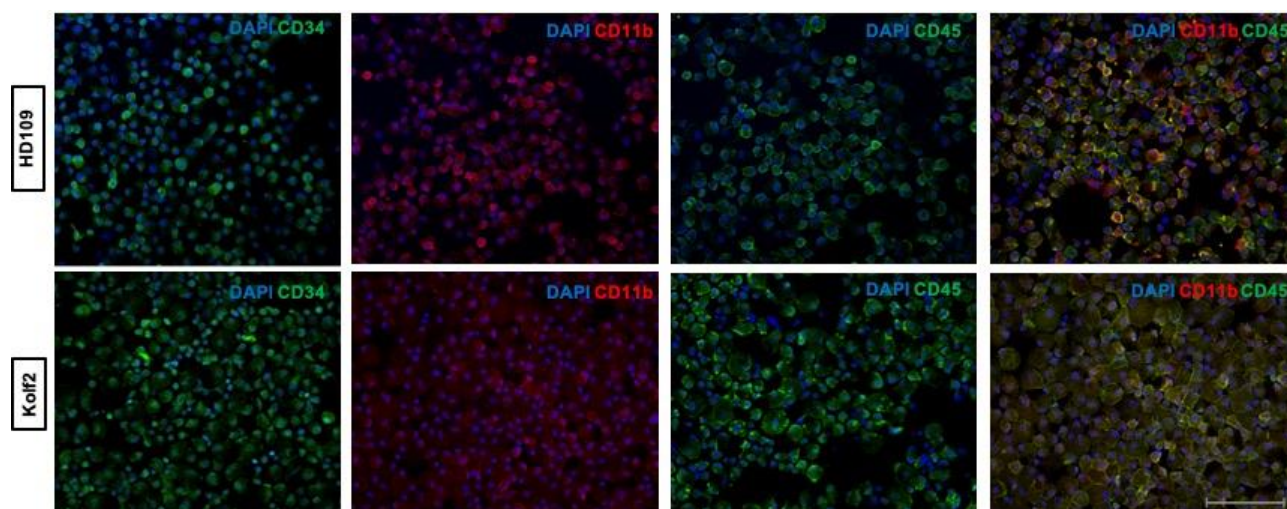
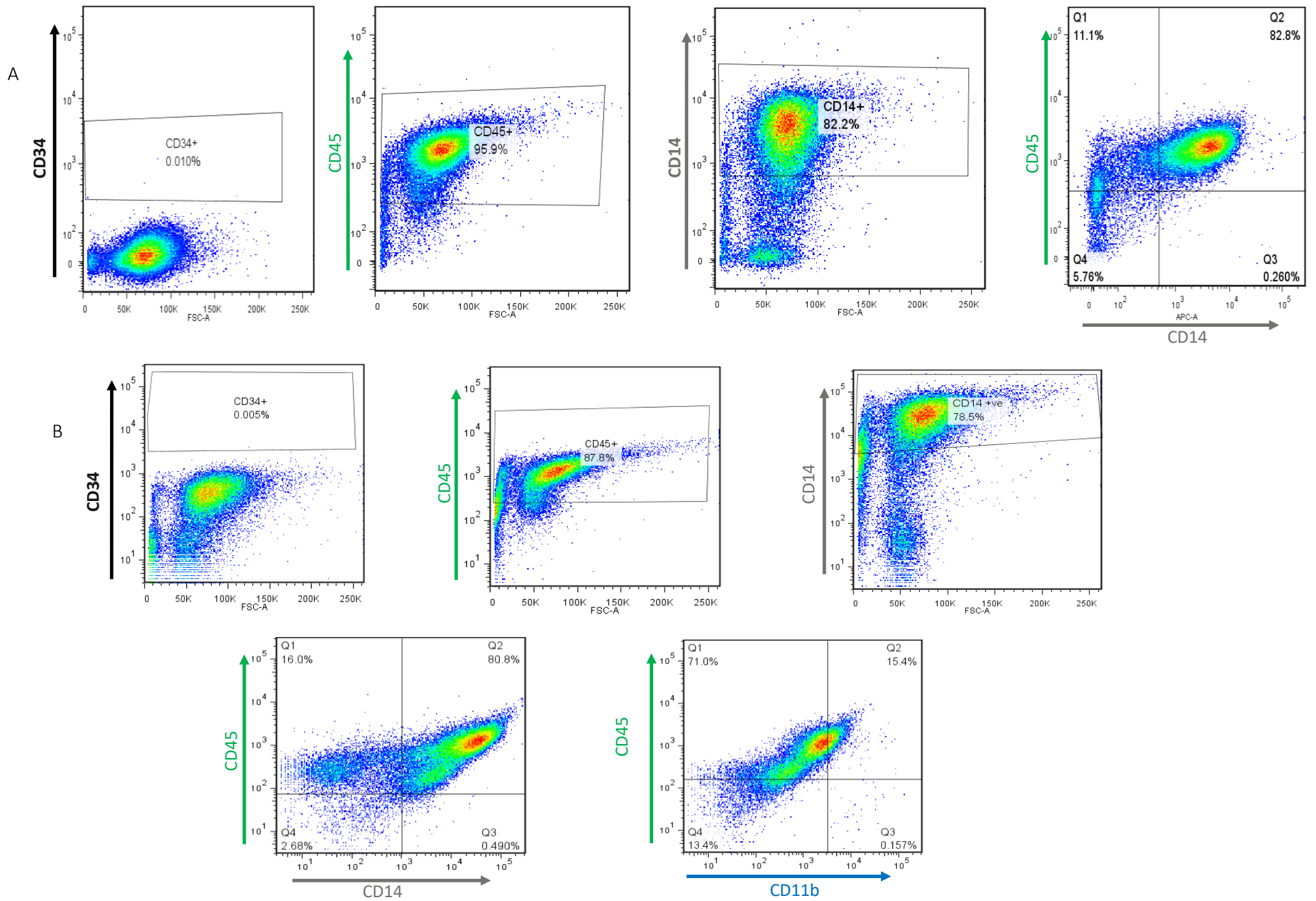


**Figure 3.2 Schematic representation of the protocol for the differentiation of human iPSCs into macrophage precursor cells.**

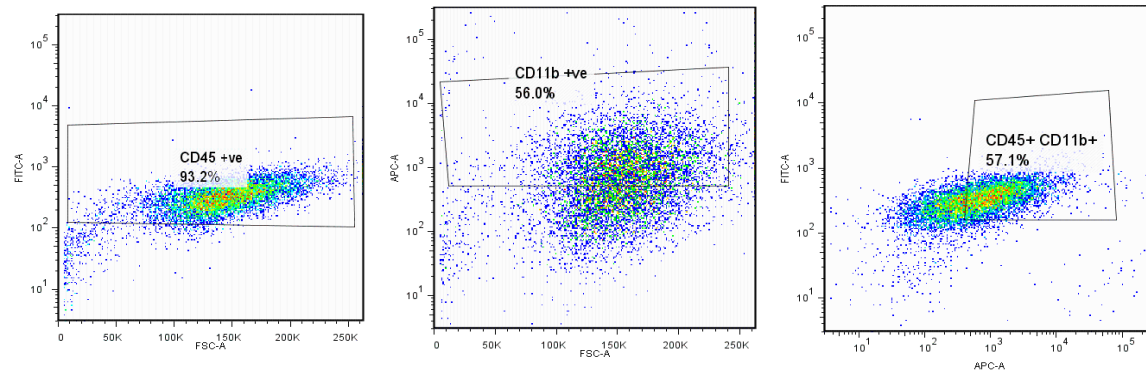
Representative images of non-adherent myeloid cells formed during M-CSF and IL-3 directed differentiation of HD109 and Kolf2 iPS cell lines. The cells were shed into the culture supernatant of the differentiated factories and harvested before cytopsin and staining for the expression of haematopoietic markers CD34 (green), CD11b (red) and CD45 (green). Scale bar represents 50  $\mu$ m.

Next, the non-adherent myeloid cells harvested at different time points from the differentiation factories (weeks 3 and 5) were analysed for the expression of CD34, CD45, CD14 and CD11b by flow cytometry (Figure 3.3). The majority of the HD109 harvested cells were positive cells at week 3 (82%), whereas CD34 expression was negligible (Figure 3.3A). Cells harvested two weeks later displayed a similar FACS profile, with an equally high proportion of CD45<sup>+</sup> CD14<sup>+</sup> double positive cells (80%), while CD11b expression was measured at 15% (Figure 3.3B). An immortalised human monocytic cell line THP-1 (Tsuchiya et al. 1980), featuring high CD45 and CD11b expression, was then used to confirm the monocyte-like antigen profile of the supernatant cells (Figure 3.3C).

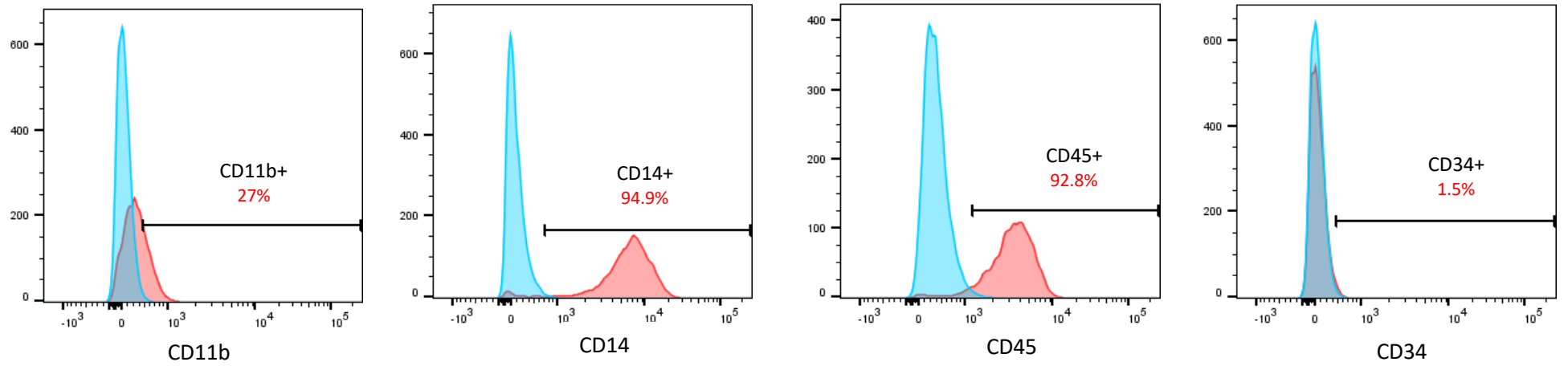
Flow cytometry analysis was extended to Kolf2 supernatant cells harvested at weeks 3 and 5 from the differentiation factories, with similar results. CD45 and CD14 expression at both time points was measured at over 90%, with CD34 equally low at 1% (Figure 3.3 D-E). CD11b was also expressed at around 30% for the two harvests, showing that the phenotype of the monocyte-like supernatant cells does not vary greatly over the course of a differentiation.



C



D



E

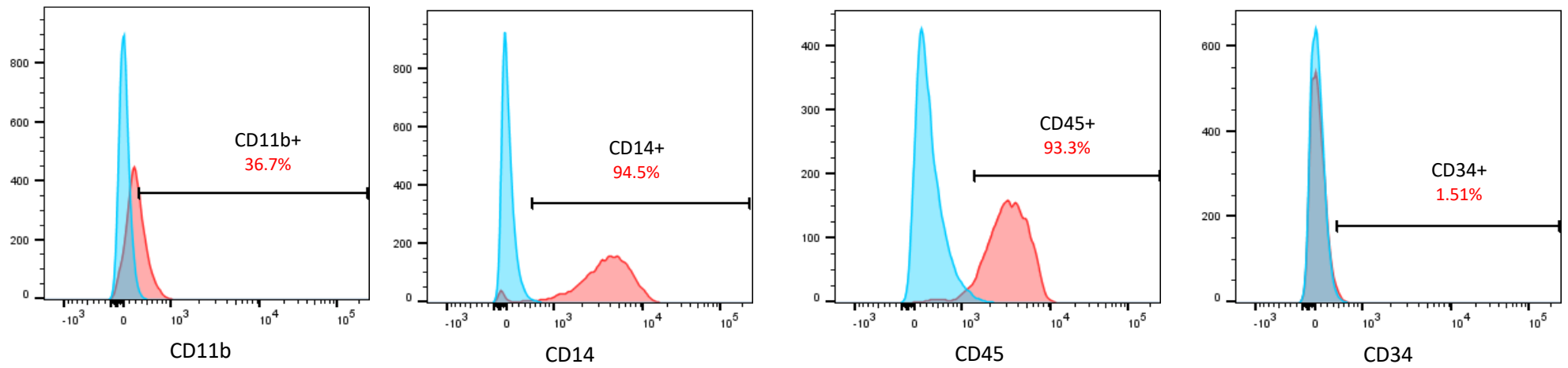


**Figure 3.3 Non-adherent supernatant cells harvested from microglia differentiation factories are positive for haematopoietic markers.**

**(A)** A high proportion of HD109 supernatant cells harvested from M-CSF & IL-3 differentiation factories at week 3 expressed the myeloid markers CD45 and CD14 (95% and 82%). CD34 expression in the cells harvested from the same differentiation factories was less than 1%. Co-expression of CD45 and CD14 showed a large population of 82%. Gates were defined by using the appropriate isotype control antibodies. **(B)** Staining for HD109 supernatant cells harvested from the same differentiation factories at week 5 showed a similarly high proportion of CD45<sup>+</sup> (over 85%), CD14<sup>+</sup> cells (78%) produced in the culture supernatant. Double staining for CD45 and CD11b showed that 15% of the harvested cells were double positive. **(C)** Expression of CD45 and CD11b in the HD109 and Kolf2 supernatant cells was compared to the myeloid control cell line THP-1 monocytes, which express high levels of CD45 (over 90%) and CD11b (57%). **(D)** Differentiation factories set up from Kol2 iPSCs produced a population of monocyte-like myeloid cells at week 3 expressing high levels of CD45 and CD14 (both, at over 90%), with CD11b expression measured at 27% and CD34 at 1%. Red peaks denote antigens and blue peaks denote isotype controls. **(E)** Kolf2 supernatant cells harvested from the same differentiation factories at week 5 displayed a similar FACS profile to those from week 3. Representative of three independent experiments.

As previously mentioned, the neuron-derived cytokine IL-34 is vital for the development and maintenance of microglia in the brain, where it binds to the colony-stimulating factor-1 receptor (CSF1R), whose ablation results in loss of microglia (Erblich et al. 2011). Moreover, a recent study demonstrated that stimulation with IL-34 and GM-CSF can induce a ramified phenotype in blood monocytes (Ohgidani et al. 2014). Therefore, to induce an in vitro microglial phenotype, Kolf2 and HD109 macrophage precursor cells (Macpre) were cultured in XVIVO15 media supplemented with 10 ng/ml GM-CSF and 100 ng/ml IL-34 for 14 days, before being stained for the canonical macrophage/microglia markers TMEM119 and IBA1 (Figure 3.4).

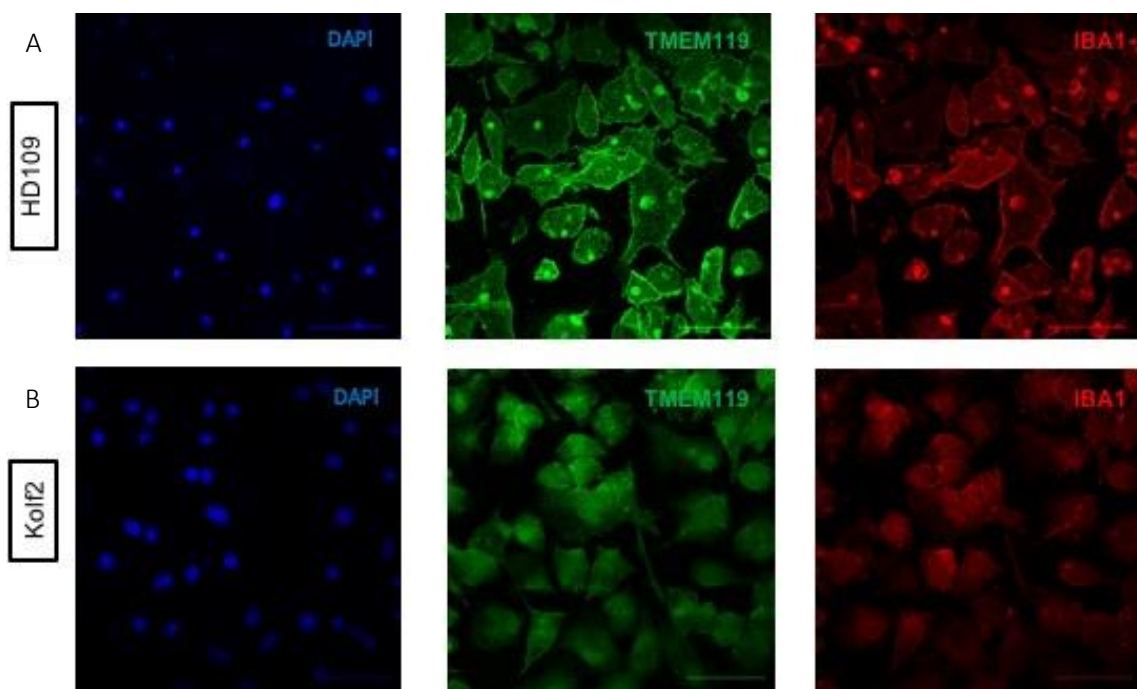
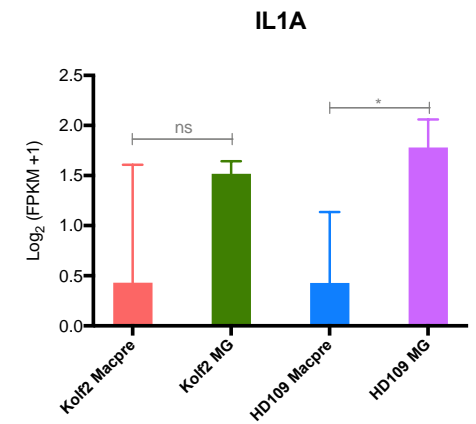
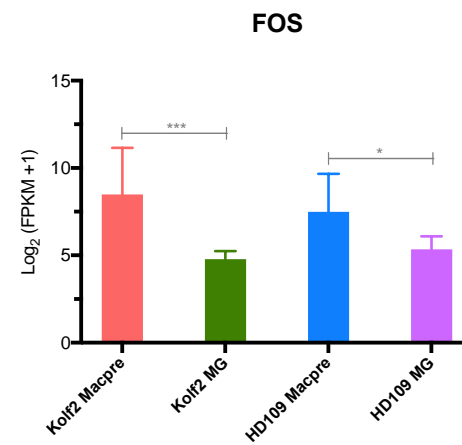
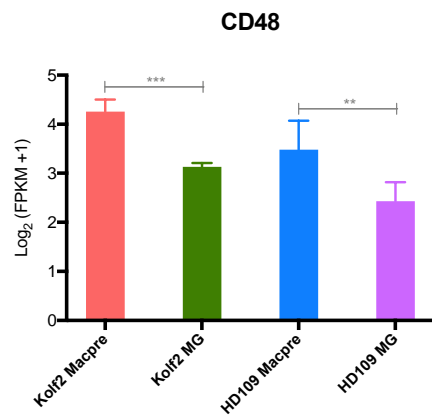
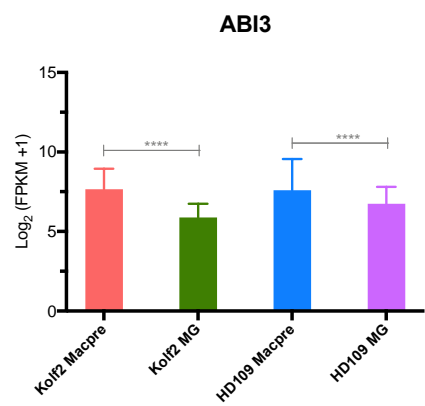
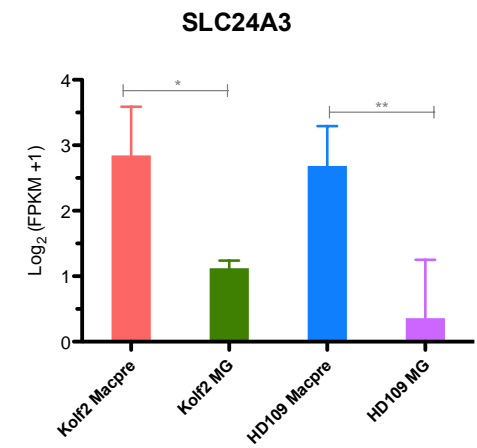
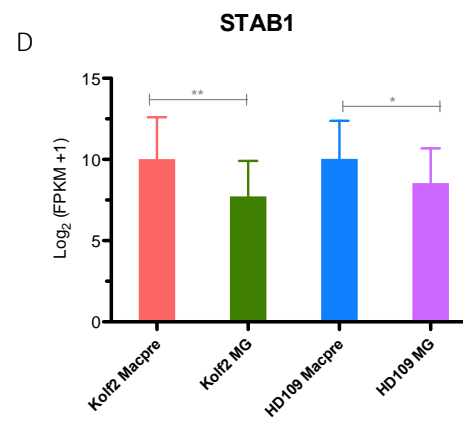
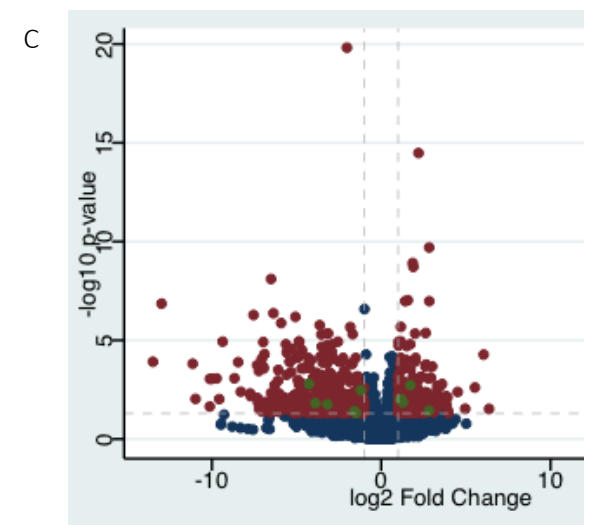
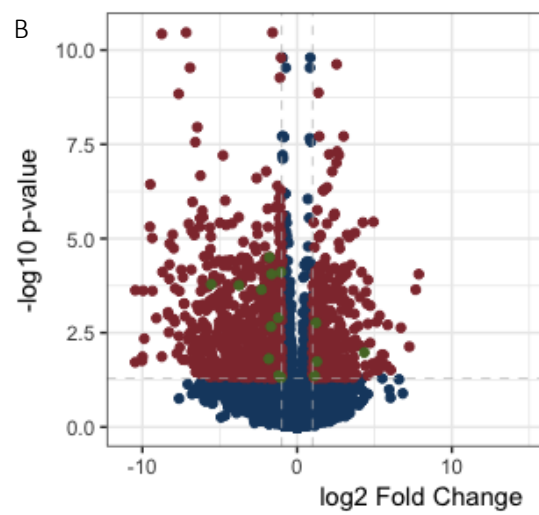
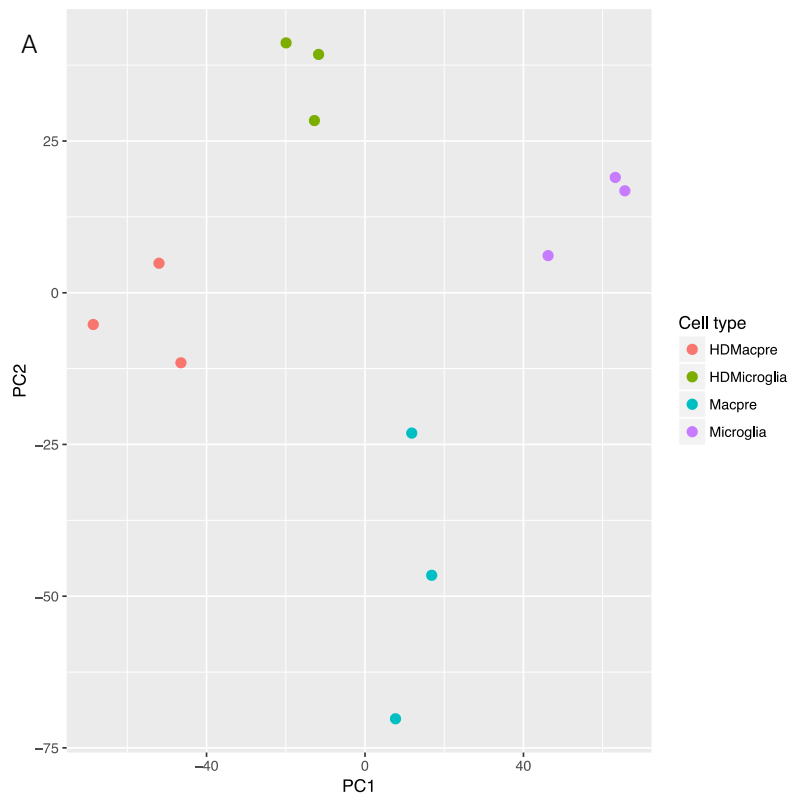


**Figure 3.4 Differentiation of macrophage precursor cells with GM-CSF and IL-34 induces a microglial-like phenotype.**

Confocal images of HD109 (A) and Kolf2 (B) microglia-like cells, which were plated on PDL-treated fibronectin-coated coverslips and cultured in XVIVO + GM-CSF + IL-34 for 14 days. MG cells were fixed and stained with TMEM119, a cell marker of unknown function highly specific to human and mouse microglia, and the macrophage/microglia marker IBA1. Scale bars represent 20 μm.

### 3.2.2 Transcriptomic profiling of human iPSC-derived microglia reveals a microglial signature

Following confirmation that the iPSC-derived IL-34 and GM-CSF-treated microglia cells (MG) express microglial markers such as IBA1 and TMEM119, RNA sequencing was employed to profile the transcriptome of the in vitro differentiated by comparing it to the macrophage precursor cells. Samples used for this experiment were drawn from three independent differentiations. Correlation analysis showed clear separation between the macrophage precursor cells and the IL-34 differentiated microglial cells for both genetic backgrounds (Figure 3.5A). Crucially, a disease effect on top of the cell type segregation was apparent between the Kolf2 and HD109 samples, as shown by the principal component analysis plot (see chapter 4). When compared to their respective macrophage precursor cells, differential gene expression analysis (fold change of 2 and p-value 0.05) demonstrated a total of 935 and 605 differentially expressed (DE) genes in the Kolf2 (Figure 3.5B) and HD109 MG cells (Figure 3.5C) respectively. In total, IL-34 and GM-CSF treatment of the respective precursor cells increased expression of 374 and 240 genes in Kolf2 MG and HD109 MG cells respectively. In contrast, 561 DE genes were downregulated in the Kolf2 WT cells, compared to 365 in the HD109 iPSC-derived microglia (Figure 3.5 B-C).



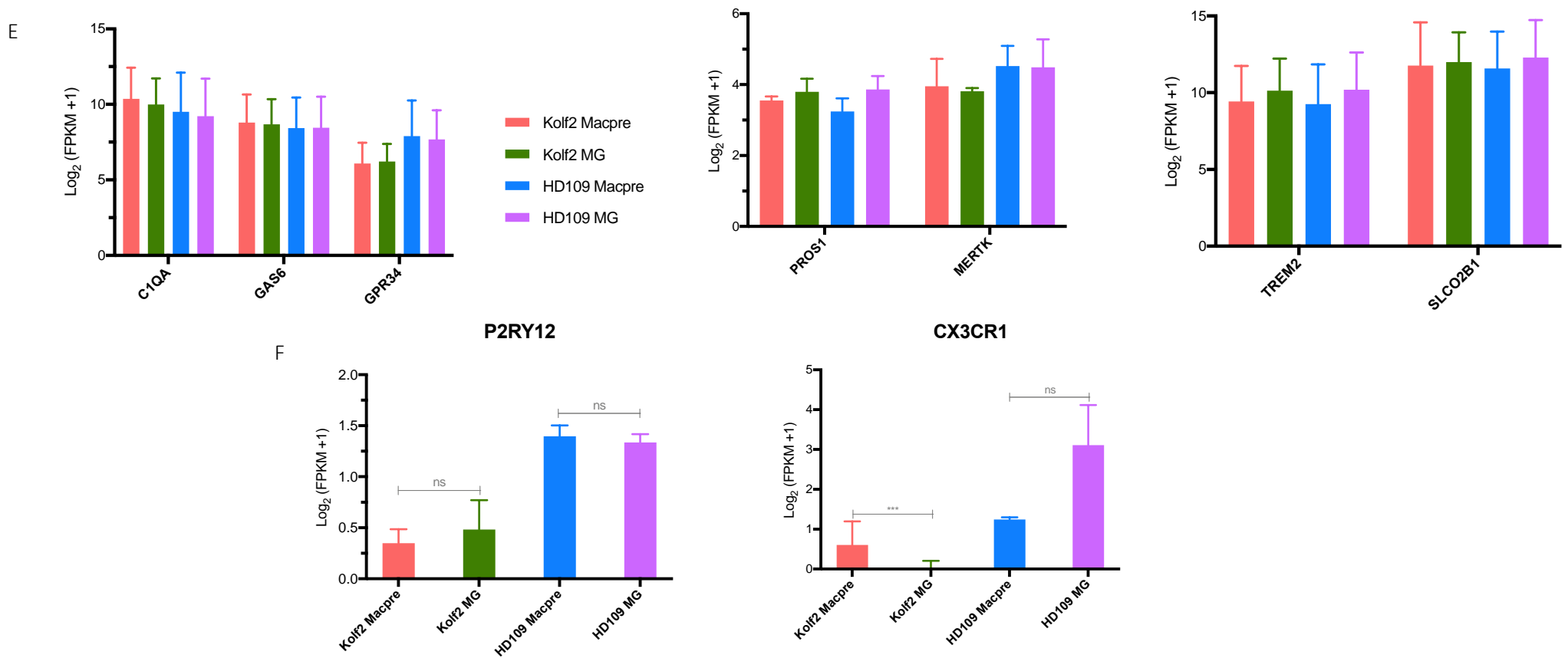


**Figure 3.5 Transcriptomic profiling of Kolf2 and HD109 iPSC-derived microglia demonstrates a microglial signature in the in vitro cells.**

Differential gene expression was carried out using DESeq2 to generate normalised expression counts. Biological replicates were used for comparative analysis to compute significant differentially expressed genes at fold change of 2 and Benjamini-Hochberg p value-adjusted < 0.05.

(A) Principal component analysis of Macpre and MG cells shows a cell-type specific segregation between Macpre samples and MG samples. PCA was performed using “prcomp” and plotted with “ggplot”. (B) Differentiation of Kolf2 Macpre cells into MG cells with IL-34 and GM-CSF resulted in 935 DE genes, with 374 upregulated ( $\log_2$  fold change > 1) and 561 downregulated genes ( $\log_2$  fold change < -1). (C) Treatment of HD109 Macpre cells with GM-CSF and IL-34 resulted in a total of 605 DE genes in HD109 MG cells, with 240 upregulated and 365 downregulated genes. The majority of microglia sensome genes were found to be comparably expressed between the Macpre and MG cells, except the genes highlighted as green dots on the volcano plots. (D) Differentially expressed microglia sensome genes between Macpre and MG samples. A pseudo-count,  $\log_2$  transformed measure of normalised gene expression counts (FPKM+1) was used to compare expression levels between samples (Abud et al. 2017). (E) Canonical microglia genes were highly expressed in Kolf2 and HD109 Macpre and MG cells. (F) Levels of the purinergic receptor P2RY12 and surface protein CX3CR1 were surprisingly low in all the Kolf2 and HD109 samples. Data analysed by DESeq2 and Benjamini-Hochberg multiple correction procedure used to compute adjusted p-values. \* p < 0.05, \*\* p < 0.01, \*\*\* p < 0.001. ns – not significant. n=3 independent differentiations.

To assess whether a microglial signature could be detected in our Kolf2 and HD109 microglia cells, a number of complementary analyses were undertaken. Firstly, the expression of microglia sensome genes was compared between Macpre and MG samples. For this purpose, a list of ~190 'microglia sensome' genes, identified in recent publications to be associated with microglia (Hickman et al. 2013; Butovsky et al. 2014; Grabert et al. 2016; Galatro et al. 2017), was compiled and included PRRs, chemoattractant and chemokine receptors, purinergic and cytokine receptors, cell-to-cell interaction and ECM-protein receptors as well as various endogenous transporters (see Table 1.1 in section 1.2.3 for examples of genes included in the list). The majority of sensome genes showed similar expression in Macpre and MG cells, with only a handful showing differential expression between the respective MG and Macpre cells, highlighted as green dots on the volcano plots (Figure 3.5 B-C). Of those genes, the AD risk gene *ABI3*, transmembrane receptor *STAB1* and sodium/calcium transporter *SLC24A3* were significantly downregulated in HD109 and Kolf2 MG compared to Macpre samples, along with the inflammatory-associated transcription factor *FOS*. Conversely, mRNA levels of *IL1A*, the cytokine released in response to injury were higher in the MG cells (Figure 3.5D). Key canonical microglial genes such as *C1QA*, *GAS6*, *GPR34*, *PROS1*, *MERTK*, *TREM2* and *SLCO2B1* were strongly expressed, and at comparable levels in both cell types (Figure 3.5E). Surprisingly, the microglial surface proteins *P2RY12* and *CX3CR1* were found to be expressed at low levels (Figure 3.5F), with *CX3CR1* significantly downregulated in the Kolf2 MG vs Macpre ( $\log_2FC = -5.547$  & p-value of  $1.59 \times 10^{-4}$ ) but not in HD109 MG vs Macpre cells ( $\log_2FC = 2.479$  & p-value of 0.113).

Secondly, the transcriptomics data was evaluated for expression of markers of leukocytes and tissue macrophages and comparisons made with expression of sensome genes. Markers for T cells (*CD3*, *CD32*), B cells (*CD19*) and dendritic cells (*CD123*) were not expressed at detectable levels. Other lowly expressed genes included *CD68* (the phagocytic-promoting lysosomal protein highly expressed in monocytes and macrophages), the carrier protein *FABP4* and the serine protease *SERPINB2* (Figure 3.6A). Many recently recognised microglia-specific genes, rather than belonging to a particular biological pathway, are mostly implicated in host

defence and regulation of immune response. Correspondingly, the iPSC-derived MG cells expressed high levels of LGMN (a cysteine protease involved in the MHC II pathway of bacterial peptide processing), SQLE (ER-localised enzyme that catalyses squalene oxidation, a rate-limiting step in sterol biosynthesis), the lysosomal protease cathepsin D and the purinergic receptor P2RX4, highly expressed in the nervous system where it has been implicated in inflammation activation and synaptic strengthening (Baxter et al. 2011; de Rivero Vaccari et al. 2012) (Figure 3.6B). The presence of immune-related transcripts highly expressed in macrophages was nevertheless notable in the Macpre and MG cells, including scavenger receptors (MSR1 and MARCO) and proteins such as TLR8 (endosomal PRR for viral ssRNA - (Cervantes et al. 2012)), IFITM (IFN-induced antiviral proteins that inhibit viral entry into the cytoplasm - (Bailey et al. 2014)) and the chemokine receptor 1 (CCR1), which enables recruitment of effector immune cells to an inflammation site and has been recently identified as enriched in a subpopulation of embryonic microglia (Hammond et al. 2018) (Figure 3.6C). Also expressed by the in vitro MG cells were a host of immune alertness genes, including inhibitory (CD33, CD47, TREM2) and classically activating molecules such as CD163 and TLR2, suggesting that the cells are in an immune vigilant and competent state, capable of reacting to pathogenic stimuli (Figure 3.6C). Several transcription factors and regulators have been identified as part of the core human microglial transcriptome and these were evaluated in the HD109 and Kolf2 stem cell-derived cells (Figure 3.6D). While the cells expressed low mRNA levels of the dendritic cell-associated transcription factor FLT3 (Figure 3.6A), microglia-specific TFs SPI1, IRF8 and MEF2C were found in relatively high levels, along with the inflammatory associated regulators IRF5 and TRIM22 (interferon-induced) (Figure 3.6F). Similarly, the cells showed robust expression of the ubiquitous MHC class I regulator NLRC5 and the MHC class II regulator CIITA (Meissner et al. 2010), stressing the importance of interactions between microglia and other immune cells.

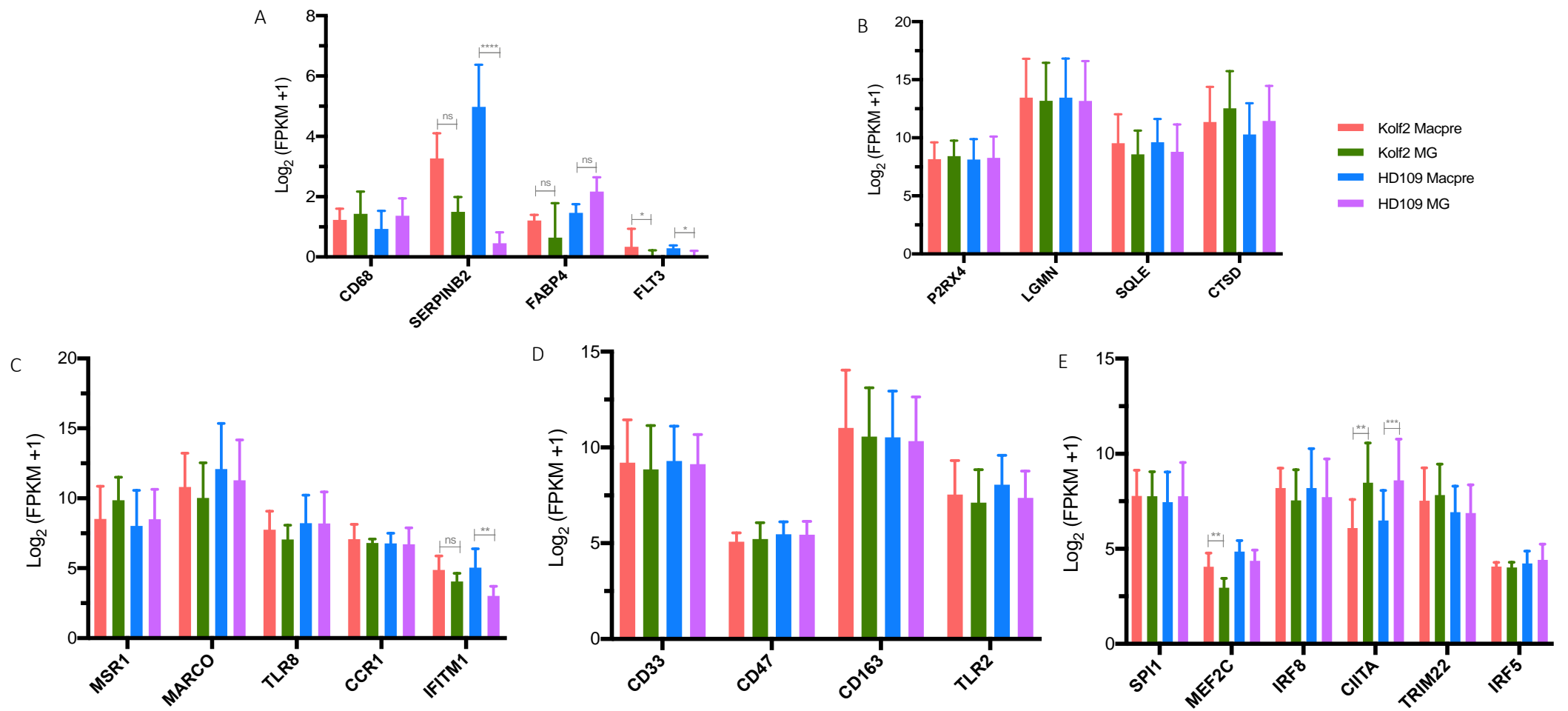


**Figure 3.6 iPSC-derived microglia display low expression levels of leukocyte markers, but high levels of immune alertness genes.**

Expression of markers for T cells (CD3, CD32), B cells (CD19) and dendritic cells (CD123) was undetected in HD109 and Kolf2 samples. **(A)** The macrophage genes CD68, SERPINB2 and FABP4 were expressed at low levels in Macpre and MG cells, along with the dendritic cell TF FLT3. **(B)** Newly identified MG-enriched genes P2RX4, LGMN, SQLE and CTSD were expressed at comparable levels in the MG and Macpre samples from both Kolf2 and HD109 cells. **(C -D)** In vitro macrophage precursors and microglia express high levels of macrophage-associated scavenger receptors (MSR1, MARCO), TLR proteins (TLR2, TLR8), viral entry IFITM proteins and immune alertness proteins (CCR1, CD33, CD47, CD163). **(E)** iPSC-derived macrophage precursors and microglia cells express several microglia-specific transcription factors such as SPI1, MEF2C, IRF8 and TRIM22. MG cells express higher levels of MHC II transcription regulator CIITA.

Expression levels are represented as log<sub>2</sub> transformed FPKM counts. Data analysed by DESeq2 and Benjamini-Hochberg multiple correction procedure used to compute adjusted p-values. Asterisks denote statistical significance: \* < 0.05, \*\* < 0.01, \*\*\* < 0.001, ns – not significant. n=3 independent differentiations.

In the final step of analysis, the microglia sensome list described above was employed to run a microglial signature enrichment analysis via Gene Set Enrichment Analysis (GSEA), in order to find out how the Kolf2 and HD109 iPSC-derived microglia compared to other brain cell types, namely brain myeloid cells, neurons and astrocytes. With the sensome gene list as the gene set of interest, GSEA was carried out using Fisher’s exact test, to determine whether the sensome gene set was significantly enriched in the MG samples compared to primary brain cell type samples. Due to lack of availability and failure to acquire good quality primary tissues, publicly available datasets were used. Direct transcriptomic comparisons to primary samples and microglia derived from recently published differentiation protocols (Muffat et al. 2016; Abud et al. 2017) were intended but not undertaken given differences in cell culture conditions and sequencing platforms – any potential gene expression changes may have reflected all those factors, as much as variations according to cell types.

Instead, the enrichment analysis described here below was carried out by identifying commonly DE genes in the iPSC-derived microglia cells when compared to human cortical neurons, astrocytes and myeloid cells from the (Zhang et al. 2016) dataset, chosen as the sequencing platform used by the authors closely matched our own. Enrichment analysis for the microglia sensome gene set by Fisher’s exact test was calculated, with the results shown in Table 3.1. In sum, both HD109 and Kolf2 iPSC-derived microglia were significantly enriched for microglia-specific genes, relative to neurons, astrocytes and cortex myeloid cells.

	Kolf2 iPSC-microglia		HD109 iPSC-derived microglia	
Comparison	Odds ratio	p-value	Odds ratio	p-value
MG vs cortex neurons	2.79	$1.57 \times 10^{-10}$	2.84	$5.4 \times 10^{-11}$
MG vs cortex astrocytes	5.47	$2.66 \times 10^{-23}$	5.54	$3.8 \times 10^{-24}$
MG vs cortex myeloid cells	3.51	$2.18 \times 10^{-15}$	4.04	$3.08 \times 10^{-18}$

**Table 3.1 Enrichment analysis of microglia sensome genes in iPSC-derived microglia.** Dataset used for this analysis was the gene list generated by comparative analysis of iPSC-derived microglia against primary neurons, astrocytes and myeloid cells.

The expression of several MG markers was further validated by Fluidigm qRT-PCR, with differential gene expression analysis carried out using the R package “Singular Analysis Toolset” (see section 2.7.1). Gene expression values are represented as  $\log_2$  expression normalised to the reference genes GAPDH,  $\beta$ -actin, SDHA, HPRT1, UBC and HMBS. Compared to THP-1 monocytes, ANOVA comparisons showed that the iPSC-derived microglia significantly expressed higher levels of CABLES1 ( $p < 0.01$ ) and TMEM119 ( $p < 0.05$ ), as well as GPR34 and C1QA (both at  $p < 0.01$ ). Transcript levels were comparable between macrophage precursor and microglia samples, confirming RNA-seq data (Figure 3.7 A-B). Equally, the expression of these genes did not vary significantly across the two genetic backgrounds of Kolf2 and HD109. However, CX3CR1 was significantly downregulated in the MG samples compared to THP-1 ( $p < 0.05$ ) and Macpre samples. Moreover, P2RY12 and MERTK expression was lower in THP-1 ( $p < 0.01$ ) but higher in precursor macrophages and microglia cells (Figure 3.7C). The family of sialic acid-binding immunoglobulin-like lectins or SIGLECs is made up of cell surface receptors that have important homeostatic functions in microglia, in particular immunosuppression and neuroprotection. They have been shown mediate a number of processes including activation, phagocytosis and inflammasome formation through cytoplasmic Immunoreceptor Tyrosine-based Inhibitory or Activation Motif or ITIM/ITAM domains (MacAuley et al. 2014). Examples include CD33, the neuroprotective SIGLEC11 and SIGLEC12, as well as the AD risk gene TREM2, which is associated with the ITAM TYROBP, which recruits and phosphorylates the tyrosine kinase SYK to activate cellular responses such as phagocytosis (Takahashi et al. 2005). As shown in Figure 3.7D, macrophage precursor and microglia samples from both cell lines expressed similarly high levels of TREM2, SYK and TYROBP, while mRNA levels of the neuroprotective SIGLEC12 were lower in comparison.

RNA-seq analysis for the enrichment of Alzheimer’s disease-associated risk genes showed that the majority of these genes were comparably expressed in the Kolf2 microglia and their precursor cells (Figure 3.8A). This observation was confirmed using qPCR, with results showing that the Macpre and MG express risk genes such as PLCG2, CR1, CD33, INPP5D and CD2AP at levels comparable with THP-1 monocytes, with only APOE being significantly upregulated in the in vitro derived cells at  $p < 0.001$  (Figure

3.8 B-C). This confirms that iPSC-derived microglia can be used to study the influence of these genes on microglia function and AD risk in vitro.

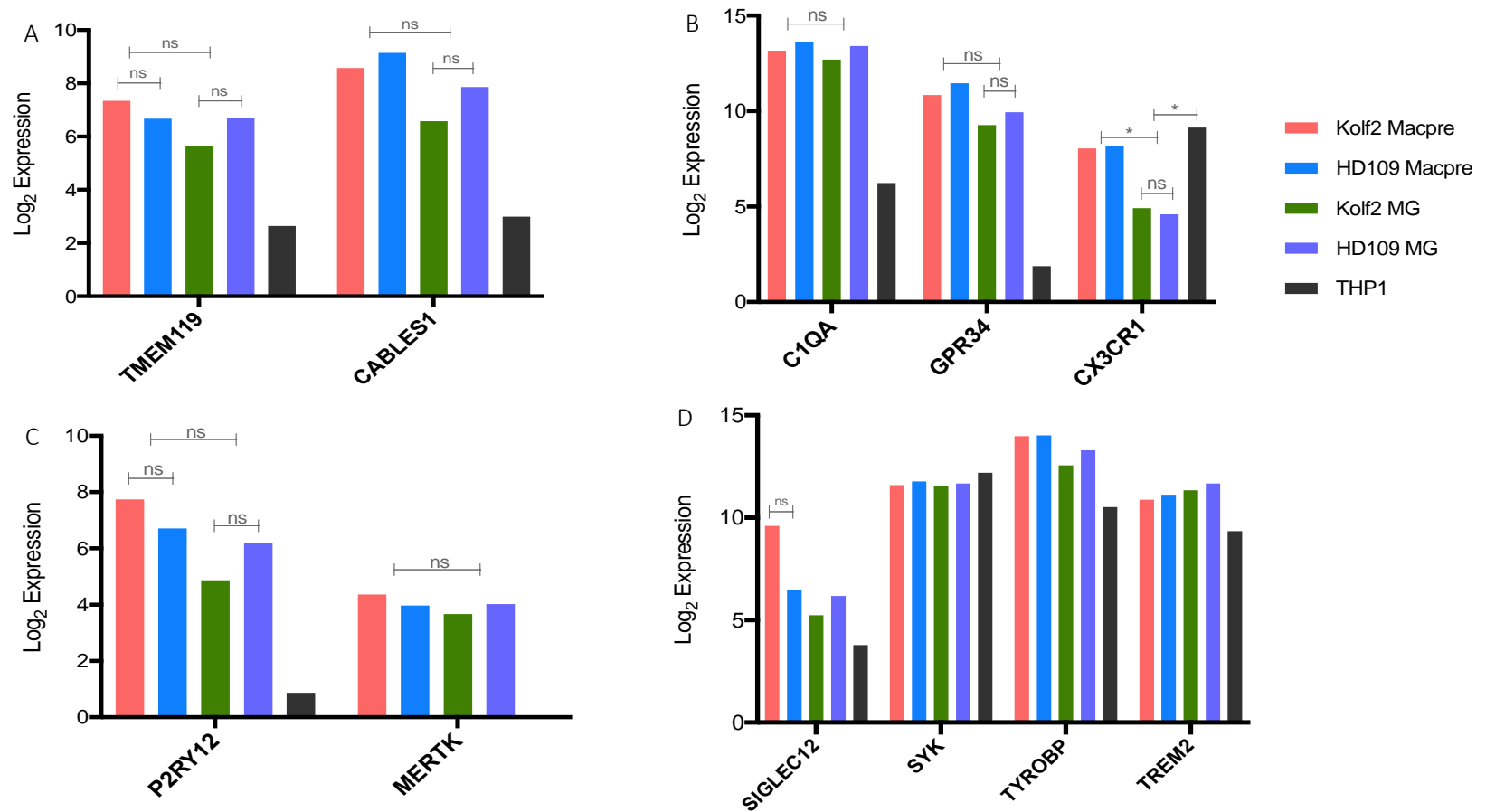


**Figure 3.7 Validation of expression of canonical microglia genes in iPSC-derived microglia by Fluidigm qRT-PCR.**

Kolf2 and HD109 MG were differentiated for 14 days in IL-34 and GM-CSF and all samples assayed by Fluidigm qRT-PCR. Ct values generated by the Fluidigm BioMark qPCR software were analysed using the R package “fluidigmSC” to gene expression values, represented here as mean Log<sub>2</sub> Expression. Log<sub>2</sub> Expression was normalised, during analysis, to reference genes GAPDH, β-actin, SDHA, HPRT1, UBS and HMBS. **(A)** TMEM119 and CABLES1 are upregulated in Macpre and MG samples compared to THP1, while levels are comparable between HD109 and Kolf2 Macpre and MG samples. **(B)** iPSC-derived Macpre and MG cells express significantly higher levels of C1QA and GPR34 than THP1 monocytes. CX3CR1 is downregulated in the MG samples (Kolf2 & HD109) compared to THP1 and Macpre cells. **(C)** Expression P2RY12 and MERTK is significantly upregulated in macrophage precursors and microglia compared THP1. Levels between HD109 and Kolf2 cells did not vary significantly. **(D)** Macpre and MG cells express members of the SIGLEC family such as SIGLEC12, CD33 and TREM2 and their associated receptors.

Statistical analysis used two-way ANOVA with Tukey’s multiple comparisons test. Asterisks denote statistical significance: \* < 0.05, ns – not significant. n=3 biological replicates for all samples, except THP1 (n=2).

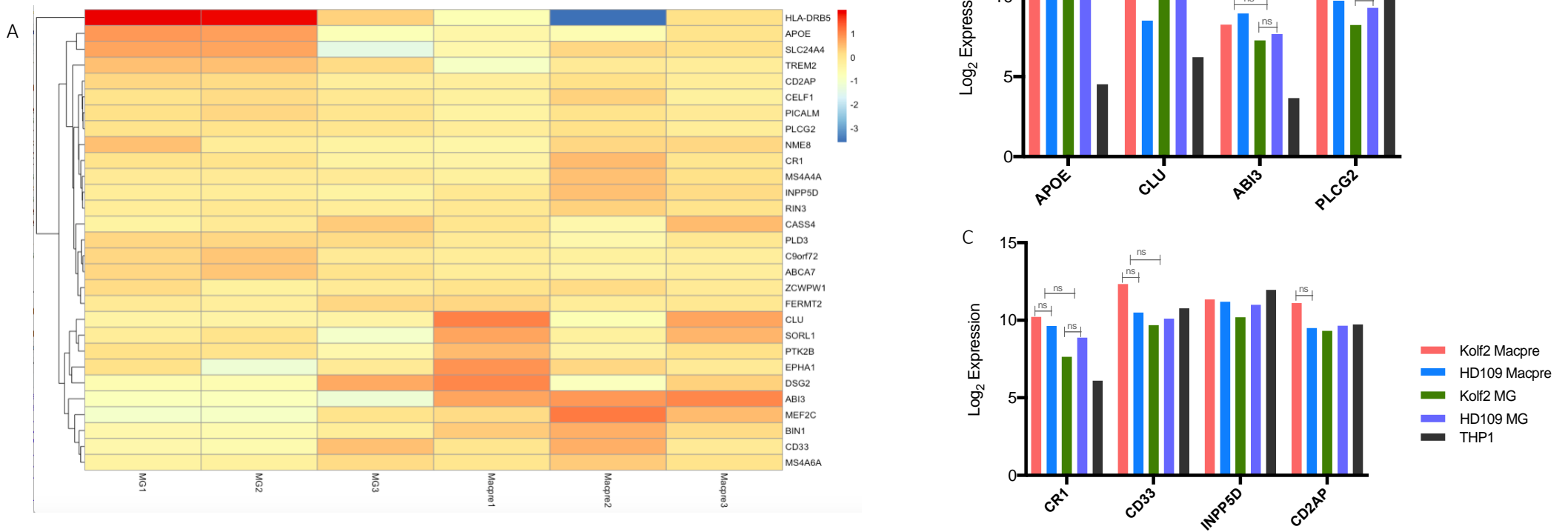


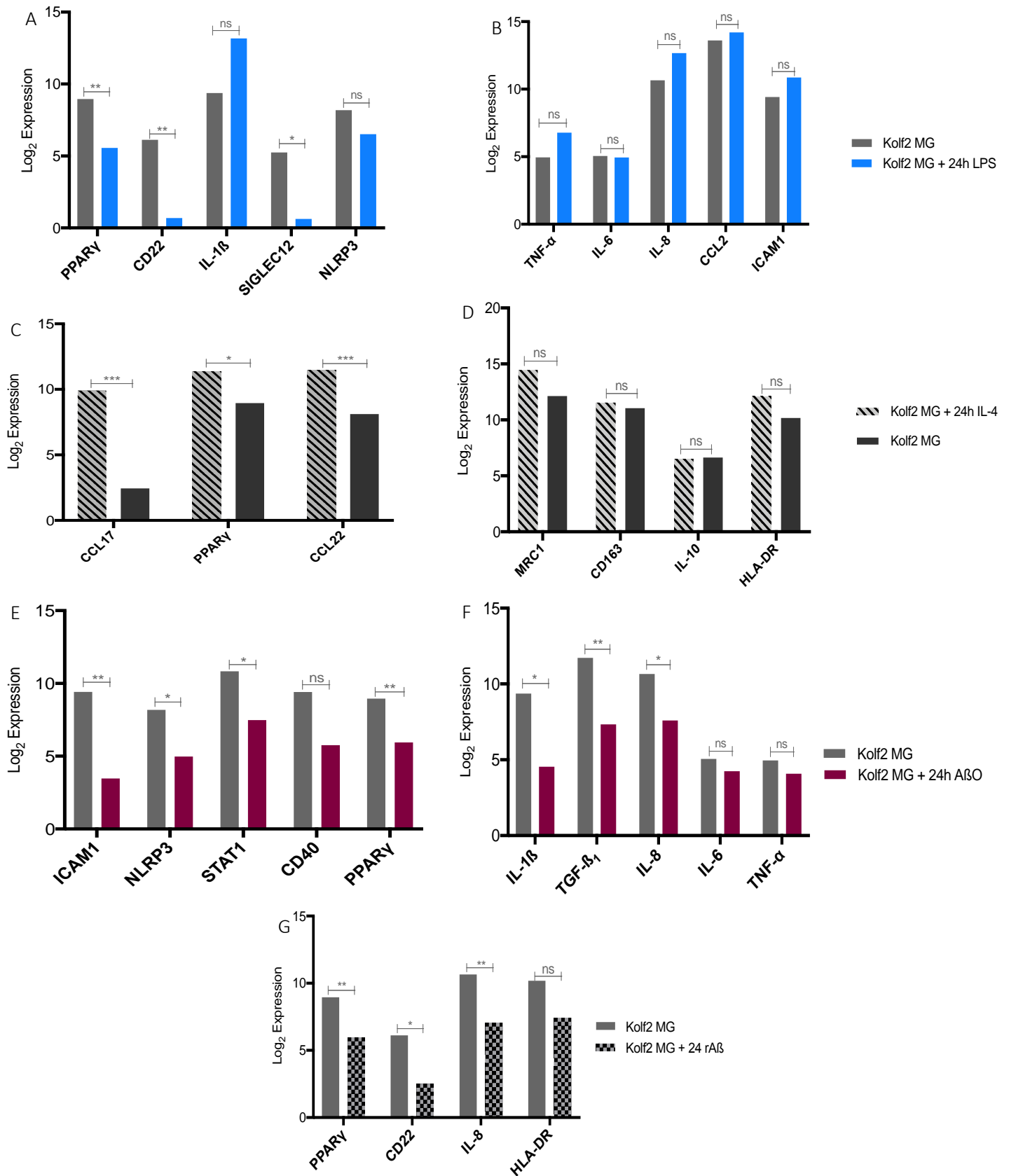
**Figure 3.8 iPSC-derived microglia express Alzheimer's disease risk genes.**

**(A)** Heatmap of 29 genes with variants associated with late onset Alzheimer's disease showed that the Kolf2 Macpre and MG express several immune genes at similar levels. Heatmap and hierarchical clustering based on normalised gene expression counts from RNA-seq data. Data plotted using R function "pheatmap". **(B)** Validation of APOE, CLU, ABI3 and PLCG2 expression in HD109 and Kolf2 Macpre and MG cells by Fluidigm qRT-PCR. Changes in expression did not show a significant difference between Macpre and MG cells. APOE is upregulated in Macpre and MG cells compared to THP1 ( $p < 0.001$ ). **(C)** Levels of CR1, CD33, INPP5D and CD2AP in microglia are comparable to expression in THP1 monocytes. Log<sub>2</sub> Expression normalised to reference genes. Statistical analysis used two-way ANOVA with Tukey's multiple comparisons test. Asterisks denote statistical significance: \*  $< 0.05$ , \*\*  $< 0.01$ , \*\*\*  $< 0.001$ , ns – not significant.  $n=3$  biological replicates for all samples, except THP1 ( $n=2$ ).

### 3.2.3 Functional analysis and validation of Kolf2 iPSC-derived microglia

Microglial activation is mediated by a complex interaction of cellular signals, metabolism and their surrounding microenvironment. They can therefore assume diverse phenotypes. Stimulation by LPS results in an M1 phenotype and is associated with expression of pro-inflammatory cytokines. Conversely, microglia can be stimulated by IL-4 to an M2 phenotype, for resolution of inflammation and tissue repair (Biswas & Mantovani 2012). Though this dichotomous nomenclature doesn't faithfully represent the spectrum of microglial polarisation states and phenotypes, it remains a useful tool for in vitro assays (see section 1.2.5). Thus, in order to functionally validate the capacity of iPSC-derived microglia to show both M1 and M2 polarisation states, the inflammatory response of Kolf2 cells under stimulation with LPS and IL-4 was investigated. 14-day-differentiated cells were incubated with 1 µg/ml LPS or 50ng/ml IL-4 for 24 hours.

LPS-activated gene expression is mediated through TLR4 signalling and involves the activation of several pathways including NFκB and STAT1, which induce the release of pro-inflammatory cytokines and chemokines such as IL-1β, TNF-α, IL-6 and CCL2. qPCR results revealed that LPS increased expression of IL-1β (though this didn't reach significance at  $p = 0.058$ ), while reducing mRNA levels of the neuroprotective molecules CD22 and SIGLEC12 (Figure 3.9A). The nuclear receptor PPARγ plays a critical immune role by inhibiting pro-inflammatory gene expression and promoting anti-inflammatory processes (Clark 2002). Interestingly, PPARγ expression was, after CD22, the most significantly downregulated gene post LPS incubation (Figure 3.9A). In addition, LPS treatment did not appreciably alter transcript levels of pro-inflammatory markers such as IL-6, TNF-α, CCL2 and IL-8 (Figure 3.9B), which suggests a diminishing immune response after 24 hours of exposure to LPS.



1  $\mu\text{M}$  oligomeric  $\text{A}\beta_{1-42}$  resulted in significant downregulation of both pro- (ICAM1, NLRP3, STAT1, IL-1 $\beta$ , IL-8) and anti-inflammatory genes (TGF- $\beta_1$ , PPAR $\gamma$ ). (G) Incubation with 1  $\mu\text{M}$  r $\text{A}\beta_{42-1}$  for 24 hours resulted in lower expression of PPAR $\gamma$ , CD22 and IL-8. No differences were found in the expression of other inflammatory genes.

Log<sub>2</sub> Expression normalised to reference genes. Statistical analysis used one-way ANOVA with Dunnett's post hoc comparison. Asterisks denote statistical significance: \* < 0.05, \*\* < 0.01, \*\*\* < 0.001, ns – not significant. n=3 biological replicates for all samples, except for Kolf2 MG 24h LPS (n=2).

Binding of IL-4 to the IL-4 receptor initiates a signalling cascade through the transcription factor STAT6 that polarises cells towards an anti-inflammatory phenotype typified by increased expression of classical M2 markers such as MRC1, IL-10 and PPAR $\gamma$  (Martinez & Gordon 2014). Stimulation of Kolf2 cells with 50 ng/ml IL-4 resulted in upregulation of CCL17, CCL22 and PPAR $\gamma$ , while mRNA levels of the M2 markers CD163, IL-10, MRC1 and HLA-DR were not significantly induced (Figure 3.9 C-D).

Microglia are also activated upon exposure to abnormal protein aggregates, releasing cytokines and other inflammatory mediators to induce a cascade of pathways and mechanisms thought to contribute to neuronal death (Block et al. 2007). In order to measure the microglial inflammatory response to  $\text{A}\beta$ , Kolf2 iPSC-derived microglia were stimulated with 1  $\mu\text{M}$  of  $\text{A}\beta$  oligomers ( $\text{A}\beta\text{O}$ ) for 24 hours. This resulted in gene expression changes characterised by downregulation of activation molecules such as ICAM1, the NLRP3 inflammasome, the interferon regulator STAT1, CD40 (expressed on professional antigen presenting cells) and PPAR $\gamma$  (Figure 3.9E). The pro-inflammatory cytokines IL-1 $\beta$  and IL-8 were also downregulated, while other M1 markers such as CCL2, IL-6 and TNF- $\alpha$  were unchanged (Figure 3.9F). In contrast, the anti-inflammatory TGF- $\beta_1$  was significantly reduced ( $p < 0.0042$ ). As a negative control, the cells were stimulated with 1 $\mu\text{M}$  r $\text{A}\beta_{42-1}$  for 24 hours, which resulted in PPAR $\gamma$ , CD22 and IL-8 downregulation (Figure 3.9G). Otherwise, the r $\text{A}\beta$  response closely matched the unstimulated samples.

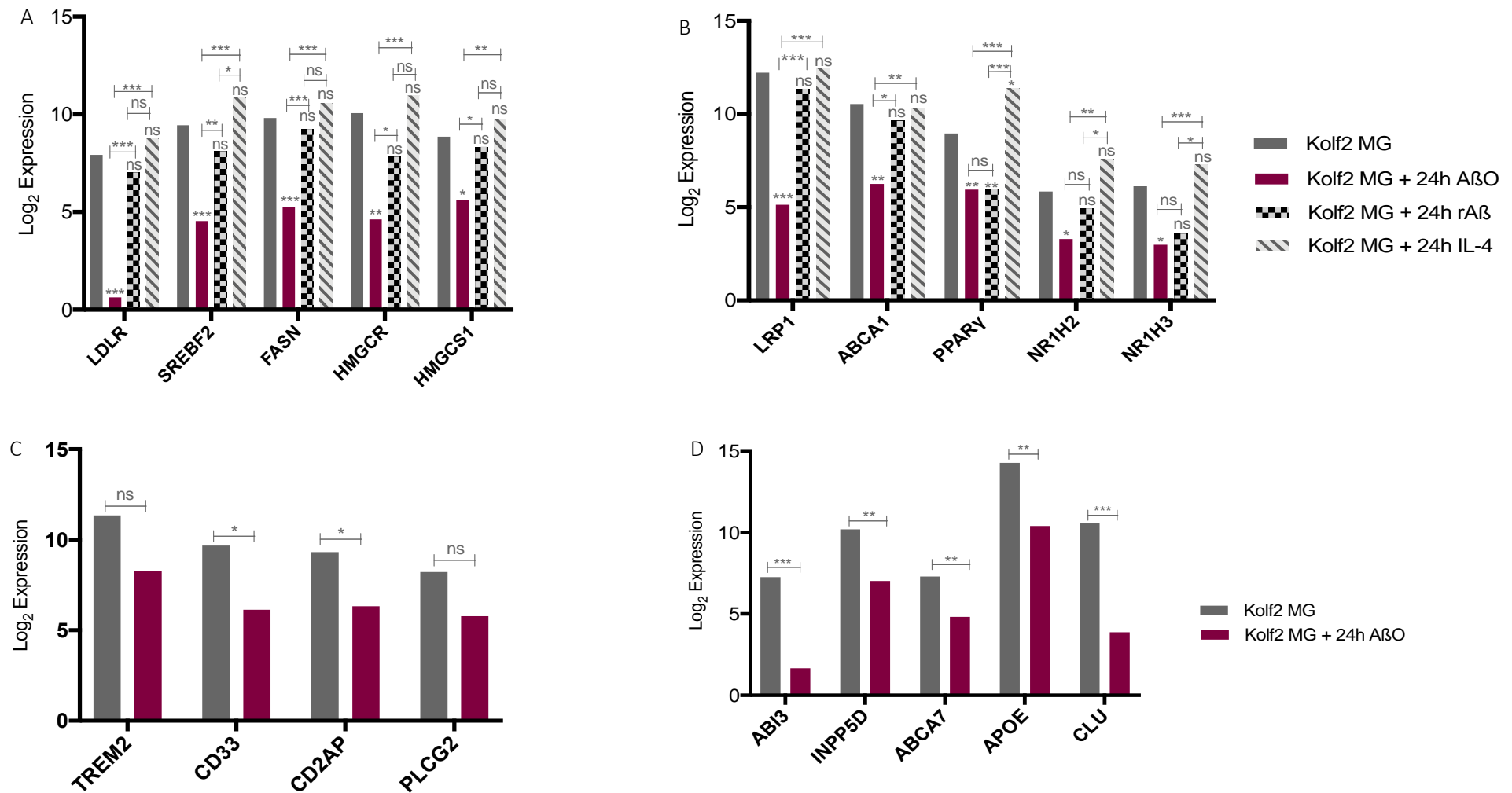
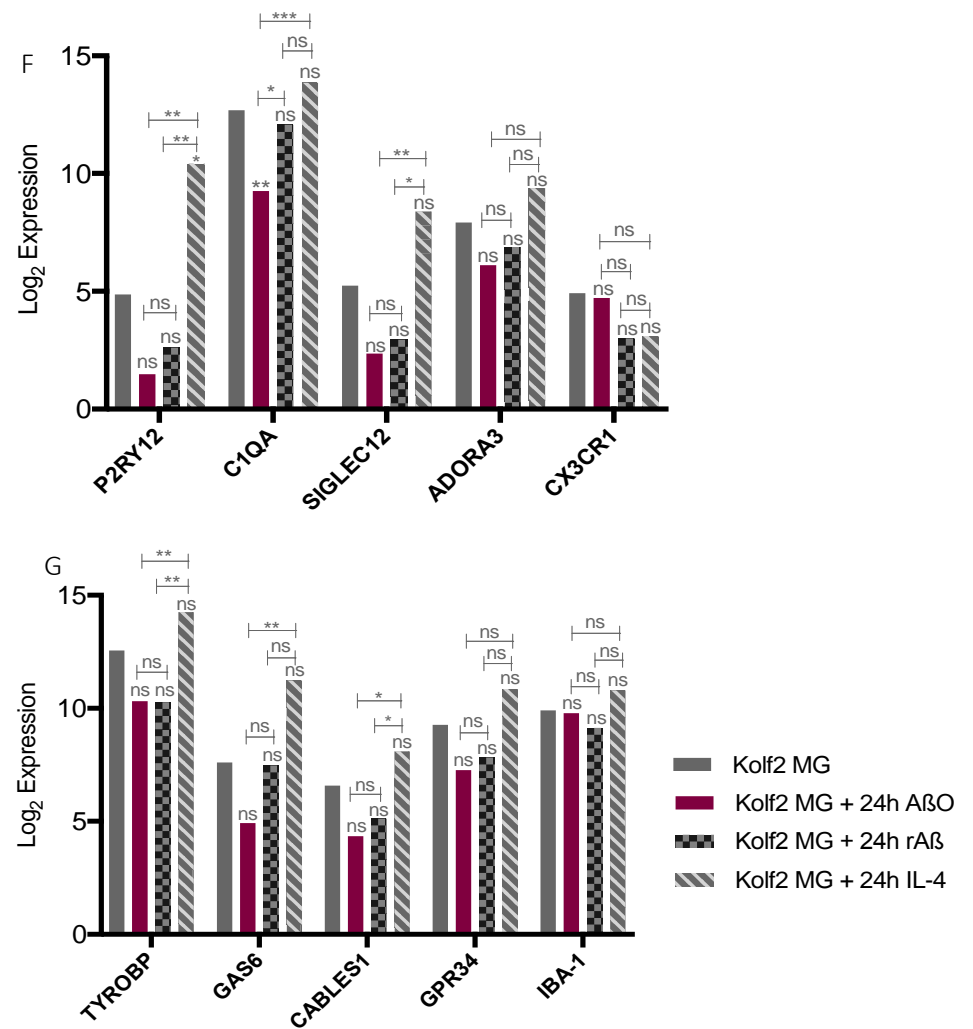
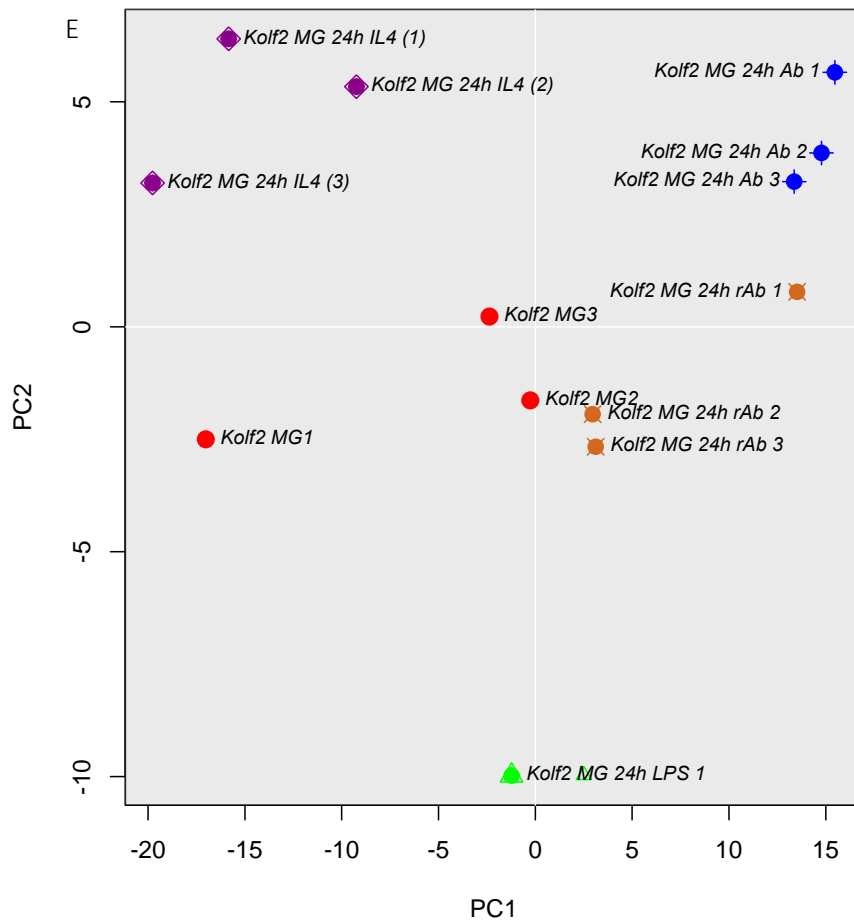


**Figure 3.10 The in vitro microglial response to oligomeric A $\beta$  is distinct from M1 and M2 polarisation states.**

**(A)** 24-hour incubation of Kolf2 iPSC-derived MG cells with 1  $\mu$ M A $\beta$ <sub>1-42</sub> oligomers resulted in significantly decreased expression of lipid synthesis genes. **(B)** Expression of cholesterol metabolism regulator ABCA1, which stimulates anti-inflammatory signalling through the PPAR $\gamma$ -LXR pathway (NR1H2 and NR1H3), was significantly downregulated, along with the A $\beta$  receptor LRP1. **(C-D)** In A $\beta$ O-treated MG cells, levels of AD CD33, CD2AP, ABI3, APOE, CLU, INPP5D and ABCA7 were significantly decreased.



(E) PCA analysis revealed that AβO-treated MG cells clustered away from LPS-treated cells. Additionally, they segregated with IL-4 treated Kolf2 MG cells, despite significant differences in expression of lipid and cholesterol metabolism genes (F-G) Treatment of MG cells with Aβ oligomers did not induce statistically significant differences in expression of canonical microglial genes, except for the downregulation of the phagocytosis-associated C1QA.

Log<sub>2</sub> Expression normalised to reference genes. Statistical analysis used two-way ANOVA with Tukey's multiple comparisons test. Asterisks denote statistical significance: \* < 0.05, \*\* < 0.01, \*\*\* < 0.001, ns – not significant. n=3 biological replicates for all samples, except for Kolf2 MG 24h LPS (n=2).

Notably, the ANOVA results highlighted significant decreases in the expression of several genes involved in lipid and cholesterol metabolism, including fatty acid synthase (FASN), HMG-CoA reductase, HMG-CoA synthase 1 and the sterol response element binding factor 2 (SREBF2); these genes not only help regulate intracellular cholesterol and are also associated with phagocytosis (Iwamoto et al. 2006). Correspondingly, levels of the multifunctional receptor LRP1, which acts as a phagocytic receptor for A $\beta$  oligomers, were similarly reduced following A $\beta$ O stimulation (Figure 3.10 A-B). The toxic effects of oligomeric A $\beta$  also influenced the expression of several AD risk genes, by downregulating CD2AP ( $p= 0.013$ ), CD33 ( $p= 0.039$ ) and more prominently ABI3, INPP5D, ABCA7, APOE, CLU and PICALM (Figure 3.10 C-D). Differences in PICALM, TREM2 and PLCG2 expression levels did not reach significance. This pattern of gene expression was found to diverge from the pro-inflammatory LPS Kolf2 microglial response, as shown by the clear segregation of the LPS-treated samples on the PCA plot, generated by using a dataset comprising inflammatory, cholesterol metabolism, sensome and AD risk genes (Figure 3.10E). Moreover, oligomeric A $\beta$  treatment impacted on expression of the MG-specific C1QA, though expression differences in CX3CR1, P2RY12 and SIGLEC12 did not reach statistical significance (Figure 3.10F). Other sensome genes including the purinergic receptor ADORA3, GPR34, TYROBP and IBA1 were not significantly altered following A $\beta$  treatment (Figure 3.10G). However, when compared with mRNA levels of IL-4 treated Kolf2 microglia cells, expression of several sensome genes were found to be significantly altered. Overall, the 24h A $\beta$ O-treated samples seemed to segregate away from the IL-4 and LPS-stimulated samples, which suggests that the microglial oligomeric A $\beta$  response differs significantly from the established M1 and M2 in vitro paradigm.

### 3.3 Summary and Discussion

The work highlighted in this chapter set out to investigate the efficacy and reproducibility of the microglia differentiation protocol described in section 2.3. The resulting iPSC-derived microglia cells displayed robust expression of microglial markers by immunocytochemistry and were enriched for several microglia-exclusive transcripts such as GAS6, C1QA, GPR34 and the recently identified immune alertness gene CCR1. RNA sequencing was then used to analyse the transcriptome of the in vitro derived cells to establish a microglial signature.

This protocol for in vitro microglial differentiation mimics development in the embryo, giving rise to a population of monocyte-like primitive macrophage precursor cells (van Wilgenburg et al. 2013). The myeloid phenotype of these cells was validated by FACS and immunostaining to confirm an expression profile of myeloid markers comparable across two cell lines of different genetic background – a wild-type Klf2 and a Huntington's disease iPSC line with a 109 CAG repeat expansion in the HTT gene (HD iPSC Consortium 2012). Recent work has elucidated the developmental origin of these in vitro microglia precursor cells, demonstrating that they are derived from a RUNX1- and SPI1-dependent lineage distinct from MYB-dependent monocytes and macrophages (Buchrieser et al. 2017). This makes them closer developmentally to yolk-sac-derived precursors of microglia (Ginhoux et al. 2010) and is in accordance with the latest findings from fate mapping mouse studies (Mass et al. 2016).

Transcriptomic analysis by RNA sequencing confirmed this close similarity between macrophage precursors and IL-34 and GM-CSF-treated microglia cells. Several genes identified as exclusive to microglia were expressed at comparable levels in the macrophage precursor cells (Figure 3.5). Furthermore, gene set enrichment analysis was used to highlight a microglial signature enrichment when the MG cells were compared to other brain cell types (see Table 3.1). Nonetheless, this signature reflected the monoculture nature of the in vitro cells and featured low expression of CX3CR1, P2RY12 and other genes involved in the homeostatic and surveillance functions of microglia (Figure 3.5). In vitro work by Abud et al. 2017 built on in vivo mouse studies data by Butovsky et al., 2014 to show that TGF- $\beta$  removal from the microglia differentiating medium strongly influences the microglial transcriptome, reducing expression of key markers such as P2RY12, CX3CR1 and TGF $\beta$ R1. Interestingly, lack of TGF- $\beta$  also downregulated expression of several key AD-associated genes such as APOE, CD33 and BIN1. (Bennett et al. 2018) recently demonstrated that microglial identity is induced by brain signalling, emphasising that microglia are highly sensitive to their environment and require brain signals to sustain homeostatic gene expression. The authors used a transplantation system to assess the survival of various macrophage populations in the microglia-deficient mouse brain and crucially found that, though tissue macrophages were able to survive and express some characteristic microglial genes, only yolk-sac derived cells were able to fully attain microglial identity – emphasising the crucial role of ontogeny on correct microglial identity. Similarly, it has been shown that though peripheral macrophages

can engraft into the brain, they maintain a unique transcriptional identity divergent to that of microglia (Cronk et al. 2018).

No significant differences in the microglial signature of Kolf2 and HD109 microglia cells were detected using gene set enrichment analysis, with transcript levels of canonical genes expressed comparably between the two cell lines, with a few exceptions (Figures 3.3 & 3.4). Fluidigm qPCR validation likewise found a similar pattern of sense gene expression in the IL-34 induced microglia from both cell lines (Figure 3.6), which strongly indicates that the expanded CAG track in the HTT gene has no discernible effect on the intrinsic microglia sense. Nonetheless, the variability in the genetic background of the cell lines was reflected in the number of differentially expressed (DE) genes in the iPSC-derived microglia samples, when compared to their respective macrophage precursors samples. Treatment of the precursor cells resulted in the upregulation of 374 DE genes in the Kolf2 microglia, compared to 240 genes in the HD109 cells. Similarly, a greater number of genes were significantly downregulated in the Kolf2 (561) than in the HD109 microglia (365). This could be attributed to a Huntington's disease effect, whereby the HD109 microglia are developmentally delayed in a fashion mirroring the developmental delay in HD iPSC-derived neural stem cells (Mattis & Svendsen 2017). However, given the presence of an intact microglial signature in the HD109 cells, this discrepancy is most likely an artefact of the in vitro differentiation process.

Microglia are capable of adopting various phenotypes. To test the functionality of the in vitro derived microglia-like cells, Kolf2 cells were activated with LPS and IL-4, which induce polarisation to an M1 and M2 phenotype respectively. LPS challenge for 24 hours was able to induce an M1 phenotype, though the characteristically increased expression of several pro-inflammatory markers did not reach statistical significance. This result suggests that the microglial response to LPS diminishes over time and hints at a different M1 polarisation phenotype in microglia compared to macrophages, underlining the distinct nature of the microglial phenotype. Polarisation to an M2 phenotype using IL-4 was also attempted and results showed no alterations in the expression of M2 markers, including the mannose receptor MRC1, CD163 as well as HLA-DR and IL-10. Intriguingly, the anti-inflammatory nuclear receptor PPAR $\gamma$  was upregulated, along with the chemokines CCL17 and CCL22. Again, this pattern of gene expression contrasts with expected changes after IL-4 induction in

macrophages, though these results compare favourably with reports of decreased sensitivity to M2 polarisation in human microglia (Durafour et al. 2012).

Previous studies carried out within our lab have shown that stimulation with monomeric A $\beta$  gives rise to a pro-inflammatory response (Emma Cope thesis, 2014). Post treatment with oligomeric A $\beta$ , Kolf2 microglia segregated away from LPS and IL-4-treated cells, proving that the A $\beta$ O-stimulated phenotype differs from M1 and M2 polarised activation phenotype of microglia. Characterised by reduced expression of both pro- and anti-inflammatory genes, this inflammatory phenotype also featured the marked downregulation of several AD risk genes. These results particularly provide strong evidence linking the microglial response to amyloid  $\beta$  to lipid and cholesterol metabolism, highlighting the PPAR $\gamma$ -LXR axis as an important player in the regulation of A $\beta$ -mediated inflammation. Induction of the anti-inflammatory PPAR $\gamma$  and LXR pathways in mouse macrophages is promoted by LRP1 signalling, which also inhibits pro-inflammation (Zurhove et al. 2008; May et al. 2013). In microglia, LRP1 downregulation results in increased production of pro-inflammatory cytokines through the JNK and NF $\kappa$ B pathways (Yang et al. 2016). Conversely, activation of LRP1 signalling in response to inflammation induces transcription of ABCA1, which regulates cellular cholesterol export and the formation of lipid rafts (Xian et al. 2017). The findings that stimulation of *in vitro* microglia with oligomeric A $\beta$  aggregates affect LRP1 levels and cholesterol metabolism reinforce the notion that cellular cholesterol homeostasis plays a crucial role in the inflammatory responses of microglia. One caveat to this approach is the fact that this is an acute model of oligomeric A $\beta$  toxicity, with 1 $\mu$ M A $\beta$ O concentration used in the experiments. This method has been shown to lead to increased neuronal death in a recent study comparing the toxicity of nanomolar and micromolar A $\beta$  concentrations to iPSC-derived neurons (Berry et al. 2018). Dahlgren and colleagues also previously showed that oligomeric A $\beta_{42}$  inhibit neural viability significantly more than unaggregated peptides and fibrils at nanomolar concentrations (Dahlgren et al. 2002). Therefore, future experiments should focus on investigating the effects of more physiological concentrations on the microglial phenotype, with particular attention to expression of AD risk genes, immune response and cholesterol metabolism genes.

Not many studies of stem cell microglia have focused on elucidating the gene expression changes associated with in vitro A $\beta$  challenge. There is a rationale for carrying out such experiments, as a way to study the impact of A $\beta$  on specific pathogenic pathways. Abud et al 2017 demonstrated this when they stimulated their iPSC microglia with fibrillar A $\beta$  to show that AD risk genes such as ABCA7, APOE, CLU, TREM2 and TYROBP were upregulated by the treatment. Equally, the focus of many ongoing studies will be to reveal how iPSC-derived microglia interact with AD pathology in vivo, by using humanised tau and amyloid mouse models. This exciting avenue of research is set to greatly advance the AD neuroinflammation field, and answer pertinent questions, for example regarding the role of microglia in tau propagation in AD (Asai et al. 2015; Maphis et al. 2015). Moreover, transplantation of stem cell microglia into AD mouse models will allow to investigate the influence of microglia-enriched risk genes and specific disease-associated mutations on pathology in vivo.

# 4. CHARACTERISATION OF THE CELL-AUTONOMOUS EFFECTS OF THE HTT GENE CAG EXPANSION ON IPSC-DERIVED MICROGLIA

## 4.1 Introduction

Immune activation in the central nervous system, primarily driven by microglia, is a major feature of Huntington's disease. Inflammation caused by a gain of toxicity of mutant HTT represents an important mechanism in HD pathogenesis (Ellrichmann et al. 2013), with current evidence suggesting that efficacy of immune system function may act as a disease modifier (Crotti & Glass 2015).

Though generally associated with neuroprotection, microglia in HD acquire an inflammatory phenotype, resulting in elevated levels of pro-inflammatory cytokines in the brains of HD patients and in several mouse models (Dalrymple et al. 2007; Silvestroni et al. 2009). Moreover, when stimulated with lipopolysaccharide (a component of the bacterial cell wall), HD immune cells cultured *ex vivo* exhibit an exaggerated immune response, secreting higher levels of pro-inflammatory cytokines (Björkqvist et al. 2008; Trager et al. 2015). Expression of mutant HTT seems key to this pathogenic phenotype. Indeed, Crotti et al. 2014 showed that mHTT-expressing microglia in R6/2 and Q175 knock-in mice (Menalled et al. 2012) are primed for an enhanced immune response through increased basal expression of pro-inflammatory and neurotoxic genes that potentiate neuronal death (Crotti et al. 2014). In particular, mHTT expression increased expression and transcriptional activity of the transcription factor PU.1, leading to higher expression of PU.1-C/EBP target pro-inflammatory genes such as *Il6*, *Irf1*, *Tnf* and *Tlr2*. The same study also found corresponding higher

expression of SPI1 (PU.1), TLR2, IL6 and IRF1 in the striatum of post-mortem HD brains in comparisons with matched controls. Elsewhere, mutant HTT has also been detected in monocytes and macrophages using time-resolved FRET, where levels tracked disease burden (Weiss et al. 2012).

The hyper-reactivity of HD immune cells is also partially mediated through altered intracellular signalling pathways centred around NF $\kappa$ B, a major regulator of inflammatory mediator activation in immune cells. Mutant HTT has been shown to interact with the IKK complex, leading to the phosphorylation and degradation of I $\kappa$ B $\alpha$ . This releases NF $\kappa$ B from cytoplasmic sequestration, allows its nuclear translocation and enhances its activity. Trager and colleagues recently demonstrated the reversibility of this cellular dysfunction by using glucan-encapsulated small interfering RNA particles to lower mHTT levels in primary monocytes and macrophages isolated from patients with HD (Träger et al. 2014). This intervention lowered cytokine production in macrophages and led to transcriptional changes in monocytes. Interestingly, cytokine production was reduced in siRNA-treated WT cells, suggesting that wild-type HTT plays a role in cytokine production.

Wild-type HTT also plays a role in actin remodelling and microtubule dynamics (Cattaneo et al. 2005), processes required for a variety of immune functions including cytokine trafficking and release (Lacy & Stow 2011), and cell migration. Fittingly, HD microglia isolated from YAC128 (yeast artificial chromosome model of human HD gene with 128 CAG repeats) and BACHD (bacterial artificial chromosome of human HD gene with 97 CAG repeats) mice (Slow et al. 2003; Gray et al. 2008) were shown to exhibit impaired migration, while aged BACHD microglia also showed a delayed response to laser-induced injury (Wanda Kwan et al. 2012). This deficit was attributed to mHTT-mediated decreased membrane ruffling and lower levels of the actin-binding protein cofilin, which plays an essential role in the regulation of actin polymerisation and is required for cell migration (Dawe et al. 2003). The same study also reported that monocytes and macrophages isolated from HD patients showed severe impairments in migration, agreeing with findings by Munsie and colleagues that revealed deficits in actin remodelling in patient-derived HD lymphocytes (Munsie et al. 2011). It is also

worth noting that impaired migration has been suggested as an explanation for the absence of infiltration of immune cells into the brain in mouse models and HD patients (Crotti & Glass 2015).

A recent RNA-sequencing study of blood-derived monocytes from HD patients found a significant enrichment in pro-inflammatory pathway activation in the transcriptome of HD monocytes at the basal level (Miller et al. 2016). Functional gene sets associated with innate immunity, cytokine production and inflammatory response, especially genes related to the NF $\kappa$ B pathway, were enriched, adding support to the notion that mHTT primes HD myeloid cells.

## 4.2 Aims

Given the overwhelming amount of evidence for pathogenic abnormalities in HD immune cells from patients as well as mouse models, experiments in this chapter were aimed at characterising the cell-autonomous phenotype of human microglia derived from HD iPSC cell lines containing 109 CAG repeats. Having established correct expression of canonical microglial markers in chapter 3, RNA-sequencing was used here to closely examine the transcriptome of the HD109 iPSC-derived microglia and compare it to Kolf2 WT microglia. Finally, differentiated HD109 microglia were assayed for their inflammatory response to stimulation with LPS to investigate whether the HD cells exhibited the exaggerated immune response characteristic of HD immune cells.

## 4.3 Results

### 4.3.1 Transcriptomic analysis of HD109 iPSC-derived microglia

Gene expression analyses uncovering the transcriptional changes in human HD immune cells have been predominantly carried out in peripheral blood cells (Runne et al. 2007; Mastrokolas et al. 2015). Indeed, while one study has looked at the transcriptome-wide effects associated with mHTT expression in HD patient-derived monocytes (Miller et al. 2016), to date no study has conducted a similar analysis of human microglia in HD. Therefore, in order to dissect any microglial-specific transcriptional changes, microglial cells and their precursors were generated from control Kolf2 and HD109 iPS cells for transcriptomic analysis by RNA sequencing.

Using principal component analysis (PCA), a correlation analysis showing the variance between data, the samples were shown to segregate by cell type, macrophage precursor samples from both cell lines showing orthogonal separation from microglia samples from both cell lines (Figure 4.1A). Analysis on the basis of disease indicated a distinct disease effect between the respective Kolf2 control and HD109 precursor and microglia samples. After processing the RNA sequencing data (see section 2.9), differential gene expression analysis was used to calculate the number of differentially expressed (DE) genes across the different samples. To investigate the possibility of a disease signature common to both HD cell types in comparison with the respective Kolf2 samples, a HD-specific meta-analysis was carried out, identifying 421 genes with significantly altered expression in both HD cell types vs Kolf2 control (Figure 4.1B). These were obtained using a threshold of 0.05 for statistical significance and a log fold change of expression with absolute value of at least 1, corresponding to a 2-fold change in mRNA expression. Of that total, 196 genes were upregulated compared to 223 downregulated genes. The gene lists were then inputted into the functional annotation tool DAVID (Huang et al. 2008) to uncover any enriched biological themes and functionally related gene groups. Among the upregulated genes, gene sets relating to ubiquitin conjugation, mitosis, cell cycle, DNA damage, DNA repair and cell division were found to be enriched. On the other hand, significantly downregulated

gene sets included those associated with cellular organelles such as lysosome, endoplasmic reticulum and Golgi membrane (see Table 4.1 below).

GO term	Fold enrichment	Benjamini corrected p value
Ubiquitin conjugation	2.398	$6.55 \times 10^{-4}$
Mitosis	5.035	$6.91 \times 10^{-3}$
Cell cycle	3.044	$1.1 \times 10^{-2}$
DNA damage	3.747	$3.55 \times 10^{-2}$
DNA repair	4.052	$3.84 \times 10^{-2}$
Cell division	3.400	$4.96 \times 10^{-2}$
Lysosome	4.768	$1.02 \times 10^{-2}$
Endoplasmic reticulum	2.484	$1.12 \times 10^{-2}$
Golgi membrane	2.652	$3.29 \times 10^{-2}$

**Table 4.1 GO terms upregulated (top) and downregulated (bottom) in HD macrophage precursor and microglia cells.**

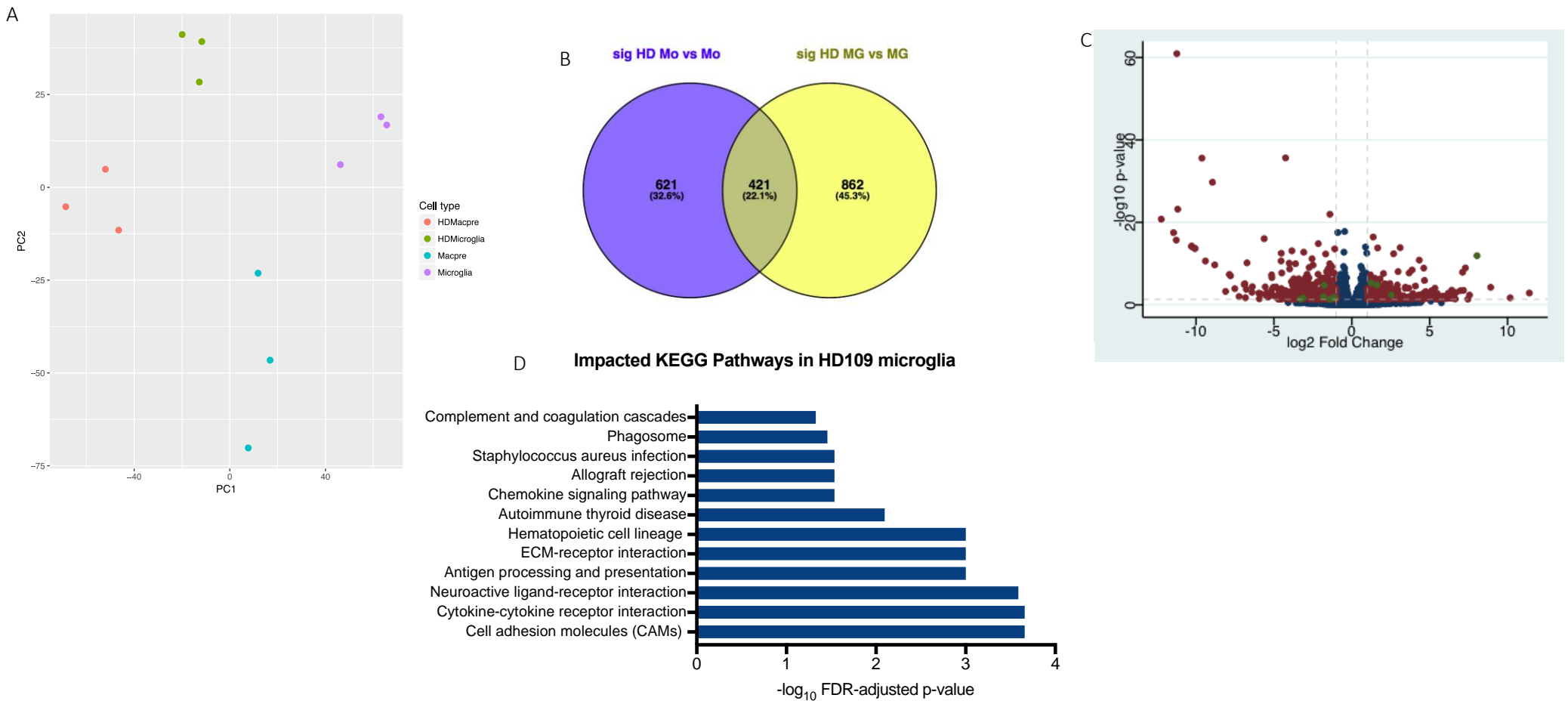


**Figure 4.1 Transcriptomic analysis of HD109 microglia by differential gene expression reveals immune pathways likely to be impacted.**

**(A)** Correlation analysis of Kolf2 and HD109 Macpre and MG cells segregation of the samples by cell type and by genotype, indicating a disease effect. Data presented here is same as in Figure 3.5A. **(B)** Differential gene expression analysis ( $> 2$ -fold,  $p < 0.05$ ) identified a common disease signature in the HD Macpre and MG cells compared to Kolf2 samples. 421 genes were significantly altered in both HD Macpre and MG cells vs their respective Kolf2 WT cells - 196 upregulated and 223 downregulated genes. **(C)** Volcano plot highlighting differential expression of 1114 genes (red dots) in HD109 compared to Kolf2 microglia. X axis shows log<sub>2</sub> fold change and BH corrected p-values shown on Y axis as negative log (base 10) values.  $n=3$  independent differentiations. **(D)** Analysis of KEGG pathways impacted by differential expression in HD109 MG cells was performed by iPathwayGuide Impact analysis package (AdvaitaBio). Top 13 Immune pathways predicted to be affected in HD109 MG include cell adhesion, cytokine-cytokine receptor interaction, antigen processing, chemokine signalling and phagosome.

The next analysis focused on the microglial-specific differences between the transcriptomes of the HD109 and Kolf2 cells. Out of a total of 17039 genes with measured expression, DE analysis of the data identified 1114 DE genes (233 upregulated and 881 downregulated) in HD109 cells compared to Kolf2 control cells (Figure 4.1C). The top 20 genes ranked by p-value correction contained several immune-related transcripts, including BDKRB1, CALR, CD151 (cell adhesion molecule), CTSB, CX3CR1, CXCL1, HLA-A/-B/-H and IL15RA (see appendix 1).

To contextualise the observed transcriptional changes in the HD109 microglia into biological relevance, the iPathwayGuide Impact Analysis package (AdvaitaBio) was utilised, as it incorporates analyses of pathways, biological processes and miRNAs (see section 2.9.4). Following analysis of impacted biological processes, a number of immune system themes and processes were represented, including immune response, response to stimulus, cell migration, chemotaxis and extracellular matrix organisation. Enrichment analysis showed that developmental and cell proliferation processes were also heavily represented outside the top 10 enriched GO terms (see Table 4.2). Table 4.3 shows the corresponding GO molecular functions. Of the enriched molecular functions, membrane receptor binding and activities including cytokine, chemokine and other signalling molecules featured prominently. It is worth noting that redundancy is a feature of these analyses, due to overlapping gene sets.

GO Biological process	DE genes (#/ALL)	FDR-adjusted p value
Immune response	151/1200	7.783 x 10 <sup>-11</sup>
Response to stimulus	531/6428	1.503 x 10 <sup>-8</sup>
Defence response	136/1142	1.503 x 10 <sup>-8</sup>
Cell migration	128/1055	1.592 x 10 <sup>-8</sup>
Chemotaxis	71/458	1.592 x 10 <sup>-8</sup>
Response to external stimulus	173/1602	3.942 x 10 <sup>-8</sup>
Cell communication	417/4835	5.188 x 10 <sup>-8</sup>
Inflammatory response	76/538	1.752 x 10 <sup>-7</sup>
Localisation of the cell	131/1141	1.752 x 10 <sup>-7</sup>
Regulation of cell migration	82/609	2.83 x 10 <sup>-7</sup>

**Table 4.2 Representation of enriched gene sets in differentially expressed genes in HD109 microglia.** GO terms list was generated by inputting DESeq2 data frame into iPathwayGuide Impact analysis package.

GO Molecular function	DE genes (#/ALL)	FDR-adjusted p value
Receptor activity	124/910	$2.979 \times 10^{-12}$
Molecular transducer activity	124/910	$2.979 \times 10^{-12}$
Transmembrane receptor activity	95/646	$4.062 \times 10^{-11}$
Transmembrane signalling receptor activity	91/607	$4.062 \times 10^{-11}$
Signalling receptor activity	97/694	$3.520 \times 10^{-10}$
Cytokine activity	32/134	$3.385 \times 10^{-8}$
Chemokine receptor binding	17/41	$5.609 \times 10^{-8}$
Chemokine activity	15/32	$6.77 \times 10^{-8}$
Receptor binding	126/1134	$6.018 \times 10^{-7}$
Collagen binding	18/60	$5.01 \times 10^{-6}$

**Table 4.3 Molecular function gene sets represented in the DE HD109 microglia cells.**

Pathway analysis identified 12 KEGG pathways significantly altered in the HD microglia, following FDR correction (Figure 4.1D). A number of immune pathways were predicted to be impacted, including cytokine-cytokine receptor interaction (KEGG:04060 – FDR =  $2.19 \times 10^{-4}$ ), antigen processing and presentation (KEGG: 04612 – FDR = 0.001), hematopoietic cell lineage (KEGG: 04640 – FDR = 0.001), autoimmune thyroid disease (KEGG: 05320 – FDR = 0.008), chemokine signalling (KEGG: 04062 – FDR = 0.029), allograft rejection (KEGG: 05330 – FDR = 0.029), Staphylococcus aureus infection (KEGG: 05150 – FDR = 0.035), phagosome (KEGG: 04145 – FDR = 0.035) and complement and coagulation cascades (KEGG: 04610 – FDR = 0.047). The most affected pathway in terms of number of DE genes was cytokine-cytokine receptor interaction (36 DE genes), followed by neuroactive ligand-receptor interaction (29 DE genes), cell adhesion molecules (24 DE genes) and chemokine signalling pathway (20 DE genes).

When considering the cytokine-cytokine receptor interaction and chemokine signalling pathways together, a pattern of dysregulation becomes evident, whereby several chemokines including CCL7, CCL17 and CCL18 and members of the CXC subfamily were found to be downregulated compared to just one, CCL24 being upregulated,  $\log_2FC = 3.284$  & p-value of 0.021 (Figure 4.2B). In addition, the chemokines (CXCL1, CXCL2, CXCL3, CXCL5, CXCL6) bind the common chemokine receptor, IL8RB or CXCR2. On the other hand, only two cytokines were shown to be

upregulated in the HD109 stem cell-derived microglia, TNFSF18 ( $\log_2FC$  of 2.657 and p-value of 0.026) and TNFSF11 ( $\log_2FC$  of 3.98 & p-value 0.041) (Figure 4.2A). Both are members of the TNF ligand family, thought to be important in the regulation of T lymphocyte survival in peripheral tissues. The anti-inflammatory IL-10 was found in lower levels ( $\log_2FC$  of -1.687 & p-value 0.010) in the HD109 microglia, along with CLCF1 or BSF3 ( $\log_2FC$  of -1.503 & p-value 0.036), a member of the IL-6 family which induces tyrosine phosphorylation of the IL-6 receptor subunit gp130, LIF receptor beta and the transcription factor STAT3. Though most chemokine receptors levels remained unchanged, levels of CCR2 ( $\log_2FC$  of 5.688 and p-value 0.010) and CX3CR1 ( $\log_2FC$  of 9.412 and p-value  $1E-06$ ) were significantly upregulated (Figure 4.2B). The important adaptor proteins [ADCY9 ( $\log_2FC$  of -1.194 and p-value 0.017), STAT1 ( $\log_2FC$  of -1.416 and p-value  $7.139E-04$ ) and GNG11 ( $\log_2FC$  of -2.17 and p-value 0.034)] were also downregulated, leading to actin regulation, cytokine production, migration and chemotaxis listed among the predicted perturbed processes (Figure 4.2C). Crucially, levels of CSF1R, the receptor which mediates microglial proliferation and survival, were shown to be significantly higher in the HD microglia ( $\log_2FC$  of 1.411 and p-value 0.020) compared to Kolf2 cells.

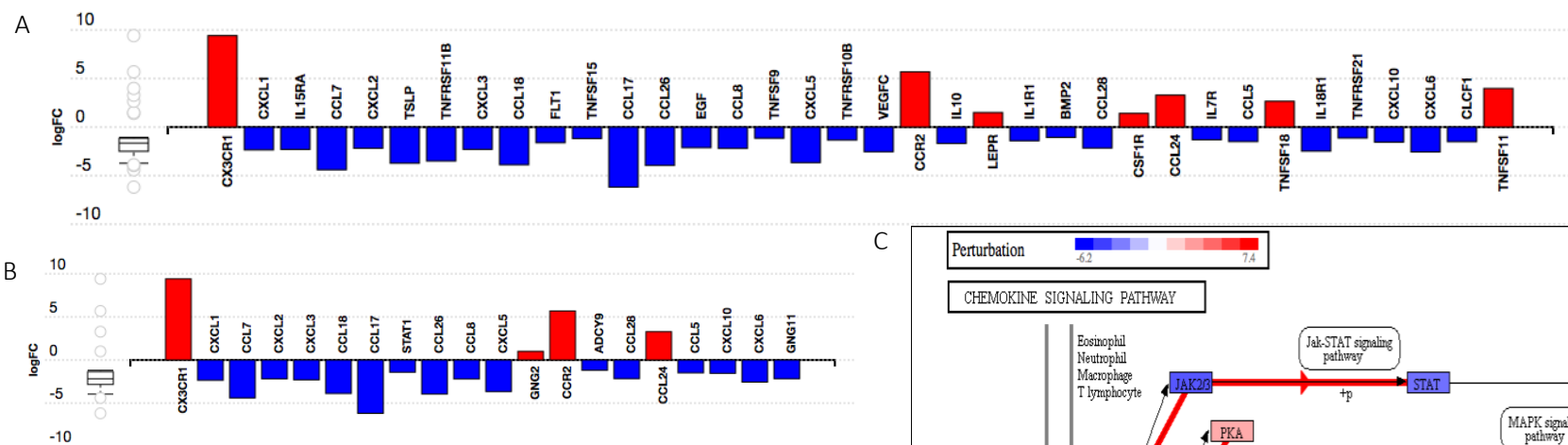
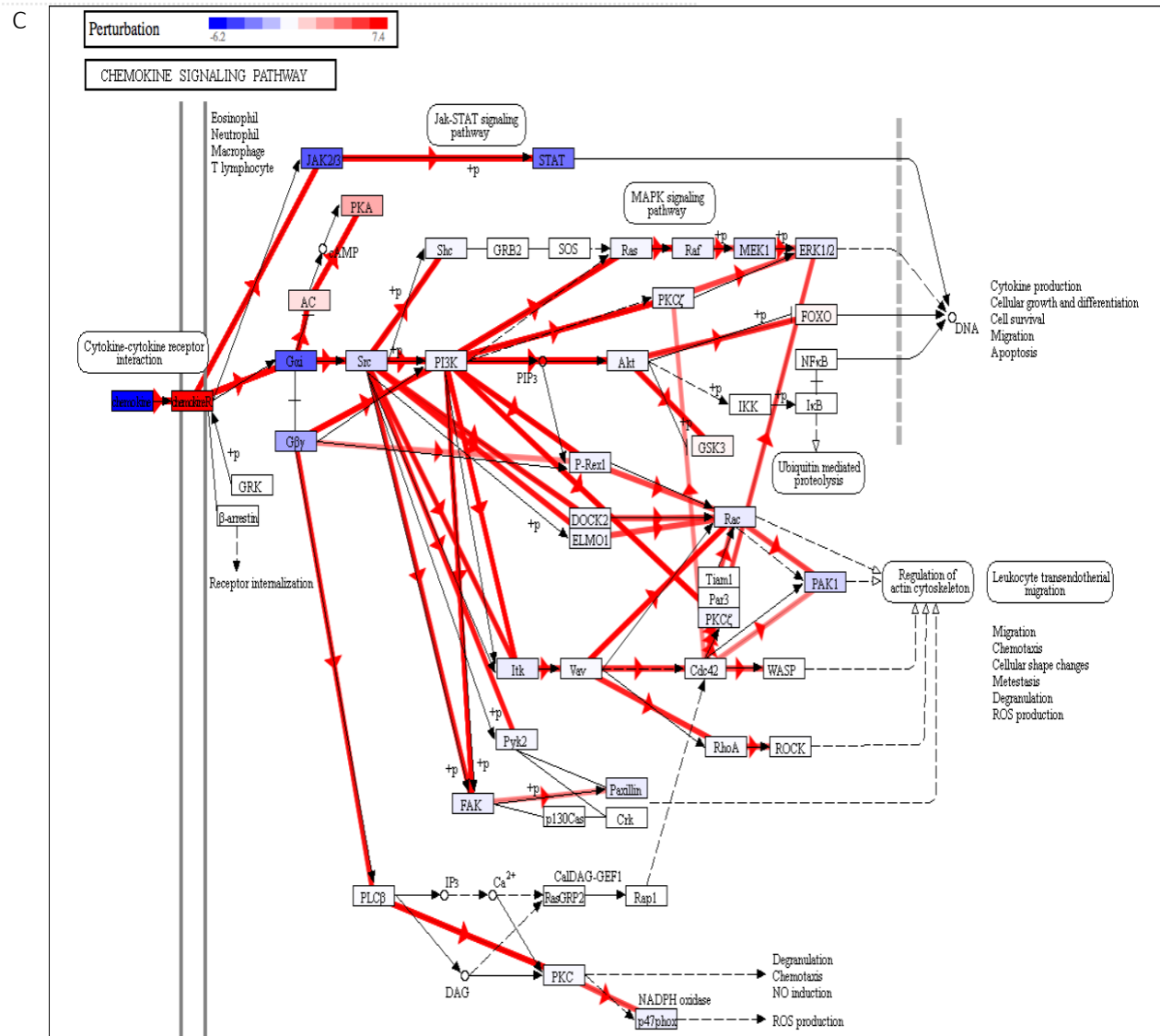


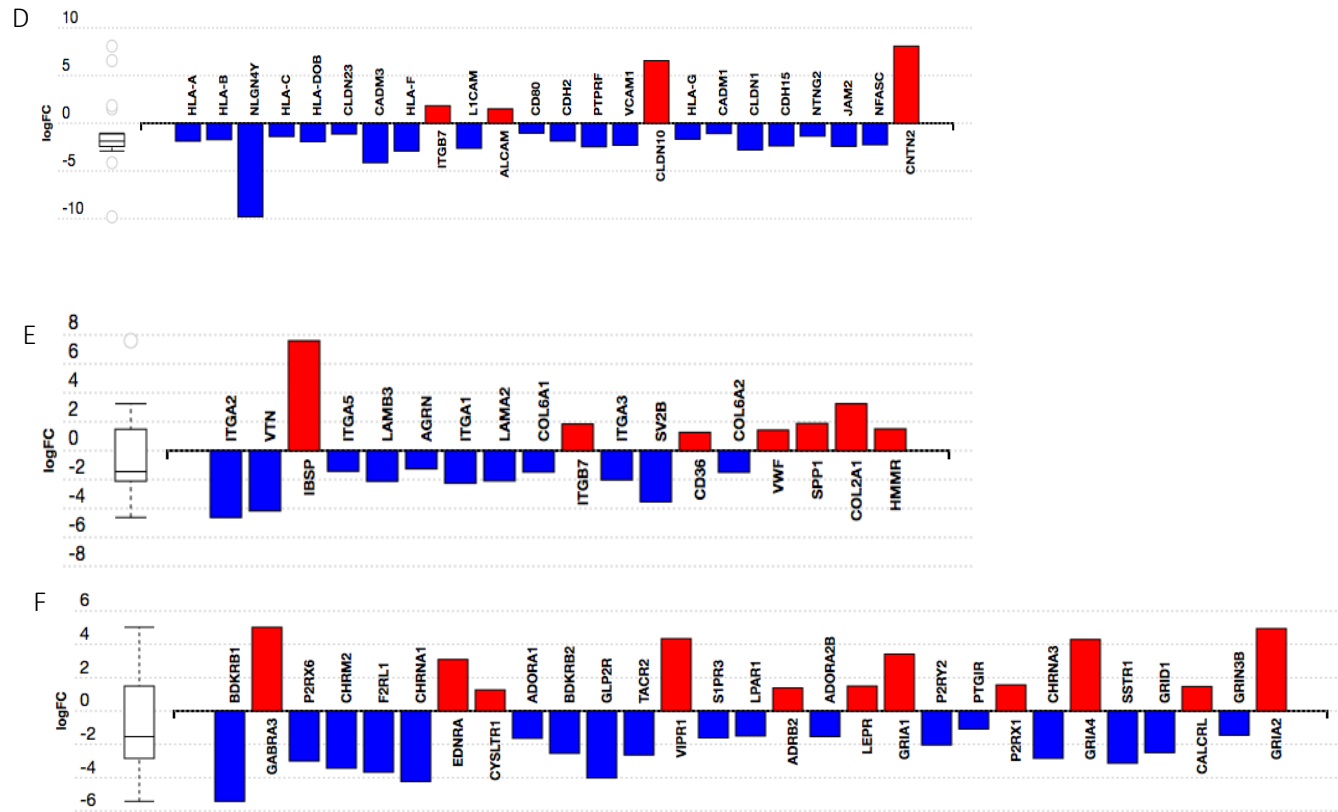
**Figure 4.2 Several immune pathways are predicted to be altered in HD109 microglia.**

**(A)** The TNF family ligands TNFSF11 and TNFSF18 were upregulated in HD109 MG, whereas the majority of cytokines including IL-10 were downregulated compared to Kof2 MG cells.

**(B)** With the exception of CCL24, the expression of several chemokines was downregulated in the HD109 MG cells. The chemokine receptors CX3CR1 and CCR2 were significantly upregulated in the HD MG cells.

**(C)** Dysregulation in chemokine signalling was predicted to perturb several processes, including cell migration and chemotaxis, actin regulation and cytokine production. Chemokine signalling pathway diagram (KEGG: 04062) overlaid with computed iPathway Guide perturbation analysis (bold red lines and arrows). Perturbation analysis accounts for measured fold change for the gene and for the accumulated perturbation propagated from any upstream genes. The highest negative perturbation is shown in dark blue, and the highest positive perturbation in dark red.





**(D)** 24 cell adhesion molecules, belonging to the KEGG pathway (04514) were reported as DE in the HD109 MG cells. **(E)** Differential expression of extracellular matrix-receptor interaction molecules (KEGG: 04512) in HD109 microglia in comparison to Kolf2 WT cells. **(F)** The neuroactive ligand-receptor interaction KEGG pathway contained 29 DE genes in the HD109 microglia.

Bar plots of top-30 genes out of total number of DE genes in a pathway. Upregulated genes displayed in red, downregulated in blue. Box and whisker plots outline the distribution of DE genes annotated to the KEGG pathway. Box represents the first quartile, the median and third quartile; outliers are shown as circles.

Two closely related pathways were also predicted as dysregulated: cell adhesion molecules (KEGG: 04514 – FDR =  $2.19 \times 10^{-4}$ ) and extracellular matrix-receptor interaction (KEGG: 04512 – FDR = 0.001). A number of cell adhesion genes that regulate pre- and post-synaptic neuronal interactions as well as interactions between neurons and other nervous system cells were altered (Figure 4.2D). Those include the neuronal adhesion genes CDH2 ( $\log_2FC$  of -1.866 and p-value 0.006), L1CAM ( $\log_2FC$  of -2.626 and p-value 0.003), NLG4Y ( $\log_2FC$  of 1-9.807 and p-value  $1 \times 10^{-6}$ ) and CADM3 ( $\log_2FC$  of -4.139 and p-value 0.001), all significantly downregulated whereas CNTN2 was the only neuronal adhesion gene markedly upregulated ( $\log_2FC$  of 8.082 and p-value 0.044). Also upregulated was the epithelial and tight junction protein CLDN10 ( $\log_2FC$  of 6.563 and p-value 0.009) while the claudin family members CLDN1 ( $\log_2FC$  of -2.798 and p-value 0.018) and CLDN28 ( $\log_2FC$  of -1.133 and p-value  $8.118 \times 10^{-4}$ ) and the endothelium adhesion proteins VCAM1 ( $\log_2FC$  of -2.315 and p-value 0.008) and JAM2 ( $\log_2FC$  of -2.419 and p-value 0.032) were significantly reduced in the HD microglia. Notably, several immune-specific cell adhesion molecules were altered, with predicted perturbing effects on antigen processing and presentation via the MHC I and MHC II pathways (below). Examples include ALCAM, an activated adhesion molecule that binds the T-cell CD6 antigen ( $\log_2FC$  of 1.506 and p-value 0.003) and CD80, a receptor that binds to T-cells when activated and induces their proliferation ( $\log_2FC$  of -1.042 and p-value 0.005).

The HD109 microglia also displayed significantly lower levels of transcripts coding for integrins, receptors that facilitate cell adhesion to the extracellular matrix: ITGA1, ITGA2, ITGA3 and ITGA5. Indeed, only ITGB7 levels were higher in HD109 vs Kolf2 microglial cells (Figure 4.2E).

The KEGG pathway neuroactive ligand-receptor interaction (KEGG: 04080) was another predicted to be dysregulated by HD109 microglia. The most perturbed gene here was the bradykinin receptor or B1BDKRB1 ( $\log_2FC$  of -5.42 and p-value  $1 \times 10^{-6}$ ), which mediates binding to bradykinin, a peptide released in inflammatory conditions. Other downregulated neuroligand receptors were the acetylcholine receptor subunit genes CHRNA1 and CHRNA3, the NDMA receptor subunit GRIN3B and the muscarinic cholinergic receptor CHRM2 (Figure 4.2F). Additional notable receptors belonging to

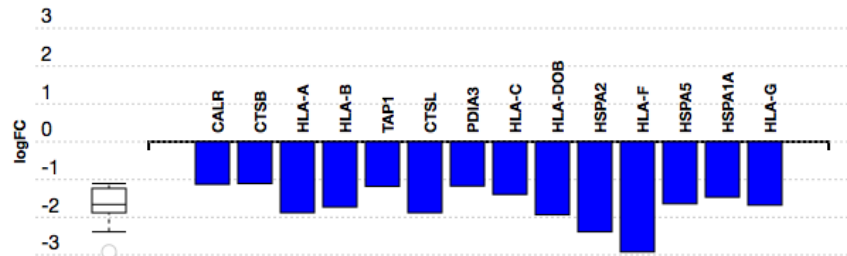
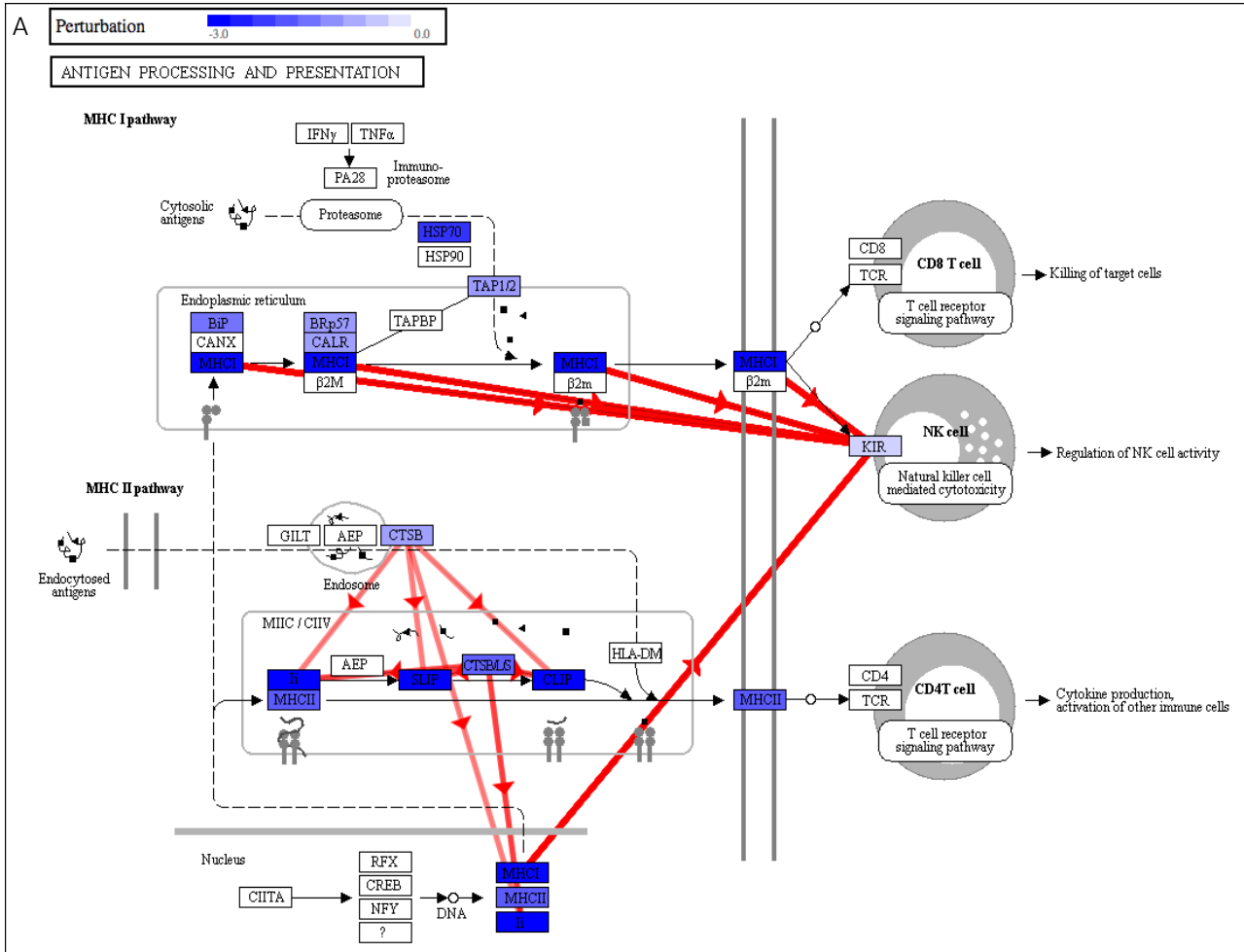
this pathway that were upregulated in HD microglia included the GABA-A receptor subunit GABRA3 ( $\log_2FC$  of 5.026 and p-value  $1 \times 10^{-6}$ ) as well the glutamate AMPA receptors GRIA1, GRIA2 and GRIA4. Intriguingly, transcript levels for the adenosine receptors A1 and A2B were markedly lower, while downregulation of the microglial sensome gene ADORA3 did not reach statistical significance ( $\log_2FC$  of -1.018 and p-value 0.253). Similarly, mRNA levels for the purinergic receptors P2RX6 and P2RY2 were also lower in the HD109 cells ( $\log_2FC$  of -3.003 and -2.039) whereas P2RX1 ( $\log_2FC$  of 1.567 and p-value 0.031) and P2RY12 ( $\log_2FC$  of 1.935 and p-value 0.152) levels were higher.

Antigen processing and presentation (KEGG: 04612 – FDR = 0.0010) was another pathway predicted to be impacted by the transcriptional changes identified in HD109 microglia (Figure 4.3A). Upon closer inspection, several MHC I and MHC II molecules were found in significantly lower levels in the HD in vitro microglia. All MHC class I molecules, expressed in nearly all cells and present peptide antigens processed by the proteasome and derived from the ER, displayed significantly lower mRNA levels. Of the class II pathway, expressed in professional antigen presenting cells, HLA-DOB ( $\log_2FC$  of -1.933 and p-value  $7.67 \times 10^{-4}$ ) was found at reduced mRNA levels in the HD MG cells, along with mRNAs for cathepsins B and L. Perturbation analysis predicted that these changes would affect presentation of endogenous and endocytosed antigens to natural killer (NK) cells.

The process of phagocytosis, an important function of microglia, was also identified among the dysregulated pathways (KEGG: 04145 – FDR = 0.035) (Figure 4.3B). Many transcripts in this pathway were shared with the antigen presentation pathway described above. The phagocytosis-promoting receptors FCAR, FCGR2B and FCGR2C exhibited markedly reduced mRNA levels, along with the scavenger receptor MARCO ( $\log_2FC$  of -4.327 and p-value  $2.154 \times 10^{-5}$ ), the complement receptor C1R and integrins ITGA2 and ITGA5. In contrast, three important genes were upregulated in the HD microglia compared to Kolf2 WT: the scavenger receptor CD36 ( $\log_2FC$  of 1.262 and p-value 0.008), the NADPH oxidase 2 gene CYBB, superoxide enzyme that generates reactive oxygen species ( $\log_2FC$  of 1.208 and p-value 0.003) and the actin-binding

protein coronin 1A, which initiates fusion of the phagosome to the lysosome ( $\log_2FC$  of 1.182 and p-value 0.008); perhaps hinting at a compensatory mechanism.

According to the iPathwayGuide Impact analysis, the final pathway predicted to be significantly affected was the complement and coagulation pathway (KEGG: 04610 – FDR = 0.047), which had 13 DE genes, of which C5 and C7 were upregulated (Figure 4.3C). CR2, CLU, MASP1, C1S, C1R and VTN were all found to be downregulated in HD109 MG cells.



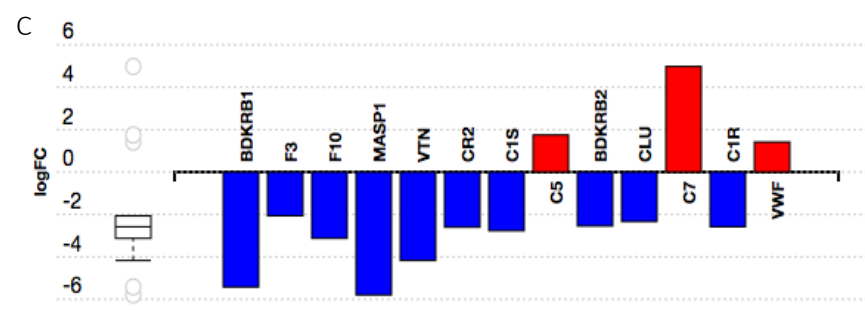
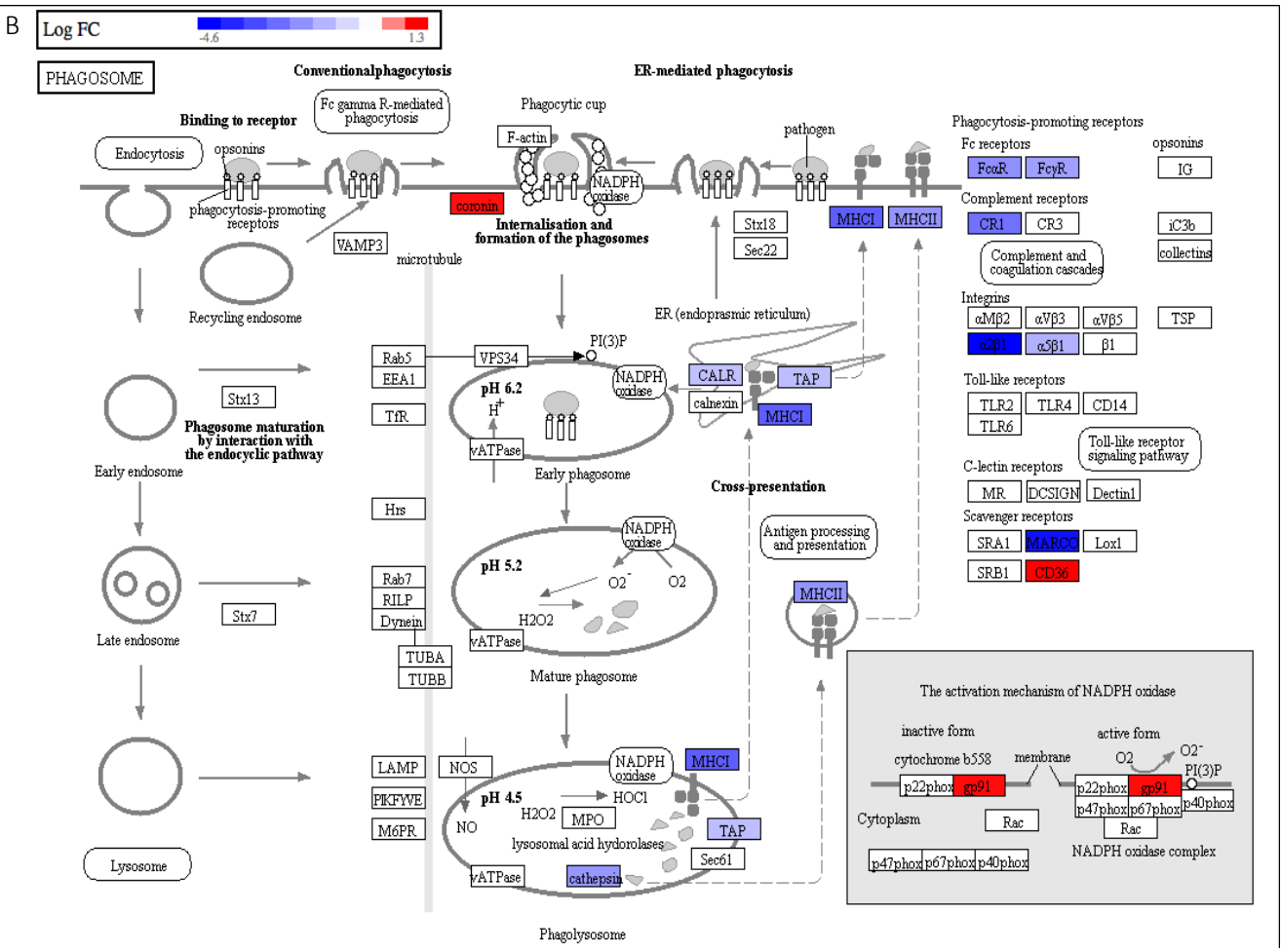
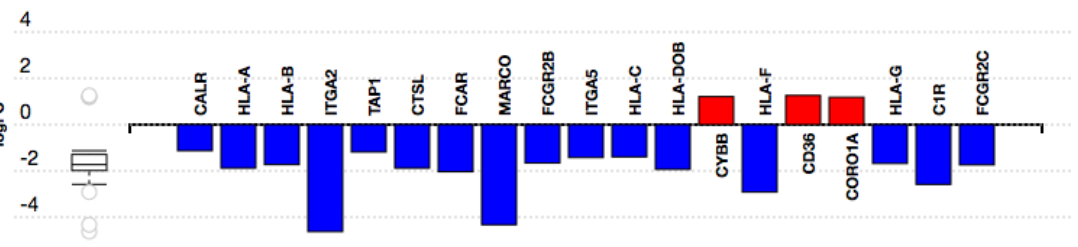


**Figure 4.3 Phagocytosis and antigen processing and presentation are among the top pathways predicted to be dysregulated in HD109 iPSC-derived microglia.**

**(A)** Perturbation analysis by iPathway Guide identified antigen processing and presentation as likely affected in HD109 MG. Highest negative perturbation shown in dark blue. Changes predicted to affect antigen presentation to natural killer cells.

**(B)** Phagosome KEGG pathway diagram overlaid with measured fold changes for genes including CYBB, CD36 and coronin (upregulated) and downregulated receptors such as FCGR2B and MARCO. **(C)** Complement pathway was enriched with 13 DE genes in HD109 MG cells.

Bar plots of top-30 genes out of total number of DE genes in a pathway. Upregulated genes displayed in red, downregulated in blue. Box and whisker plots outline the distribution of DE genes annotated to the KEGG pathway. Box represents the first quartile, the median and third quartile; outliers are shown as circles.



To gain further insight into the underlying mechanisms driving the differential gene expression observed in the HD109 stem cell-derived microglia, upstream regulator analysis was performed using Ingenuity Pathway Analysis software (IPA, Qiagen). This software compares gene expression in a dataset with known gene lists regulated by specific upstream signalling molecules and networks (p-value of overlap) and predicts whether a specific molecule is likely to be activated or inhibited (z score). Using a z score of > 2 or < -2 and p value of < 0.01 as cut-offs for ascribing significance, the extensive list of predicted upstream regulators was narrowed down to 41, with the majority (28 out of 41) found to be significantly inhibited (see Table 4.4) compared to 13 predicted to be activated (see appendix 3).

Upstream regulator	Activation z-score	P value of overlap	Function
Lipopolysaccharide	-4.272	6.42E-14	Bacterial cell wall component that elicits strong immune response
NFκB complex	-4.222	0.0022	Family of TFs that regulate inflammatory response
TP53	-4.17	1.7E-05	Tumour suppressor involved in regulation of apoptosis
IFN-α2	-4.114	6.16E-05	Type I IFN cytokine produced by virus-infected cells
poly rI:rC-RNA	-3.806	2.05E-05	Synthetic drug that activates IFN-inducible genes
IFN-γ	-3.668	1.04E-10	Immune response-mediating cytokine
IL1A	-3.609	2.15E-03	Pro-inflammatory cytokine
TNF	-3.545	1.53E-15	Pro-inflammatory cytokine
F2	-3.502	1.94E-03	Serine protease involved in clotting process
IFN-β	-3.399	7.75E-04	Type I IFN cytokine involved in innate immune response

**Table 4.4 IPA of upstream transcriptional regulators inhibited in HD109 iPSC-derived microglia.** IPA was used to predict activation of specific transcription regulators that overlap with the transcriptome changes observed in HD109 microglia. The upstream regulators were ranked by activation z-score, with a significant p value cut-off of < 0.01. The 10 most significant regulators and networks were included in the table above (for the remaining inhibited regulators – see appendix 2).

The top activated regulator in terms of z score was the p38 MAPK kinase inhibitor SB203580 (z score of 3.885 and p-value overlap  $1.33 \times 10^{-8}$ ), followed by the nuclear receptor retinoic acid receptor alpha or RARA (z score of 3.414 and p-value of overlap

$5.41 \times 10^{-7}$ ). The cytokine IL1RN, whose expression was upregulated ( $\log_2FC$  of 2.254 & p-value 0.034), was identified as one of the activated upstream regulators (z score of 2.279 and p-value  $1.64 \times 10^{-3}$ ), along with the growth factor DKK1 (z score of 2.005 and p-value  $1.94 \times 10^{-4}$ ). Predictive activation of the transcription factor STAT3, previously identified as an activated regulator in HD monocytes (Miller et al. 2016), failed to reach significance (z score of 1.12 and p-value  $7.29 \times 10^{-4}$ ) whereas NKX2-3 (z score of 2.103 and p-value  $6.63 \times 10^{-6}$ ) and MYCN (z score of 2.671 and p-value  $7.85 \times 10^{-4}$ ) were predicted as significantly activated.

In contrast, a large number of cytokines, transcription factors and pathways were predicted to be inhibited in the HD109 microglial cells. Top of this list were the LPS pathway (z score of -4.272 and p-value overlap  $6.42 \times 10^{-14}$ ), NF $\kappa$ B complex (z score of -4.222 and p-value overlap  $2.2 \times 10^{-3}$ ), TP53 (z score of -4.17 and p-value overlap  $1.7 \times 10^{-5}$ ), IFN $\alpha$ 2 (z score of -4.114 and p-value overlap  $6.16 \times 10^{-5}$ ), IFN- $\gamma$  (z score of -3.668 and p-value overlap  $1.04 \times 10^{-10}$ ) and TNF (z score of -3.545 and p-value overlap  $1.53 \times 10^{-15}$ ). Several other regulators including IL6, IL1 $\beta$ , IFN $\alpha$ , IL4, ERK1/2, p38 MAPK, IRF3, IRF1 and STAT1 were similarly predicted to be significantly inhibited, though TLR4 didn't fit the z score criterion (-1.58 and p-value overlap  $6.65 \times 10^{-4}$ ). Overall, these data firmly suggest that the transcriptional changes observed in the HD109 stem cell-derived microglia are associated with inhibition by several upstream regulators.

### 4.3.2 Functional validation of HD109 of iPSC-derived microglia

Upstream regulator analysis carried out using IPA (see section 4.3.1) projected several inflammatory pathways to be inhibited in HD109 MG, including the NF $\kappa$ B (Figure 4.4A) and LPS pathways (Figure 4.5A). To test this hypothesis, the expression of NF $\kappa$ B pathway genes in the RNA-seq data was compared to WT Kolf2 cells. Out of a total of 50 genes, only three were differentially expressed: IL1R1 ( $\log_2$ FC of -1.411 and p-value 0.018), IL10 ( $\log_2$ FC of -1.687 and p-value 0.01) and STAT1 ( $\log_2$ FC of -1.416 and p-value  $7.14 \times 10^{-4}$ ) were downregulated (Figure 4.4B). All other genes in this pathway, including important adaptor proteins such as MYD88 were expressed at comparable levels in both cell lines, though differences in IL-1 $\beta$  did not reach statistical significance ( $\log_2$ FC 1.115 and p-value 0.241) (Figure 4.4C). The expression of key NF $\kappa$ B pathway genes was further validated by Fluidigm qRT-PCR and results confirmed RNA-seq data observations that mRNA levels of NF $\kappa$ B genes did not vary significantly between HD109 and Kolf2 microglia samples (Figure 4.4 D-E).

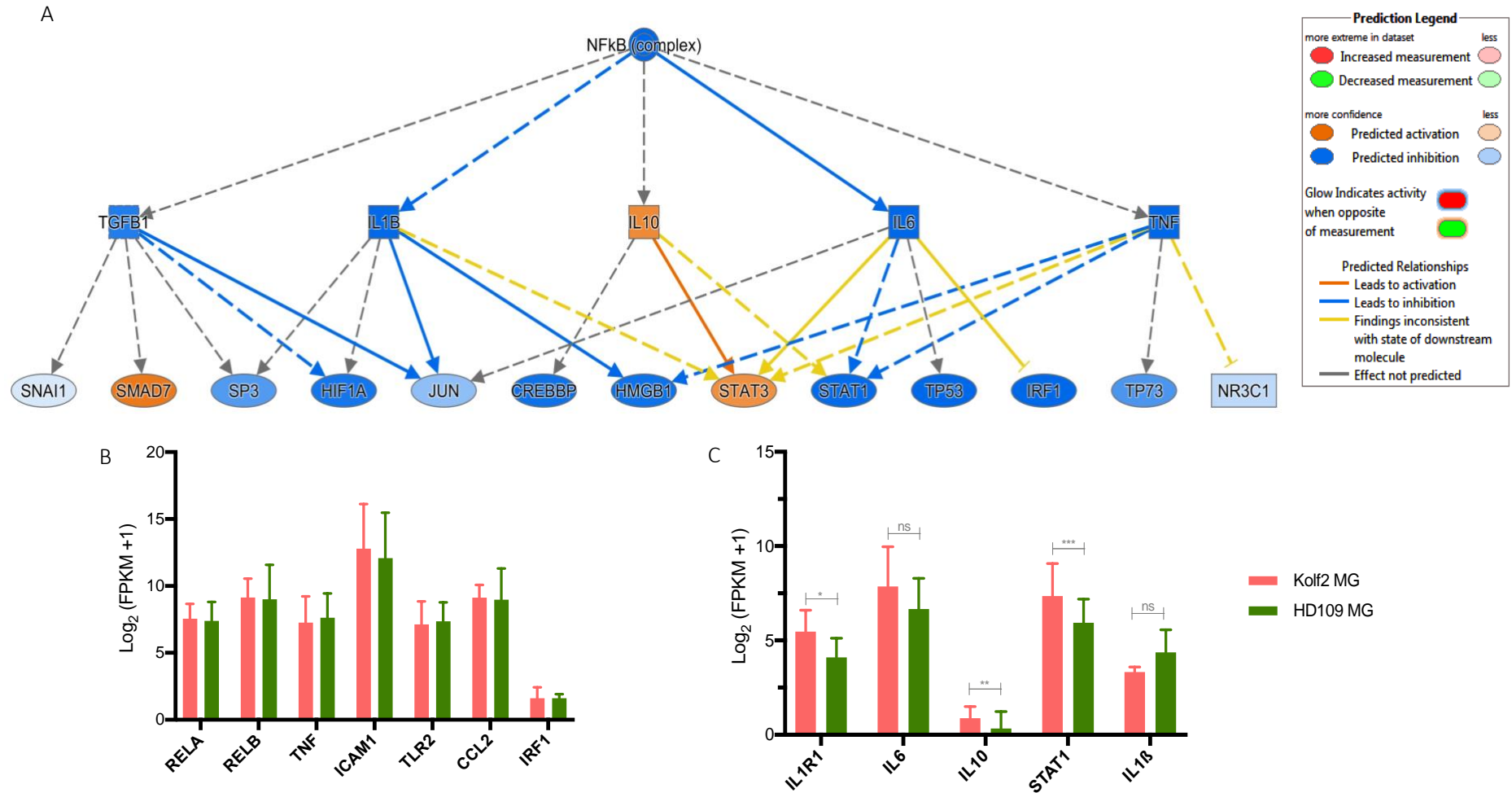
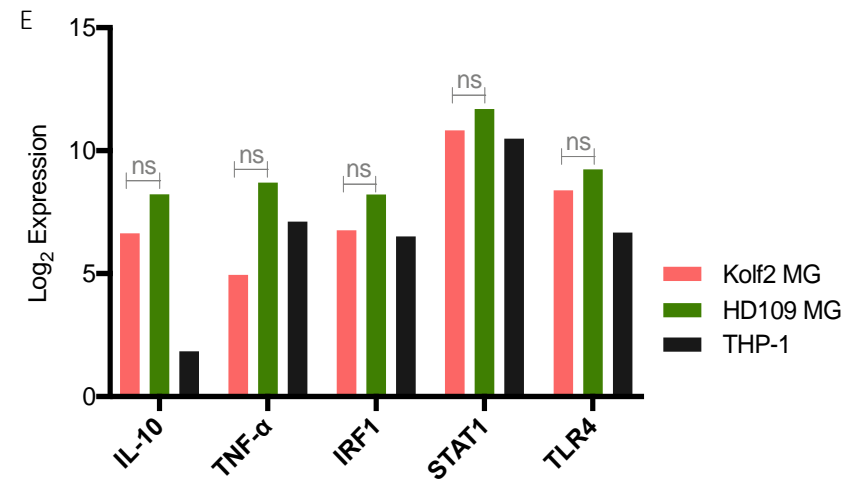
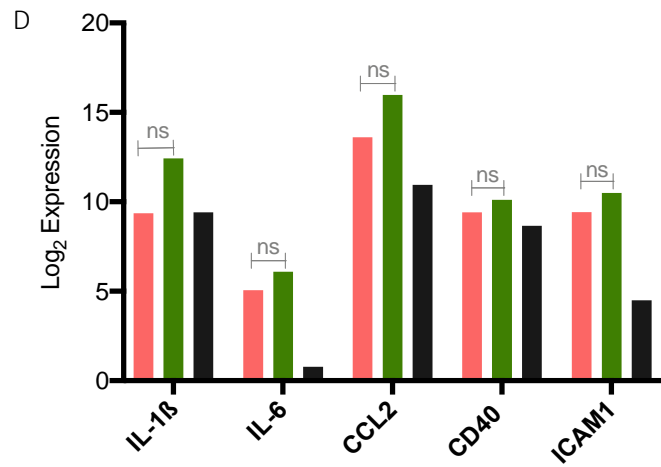


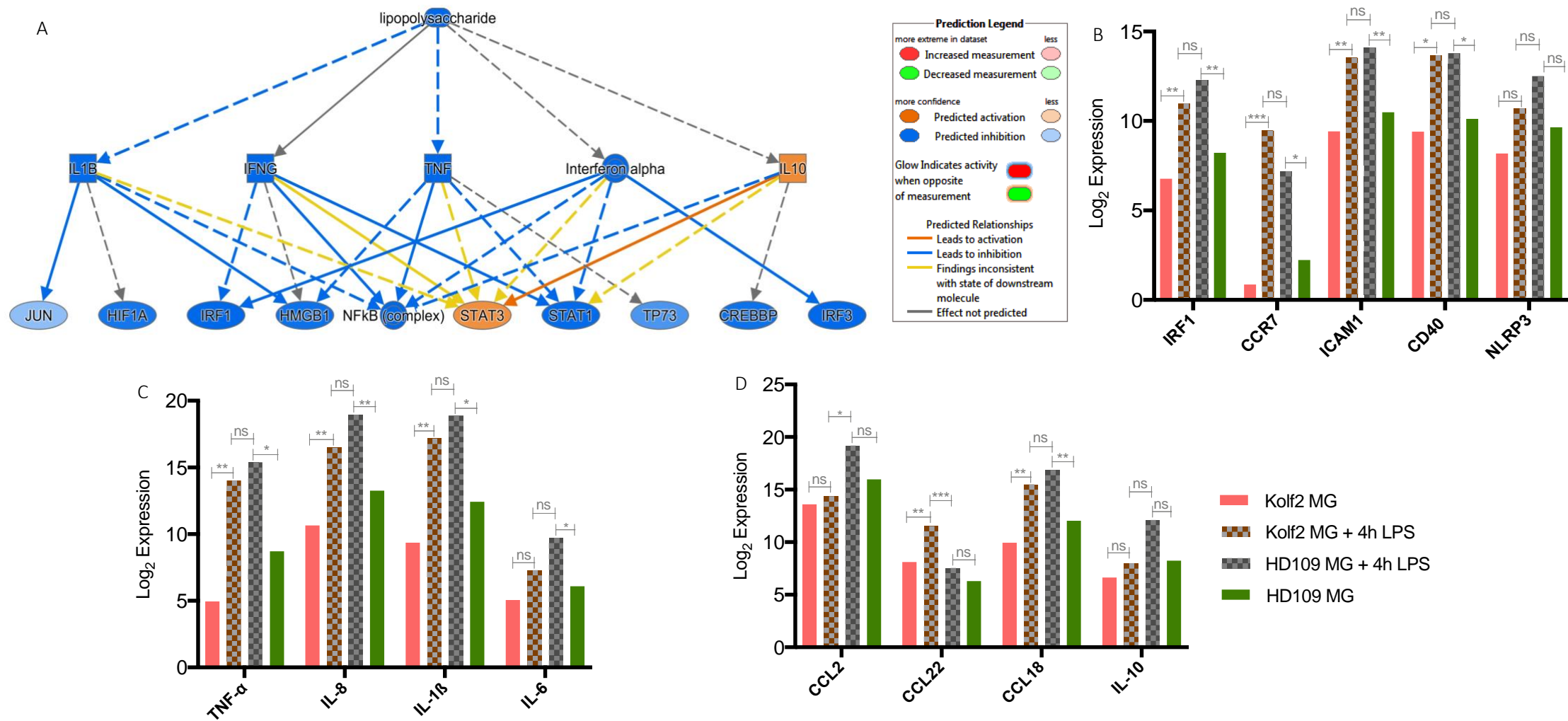
**Figure 4.4 The expression of NF $\kappa$ B pathway genes is unaltered in HD109 microglia compared to WT Kolf2 microglia.**

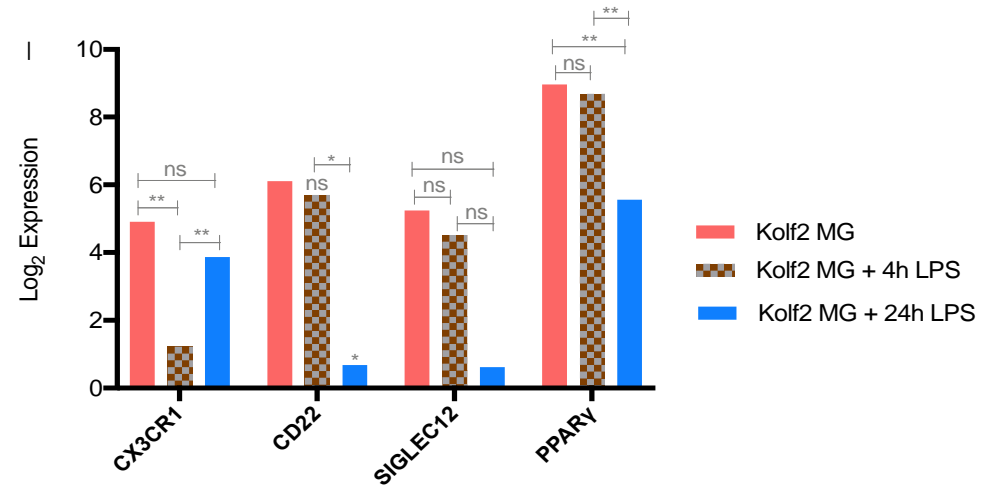
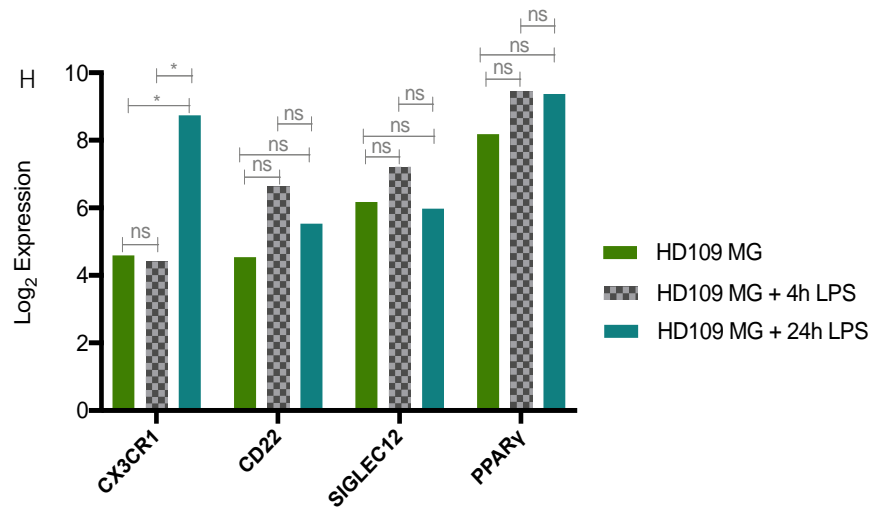
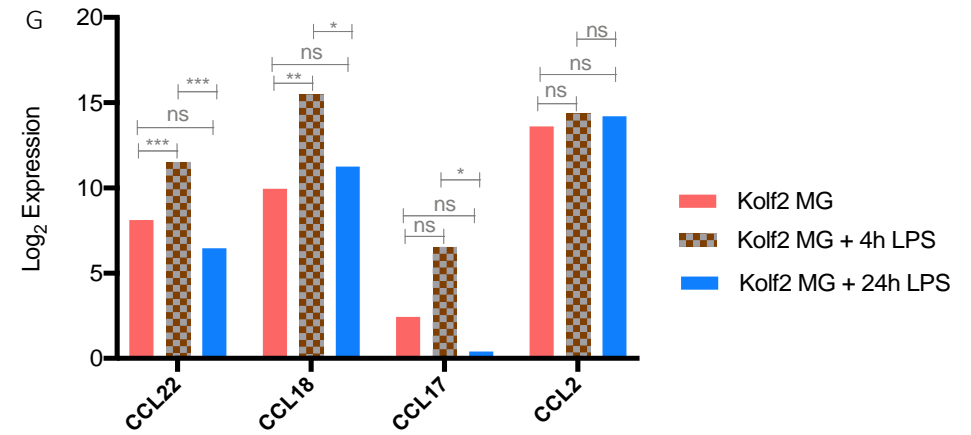
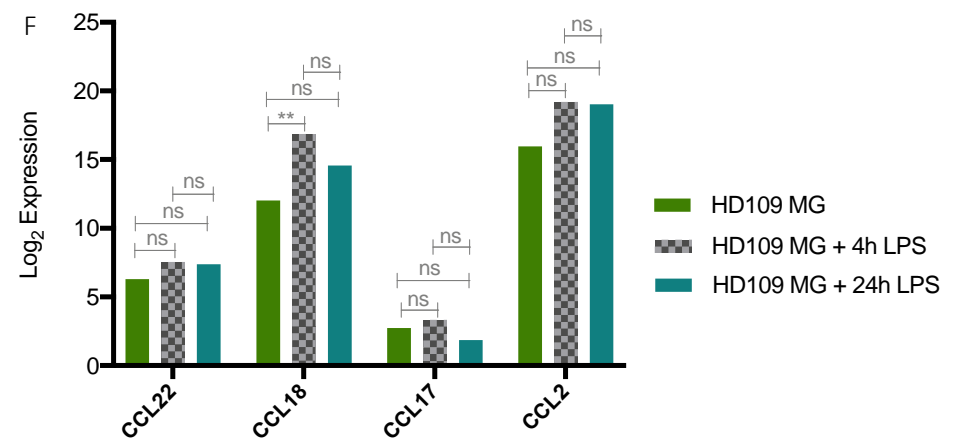
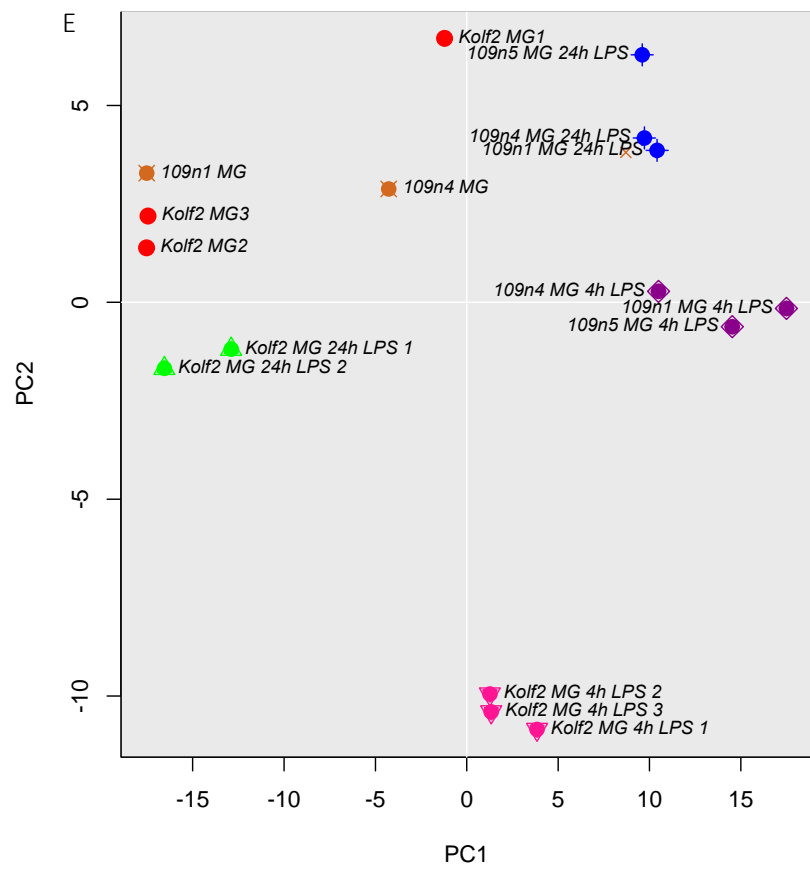
(A) IPA's Upstream regulator analysis of the DE genes in the HD109 microglia RNA-seq dataset predicted the inhibition of several inflammatory pathways including the NF $\kappa$ B complex. Regulators with significantly inferred activation (IL-10, SMAD7 and STAT3) are shown in orange, inhibited regulators (TNF, IL-6, IL-1 $\beta$ , TGFB1, STAT1 and IRF1) are shown in blue. (B) Expression of various components of the NF $\kappa$ B pathway was assessed by RNA-seq. No significant differences were found in levels of NF $\kappa$ B subunits RELA and RELB, as well as the inflammatory activation markers TNF, ICAM1, CCL2 and IRF1. (C) Out of 50 genes in the pathway, three were differentially expressed (downregulated) in HD109 microglia: IL1R1, IL-10 and STAT1. RNA-seq expression levels are represented as log<sub>2</sub> transformed FPKM pseudo-counts. Data analysed using one-way ANOVA with Tukey's multiple comparison test. Asterisks denote statistical significance: \* < 0.05, \*\* < 0.01, \*\*\* < 0.001, ns – not significant. n=3 independent differentiations.



**(D-E)** Fluidigm qPCR validation of NFκB pathway genes expression in the HD109 microglia. No statistically significant differences were found in the expression levels of several genes between Kolf2 and HD109 iPSC-derived microglia, despite a notable trend towards upregulation. Fluidigm qRT-PCR data are presented as log<sub>2</sub> expression normalised to reference genes. Statistical analysis used one-way ANOVA with Dunnett's post hoc comparison. ns – not significant. n=3 biological replicates, except THP-1 (n=2).

Mouse model studies have shown how HD immune cells cultured *ex vivo* exhibit a hyper-reactive profile upon LPS stimulation, secreting higher levels of pro-inflammatory cytokines compared to controls (Björkqvist et al. 2008; Trager et al. 2015). Thus, the hypothesis that LPS-stimulation of HD109 microglia may result in a hyper-reactive was investigated, with expression of classical M1 markers and LPS pathway genes assessed by qPCR. HD109 and Kolf2 microglia were differentiated for 14 days in IL-34 and GM-CSF, after which the cultures were incubated with 1 µg/ml LPS for 4 and 24 hours, as gene expression changes following LPS stimulation peak at around 4 hours (Yamamoto et al. 2004; Aung et al. 2006). No notable differences were evident in the magnitude of change in expression of activation molecules after 4 hours between HD and Kolf2 microglia, which suggests that both cell lines exhibited the expected M1 activation or polarisation state. Genes such as IRF1, CCR7, ICAM1, CD40 and NLRP3 were upregulated to similar levels in both LPS-treated cell samples (Figure 4.5B). Though these differences were not statistically significant, there was a trend towards higher mRNA levels of M1 pro-inflammatory cytokines in unstimulated HD109 microglia, including TNF- $\alpha$ , IL-8, IL-6, IL-1 $\beta$  and CCL2. Subsequently, these genes were upregulated in response to LPS incubation at 4 hours, with no differences in mRNA levels post incubation between the cell lines (Figure 4.5C). However, the magnitude of the mRNA increases between the LPS-treated microglia samples differed for two genes, TNF- $\alpha$  and IL-1 $\beta$ . For TNF- $\alpha$ , mRNA levels increased by a greater magnitude in the Kolf2 WT cells (3-fold increase at  $p = 0.0024$ ) compared to HD109 cells (2-fold increase at  $p = 0.0217$ ) (Figure 4.5C). A similar pattern was observed for IL-1 $\beta$ , with a 3-fold increase in gene expression for Kolf2 cells ( $p = 0.0073$ ) versus 2.5-fold increase in the HD109 cells ( $p = 0.0256$ ). The 4h LPS challenge also resulted in higher CCL2 expression in HD109 microglia compared to Kolf2, whereas CCL22 expression was higher in 4h LPS-treated HD109 compared to 4h LPS-treated WT Kolf2 cells. The chemokine CCL18, a cytokine with both immune activation and suppressive properties, was equally upregulated by LPS induction in both genotypes (Figure 4.5D). Taken together, these observations hint at a tighter regulation of pro-inflammatory cytokine production in the HD109 microglial cells.





(E) Cluster analysis of unstimulated and LPS-treated Kolf2 and HD109 MG cells showed a greater segregation between Kolf2 4h and 24h LPS-stimulated samples than for the corresponding HD109 cells. (F-G) LPS-induced expression of the anti-inflammatory chemokines CCL17, CCL18 and CCL22 was differentially regulated in Kolf2 vs HD109 MG cells. In HD109 MG cells, no significant differences were found in the expression of the chemokines over a 24-hour course of LPS stimulation. In Kolf2 MG cells, expression of all three chemokines peaked at 4 hours post LPS before significantly decreasing at 24 hours. (H-I) LPS treatment significantly affects expression of calming molecules in Kolf2 MG but not HD109 cells.

Fluidigm qRT-PCR data are presented as  $\log_2$  expression normalised to reference genes. Statistical analysis used two-way ANOVA with Tukey's multiple comparisons test. ns – not significant, \* < 0.05; \*\* < 0.01; \*\*\* < 0.001. n=3 biological replicates, except Kolf2 MG + 24h LPS (n=2).

Next, a PCA plot was used to examine the divergence of all LPS-treated samples from their corresponding unstimulated samples. For both cell lines, 4h LPS samples were segregated away from 24h samples, with the Kolf2 LPS-treated cells showing greater separation than the corresponding HD109 cells (Figure 4.5E). Furthermore, the plot demonstrated that the 4h and 24h HD109 cells were closely matched to each other and to unstimulated HD109 control cells. For the Kolf2 samples, the control cells segregated with the 24h LPS-stimulated cells, which were clearly separate from the 4h treated cells. This hinted at significant differences in the maximal LPS response at 4 hours of cells from both genotypes. To delve further into these differences, the profile of LPS response of both cell lines was compared for meaningful trends. Chemokine expression in response to LPS was found to differ in HD109 vs Kolf2. Except for increased CCL18 release, all levels of chemokines remain constant over the 24h course of LPS treatment in HD109 microglia (Figure 4.5F). In comparison, CCL22, CCL18 and CCL17 were upregulated in Kolf2 cells after 4 hours of LPS treatment, with levels decreasing significantly thereafter (Figure 4.5G).

Moreover, LPS stimulation appeared to impact the expression of a number of neuroprotective genes in Kolf2 microglia (Figure 4.5H). CX3CR1, CD22 and SIGLEC12, sensing molecules that provide a constitutive and calming 'off' signal were downregulated in Kolf2 microglia over the course of LPS treatment, whereas levels of the same genes remained constant in the control and LPS-stimulated HD109 microglia (Figure 4.5I). In conclusion, these experiments demonstrated that HD109 microglia did not exhibit a hyper-reactive phenotype in response to challenge with LPS.

## 4.4 Summary and Discussion

In this chapter, a HD iPSC line containing 109 CAG repeats and a WT Kolf2 iPSC line were differentiated into microglia and the phenotype of the in vitro derived microglial cells characterised using RNA sequencing in order to analyse the microglia-specific transcriptome effects of the HD CAG expansion. Gene Ontology analysis revealed that developmental processes, including development of the embryo, mesenchyme, vasculature and epithelium were among those significantly enriched in the HD109 microglia gene sets. The fact that these processes aren't specific to the nervous or immune system suggests that these transcriptional changes reflect development as a whole being altered in HD. Recent studies have shown that CAG repeat expansion results in the dysregulation of genes involved in neuronal development and dorsal striatum formation (Ring et al. 2015). Similarly, Molero et al. 2009 found that CAG expansion-associated developmental abnormalities in neurogenesis in the striatum subsequently made medium spiny neurons more susceptible to degeneration in later life (Molero et al. 2009). These findings seem to support the notion of HD as a neurodevelopmental disorder (Kerschbamer & Biagioli 2016). Genes related to skeletal and limb morphogenesis were also represented among the gene sets altered in the HD109 microglia, likely as a result of non-specific transcriptional changes due to aberrant mutant HTT transcription factors interactions. These findings agree with recent RNA-seq data from Labadorf et al. 2015, who analysed gene expression in the prefrontal cortex of HD post-mortem samples and found evidence of a developmental signal, although it was unclear which brain cell type was responsible for this signal (Labadorf et al. 2015). The same study also uncovered evidence of an enrichment in inflammatory and immune response gene sets in HD brains.

According to pathway impact analysis of the in vitro HD microglia transcriptome data, several immune-related pathways were predicted to be dysregulated. Transcripts coding for cell adhesion molecules that mediate antigen presentation and immune cell regulation were downregulated in HD109 vs Kolf2 cells. Given that microglial cell adhesion molecules play a critical role in many processes, including neural tissue development, it was unsurprising to note a predicted dysregulation in the KEGG pathway 04080, enriched with genes coding for neuroactive ligand-receptor interactions. This may hint at an impairment of HD microglia in their capacity to aid the construction and development of neuronal networks. Another

pathway impact analysis prediction was the likely perturbation of interactions between HD microglia and the extracellular matrix, which are mainly mediated by integrins and cell adhesion molecules whose expression was found to be dysregulated. Given that the ECM plays a key role in the morphogenesis and maintenance of cell and tissue structure and function, these data appear to tally well with reports of neurovasculature disruptions in HD patients, R6/2 mouse models and iPSC models of blood-brain barrier (Drouin-ouellet et al. 2015; Lim et al. 2017; Vatine et al. 2017).

Chemokine signalling was among the biological pathways revealed to be significantly affected by transcriptional changes in HD109 microglia. Chemokines involved in the recruitment of blood myeloid cells (CCL7, CCL8, CCL17) were significantly downregulated. mRNA levels of CCL24, strongly chemotactic to resting T lymphocytes, was upregulated while levels of T cell recruiting chemokines such as CCL1, CCL2 and CCL22 were unchanged. This pattern of expression seems to contradict data from previous findings, which have shown that levels of chemokines, complement proteins and the anti-inflammatory cytokine IL-10 increase with HD burden (Dalrymple et al. 2007; Bjorkqvist et al. 2008; Wild et al. 2011). Equally, these observations could be reflective of a dysregulation in chemokine signalling and thus compare favourably with reports of a lack of infiltration of blood myeloid cells into the HD brain (Lucin & Wyss-Coray 2009; Rocha et al. 2016); a phenomenon previously thought to be a consequence of impaired immune cell migration in HD (Wanda Kwan et al. 2012). Finally, altered chemokine signalling is likely to affect crosstalk between the HD microglia in the CNS and cells of the adaptive immune system, and potentially have an impact on the involvement of other immune cells in the striatum. Certainly, this view is supported by predicted deficits in the antigen processing and presentation machinery of the HD109 microglia, perhaps an adaptation to keep out infiltrating blood immune cells such as cytotoxic T-cells, NK cells and monocytes.

Expression of three important cytokines and chemokine receptors (CCR2, CX3CR1 and CSF1R) was increased in HD microglia, perhaps an indication of a proliferative and neuroprotective adaptation of the cells to the HD neuronal environment. Interestingly, a recent study showed in a rodent brain slice model that mutant HTT aggregation triggered by neuronal stressors led to increased IL-34 production and corresponding microglial proliferation, exacerbating degeneration of medium spiny neurons (Khoshnan et al. 2017). In addition, deletion of CCR2 has been shown to hamper microglial accumulation in a transgenic mouse model of

Alzheimer's disease, resulting in higher amyloid burden and increased mortality (El Khoury et al. 2007), implying that CCR2-dependent microglial accumulation can be neuroprotective. Of course, deletion of the fractalkine receptor CX3CR1 has been shown to regulate microglial activation in a mouse model of tauopathy (Bhaskar et al. 2010), while its overexpression suppresses activation and diminishes tau pathology (Nash et al. 2013).

The inflammatory response of the HD109 cells was subsequently validated, to investigate the hypothesis that HD microglia are primed for an exaggerated response to exogenous stimuli. Following stimulation with LPS, both HD109 and Kolf2 cells exhibited the expected M1 polarisation state featuring a similar upregulation in pro-inflammatory markers including CD40, ICAM1 and IRF1. In contrast, the same challenge appeared to induce a maintenance of the core microglial phenotype in the HD109 microglia, with neuroprotective and calming molecules such as SIGLEC12, CD22 and CX3CR1 being expressed at similar levels during and following LPS treatment, whereas the same genes were downregulated in the Kolf2 cells (Figure 4.5). Another particular point of difference in the HD109 inflammatory response profile was that the increase in TNF- $\alpha$  and IL-1 $\beta$  expression post LPS of a higher magnitude in Kolf2 compared to HD109 microglia. All things considered, it appears that the immune response of HD109 microglia is more tightly regulated to prevent excessive release of deleterious pro-inflammatory cytokines and loss of a neuroprotective signature. Cytokines such as TNF and IL-6 are contained in carrier vesicles that are trafficked to the cell surface for release (Stanley & Lacy 2010). Upon TLR-mediated LPS stimulation, carrier vesicles accumulate in the Golgi prior to release. Several molecules are involved in the vesicular transport of TNF-containing vesicles, including the lysosomal cysteine protease cathepsin B (Ha et al. 2008), which is downregulated in HD109 microglia. Given the importance of the Golgi network in cytokine trafficking, and given the fact that several Golgi and lysosome-associated proteins were found to be decreased in the HD109 cells, it is plausible that altered vesicle transport and trafficking pathways form part of the inhibitory mechanisms that regulate cytokine release in HD stem cell derived microglia.

The hypothesis that the HD CAG expansion results in a more neuroprotective microglial phenotype is further supported by findings from the upstream regulator analysis, which predicted inhibition of several inflammatory pathways and signalling cascades in the HD109

microglia (see Table 4.4). In particular, the TNF and LPS pathways, previously shown to be dysregulated in HD patient-derived monocytes (Miller et al. 2016), were predicted to be inhibited, in comparison with the Klf2 microglia cells. The NF $\kappa$ B pathway, another dysregulated pathway in HD immune cells (Trager et al. 2014), was similarly predictively inhibited. These results imply a protective anti-inflammatory phenotype in the HD109 cells, in stark contrast to the cell-autonomous pro-inflammatory state of HD mouse microglia cited in the literature (Crotti & Glass, 2015). This discrepancy intriguingly invites questions about the origin of this immune dampening effect – is this effect an accurate reflection of the HD microglial phenotype or an artefact of in vitro differentiation? If this is an HD microglia-specific effect, what are the mechanisms mediating it? The first question is the subject of the investigation in chapter 5. To answer the second question, one has to consider the crucial role of the brain microenvironment on the microglial phenotype.

Recent studies have intimated that neuronal co-culture highly modulates the transcriptome of iPSC-derived microglial cells, suppressing pro-inflammatory signalling pathways relative to monocultures (Abud et al. 2017; Haenseler et al. 2017). Despite the lack of neuronal co-culture in this differentiation protocol, the predicted inhibitory effects observed in our HD microglia dataset are evident when compared to the HD macrophage precursors upstream regulator analysis dataset (see appendix 4), demonstrating that the neuronal IL-34 is partly responsible for this particular inhibitory signal. In addition, it could be argued that in vitro microglia are protected from this mutant HTT-mediated priming effect due to their distinct ontogeny to other immune cell types. Indeed, the primitive macrophages used as precursors for differentiation in this protocol have been shown to arise from a MYB-independent, RUNX1 and SPI1 lineage (Buchrieser et al. 2017) that is separate from the MYB-dependent wave of haematopoiesis that gives rise to monocytes and macrophages (Orkin & Zon 2008). Therefore, it is plausible that the distinct ontogeny of microglia combined with the immune-privileged nature of the CNS and the fragility of the HD brain environment mediate the immune dampening and inhibitory effects observed on the transcriptome of HD iPSC-derived microglia.

# 5. EXPLORING THE EFFECTS OF CORRECTING THE HD MUTATION ON IMMUNE DYSFUNCTION IN iPSC- DERIVED HD MICROGLIA

## 5.1 Introduction

Huntington's disease is a fatal neurodegenerative disorder caused by expansion of a polymorphic CAG repeat tract in exon 1 of the huntingtin (HTT) gene (MacDonald et al. 1993). Though neurodegeneration in the HD brain primarily affects medium spiny neurons in the striatum, mutant HTT is broadly expressed, including in immune cells where its levels track with disease progression (Weiss et al. 2012). Thus, mutant HTT expression in cells of the immune system has been suggested to contribute to HD neuropathology. Activation of microglia, the brain's resident immune cells, as evidenced in HD post-mortem brains (Sapp et al. 2001), is not only widespread in symptomatic patients, but it also occurs years before disease onset in HD gene carriers (Pavese et al. 2006; Tai et al. 2007). Indeed, these pathological microglial changes mirror those reported in dysfunctional peripheral immune cells (Dalrymple et al. 2007; Bjorkqvist et al. 2008). Several studies have put forward convincing evidence for the peripheral and central immune systems acting as modifiers of HD pathogenesis. In 2012, Kwan and colleagues showed that transplantation of WT bone marrow cells attenuates motor deficits, enhances synaptogenesis and lowers plasma cytokine levels in HD mice (W. Kwan et al. 2012). An earlier study determined that inhibiting the enzyme kynurenine 3-monooxygenase (KMO), a key metabolite in the kynurenine pathway, is neuroprotective, resulting in reduced microglial activation, attenuated synaptic loss and a prolonged life span in HD mice, despite the inhibitor's inability to cross the BBB (Zwilling et al. 2011). Furthermore, signalling through the cannabinoid

receptor 2, expressed in microglia and peripheral immune cells and whose levels increase in post-mortem HD brains and mice, was recently shown to modulate immune activation (Palazuelos et al. 2009). Administration of a CB2 agonist dampened CNS inflammation and inhibited motor defects and synaptic loss in R6/2 HD mice (Bouchard et al. 2012).

The development of protocols for the differentiation of human iPSCs into several cell types of interest has unlocked new prospects in disease modelling. Nevertheless, one challenge of iPSC-based disease modelling that remains is the inconsistency in differentiation quality due to variations in genetic background (Kajiwara et al. 2012), which may affect the interpretation of in vitro diseased phenotypes. Moreover, the impact of genetic background on observed phenotypes in iPSC-based models can be substantial, even for a monogenic disease like HD where numerous disease-modifying loci alter age of neurological onset (GeM-HD Consortium 2015). This should therefore encourage the use of genetically identical control iPSC lines, to increase confidence and authenticate observed HTT-specific mechanisms and phenotypes. For this reason, work carried out within our lab by Jasmine Donaldson was successful in generating isogenic control iPSC lines from the HD109n1 iPSC line, which is heterozygous for the HD mutation with one WT allele of 21 CAG repeats and an expanded allele of 109 CAG repeats. Using a homologous gene-targeting approach, CRISPR gRNAs were used to target the 5' UTR and exon 1 sequences of the expanded HTT allele. The donor DNA featured a piggyBac transposon to allow a footprint-free removal of the selection cassette from the targeted locus. Targeted clones were identified by PCR amplification of exon 1 of the HTT allele, and following excision of the selection cassette by piggyBac transposase, correct footprint-free editing of the HD iPSCs was confirmed by Sanger sequencing and SNP array genotyping. In all, three isogenic HD109 corrected clones were generated (5H9, 3H2 and 2H1), along with a non-corrected HD iPSC line (11B11) that did not undergo piggyBac selection cassette to be used as an additional control HD iPSC line. All lines were validated for pluripotency and shown to retain a normal karyotype.

Successful correction of the HD mutation in iPSCs has been previously reported (An et al. 2014; Shin et al. 2016). Efforts to characterise the effects have focused on phenotypic abnormalities in iPSC-derived neural stem cells, namely impaired neural rosette formation, increased susceptibility to growth factor removal and mitochondrial respiration deficits (An et al. 2012; Mattis et al. 2015; Xu et al. 2017). In an attempt to assess the effects of HD correction on immune cell function, a study by the Tabrizi group used anti-HTT small interfering RNA to demonstrate that immune dysfunction and hyperactivity caused by NF $\kappa$ B dysregulation can be reversed by reducing mutant HTT expression in patient-derived monocytes and macrophages (Trager et al. 2014).

## 5.2 Aims

In chapter 4, RNA-seq was used to reveal any microglia-specific transcriptome changes associated with mutant HTT expression in the HD109 iPSC-derived cells. Pathway analysis identified several immune-related functions and pathways as being potentially impaired or dysregulated in these cells. Following on from this earlier work, this chapter had two principal objectives. Firstly, isogenic control HD corrected iPSC lines were differentiated into microglia in order to study the effects of correcting the HD mutation on the gene expression changes reported in the HD109 iPSC-microglia. Secondly, a series of experiments aimed to investigate the predicted impaired functions of HD microglia, characterise any potential impairments and ascertain the extent to which any phenotypic abnormalities were rescued by correcting the Huntington disease CAG expansion.

## 5.3 Results

### 5.3.1 Does correcting the HTT CAG expansion reverse the gene expression changes observed in HD109 iPSC-derived microglia?

The presence of the expanded CAG track in the HTT gene resulted in widespread changes in the transcriptome of the HD109 stem cell-derived microglia, as described in chapter 4. In order to disentangle whether these transcriptional changes were mutant HTT-specific or due to differences in genetic background between the HD109 and Kolf2 cells, isogenic control HD corrected iPSC lines were differentiated into microglia. As well as the three HD corrected clones (5H9, 3H2 and 2H1), one non-corrected HD iPSC line (11B11) was also used as control.

Initially, HD corrected microglia were assayed for expression of canonical markers by immunocytochemistry. As highlighted in chapter 3, treatment of macrophage precursors with IL-34 and GM-CSF results in robust expression of several microglial markers. Confocal imaging analysis of microglia derived from isogenic corrected iPSCs showed clearly that the IL-34 induced cells were positive for the microglial markers IBA1, P2RY12 as well as the leucocyte-specific CD45 (Figure 5.1). Also expressed was the microglia-enriched TGFBR1, a protein kinase receptor that binds the astrocyte-derived cytokine TGF- $\beta$  (Schilling et al. 2001) shown to be essential for microglial development and maintenance (Abutbul et al. 2012; Butovsky et al. 2014).

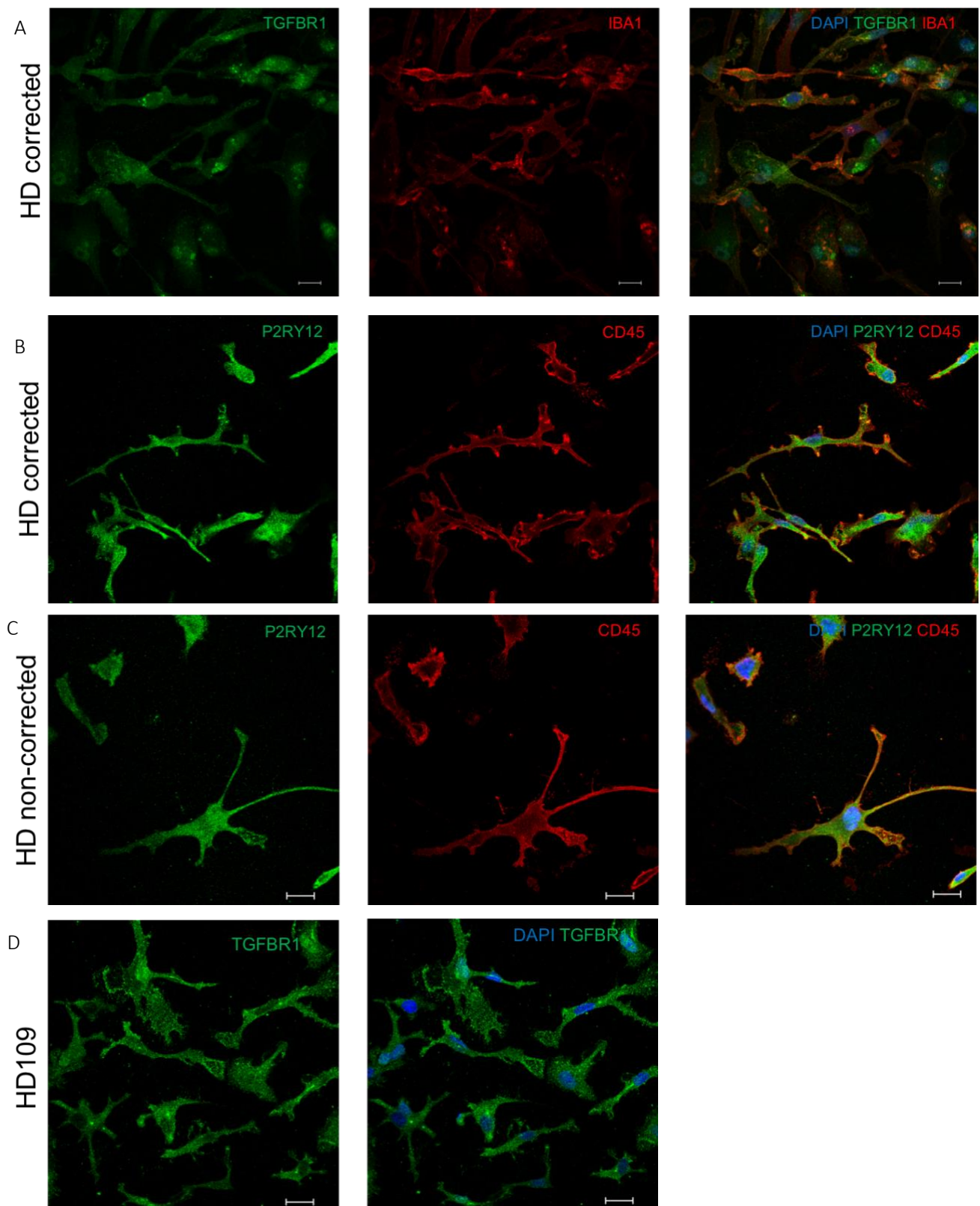


**Figure 5.1 HD109 Corrected and non-corrected iPSC-derived microglia express microglial markers and display the characteristic ramified morphology of microglia.**

(A-B) Confocal images of microglia-like cells derived from HD109 corrected lines 3H2 (A) and 5H9 (B) shows robust expression of MG markers IBA1, TGFBR1, P2RY12 and CD45. (C) Non-corrected HD iPSC-derived MG cells were cultured for 14 days in GM-CSF and IL-34, fixed and stained with P2RY12 and CD45. (D) HD109 MG cells express the MG-enriched protein kinase TGF- $\beta$  receptor 1. Scale bars represent 20  $\mu$ m.

Next, the expression of microglia-specific markers was analysed by Fluidigm qRT-PCR and results showed that genes such as C1QA, GPR34, MERTK, P2RY12 and CABLES1 were expressed at similar levels in the HD corrected microglia compared to Kolf2 and isogenic HD109 cells. Although its expression was decreased compared to THP1 monocytes, CX3CR1 followed a similar trend to other microglia sensome genes, with transcript levels consistent across cells of different genotypes (Figure 5.2 A-B). Also, two other sensome genes P2RY12 and ADORA3 found to be differentially expressed in the HD109 microglia after RNA-seq data analysis were expressed at comparable levels between the different genotypes.

The expression of AD risk genes in the HD corrected iPSC-derived microglia was assessed, with CLU and CR2 being identified as differentially expressed in the HD109 microglia compared to Kolf2. qPCR results showed that CLU expression did not vary markedly between the Kolf2, HD109 and HD109 corrected microglia samples. CR2 expression was not detected in THP1 monocytes and low in the microglia samples, with the highest expression in the HD109 microglia and transcripts levels in the corrected HD109 cells matching the low levels in the Kolf2 cells. However, these differences did not reach statistical significance (Figure 5.2C).

Findings presented in chapter 4 established that expression levels of NF $\kappa$ B genes were similar in Kolf2 and HD109 microglia (see section 4.3.2). Expression of the core microglial transcription factor PU.1 (SPI1) and its target genes, which is increased in HD mouse immune cells, was equally similar. When the same genes were evaluated in the corrected HD109 microglia by qPCR, results established that expression of both sets of genes were comparable to the WT Kolf2 and HD109 microglia (Figure 5.2 D-E). Overall, these results are consistent with the lack of altered NF $\kappa$ B signalling observed in HD109 microglia and suggest that reversal of the CAG mutation in HD microglia may not affect basal activation of pro-inflammatory signalling through NF $\kappa$ B.

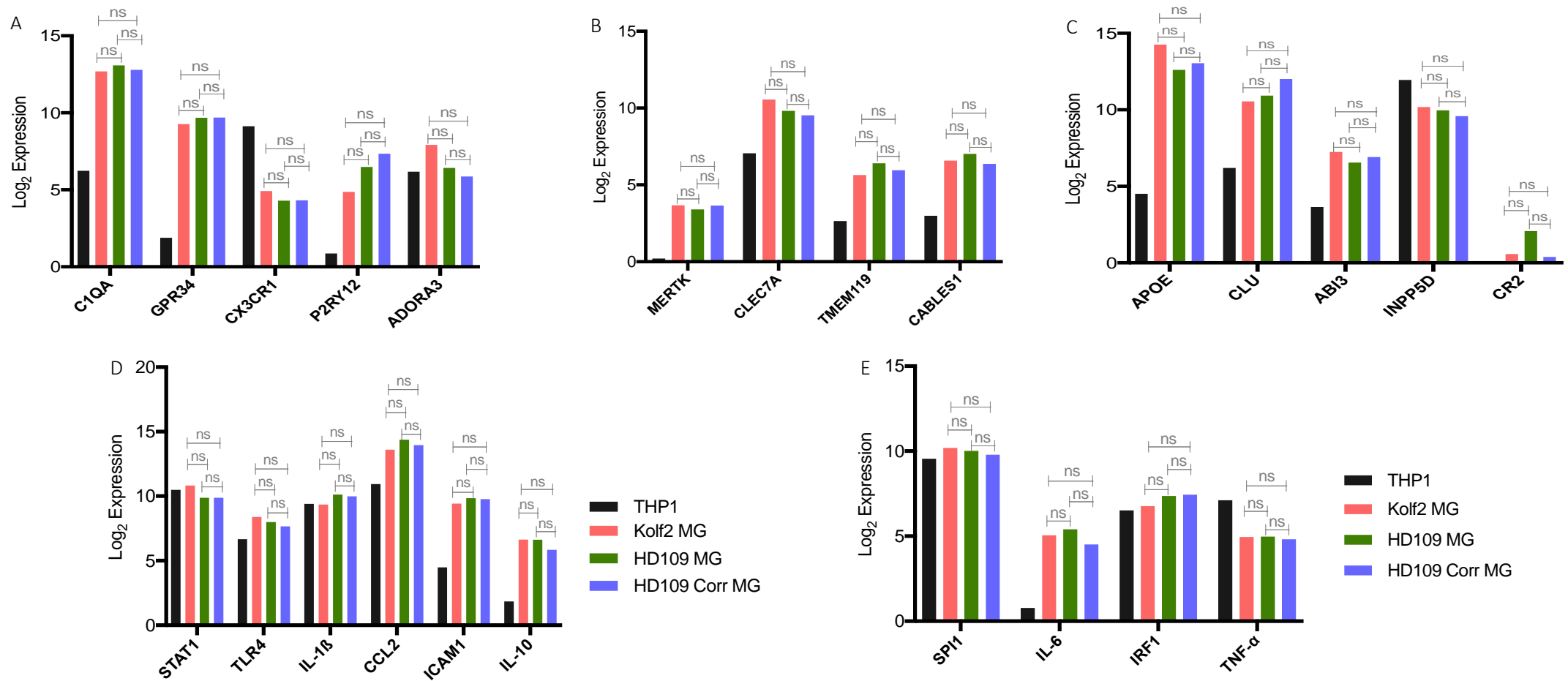


**Figure 5.2 The expression of canonical microglial and NFκB pathway genes is unaffected by reversal of HD CAG repeat expansion.**

Kolf2, HD109 and HD109 corrected MG cells were differentiated for 14 days in IL-34 and GM-CSF and all samples assayed by Fluidigm qRT-PCR. **(A-B)** No significant differences were found in the expression of microglia-enriched markers between HD109 corrected MG cells, Kolf2 and HD109 MG samples. **(C)** ABI3, CLU and CR2 were identified as DE in HD109 MG compared to Kolf2 by RNA-seq. Validation by qPCR shows comparable expression levels between HD109, Kolf2 and HD109 corrected samples. **(D)** NFκB pathway genes are comparably expressed in HD109 and isogenic corrected MG cells. **(E)** Expression of the TF SPI1 and of its target genes is unaltered in HD109 and following correction of the CAG mutation.

Log<sub>2</sub> Expression normalised to reference genes. Statistical analysis by two-way ANOVA with Tukey's multiple comparisons test. Asterisks denote significance: \* < 0.05, \*\* < 0.01, \*\*\* < 0.001, ns – not significant. n=3 biological replicates for all samples, except for THP1 (n=2).

### 5.3.2 Effects of correcting the HD mutation on the microglial inflammatory response under stimulatory conditions

Having previously established that HD109 microglia exhibited an inflammatory activation profile distinct from Kolf2 WT cells, the next set of experiments aimed at investigating the immune response of the HD corrected iPSC-derived microglia. 14-day-differentiated microglia derived from HD109 corrected iPSC were stimulated with 1  $\mu\text{g/ml}$  LPS for 4 hours, and the expression of pro-inflammatory markers compared to 4-hour LPS-treated Kolf2 and HD109 microglia. The activation profile of the corrected HD109 microglia was found to be consistent with that of Kolf2 and HD109 cells, with expected increases in the M1 markers IRF1, CCR7 and ICAM1 that were comparable in magnitude between the corresponding unstimulated and 4h LPS samples; the only notable difference being that CCR7 mRNA levels post LPS were significantly higher in Kolf2 vs corrected HD109 cells (Figure 5.3A). The two main pro-inflammatory cytokines TNF- $\alpha$  and IL-1 $\beta$  were upregulated after LPS stimulation in all three cell lines, with comparable mRNA levels post incubation (Figure 5.3B). Intriguingly, differences in the magnitude of these changes were again apparent, with a 3-fold upregulation in both genes for the WT Kolf2 and corrected HD109 microglia compared to a 2.5-fold increase in TNF- $\alpha$  and IL-1 $\beta$  for the HD109 cells. Inflammatory regulation of these two genes may therefore be an indication of the effects of correcting the CAG mutation on HD109 microglia. The other pro-inflammatory cytokines IL-8 and IL-6 were also upregulated after LPS incubation, with non-significant variations between the genotypes (Figure 5.3C).

The genetic background of the cells also seemed to dictate their LPS response. Whereas levels of the anti-inflammatory IL-10 and the pro-inflammatory CCL2 were unchanged in the LPS-treated Kolf2 cells, these two genes were correspondingly upregulated in the HD109 and isogenic corrected microglia (Figure 5.3D). Expression of the main anti-inflammatory cytokine IL-10 hinted at a balanced secretion of pro- and anti-inflammatory molecules. Fittingly, the upregulation of the chemokines CCL22 (in Kolf2 microglia only) and CCL18 (in all three samples) after LPS exposure seemed to support this idea (Figure 5.3E). To illustrate the segregation between the unstimulated and LPS-treated samples, a principal component analysis was carried

out, with the results plotted using a t-distributed Stochastic Neighbour Embedding (tSNE) (Van Der Maaten & Hinton 2008). The resulting plot showed close proximity between HD corrected microglia, HD109n1 and two Kolf2 microglia samples, hinting at a close similarity between the unstimulated microglia (Figure 5.3F). The LPS-treated samples from all three cell lines formed separate clusters that segregated according to genotype, which suggested that LPS treatment resulted in a HD corrected phenotype distinct from that observed in the WT Kolf2 and HD109 microglia. This therefore hinted at differences between the HD109 and the corrected microglia and demonstrated that correction of the CAG mutation on the HD gene had an effect on the phenotype of microglia.

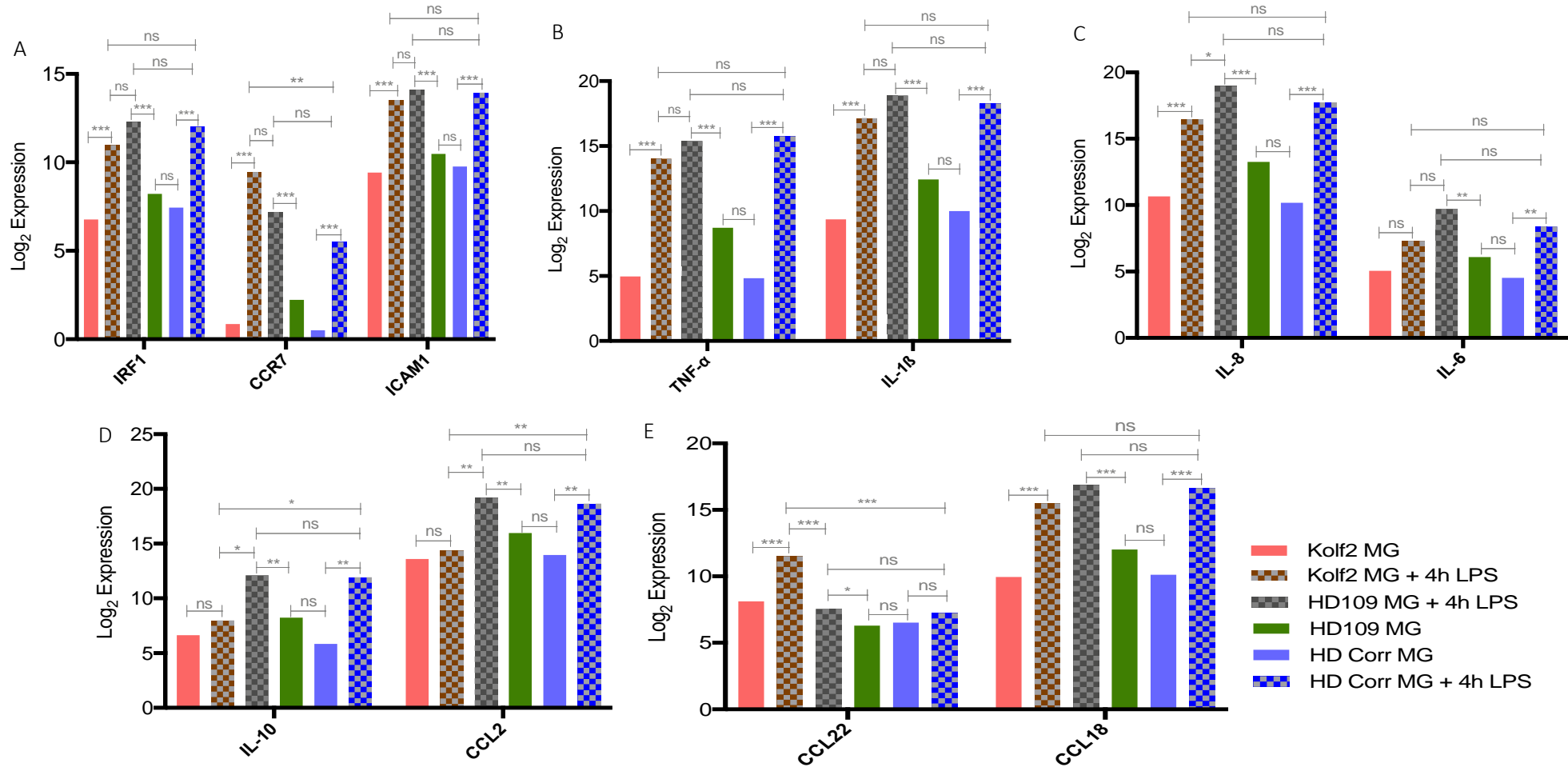
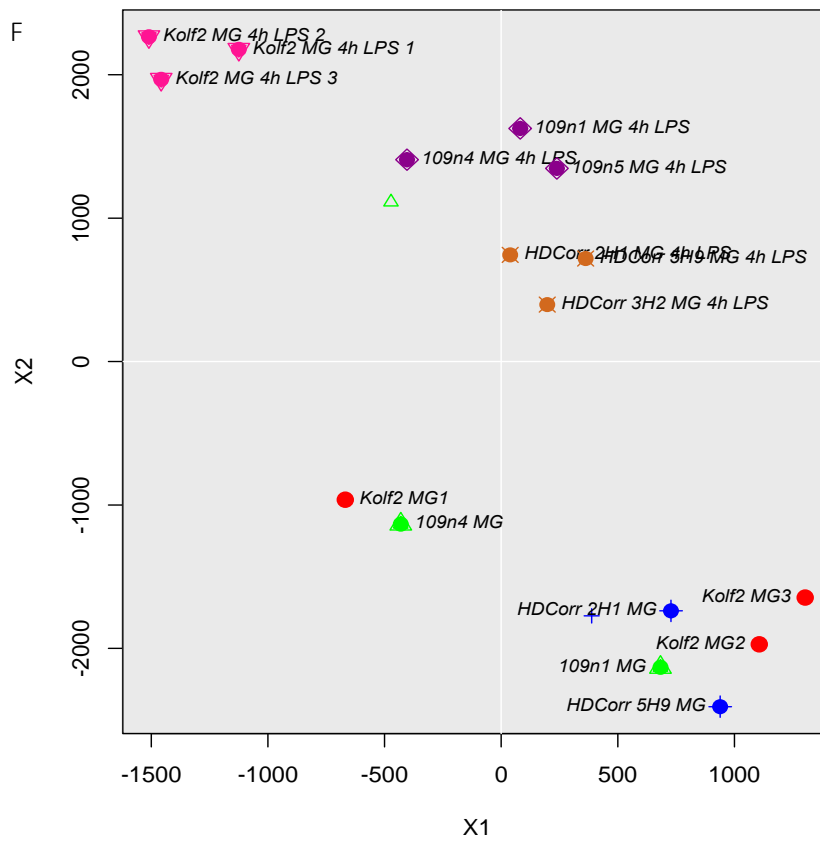


**Figure 5.3 The LPS inflammatory response of HD corrected microglia is similar to that of HD109 microglia.**

(A) 4h LPS stimulation of HD109 corrected MG cells leads to upregulation of IRF1, CCR7 and ICAM1 comparable with Kolf2 and HD109 cells. (B) Despite a trend towards lower expression of TNF- $\alpha$  and IL-1 $\beta$  in corrected compared to HD109 MG, no significant differences were found in expression of both genes in the corresponding LPS-treated MG samples. (C) Expression of the pro-inflammatory cytokines IL-8 and IL-6 did not vary significantly between the HD genotypes following LPS incubation. (D) LPS-induced changes in IL-10 and CCL2 expression are dictated by the genetic background of the MG cells; expression of both genes is upregulated in both HD genotypes and unchanged in Kolf2 cells. (E) Expression of the anti-inflammatory chemokine CCL18 is significantly increased in LPS-treated corrected MG cells and HD109 MG cells. Kolf2 MG cells upregulate CCL18 and CCL22 expression in response to LPS incubation.

Fluidigm qRT-PCR analysis used to generate log<sub>2</sub> Expression values normalised to reference genes. Statistical analysis by two-way ANOVA with Tukey's multiple comparisons test. Asterisks denote significance: \* < 0.05, \*\* < 0.01, \*\*\* < 0.001, ns – not significant. n=3 biological replicates for all samples.



**(F)** 4-hour LPS stimulation of *Kolf2*, HD109 and HD109 corrected microglia resulting in clustering effect, with MG samples segregating according to genotype. tSNE plot generated using “Fluidigm SC” package analysis of raw Ct data. Each data point represents one MG sample.

### 5.3.3 HD109 microglia do not manifest transcriptome-associated functional deficits in phagocytosis and chemotaxis

As described in chapter 4, several KEGG pathways were predicted through impact analysis to be impaired or dysregulated in HD109 microglial cells. These included cytokine-cytokine interaction, chemokine signalling, cell adhesion and ECM-receptor interaction as well as phagosome. Two pathways were chosen for functional validation: phagocytosis (FDR= 0.035) and chemotaxis (0.029). Levels of chemokines such as CCL17 and CCL18 were also downregulated in HD109 microglia, with qPCR results confirming that only one gene followed the same trend, with negligible CCL17 levels in the HD109 and corrected microglia compared to Kolf2. Elsewhere, transcript levels of CCL22 and CCL18 in HD109 and corrected cells matched those in Kolf2 cells (Figure 5.5A).

Phagocytosis is a key function of microglia, enabling clearance of pathogens, protein aggregates and apoptotic cells in the CNS. Differential gene expression identified downregulation of several phagocytosis-promoting receptors (FCAR, FCGR2B and FCGR2C, C1R, ITGA2, ITGA5, MARCO) in HD109 microglia compared to Kolf2 WT microglia. Interestingly, genes coding for the multi-ligand scavenger receptor CD36 and the enzyme NADPH oxidase or CYBB were upregulated. Validation of CD36 and CYBB expression by qPCR indicated that both genes were comparably expressed in the Kolf2 and HD microglia from both genotypes (Figure 5.4A). Also downregulated was CORO1A, a protein that initiates fusion of the phagosome to the lysosome during pathogen killing. These findings seemed to indicate a compensatory mechanism. To confirm this observation, phagocytosis of pHrodo red E. coli particles was monitored in real time using the IncuCyte S3 live imaging platform, which quantifies the increase in red fluorescence triggered by the uptake of pHrodo cells and internalisation into the acidic phagosome by professional phagocytes (Kapellos et al. 2016). Microglia from Kolf2, HD109 and HD109 corrected iPSCs were seeded on 96-well plates at 35,000 cells per well, differentiated for 14 days and then incubated with 10 µg pHrodo red particles for 6 hours while confocal images were taken every 10 min. All HD derived microglial cells (HD109, non-corrected and corrected) displayed a higher rate

of uptake compared to Kolf2 microglia, indicating that they retained efficient ability to phagocytose bioparticles (Figure 5.4B). Interestingly, Kofl2 WT cells pre-treated with the phagolysosome v-ATPase inhibitor bafilomycin A1 were capable of ingesting the fluorescent particles, though the final count of phagocytosed particles was significantly reduced compared to Kolf2 and all HD genetic backgrounds (two-way ANOVA with Tukey's post hoc test,  $p < 0.0001$ ). This was hypothesised to be due to the high cell density in each well (Figure 5.4C). Comparisons between the HD109n1 and the HD109 corrected clones showed that correction of the HD CAG mutation had no effect on the cells' ability to phagocytose bioparticles, despite clonal variations in pHrodo *E. coli* bioparticle uptake. This experiment was repeated with a lower number of 20 000 plated cells per well (Figure 5.5D). On this occasion, pre-treatment of the cells with bafilomycin A1 and cytochalasin D resulted in a larger reduction in fluorescence signal, demonstrating that the rate of bioparticle uptake is dependent on cell numbers (Figure 5.4E). At the peak of around 6 hours of incubation, MG cells from two of the HD109 corrected clones (5H9 and 2H1) ingested more particles than cells derived from the isogenic HD109 line. The HD109 corrected clone 3H2 phagocytosed less particles than cells generated from the parental HD109n1 ( $p < 0.0001$ ), although this rate of phagocytosis was found to be as efficient as that of the HD109 non-corrected iPSC-derived microglial cells ( $p = 0.5897$ ). To conclude, while clonal differences in the kinetics of pHrodo phagocytosis were evident, HD microglia have shown to be competent phagocytes of bioparticles.

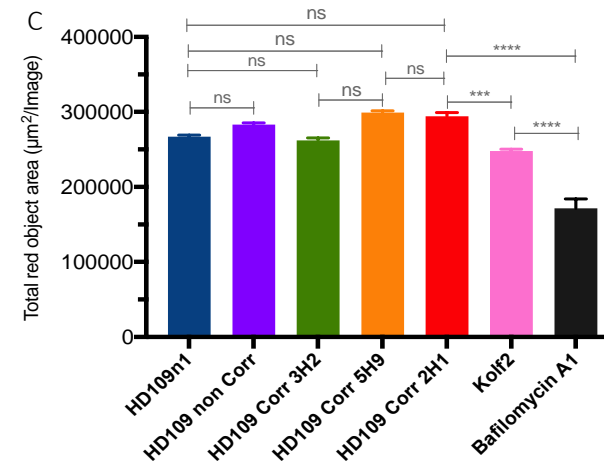
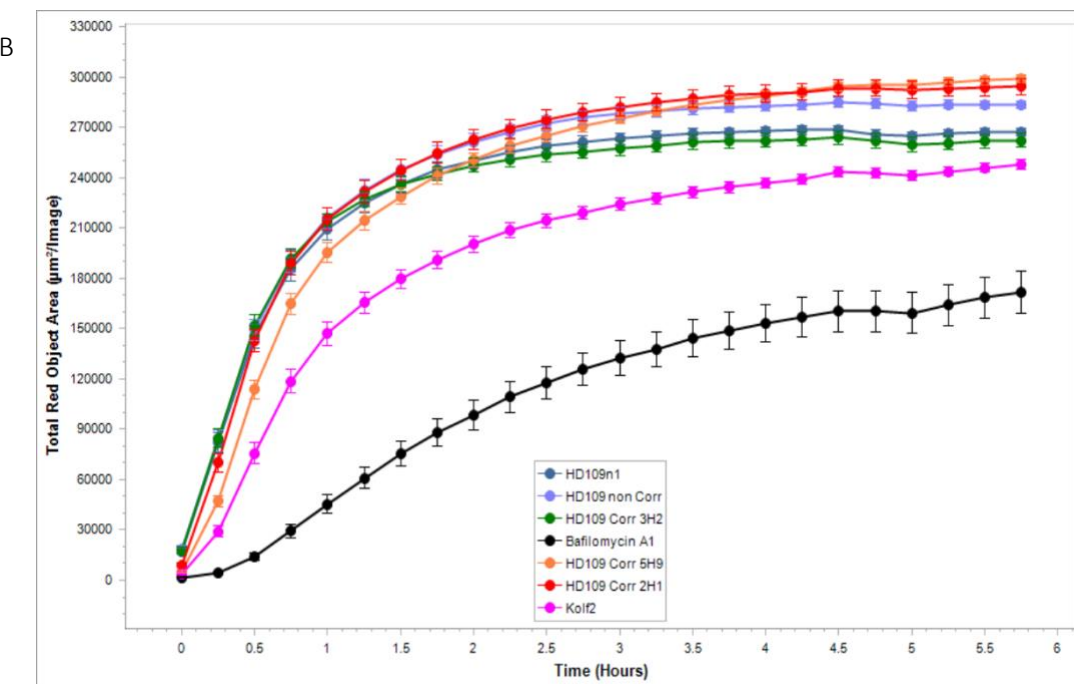
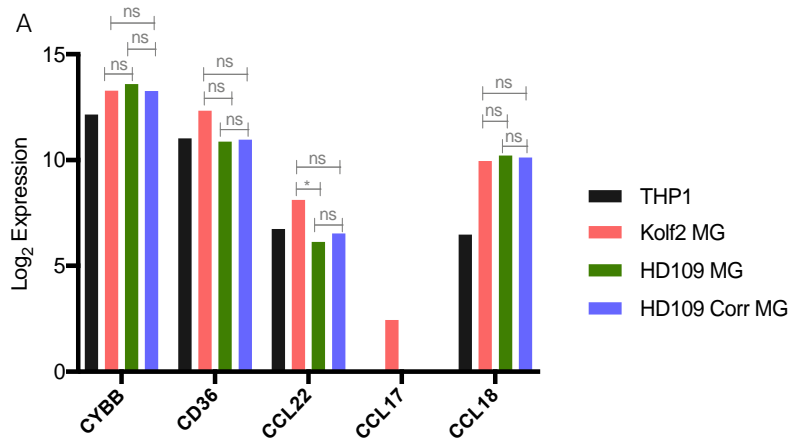
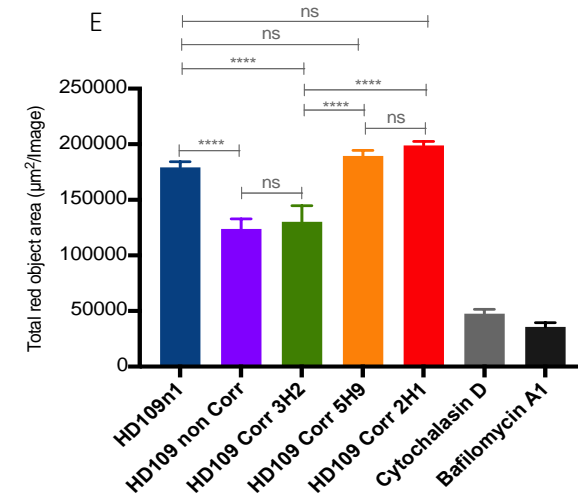
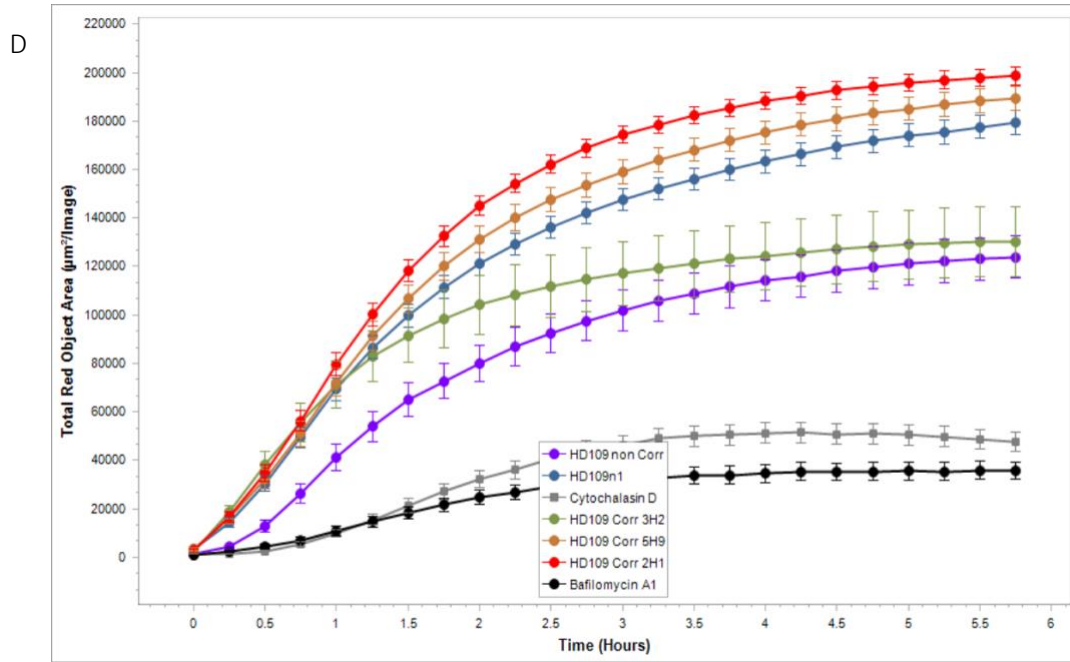
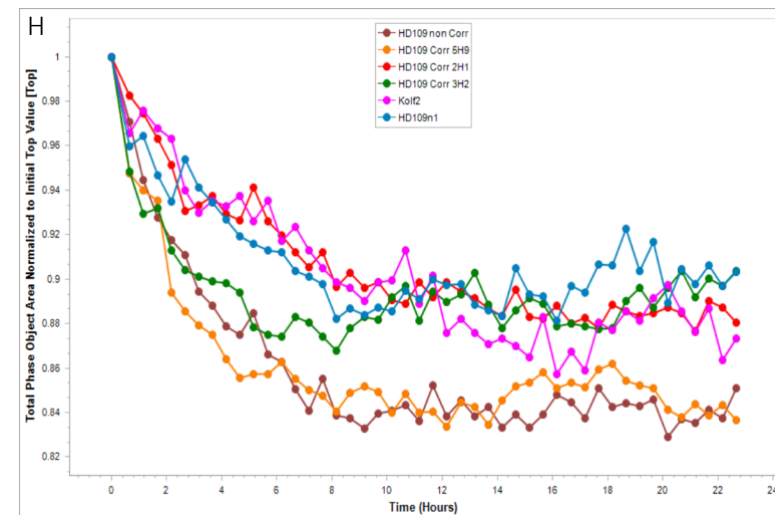
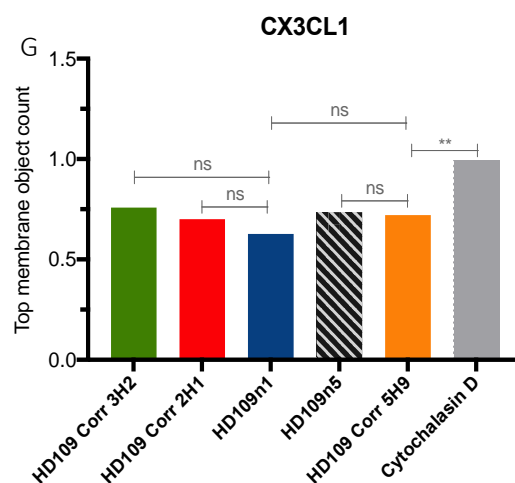
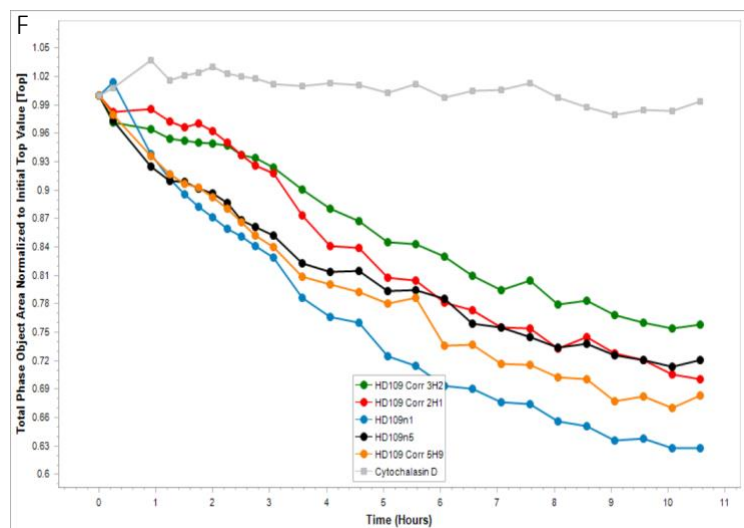


**Figure 5.4 Phagocytosis of *E. coli* bioparticles and chemotaxis are not impaired in HD109 iPSC-derived microglia.**

(A) qPCR validation of phagocytosis and chemokine transcripts shows expression of CCL17 and CCL22 is higher in Kolf2 MG than HD109 MG. CYBB and CD36 expression levels are comparable in HD109 and Kolf2 MG. (B) MG cells from HD109 and HD109 corrected iPSCs exhibit a higher rate of uptake of bioparticles than Kolf2 MG cells. MG cells were plated on a 96-well plate at 35,000 per well and incubated with 10 µg pHrodo *E. coli* for 6 hours. For negative control, Kolf2 MG cells were pre-treated with 10 µM bafilomycin A1 before 1hr before *E. coli* incubation. (C) End point fluorescence values from (B) were plotted. Data presented as mean ± SEM from each condition with 8 technical replicates. n=1 independent experiment.



**(D)** HD109 corrected microglia phagocytose *E. coli* bioparticles as efficiently as microglia derived from the HD109 parental clonal line. MG cells were plated at 20,000 cells per well. HD109 MG cells were pre-incubated with 10 µM cytochalasin D for 1hr before *E. coli* treatment. End point fluorescence values were plotted in **(E)**. Data presented as mean ± SEM from each condition or genotype with 8 technical replicates. n=2 independent experiments.



**(F)** HD109 and HD109 corrected MG cells display efficient cell migration in response to stimulation with CX3CL1. **(G)** End point (12h) values for top membrane index show that compared to cytochalasin D-treated MG cells, HD109 and HD109 corrected microglia retain proper chemotactic functions. **(H)** Chemotactic response of MG cells to ADP is unaffected in HD109 iPSC-derived microglia.

For pHrodo E. coli phagocytosis assays, red channel fluorescence (400ms) was measured every 10 mins in an IncuCyte S3 live imaging platform. Data was analysed using the IncuCyte S3 Base software (see section 2.5.3 for analysis parameters).

For chemotaxis assays, MG cells were plated and differentiated for 14 days on the upper chamber of 96-well ClearView chemotaxis plates. Cells were stimulated with 200 ng/ml CX3CL1 or 8  $\mu$ M ADP to induce migration to the lower chamber of the chemotaxis plate. Phase channel images were taken using IncuCyte S3 every 30 mins for 12-24 hours and quantified by IncuCyte analysis software. n=1 independent experiment.

Statistical significance was tested using two-way ANOVA with Tukey's multiple comparisons test. \* < 0.05, \*\* < 0.01, \*\*\* < 0.001, \*\*\*\* < 0.0001, ns – not significant. n=1 independent experiment.

Kwan et al. 2012 revealed using myeloid cells isolated from premanifest HD patients and early postnatal mouse microglia overexpressing mutant HTT that immune cells display mHTT-dependent deficits in migration to chemotactic stimuli. In order to characterise any potential impairments in chemotaxis in HD109 iPSC-derived microglia, cell migration assays were carried out using the IncuCyte S3 platform (see section 2.5.3). Microglial cells from Kolf2, HD corrected and HD109 iPSCs were differentiated for 14 days on a 96-well ClearView Chemotaxis, where each well is made up of a membrane that contains a lower and upper chamber. Cells are required to migrate across the membrane, through 8µm pores to reach the lower chamber, a process visualised and quantified in real-time by the IncuCyte analysis software. Migration in response to two chemoattractants, CX3CL1 and ADP was assayed. Cells stimulated with 200 ng/ml CX3CL1 were shown to be responsive to the chemotactic stimulus (Figure 5.4F), as shown by the reduced top membrane index (Figure 5.4G). When compared to cytochalasin D-treated MG HD 109 cells, all cell lines were found to be efficient at cell migration through the membrane. Interestingly, no significant variations in response were found between the HD109 and the corrected iPSC-derived microglia. Chemotactic response to ATP was then investigated. Along with CX3CL1, sphingosine-1-phosphate (S1P) and lysophosphatidylcholine (lysoPC), ATP and other nucleotides are so called “find-me signals” released by cells undergoing apoptosis that attract phagocytes towards them (Lauber et al. 2004). Chemotactic response of the HD MG cells to 8 µM ADP was quantified and results showed no statistically significant differences in the migration of HD109 and HD109 corrected microglia compared to Kolf2 WT microglia (Figure 5.4H). Overall, these results suggest that migration and regulation of actin remodelling of HD iPSC-derived microglia is not impaired, with no rescue effect of the CAG expansion excision on those properties.

#### 5.3.4 HD109 microglia do not exhibit deficits in mitochondrial respiration associated with other HD cell types

Mitochondrial dysfunction has been strongly implicated in HD pathogenesis, with impairments in ATP production, mitochondrial basal respiration and glycolysis among early reported disturbances in the HD brain (Damiano et al. 2010; Costa & Scorrano

2012). Studies in mouse models and post-mortem human brains have described mitochondrial impairments in several HD cell types, e.g. primary lymphoblasts, fibroblasts and striatal cells (Polyzos & McMurray 2017) and stem cell-derived neural stem cells (An et al., 2012; Xu et al. 2017). To date, impairments in HD microglia have not been extensively reported or characterised. Given the metabolic demands that homeostatic and immune functions place on microglia (Cherry et al. 2014), an investigation of the bioenergetics profile of HD109 microglia was performed to initially compare it to that of WT Kolf2 microglia (Figure 5.5A). For this series of preliminary experiments, microglial cells from Kolf2, HD109 and corrected HD109 iPSC lines were differentiated in Seahorse XF96 plates and responsiveness to the mitochondrial stressors oligomycin, FCCP and rotenone measured to calculate the oxygen consumption rate (OCR). The Seahorse XF Cell Mito Stress Test protocol was used (see section 2.5.4), which allows the assessment of different aspects of mitochondrial respiration, including basal respiration, maximal respiration, spare respiratory capacity and ATP production.

Though earlier results had hinted at the HD109 MG cells exhibiting a lower basal respiration rate, the preliminary examinations presented here showed that basal respiration was similar between the WT and HD109 microglial cells (Figure 5.5B). Microglia derived from the HD109n1 clonal line seemed to exhibit a greater mitochondrial spare respiratory capacity compared to cells derived from Kolf2, HD109n4 and HD109n5 lines, with a similar pattern emerging in the maximal respiration OCR rates between the lines (Figure 5.5C). ATP production rates were also comparable between the HD109 and Kolf2 WT MG cells (Figure 5.5D).

Similarly, the profile of HD corrected iPSC-derived microglia was compared to that of HD109n1, the parent clonal line (Figure 5.5E), with preliminary data showing small increases in maximal respiratory capacity for two out of three clones (Figure 5.5F), but no changes in ATP production or basal respiration (Figure 5.5 G-H). Taken together, these preliminary results into the bioenergetics profile of iPSC-derived microglia suggest that mitochondrial function may not be impaired in the HD109 microglia.

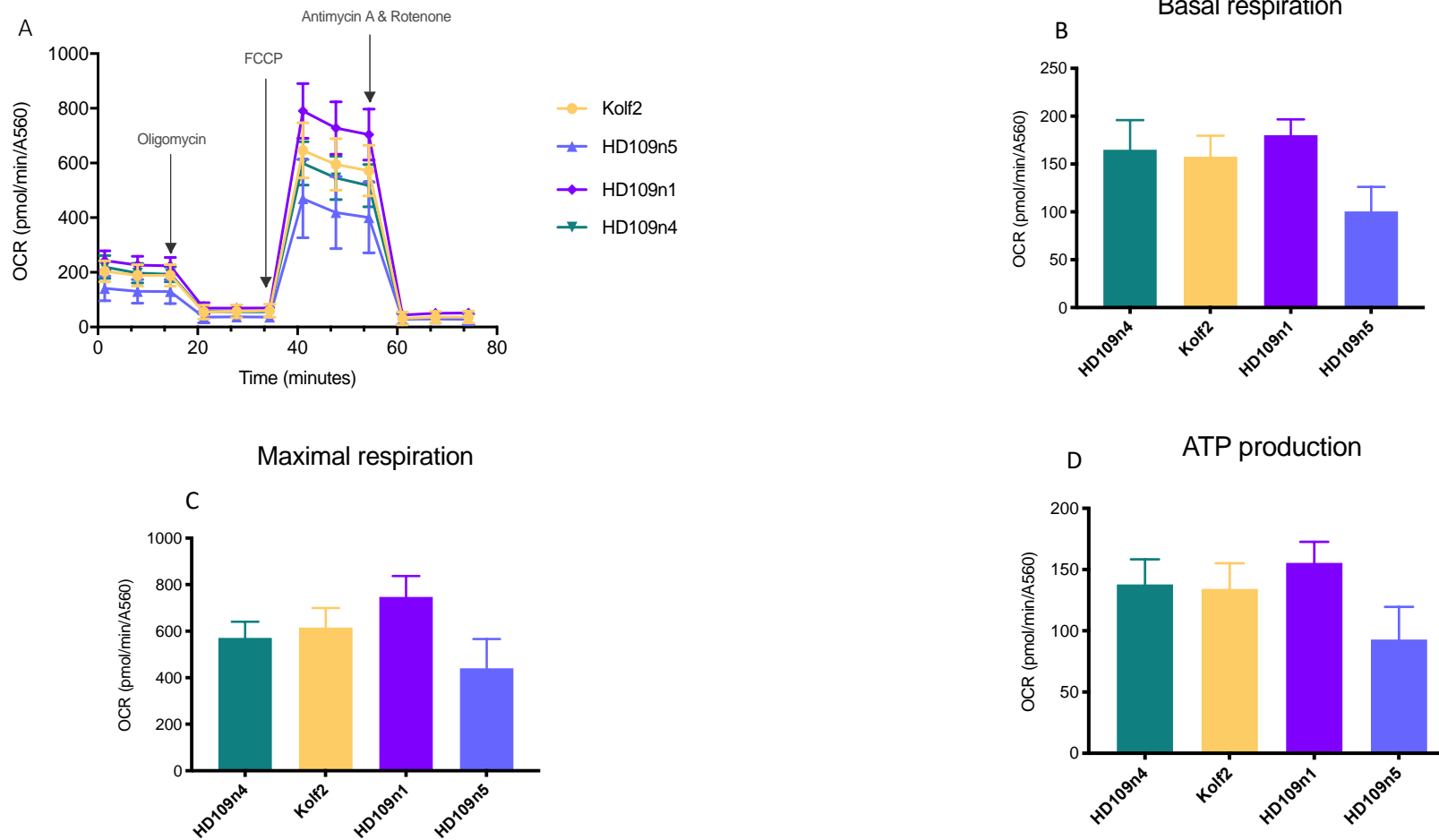
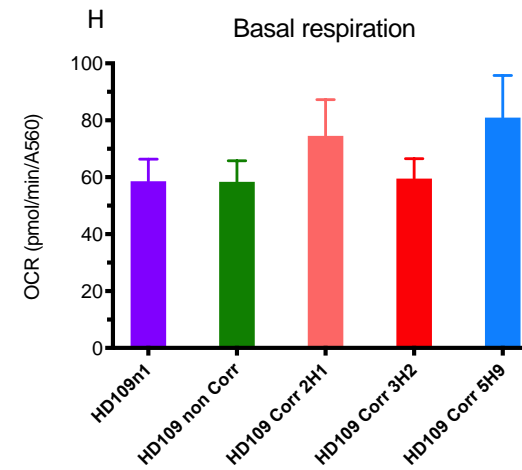
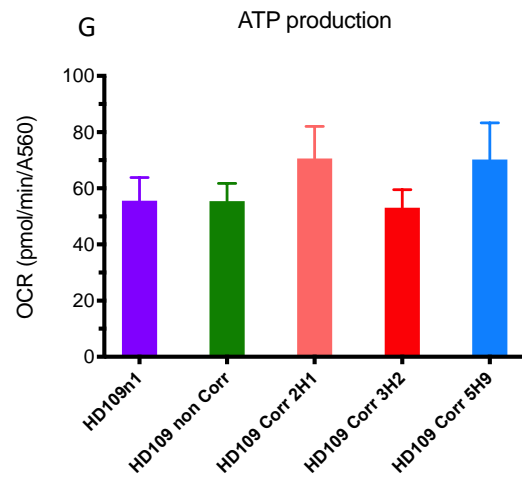
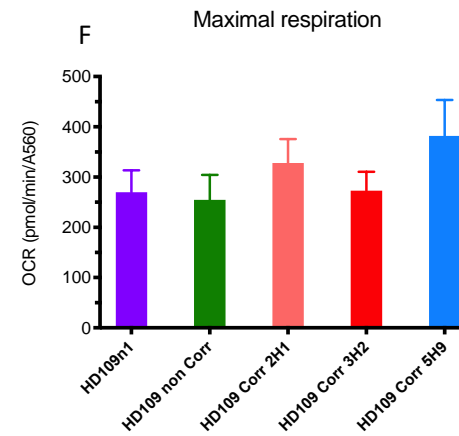
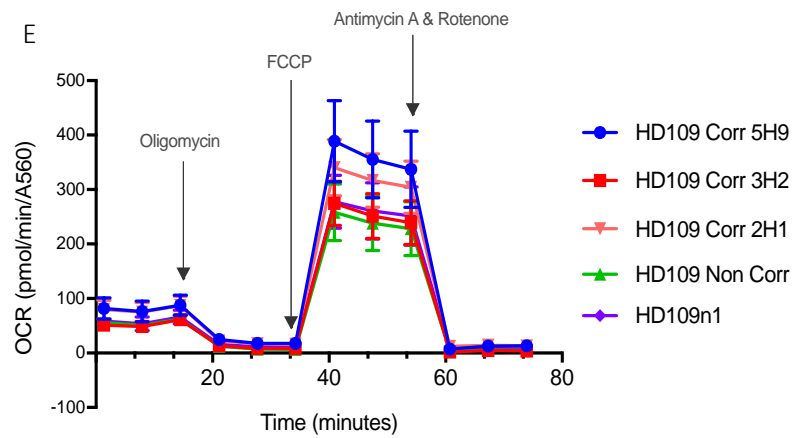


**Figure 5.5 Preliminary results show that mitochondrial oxidative phosphorylation is unimpaired in HD109 iPSC-derived microglia.**

MG cells (20,000 per well) were plated and differentiated on Seahorse XF 96-well plates. Oxygen consumption rate (OCR) was measured with sequential injections of 2  $\mu$ M oligomycin, 2.5  $\mu$ M FCCP and 0.5  $\mu$ M antimycin A & rotenone. **(A-D)** Measurements of basal respiration and ATP production show no differences between HD109 and Kolf2 MG cells. MG cells derived from HD109n1 iPSCs seemed to show greater maximal respiration rate than WT Kolf2 MG cells. Data presented as mean  $\pm$  SEM from each genotype with at least 8 technical replicates; OCR measures normalised to absorbance at 560 nm; n=1 independent experiment.



(E-H) Mitochondrial basal respiration, maximal respiration and ATP production rates in HD109 corrected microglia are comparable to measurements in the microglia cells derived from the parental clonal line HD109n1. n=1 independent experiment.

A complex interplay exists between the immune response and the major metabolic pathways of glycolysis, the TCA cycle, fatty acid synthesis and oxidation, amino acid metabolism and the pentose phosphate pathway. In particular, changes in the metabolites of these pathways have been shown to regulate the innate inflammatory response (Galván-peña & O'Neill 2014; O'Neill et al. 2016). For example, Tannahill et al. 2013 showed that LPS stimulation of mouse macrophages causes an increase in intracellular levels of the TCA cycle intermediate succinate, which subsequently drives production of IL-1 $\beta$  (Tannahill et al. 2013). Stimulation by LPS, which results in an M1 phenotype and is associated with expression of pro-inflammatory cytokines, is accompanied by a shift from oxidative phosphorylation to glycolysis for energy production, called the Warburg effect (López-Lázaro 2008). A second aspect of this shift during inflammation is mitochondrial dysfunction, whereby mitochondria are reprogrammed by undergoing fission, which induces formation of ROS and other inflammatory mediators such as NF $\kappa$ B (Park et al. 2013; Park et al. 2015). To investigate mitochondrial contribution to the energetic demands concurrent with inflammation, preliminary experiments were undertaken to study the effects of LPS stimulation on the bioenergetics of microglia. Cells were plated and differentiated on Seahorse XF96 plates for 14 days. After differentiation, the microglia were stimulated in situ with 1  $\mu$ g/ml LPS for 4 hours before measurements of mitochondrial respiration (Figure 5.6A). LPS challenge was found not to cause any changes in ATP production or basal respiration in the respective HD109 and Kolf2 microglial cells (Figure 5.6 B-C). A similar pattern was observed with microglia derived from the HD corrected iPSC lines (Figure 5.6 D-F). When comparing challenged and unstimulated cells, LPS stimulation only resulted in subtle differences in the maximal respiration rates (Figure 5.6E). Taken together, these preliminary experiments appear to indicate that LPS activation of in vitro microglia does not result in deficits in mitochondrial respiration.

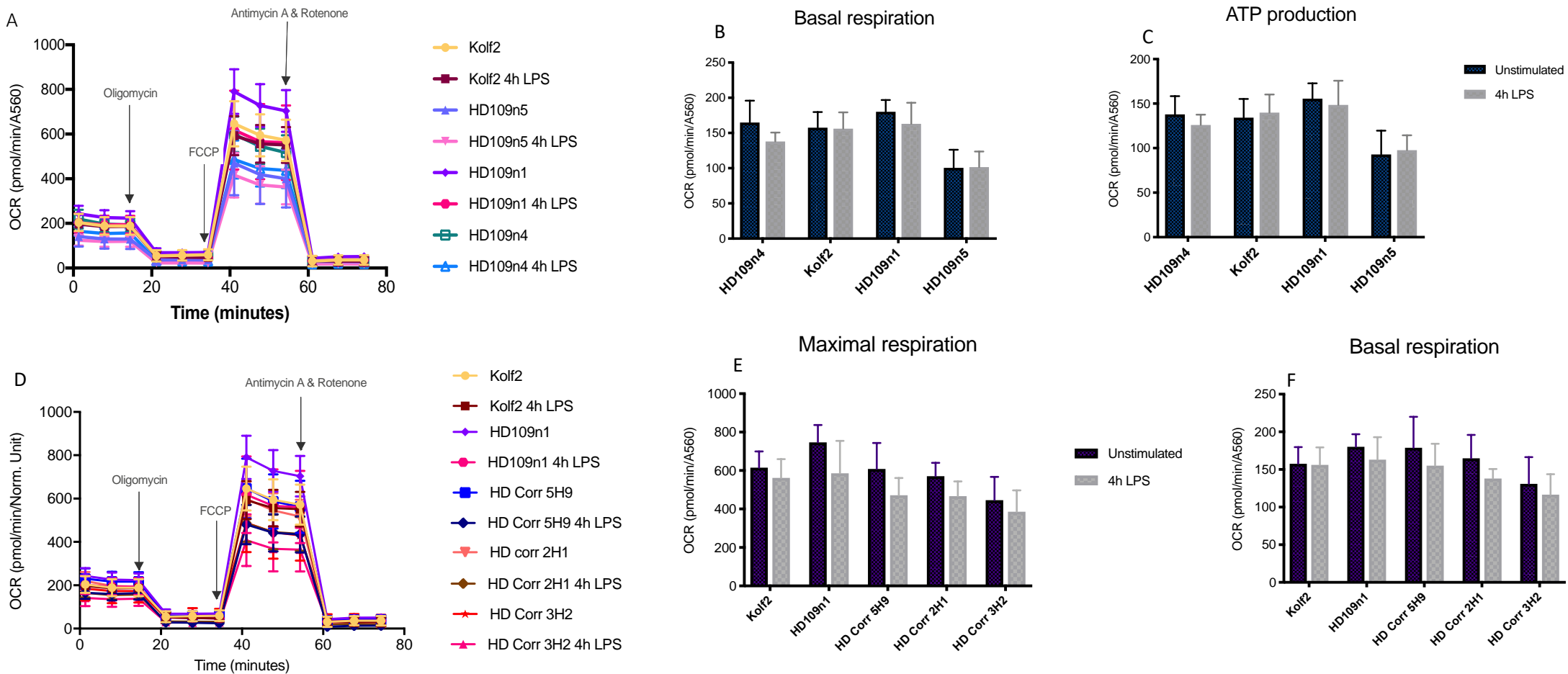


**Figure 5.6 LPS stimulation of iPSC-derived microglia does not seem to impair mitochondrial respiration.**

MG cells (20,000 per well) differentiated on Seahorse XF 96-well plates were stimulated with 1  $\mu\text{g/ml}$  LPS for 4 hours before OCR measurements. **(A-C)** Measurements of basal respiration and ATP production in HD109 and Kolf2 MG cells show that LPS stimulation does not affect mitochondrial function in iPSC-derived microglia. **(D-F)** Preliminary comparisons of mitochondrial respiration measures between HD109 and HD109 corrected microglia suggest that mitochondrial function is unchanged following LPS stimulation.

Data presented as mean  $\pm$  SEM from each genotype with at least 8 technical replicates; OCR measures normalised to absorbance at 560 nm; n=1 independent experiment.

## 5.4 Summary and Discussion

As described in chapter 4, pathway impact analysis of changes in the transcriptome HD109 microglia predicted potential impairments in crucial immune functions such as chemotaxis, antigen processing and presentation, phagocytosis. The work undertaken in this chapter was thus based on these transcriptomic findings and experiments were carried out to characterise any phenotypic and functional abnormalities in the HD109 microglia. In parallel, isogenic control HD corrected iPSCs, generated by CRISPR-Cas9 and piggyBac transposon editing, were used to derived microglia, with the aim of establishing the extent to which any functional abnormalities observed in the HD109 microglia could be rescued by correction of the HD CAG expansion mutation.

Differential gene expression of RNA-seq data highlighted decreased expression levels of several phagocytosis-associated transcripts in HD109 microglia, prompting questions about whether these expression changes could translate to an observed phenotype. This was assayed with pHrodo E. coli particles, where no functional abnormalities in the HD109 microglia were apparent. The lack of phenotypic manifestations of these transcriptional changes was first suggested to be due to the likely compensatory upregulation of CD36, CORO1A and CYBB, key genes in the phagocytosis pathway. Indeed, the scavenger receptor CD36 is crucial to engagement of apoptotic particles and the subsequent actin cytoskeleton signalling that facilitates phagocytosis (Stuart et al. 2007). In addition, it has been shown to mediate phagocytosis through interactions with TLRs (Erdman et al. 2009). However, qPCR validation of CD36 and CYBB revealed that mRNA levels of these two genes were similar in the Kolf2 and HD109 microglia. Alternatively, the absence of observed phagocytosis deficits may reflect the relatively young age of the microglial cells in the monocultures. Since iPSC microglial differentiation mimics embryonic haematopoiesis, it is conceivable that these phenotypic abnormalities would not manifest at the embryonic stage of microglial development, but rather later as the cells age and mature. Another point to consider is that phagocytosis has been shown to differ according to macrophage polarisation, whereby a slower rate of phagosome acidification and maturation is thought to facilitate antigen presentation (Canton

2014). Thus, it could be hypothesised that any phagocytic deficits in the HD109 microglia would become more apparent upon stimulation with LPS for example. Likewise, these deficits could be more evident in the inflamed environment of the HD brain, using viable humanised transgenic mouse models.

Similarly, cell migration in response to a chemotactic gradient was not altered in the HD109 microglia. Given that these microglial functions were intact in the HD109 microglia, it was unsurprising to discover that cells derived from corrected HD iPSC cell lines did not exhibit any impairments when chemotaxis was assayed in response to CCL5, ADP and CX3CL1. Despite transcriptomic evidence pointing to the contrary, these findings indicate that the CAG track expansion in the HTT gene is unlikely to impact the phagocytosis and chemotaxis-associated homeostatic functions of HD microglia. However, these results should also be analysed in the context of a recent study by Galatro et al. 2018, which analysed the transcriptome of human microglia isolated from aged patients and identified several age-related transcriptional changes in genes associated with actin cytoskeleton dynamics and cell motility. This could mean that ultimately the HD cells have either adapted to their transcriptome or, as with the prediction of phagocytic deficits, that the embryonic nature of the HD109 iPSC-derived microglia is masking manifestations of any potential deficits. Ultimately, these findings demonstrate that HD iPSC-derived microglia-like cells are competent immune cells capable of phagocytosis and chemotaxis.

There is currently little published data on the direct contribution of metabolic pathways to in vivo microglial function, an important area of research, given recent mouse model findings that variations in metabolic and bioenergetic pathways contribute to regional diversity in microglial population (Grabert et al. 2016). Furthermore, mitochondrial dysfunction has been strongly implicated in HD pathogenesis, with impairments described in several HD cell types but not microglia (Polyzos & McMurray 2017). The hypothesis that HD microglia would exhibit potential mitochondrial deficits was investigated in preliminary experiments, with the assay results suggesting that in vitro HD microglia did not present deficiencies in mitochondrial respiration. This implies that impairments in mitochondrial function

may be due to cell type specific effects of mutant HTT. These findings are in contrast to reports of impairments in HD iPSCs and iPSC-derived neural precursor cells (Xu et al. 2017). However, these results seem to align with our transcriptomic data where we found no differences in the expression of genes required for glycolysis and oxidative phosphorylation were found in the HD109 microglia dataset compared to Kolf2. They also confirm the intact metabolic capacity of HD109 microglia and are in agreement with other functional data proving the competency of HD microglia in phagocytosis, chemotaxis and inflammatory response. Exploratory mito stress results showed no changes in OCR levels in response to LPS activation, indicating that microglia maintain mitochondrial function under inflammatory stimulatory conditions in vitro. This suggests that the bioenergetic profile of human iPSC-derived microglia is distinct from that of mouse microglia (Orihuela et al. 2016; Park et al. 2013; Park et al. 2015) and macrophages (Everts et al. 2012; Everts et al. 2014). In those cells, inflammatory stimulation is characterised by a metabolic shift towards glycolysis for energy production, whereas preliminary results from proton efflux rate experiments hinted that microglia undergo a less pronounced glycolytic shift under stimulatory conditions (data not shown).

Aberrant NF $\kappa$ B signalling, which is mediated by mutant HTT transcriptional activity, is a widely reported feature of HD immune cells. In particular, mHTT expression leads to increased expression and transcriptional activity of the transcription factor PU.1 (SPI1) and results in higher expression of SPI1 target pro-inflammatory genes such as *Il6*, *Irf1*, *Tnf* and *Tlr2* in microglia isolated from new-born R6/2 mice, with similar findings reported in primary microglia derived from Q175/Q175 mutant mice (Crotti et al. 2014). Fluidigm qRT-PCR was therefore used to validate expression of genes belonging to this pathway, with comparisons made between Kolf2, HD109 and HD corrected microglial cells. It was found that expression of NF $\kappa$ B pathway and SPI1-target pro-inflammatory genes in the HD109 corrected were expressed at comparable levels to those in WT Kolf2 and HD109 microglia. Notably, these results were consistent with findings of a lack of pro-inflammatory NF $\kappa$ B-mediated signature in the HD109 iPSC-derived microglia, as described in chapter 4.

Mutant HTT expression in mouse models has been shown to have several other cell-autonomous effects on immune cells. These include a priming effect, such that the cells exhibit an exaggerated inflammatory response to exogenous stimuli (Crotti & Glass 2015). The same priming effect has been recapitulated in HD patient-derived monocytes (Miller et al. 2016). However, qPCR data from the LPS stimulation experiments revealed an activation profile similar to that of microglia derived from the parental clonal line HD109 iPSCs (Figure 5.3). Yet, principal component analysis of the LPS-treated samples showed a separation between HD corrected and HD109 LPS-treated samples, hinting at slight differences in the immune response of the cells. Given that the unstimulated HD corrected microglia clustered together with the HD109 microglia, these overall findings suggest that correction of the HTT gene CAG mutation did impact on the phenotype of the HD microglia, with these effects evident only after inflammatory stimulation.

Moreover, the LPS experiments indicated that aspects of the immune response of the *in vitro* microglia varied according to the genetic background of the cells. For example, whilst unaffected in the HD genotypes, LPS stimulation in the Kolf2 microglia led to increased expression of the CCR4 agonist CCL22, an inflammatory chemokine associated with M2 polarisation expressed by various cells (Mantovani et al. 2004). Likewise, this was noted for the M2a-associated chemokine CCL17 (data not shown), which also binds to CCR4 and is induced by production of IL-10 to inhibit M1 activation (Katakura et al. 2004). These observations may reflect a genotype-specific divergent regulation of immune response in microglia. Still, despite these genetic background-related differences, there were parallels in the LPS response of the three cell lines, centring around the upregulation of activation markers such as ICAM1, IRF1 and CCR7, and the pro-inflammatory molecules IL-8 and IL-6. In this regard, the response from all three cell lines exhibited a consistent M1 activation profile. Logically, this variability in microglial immune response across different iPSC lines highlights the need for careful thought and planning of experiments, especially those involving the use of non-isogenic control-matched iPSC models.

LPS exposure was also found to elicit expression of CCL18, induced by anti-inflammatory cytokines such as IL-4, IL-13 and IL-10 (Politz et al. 2000). The presence of this anti-inflammatory signature in an overall pro-inflammatory environment

suggests that the gene expression changes evident in the results do not take into account and/or may mask the immune response and behaviour at the single cell level. It is likely, that individual cells or a subpopulation of cells are driving the expression of specific anti-inflammatory mediators. In addition, based on the prediction of potential inhibition of specific inflammatory pathways in HD microglia, it may transpire that the transcription and inhibitory nuances sought after are more apparent at the level of the single cell, but may be masked overall. Therefore, future experiments should endeavour to investigate the transcriptome of LPS-treated HD109 and HD corrected iPSC-derived microglia at the single cell level, in combination with comparisons of bulk samples of HD corrected and HD109 iPSC-derived microglia. In addition, a proteomics approach using mass spectrometry analysis of culture supernatants could be integrated to these experiments, by assessing whether any gene expression changes observed at the transcriptomic levels match protein and cytokine expression at the level of the secretome.

Finally, it should be noted that while the results described herein have considered the downstream effects of their immune response, the transcriptomic data hinted at complex changes upstream of HD microglia's immune response genes. These could include transcription factor interactions and regulatory gene networks, which could be the focus of future transcriptomic studies of HD109 and corrected iPSC-derived microglia. Several analysis tools are available to help with these imputations, for example weighted gene co-expression network analysis or WGCNA, which can be used for finding clusters of highly correlated genes and identifying patterns of expression (Langfelder & Horvath 2008). Another example is the Bioconductor package CoRegNet, which analyses large-scale gene expression datasets and imputes the transcriptional co-regulator networks responsible. It integrates data from CHIP and TF binding sites (Nicolle et al. 2015). These packages could be used in conjunction with the upstream regulator analysis from IPA to build a more complete map of the transcriptional changes specific to the HD microglia.

# 6. INVESTIGATION OF THE EFFECTS OF ABCA7 LOSS-OF-FUNCTION IN HUMAN IPSC-DERIVED MICROGLIA

## 6.1 Introduction

Phagocytosis is an important and highly complex process central to several biological processes, including development, tissue homeostasis and innate immunity. Mechanistically, it involves the recognition and ingestion of particles larger than 0.5  $\mu\text{m}$  into membrane-bound vacuolar structures known as phagosomes. It is primarily performed by professional phagocytes, a subset of cells that comprises monocytes, macrophages, dendritic cells, neutrophils, eosinophils and osteoblasts (Rabinovitch 1995). Phagocytes express a spectrum of distinct receptors that mirrors the diversity of particles they encounter, ranging from foreign pathogens such as bacteria and yeast to apoptotic cells.

As the resident phagocytes of the CNS, microglia express a range of PRRs, PAMPs and DAMPs (see section 1.2.4) that facilitate particle recognition, engagement and initiation of appropriate downstream signalling. Their phagocytic ability is thus crucial in modulating their response to apoptotic or damaged neurons (Stolzing & Grune 2004; Fraser et al. 2010), harmful protein aggregates such as amyloid beta (Ard et al. 1996), as well as the capacity to shape neural circuits (Paolicelli et al. 2011; Schafer et al. 2012). Following on from the notion of microglial phagocytosis being essential to normal brain health, variants in phagocytosis-related genes such as TREM2 and CD33 have been identified as risk factors for Alzheimer's disease (Kleinberger et al. 2014; Griciuc et al. 2013).

First identified as a risk factor for AD by two genome-wide association studies in 2011 (Naj et al. 2011; Hollingworth et al. 2011), and later by Lambert et al. 2013, ABCA7 is one of four risk loci significantly associated with plaque burden in Alzheimer's disease,

alongside CR1, APOE and CD2AP (Shulman et al. 2013). The common ABCA7 GWAS risk allele rs3764650G, located in intron 13, is associated with reduced expression in the brain and increased plaque burden (Vasquez et al. 2013), suggesting that lower levels of ABCA7 protein may underline increased disease risk. Fittingly, rare loss-of-function coding variants were found in a Belgian cohort by Cuyvers et al. 2015, demonstrating that several ABCA7 coding mutations segregate with disease in an autosomal dominant manner. Some of these findings were replicated in an Icelandic cohort (Steinberg et al. 2015), while a recent study by the European Early-Onset Dementia consortium identified ten novel deleterious ABCA7 mutations (Figure 6.1) (Roeck et al. 2017). Le Guennec et al. 2016 performed a meta-analysis of recently published data from France and Belgium cohorts to find that ABCA7 rare loss-of-function variants of ABCA7 account for around 3% of AD cases (Le Guennec et al. 2016). These and more recent early onset AD findings from Bellenguez et al. 2017 provide strong genetic evidence that ABCA7 mutations significantly contribute to AD risk (Bellenguez et al. 2017).

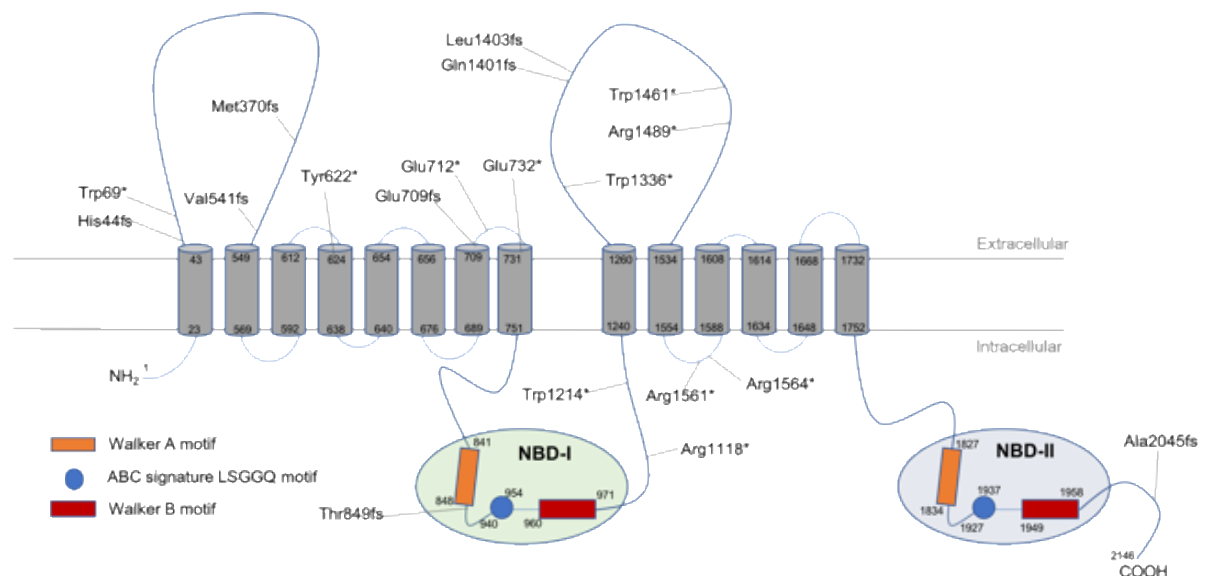


**Figure 6.1 Schematic representation of rare loss-of-function variants in ABCA7.**

Loss-of-function variants identified by Steinberg et al. 2015, Cuyvers et al. 2015 and Roeck et al. 2017. fs denotes frameshift mutations; \* denotes nonsense mutations. Figure adapted from Cuyvers et al. 2015; Aikawa et al. 2018.

ABCA7 encodes ATP-binding cassette transporter A7, a member of the ABC transporter superfamily involved in the transport across cell membranes of a variety of substrates ranging from small molecules such as amino acids and sugars to larger compounds including peptides, oligonucleotides and lipids (Dean & Annilo 2005). Its expression can be detected in several tissues including thymus, spleen and the brain, where it is most abundant in microglia (Kim et al. 2006). Structurally, ABC transporters are organised into four functional units: two nucleotide-binding domains (NBDs) and two transmembrane domains (TMDs). The NBDs or ATP-binding cassettes are highly conserved in sequence and structure across all ABC transporters, with each composed of seven motifs that include the Walker A, Walker B and ABC signature LSGGQ motif (Beek et al. 2014). The  $\alpha$ -helices of the two TMDs are arranged such that they form a transmembrane pore accessible either from the cytoplasm (inward-facing conformation) or the outside of the cell (outward-facing conformation) (Rees et al. 2009).

ABCA7 has previously been shown to regulate phagocytosis of apoptotic cells. Jehle et al. 2006 demonstrated that *Abca7*<sup>+/-</sup> mice-derived macrophages exhibit a deficiency in the phagocytosis of apoptotic Jurkat T cells and neutrophils. Similarly, Iwamoto and colleagues have shown that siRNA-knockdown of ABCA7 in BALB/3T3 fibroblasts significantly reduces phagocytic activity (Iwamoto et al. 2006). Studies assessing ABCA7 function in AD mouse models have shown that ABCA7 deletion increases amyloid plaque load (Kim et al. 2013; Li et al. 2015; Sakae et al. 2016). Importantly, ABCA7 deficiency has been shown to impair A $\beta$  phagocytosis in mouse macrophages and microglia, suggesting that ABCA7 may play a role in phagocytic clearance of amyloid from the brain. However, given the lack of direct mechanistic evidence for the link between ABCA7 and microglial phagocytosis, more work is required to further our understanding of the role of ABCA7 in microglia and of its contribution to the pathogenesis of Alzheimer's disease.

## 6.2 Aims

The objective of this chapter was to investigate the function of ABCA7 in human microglia derived from iPSCs. ABCA7 single and double allele KO iPSC lines were

generated by CRIPSR-Cas9 genome editing and validated. Microglia were subsequently differentiated from the successfully generated ABCA7-edited clones and the cells used to analyse the effects of these ABCA7 mutations on phagocytosis, immune response and lipid metabolism.

## 6.3 Results

### 6.3.1 Generation of ABCA7 KO iPSC lines by CRIPSR-Cas9

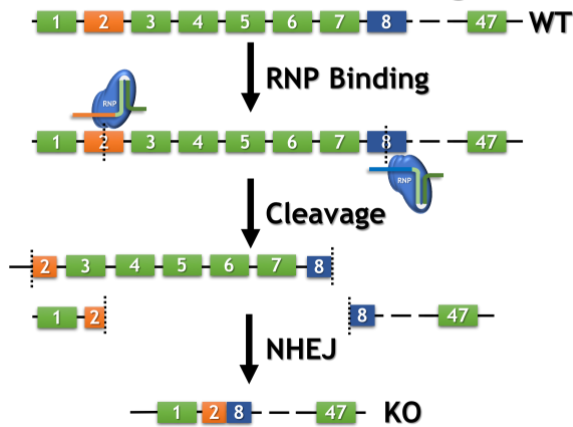
The full length (type I) ABCA7 encodes a protein of 2146 amino acids (Abe-Dohmae et al. 2006). Ikeda et al. 2003 detected a splicing variant of the protein (designated type II), with a translation initiation codon between exon 5 and 6 of the full-length isoform. This novel N-terminus in type II ABCA7 is thought to affect both the size, subcellular localisation and lipid release function of the protein. To generate a loss-of-function allele of ABCA7 in iPSCs, two CRISPR guide RNAs were designed to target the coding exons 2 (Ex2P1) and 8 (Ex8P1) in the N-terminus of the protein. The guide RNAs were chosen as they were predicted to have no potential off-target sites – this was confirmed by using the Cas-OFFinder algorithm (Bae et al. 2014) (<http://www.rgenome.net/cas-offinder/>). In addition, this combination of gRNAs would result in a successful excision of a 2.4kb region at the 5' end of the gene and a subsequent frameshift mutation (Figure 6.2A).

Following transfection and the first round of single colonies picking and screening (see section 2.8.2), 9 clones were initially identified as potential ABCA7 positive KO by PCR screening, from which four (2G, 7G, 11H and 12H) were chosen for sub-cloning onto 10 cm culture dishes (Figure 6.2B). A total of ~ 200 single sub-clones were picked from this pool (48 colonies per clones) and PCR screened for successful ABCA7 excision. A number of potential KO positive sub-clones were identified by PCR screen, from which 4 mutant clones were expanded and re-screened to confirm excision of the intervening DNA between exons 2 and 8 (Figure 6.2C). The PCR fragments from these screens were sequenced to reveal the Cas9 cleavage sites on ABCA7 exon 2 and exon 8 loci. Sequencing results revealed a great degree of variability in the Cas9 cleavage sites between clones. Cleavage resulted in identical sequences for two clones 11H-7C and 11H-11B, with the Cas9 cleaving the target sequence 5 base pairs upstream of the PAM sequence and the insertion of two base pairs (Figure 6.2D). In both cases, the

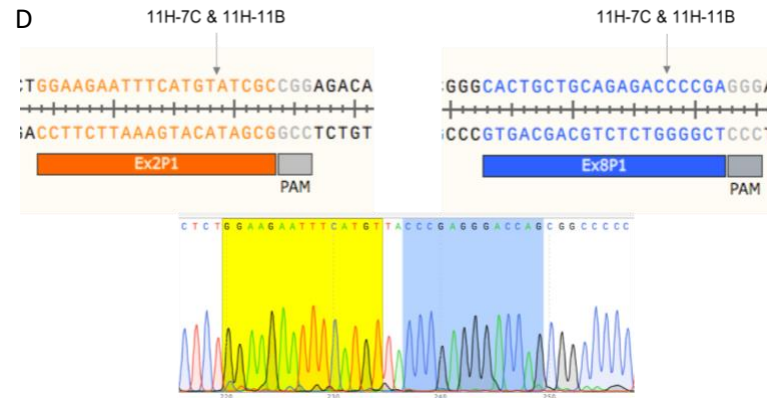
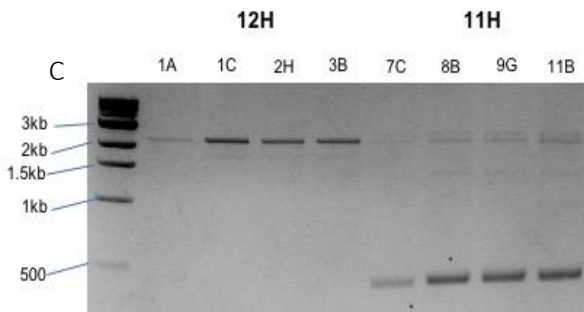
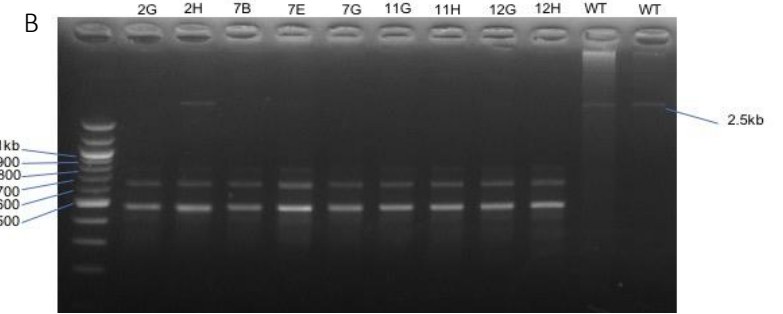
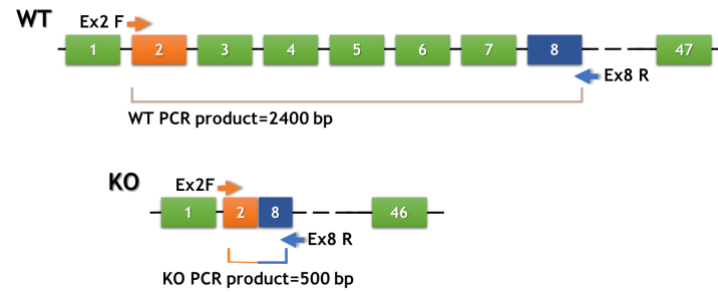
mutation would result in a premature stop codon. Sequencing for the third single KO clone 11H-9G showed the Cas9 cut site to be 3 base pairs upstream of the PAM sequences in both exons 2 and 8 (Figure 6.2E), resulting in a frameshift mutation, as verified using the CRISPR-mediated indel detection tool CRISPR-ID (Dehairs et al. 2016).

ABCA7 double KO alleles were generated using the same strategy, by submitting the ABCA7 heterozygous clone 11H-11B to a round of transfection, picking and screening, followed by sub-cloning and expansion of potential double KO positive clones. PCR screening showed the presence of single 500 bp bands indicative of successful excision of the target region between the exons 2 and 8 of ABCA7 gene (Figure 6.2F). The double KO clones identified in this way were subsequently sequenced: clones T2-9G and T2-11B returned similar sequences, as shown in Figure 6.2G. On the other hand, sequencing for the T2-1F and T2-1G clones revealed the Cas9 cut site for the exon 8 Ex8P1 guide RNA to be located three base pairs upstream of the PAM site, with the exon 2 cut site five base pairs upstream of the CGG sequence (Figure 6.2H). To further differentiate between heterozygous and homozygous ABCA7 mutants, an additional PCR screen was carried using the Ex2F forward primer and Ex2R reverse primer, which binds in the guide RNA-targeted region (Figure 6.2I). PCR products of 800 bp could be detected for WT Kolf2 and ABCA7<sup>+/-</sup> cells, with no bands detected for the homozygous clones T2-1F, T2-9G and T2-11B.

## A CRISPR KO Design



## ABCA7 KO Screening



Normal ABCA7 protein sequence

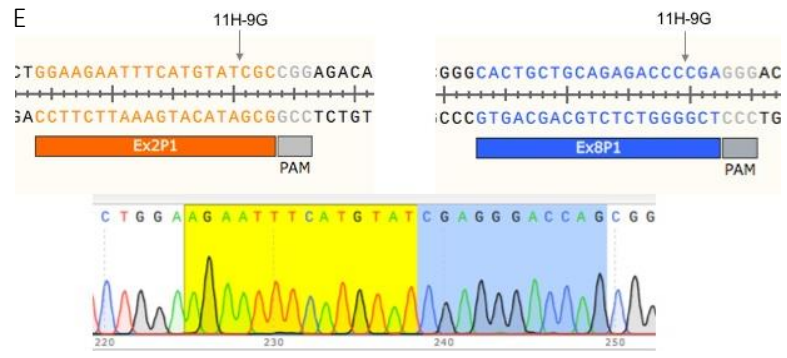
MAFWTQLM~~LL~~LWKNFMYRRRQPVQLLVE~~LL~~WPLFLFFILVAVRHSHP  
PPLHHECHF~~PN~~KP

11H-7C & 11H-11B clones

MAFWTQLM~~LL~~LWKNFMYPDGPAAPWSCCQRPSAVSGDLAAQ  
WAPRSTGTRLVT|Stop|

**Figure 6.2 CRISPR/Cas9-edited generation of ABCA7 knock out mutants in Kolf2 iPSCs.**

(A) Guide RNAs (Ex2P1 and Ex8P1) were designed to target exons 2 and 8 at the N-terminal end of ABCA7 in Kolf2 iPSCs. Successful Cas9 cleavage would result in deletion of a 2.4kb region that could be identified by PCR screen using Ex2F and Ex8R primers flanking the target DNA sequence to give a knock out PCR fragment of 500 bp and WT fragment of 2400 bp. (B) Following transfection and picking of single colonies in a 96-well plate, 9 clones were identified as potential KO clones by the initial PCR screening – targeted efficiency of 9%. From those potential clones, four (2G, 7G, 11H and 12H) were selected for sub-cloning on 10 cm TC dishes and single colonies picked for further screening. (C) 200 sub-clones were picked and screened, with four 11H sub-clones identified as potential ABCA7<sup>+/-</sup> mutants. (D) Sequencing analysis showed Cas9 cleavage sites for 11H-7C and 11H-11B ABCA7<sup>+/-</sup> mutants were 5 bp upstream of PAM sites, with 2 bp insertion. The mutated DNA sequence would result in the insertion of a premature stop codon in the translated protein.

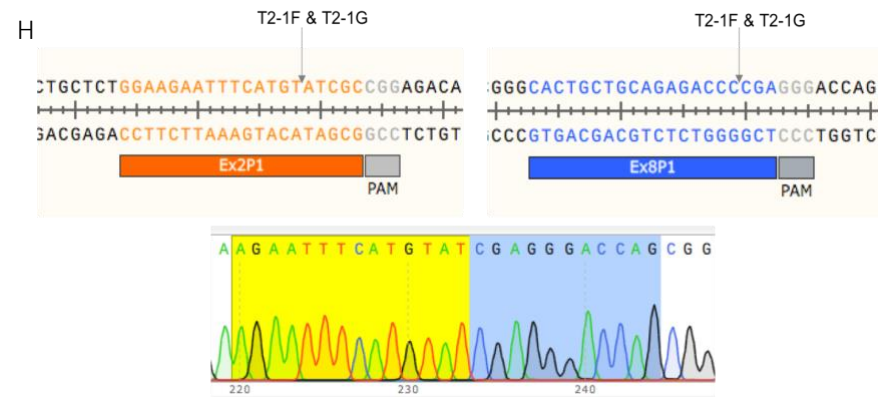
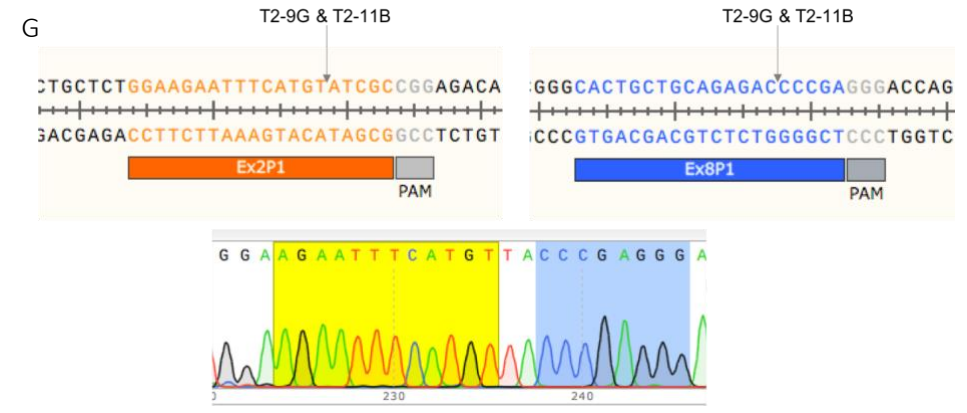


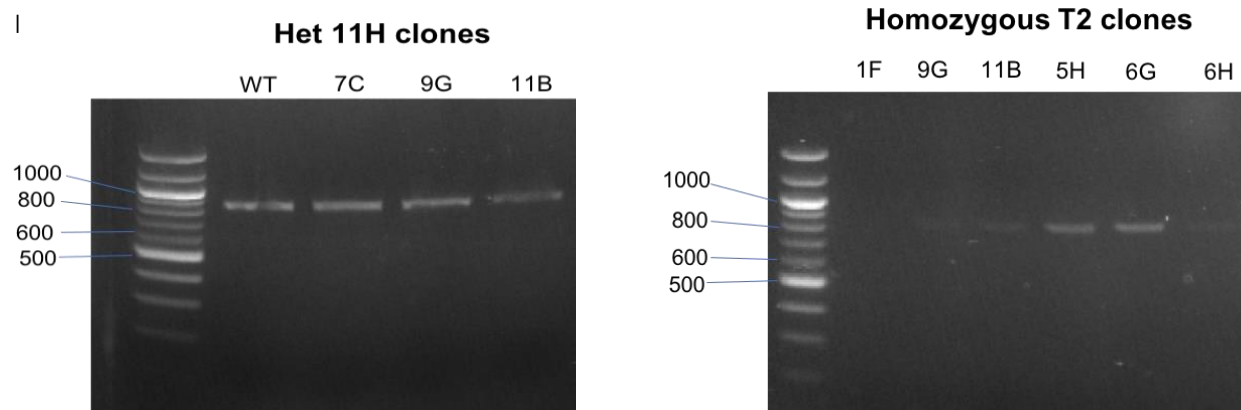
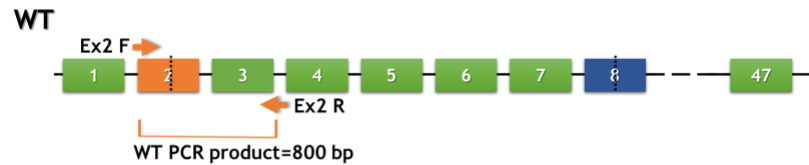
Normal ABCA7 protein sequence

**MAFWTQLMLLLWKNFM YRRRQPVQLLVELLWPLFLFFILVAVRHSHP**  
**PPLEHHECHFPNKPLPSAGTVPWLQGLICNVNNTCFPQLTPGEEPG**  
**RLSNFNDSLVSRLLDARTVLGGASAHR**

11H-9G clone

**MAFWTQLMLLLWKNFMSRGTSGPLELLSEALCSVRGPSS**  
**TVGPSLNWYEASDL Met ELVGQEPESALPDSSLSPA**  
**CSELIGALD SHPLSRLWRRLKPLILGKLLFAPDTPF**  
**TRKLMet AQVNRTFEELTLR DVREWVEMet LGPRIFT**





**(E)** Sequencing for the  $ABCA7^{+/-}$  mutant 11H-9G revealed the Cas9 cleavage sites to be 3 bp upstream of the PAM sites, leading to a frameshift mutation. **(F)**  $ABCA7^{-/-}$  mutants were generated by transfecting the heterozygous mutant 11H-11B, followed by colony picking and sub-cloning. PCR screening identified seven T2 homozygous clones, by the presence of 500 bp bands of stronger intensity than the heterozygous 11H  $ABCA7^{+/-}$  mutants. **(G-H)** Sequencing analysis of the homozygous T2 clones identified variability in the Cas9 cleavage sites between the different clones. **(I)** PCR screens revealed differences between  $ABCA7$  heterozygous and homozygous clones, using the Ex2R reverse primer that binds in the guide RNA-targeted region. For heterozygous clones, the reaction would yield a PCR product of 800bp while no band would be produced for homozygous clones.

### 6.3.2 Validation of ABCA7-edited iPSC-derived microglial cells

Having generated the ABCA7 mutant iPSC lines, microglia were derived from the edited iPS cells before the expression of canonical MG markers was confirmed by immunostaining (Figure 6.3 A-B). Expression of MG-specific transcripts CABLES1, C1QA and GPR34 was also measured by qPCR, with comparisons showing significant upregulation in the microglial samples compared to THP1 monocytes and comparable expression across the ABCA7 genotypes (Figure 6.3C). Validation of protein expression in the ABCA7-edited MG cells by immunocytochemistry and western blotting was attempted over the course of the study, but no suitable antibodies could be found. As a result, Fluidigm qRT-PCR analysis was used to assess reduction of ABCA7 mRNA expression in the ABCA7 mutant microglia generated from the heterozygous KO clones 11H-7C and 11H-11B as well as the homozygous KO clones T2-1G, T2-9G and T1-11B. Principal component analysis showed a clear separation between samples from the double KO microglia and Kolf2 WT microglia, while the ABCA7<sup>+/-</sup> mutants segregated with the Kolf2 WT samples (Figure 6.3D). Gene expression results revealed no significant differences in the ABCA7 mRNA levels between the samples, although there was a trend towards lower expression in the homozygous KO samples (Figure 6.3E). ABCA7 shares sequence homology with ABCA1, the ATP cassette transporter essential for the regulation of intracellular cholesterol levels (Kaminski et al. 2000). The potential for a compensatory upregulation of ABCA1 after ABCA7 deletion was also investigated, with results showing that ABCA1 expression levels did not differ between WT and ABCA7-edited MG cells (Figure 6.3E).

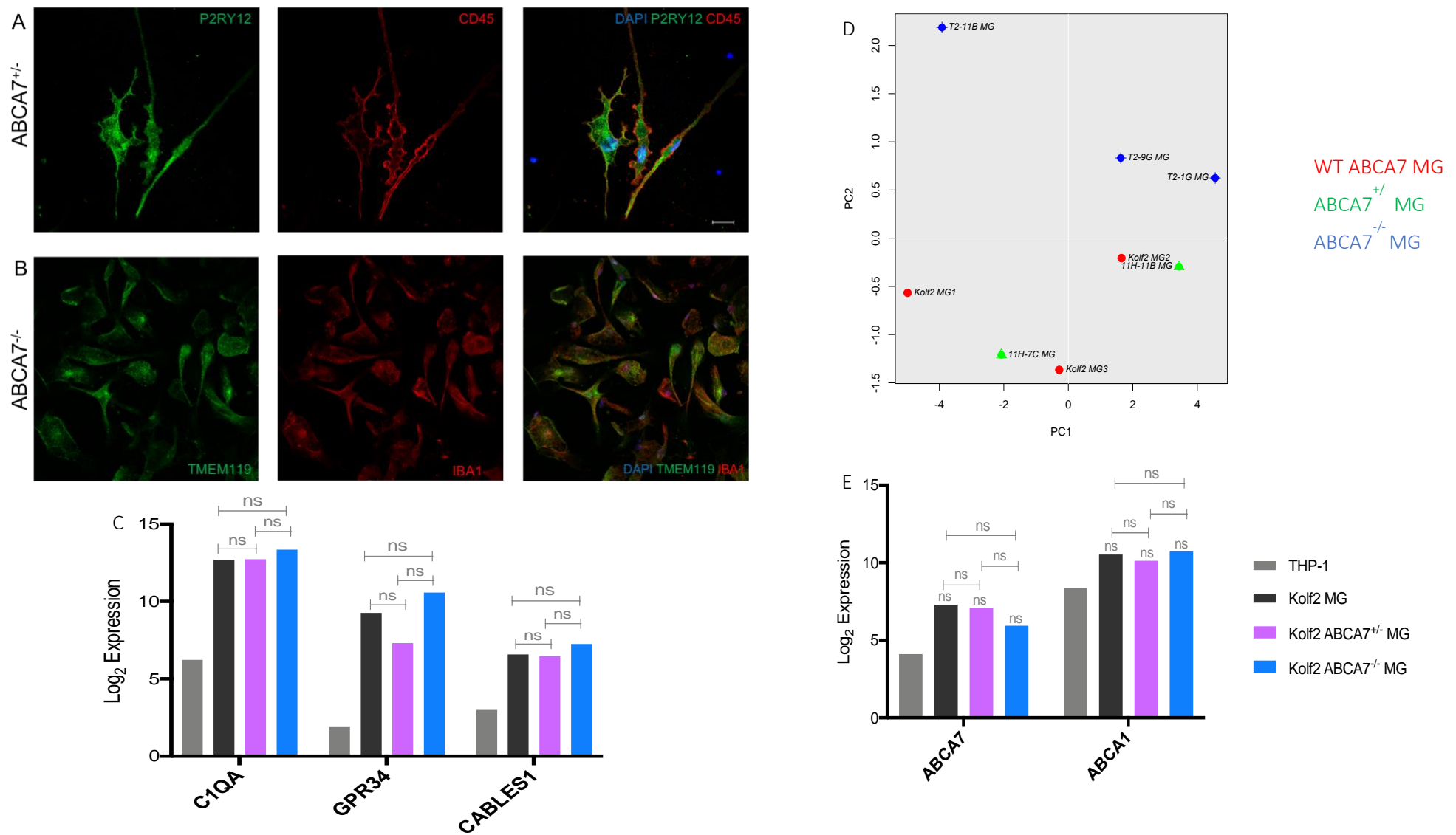
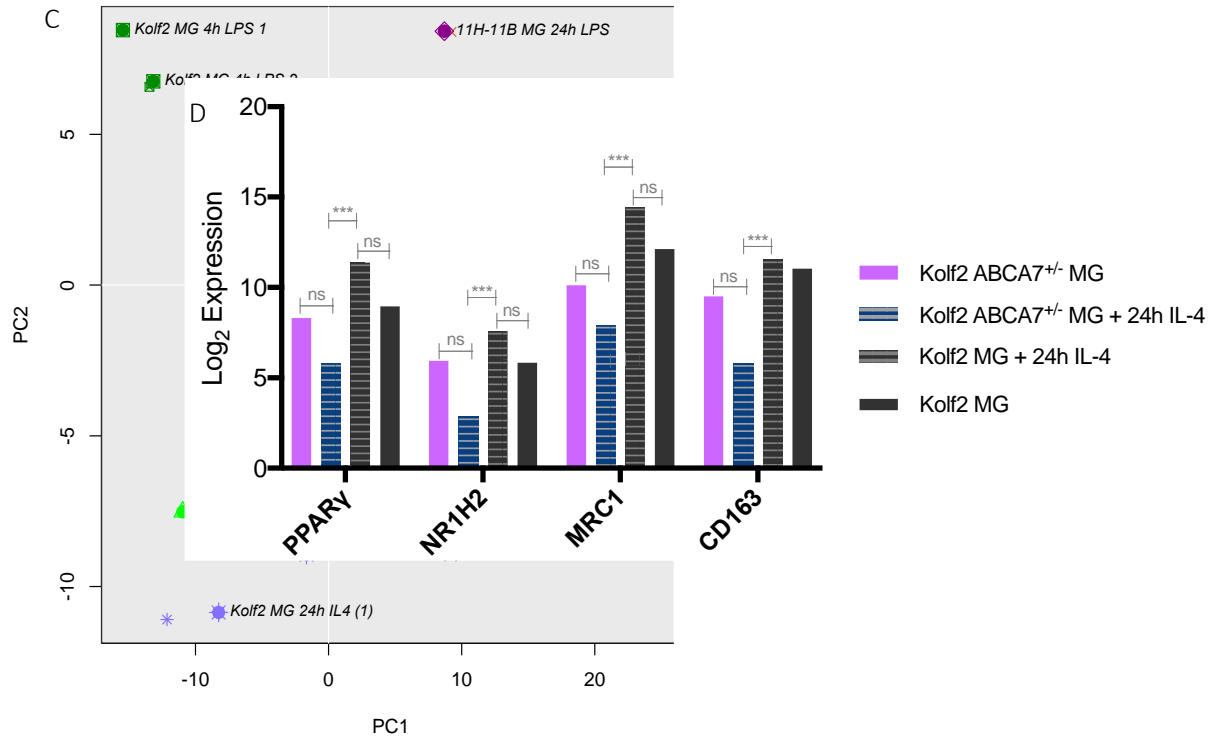
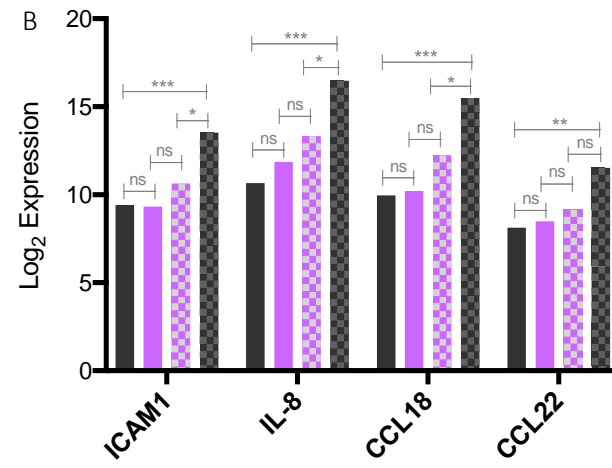
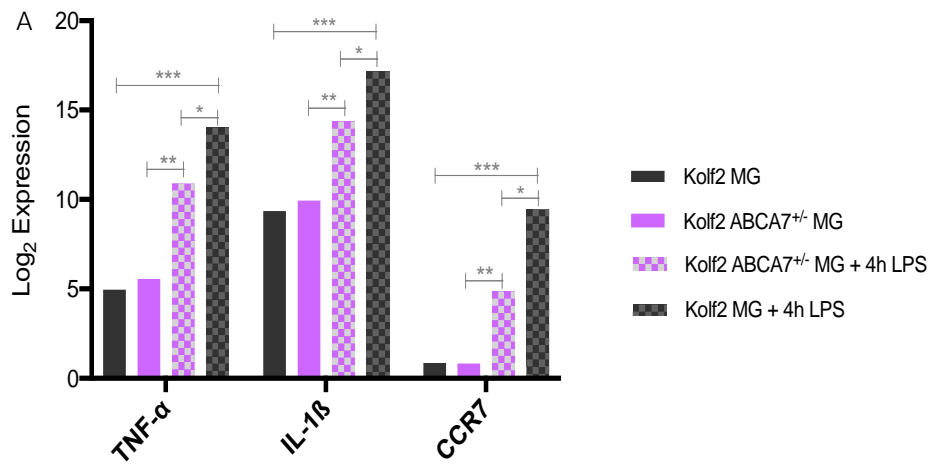


**Figure 6.3 Microglia derived from ABCA7<sup>+/-</sup> and ABCA7<sup>-/-</sup> iPSCs express canonical microglia markers.**

**(A)** Confocal images of ABCA7<sup>+/-</sup> microglia-like cells positive for P2RY12 and CD45. **(B)** Differentiation of ABCA7<sup>-/-</sup> clones generated TMEM119<sup>+</sup> IBA1<sup>+</sup> iPSC-derived microglia. Scale bar represents 20  $\mu$ m. **(C)** Expression of microglia-enriched genes C1QA, GPR34 and CABLES1 in microglia differentiated from ABCA7-edited Kolf2 iPSCs was validated by Fluidigm qPCR. **(D)** Cluster analysis revealed that ABCA7<sup>-/-</sup> samples segregated away from WT and ABCA7<sup>+/-</sup> samples.

**(E)** ANOVA comparisons revealed no significant differences in ABCA7 mRNA expression between ABCA7<sup>+/-</sup>, WT and ABCA7<sup>-/-</sup> Kolf2 microglia. Levels of the related ATP transporter ABCA1 were similarly unchanged in the ABCA7-edited MG cells. Log<sub>2</sub> Expression normalised to reference genes. Statistical analysis used two-way ANOVA with Tukey's multiple comparison test. Asterisks denote statistical significance: \* < 0.05, \*\* < 0.01, \*\*\* < 0.001, ns – not significant. n=3 biological replicates for all samples, except for THP-1 (n=2), Kolf2 ABCA7<sup>+/-</sup> MG (n=2).

Next, the impact of the ABCA7<sup>+/-</sup> mutations generated on the microglial immune response was investigated. ABCA7<sup>+/-</sup> cells were differentiated on 6-well plates for 14 days and stimulated with 1 µg/ml LPS for 4 hours or 50 ng/ml IL-4 for 24 hours. Under control unstimulated conditions, both ABCA7<sup>+/-</sup> and WT MG cells expressed comparable mRNA levels of M1 activation markers. Following LPS treatment, only three markers CCR7, TNF-α and IL-1β were significantly upregulated in the Kolf2 ABCA7<sup>+/-</sup> cells vs control ABCA7<sup>+/-</sup> cells (p < 0.01) (Figure 6.4A). In contrast, transcript levels of several other activation markers were significantly upregulated in the LPS-treated WT Kolf2 cells (p < 0.001), including the chemokines IL-8, CCL18 and CCL22 (p < 0.01) and the inflammation-induced adhesion molecule ICAM1 (Figure 6.4B). This suggests that though the LPS-treated cells displayed the classical M1 phenotype, the ABCA7 mutations restricted the magnitude of the induced pro-inflammatory response.



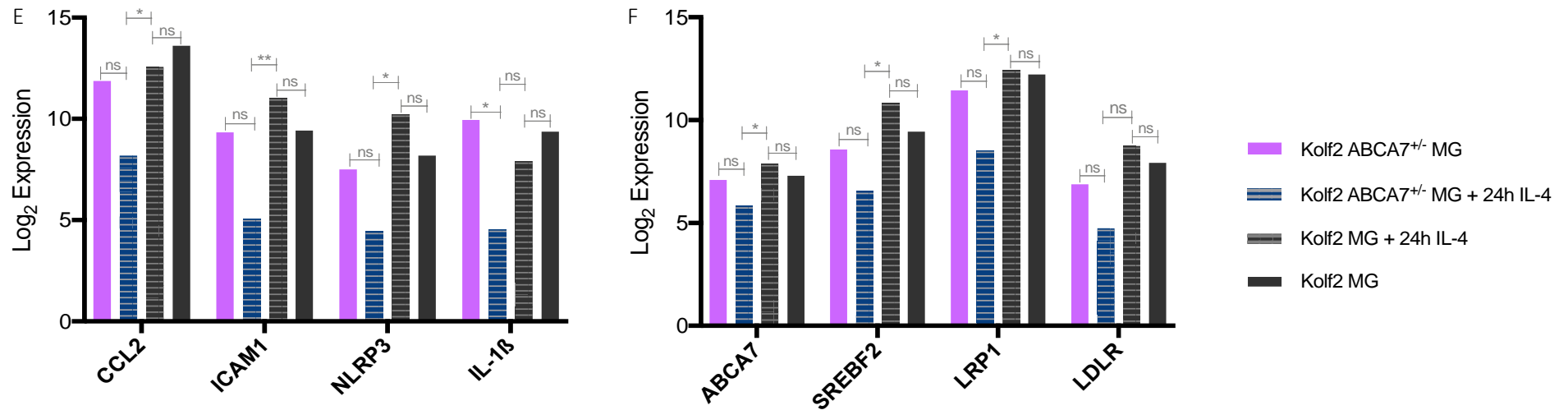


**Figure 6.4 The inflammatory response of iPSC-derived microglia to LPS and IL-4 stimulation is influenced by ABCA7 deleterious mutations.**

**(A)** Stimulation of Kolf2 ABCA7<sup>+/−</sup> MG cells with 1 μg/ml LPS for 4 hours resulted in increasing expression of three M1 markers, TNF-α, IL-1β and CCR7. Compared to WT 4h LPS-treated MG cells, this pro-inflammatory response was markedly restrained, as demonstrated by higher expression levels of those three genes in the corresponding Kolf2 WT LPS samples. **(B)** Expression of ICAM1, IL-8, CCL18 and CCL22 was unchanged in the ABCA7-edited MG cells after the same LPS challenge, whereas the same genes were significantly upregulated in 4h LPS-stimulated WT MG cells. **(C)** Kolf2 WT and ABCA7<sup>+/−</sup> MG cells were stimulated with 50 ng/ml IL-4 for 24 hours. Cluster analysis showed that the M2 phenotype of ABCA7-edited IL-4 treated MG cells was markedly different from that of IL-4 treated WT Kolf2 MG cells. **(D)** IL-4 stimulation resulted in lower expression of the anti-inflammatory genes (PPARγ and NR1H2) and M2-specific markers (MRC1 and CD163) in the ABCA7<sup>+/−</sup> MG cells compared to WT MG cells. **(E)** The pro-inflammatory genes CCL2, ICAM1 and NLRP3 were expressed at lower levels in compared to WT MG cells. **(F)** Differences in the expression of ABCA7 and cholesterol-associated genes were statistically significant between WT and ABCA7<sup>+/−</sup> MG cells after treatment with IL-4.

Log<sub>2</sub> Expression normalised to reference genes. Statistical analysis used two-way ANOVA with Tukey's multiple comparison test.

Asterisks denote statistical significance: \* < 0.05, \*\* < 0.01, \*\*\* < 0.001, ns – not significant. n=3 biological replicates for all samples, except for Kolf2 ABCA7<sup>+/−</sup> MG (n=2); Kolf2 ABCA7<sup>+/−</sup> MG + 4h LPS (n=2); Kolf2 ABCA7<sup>+/−</sup> MG + 24h IL-4 (n=2).

This immune response-altering effect was more apparent with stimulation with IL-4, which induces an M2 phenotype. As shown by the PCA plot in Figure 6.4C, the inflammatory phenotype of the ABCA7<sup>+/-</sup> cells was markedly different from that of WT microglia after IL-4 treatment, with a distinct segregation based on expression of several immune response genes. This difference was particularly illustrated by the fact that the M2-specific markers PPAR- $\gamma$  and CD163, and the nuclear factor NR1H2 (or LXR- $\beta$ ), which showed a trend towards upregulation in the WT IL-4 stimulated cells, trended towards downregulation in the corresponding ABCA7-edited MG cells (Figure 6.4D). In addition, the pro-inflammatory markers ICAM1, NLRP3 and CCL2 showed a trend towards reduction in the IL-4-treated ABCA7 mutant microglia, while IL-1 $\beta$  reduction was found to be statistically significant. Crucially, the differences in expression levels of these genes were significant when comparing WT and ABCA7<sup>+/-</sup> IL-4 treated cells (Figure 6.4E). It is also worth noting that, following IL-4 stimulation, levels of ABCA7 and the cholesterol related transcripts SREBF2 and LRP1 were lower in ABCA7<sup>+/-</sup> cells vs WT cells (Figure 6.4F). Taken together, these results showed that, along with pro-inflammation, M2 anti-inflammatory responses were likely to be affected by ABCA7 loss-of-function mutations.

### 6.3.3 ABCA7 loss of function impairs phagocytosis in iPSC-derived microglia

ABCA7<sup>+/-</sup> and ABCA7<sup>-/-</sup> microglia cells were functionally validated for their capacity to phagocytose pHrodo red E. coli particles. 96-well plate differentiated microglial cells (20,000 per well) were incubated with 10  $\mu$ g pHrodo particles and red channel fluorescence measurements were taken every 15 minutes for 4 hours in the IncuCyte S3 live imaging platform (see section 2.5). pHrodo red fluorescence was found to be markedly reduced in ABCA7<sup>+/-</sup> and ABCA7<sup>-/-</sup> cells compared to Kolf2 WT microglial cells (Figure 6.5A). Quantification of the endpoint fluorescence indicated that ABCA7 homozygous and heterozygous mutant microglia cells ingested significantly fewer particles than WT Kolf2 cells ( $p < 0.0001$ ) (Figure 6.5B). Pre-treatment of the WT cells with 1  $\mu$ M bafilomycin A1 resulted in ablation of the fluorescent signal, confirming that phagolysosome acidification is a prerequisite for this process. Tellingly, ABCA7 mutant cells showed a higher rate of particle uptake than the inhibitor-treated cells,

except for one ABCA7<sup>-/-</sup> clone T2-1F where the difference was non-significant. Differences in rate of particle uptake were also uncovered between the three different ABCA7<sup>-/-</sup> clones, which individually ingested significantly fewer particles ( $p < 0.0001$ ) than the single ABCA7<sup>+/-</sup> clone studied in this experiment. Therefore, these preliminary results suggest that microglial phagocytosis of red E. coli bioparticles is considerably impaired by genetic modification of ABCA7, implying that ABCA7 is essential for phagocytosis of pathogenic particles.

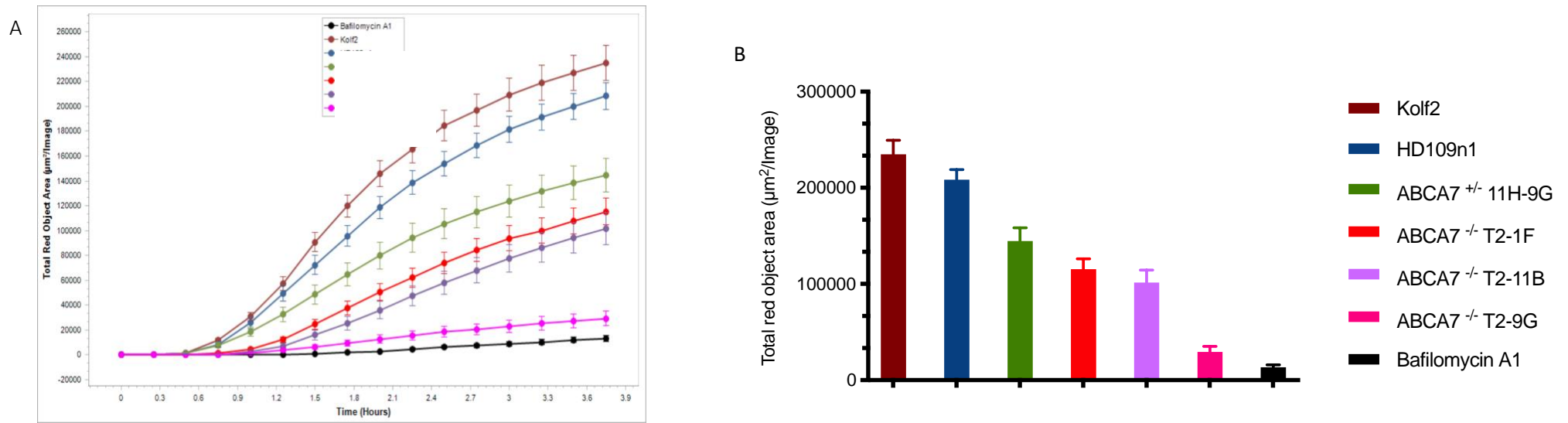


**Figure 6.5 Phagocytosis of pHrodo *E. coli* bioparticles seems to be impaired by ABCA7 heterozygous and homozygous KO mutations in preliminary examinations.**

iPSC-derived MG cells plated at 20,000 per well were incubated with 10 µg pHrodo *E. coli* for 4 hours. **(A)** For negative control, WT MG cells were pre-treated with 10 µM of bafilomycin A1 for 1 hour before *E. coli* treatment. **(B)** End point fluorescence values from the experiment in (A) were plotted. Data are presented as mean ± SEM from each genotype or condition with 8-16 technical replicates. n=1 independent experiment.

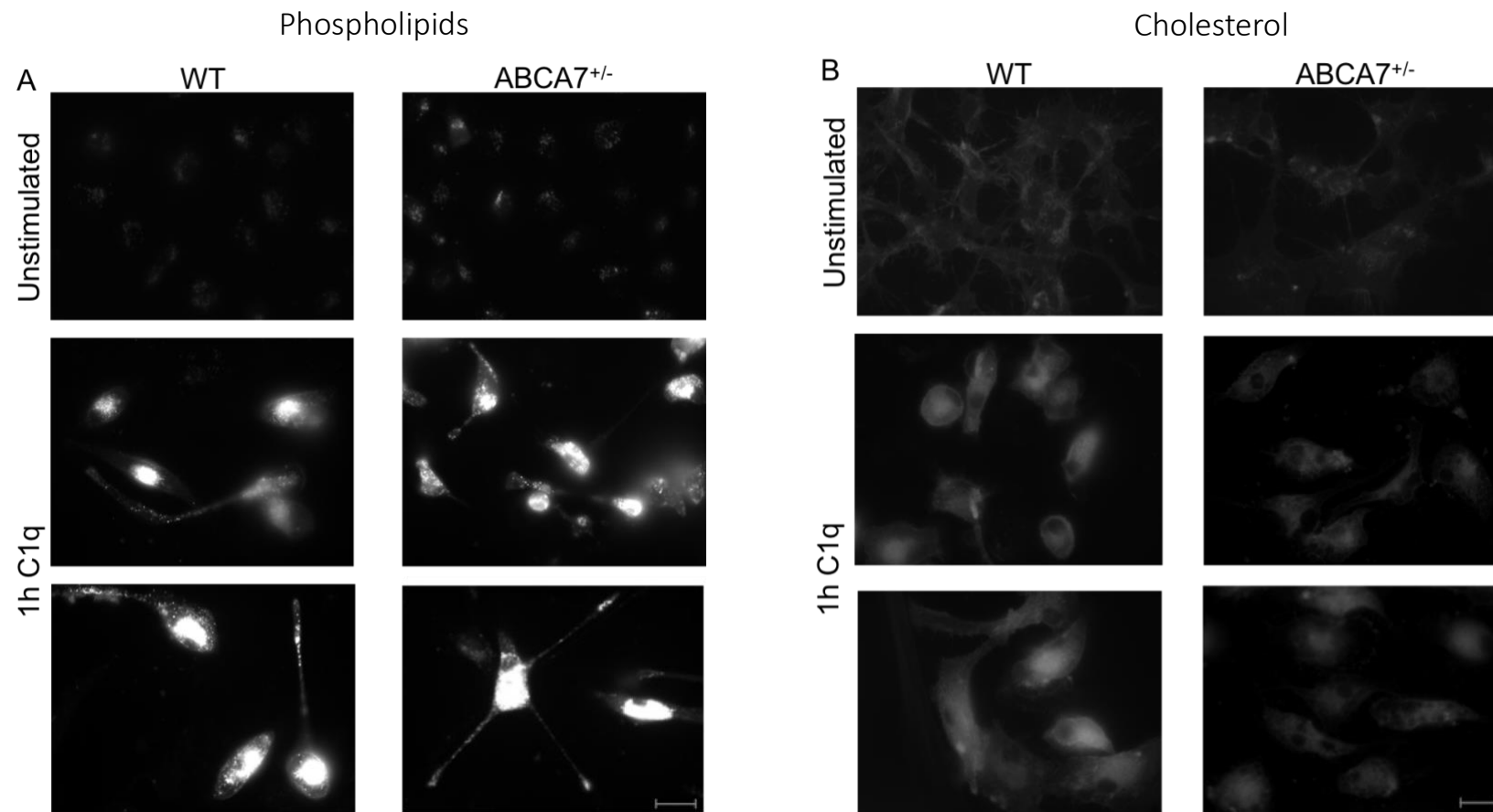


**Figure 6.6 Stimulation with the apoptotic molecule C1q induces intracellular accumulation of phospholipids and cholesterol in iPSC-derived microglia.**

Kolf2 WT and ABCA7<sup>+/-</sup> MG cells were cultured on PDL-treated and fibronectin-coated Ibidi 8-well chamber slides before stimulation with 10 μg/ml C1q for 1 hour. **(A)** MG cells were incubated with the phospholipidosis detection reagent LipidTOX for 4 hours. Fluorescence images were taken with a high-resolution microscope – LipidTOX was excited at 543 nm and its emission detected at 594 nm. **(B)** Following C1q stimulation, MG cells were incubated for 30 mins with 125 μg/ml of the cholesterol-specific probe filipin. Fluorescence images were taken at 300nm.

Scale bars represent 20 μm.

#### 6.3.4 Is ABCA7 involved in intracellular lipid trafficking?

ABCA7 has been reported to exert its phagocytosis-mediating activity in mouse macrophages through recruitment to the cell surface of the low-density lipoprotein receptor-related protein 1 or LRP1, with both proteins colocalised to phagocytic cups when the cells were stimulated with C1q (Jehle et al. 2006). C1q is expressed on apoptotic cells, where it binds to LRP1 on phagocytes, initiating uptake of apoptotic cells (Ogden et al. 2001).

Particle engulfment by phagocytes is a tightly orchestrated process that requires several proteins operating in concert to generate approximately 100 lipids in order to replenish the cell membrane expended during initial engulfment (Aderem 2002). This rapid rate of lipid synthesis is accompanied by increased transcription of many proteins, including the LDL receptor, fatty acid synthase and the cholesterol synthesis enzymes 3-hydroxy-3-methylglutaryl CoA synthase and 3-hydroxy-3-methylglutaryl CoA reductase (Castoreno et al. 2005). In order to explore the dynamics of cell membrane biogenesis and lipid metabolism during microglial phagocytosis, lipid trafficking assays focusing on two species (cholesterol and phospholipids) were carried out. Microglia differentiated from WT and ABCA7<sup>+/-</sup> cell lines were cultured on Ibidi 8-well chamber slides and incubated with 10 µg/ml C1q for 1 hour before staining for cholesterol and phospholipids with filipin and LipidTOX respectively (see section 2.5). High resolution images showed that unstimulated microglial cells exhibited low levels of phospholipids, with the LipidTOX staining enclosed in intracellular puncta (Figure 6.6A). Upon stimulation with C1q, cells exhibited a noticeable intracellular accumulation of phospholipids, indicative of an increased rate of lipid synthesis. Crucially, no differences in staining pattern were observed between WT and single KO microglial cells, suggesting that ABCA7 mutations do not affect phagocytosis-mediated synthesis of phospholipids in microglia cells (Figure 6.6A). Cholesterol was similarly observed in intracellular punctate structures, as shown by staining with filipin (Figure 6.6B). ABCA7<sup>+/-</sup> and WT microglia treated with C1q for 1 h showed elevated levels of filipin staining, the accumulation of cholesterol being concentrated in intracellular compartments (Figure 6.6B). Though not quantified, cholesterol staining in the ABCA7<sup>+/-</sup> cells was less pronounced compared to WT cells, hinting at an altered capacity to regulate cholesterol levels in response to a phagocytic challenge.

### 6.3 Summary and Discussion

Transcriptomic and gene expression studies described in chapter 3 demonstrated that the human iPSC-derived microglia generated using the protocol described in this study express several disease-associated risk genes for AD. To validate the suitability of these in vitro differentiated cells for modelling the function of microglial-enriched AD risk genes, ABCA7 was chosen as a candidate gene with the intention of knocking out the gene and studying the subsequent effects of these mutations on microglial function. Using CRISPR/Cas9 genome editing, ABCA7 mutant clones were generated by excision of a 2.5 kb region at the N-terminal end of the protein. Potential heterozygous and homozygous KO clones were identified by PCR screening and sequencing.

Validation by Fluidigm qRT-PCR showed that ABCA7 mRNA expression was found to be unaltered following genome editing. The mRNA primers used were mapped to the coding exons 40 and 41 of the full-length protein, with the forward mRNA primer flanking the exon-exon boundary for increased specificity. No reduction in ABCA7 mRNA levels in either the heterozygous or homozygous mutants suggests that the mutated mRNA transcripts may have escaped the nonsense mediated decay machinery. One important limitation of this investigation was the failure to validate ABCA7 protein expression and therefore the KO lines generated by Western blotting. A number of antibodies were trialled, namely the rabbit polyclonal antibody 25339-1-AP from ProteinTech Europe and another rabbit polyclonal antibody ARP-43690\_P050 from Aviva Systems Biology (USA), which targets the middle region of the protein. Neither antibody worked convincingly by producing any bands when Western blots experiments were carried out. Recently, a study published the first paper using an antibody specific to human ABCA7 (Allen et al. 2017), designed to bind the epitope aa 2096-2146 in the C-terminus of the full-length protein (LS-C291064, LifeSpan BioSciences - USA). This antibody looks like a good candidate for validation of the KO lines generated in this study.

Nevertheless, preliminary functional assays carried out with pHrodo red E. coli bioparticles demonstrated a deficit in phagocytosis in ABCA7-edited microglia, showing that ABCA7 is required for efficient phagocytosis of bioparticles. In addition, the findings underlined the importance of actin remodelling and phagolysosome fusion in microglial phagocytosis, as the

use of the respective inhibitors cytochalasin D and bafilomycin A1 resulted in loss of pHrodo fluorescence. These observations are in agreement with recent studies of iPSC-derived macrophage and microglia phagocytosis performed using similar live cell imaging platforms (Kapellos et al. 2016; Brownjohn et al. 2018). Though this study recapitulates previous mouse model findings that ABCA7 mediated phagocytosis, another limitation is that only one aspect of bioparticle phagocytosis, through engagement of the TLR4 was investigated herein. Future experiments would need to establish whether mechanisms of phagocytosis impairment through ABCA7 loss-of-function are receptor- and particle-dependent, by challenging cells with larger bioparticles such as zymosan, a ligand found on the surface of fungi that stimulates TLR2-mediated uptake. Another essential question that has to be answered is whether these ABCA7 mutations would affect binding and internalisation of oligomeric A $\beta$ , as ABCA7 deletion in AD mouse models enhances plaque load (Kim et al. 2013; Li et al. 2015; Sakae et al. 2016). Given that iPSC-derived microglia were shown to express several A $\beta$  receptors including TREM2, CD36 and CR1, impairments in A $\beta$  phagocytosis would likely point towards a general phagocytic mechanism that requires ABCA7.

Studies in mouse macrophages have shown that ABCA7 staining is mostly intracellular (Liensel-Nitschke et al. 2005), whereas the protein co-localises with LRP1 following stimulation with C1q (Jehle et al. 2006). The latter work also proved that ABCA7 is required for signalling through LRP1. The ubiquitously expressed receptor LRP1 regulates a diverse range of physiological processes including endocytosis, lipid metabolism and signal transduction (May et al. 2005). In macrophages, it promotes anti-inflammatory signalling via inhibition of pro-inflammatory gene expression (Zurhove et al. 2008; May et al. 2013). This in turn affects polarisation by favouring an M2 anti-inflammatory phenotype. Correspondingly, LRP1 downregulation in mouse microglia leads to increased pro-inflammation via JNK and NF $\kappa$ B activation (Yang et al. 2016). LPS and IL-4 stimulation experiments showed that the inflammatory response of microglia was affected by ABCA7 mutations, suggesting that the ATP transporter may play a role in microglial anti-inflammatory signalling. ABCA7<sup>+/-</sup> microglia exhibited a more restrained inflammatory response to LPS incubation compared to WT Kof2 cells, as indicated by fewer and statistically smaller increases in pro-inflammatory and M1 activation molecules (Figure 6.4). Similarly, a distinct immune profile was obtained following stimulation with the anti-inflammatory cytokine IL-4. These data therefore provide

preliminary evidence for the involvement of ABCA7 in both the pro- and anti-inflammatory response of microglial cells, perhaps in modulating the appropriate response to pathogens and inflammatory stimuli. Given the evidence for LRP1 in this context and that ABCA7 is required for LRP1 signalling, it is plausible that ABCA7 exerts its inflammation- and phagocytosis-mediating effects through interactions with LRP1 in lipid rafts. Consequently, more work is needed to certify these potential links between LRP1 and ABCA7, including their intracellular localisation in unstimulated microglia and during phagocytosis. This could be done using confocal microscopy, as well as using co-immunoprecipitation assays that could enable the identification of proteins and complexes that interact with ABCA7 during phagocytosis.

C1q treatment of iPSC-derived microglia resulted in increased intracellular cholesterol and phospholipid staining, indicative of a higher rate of lipid and cholesterol synthesis in response to or during phagocytosis. Future experiments should aim to quantify these increases and assess whether ABCA7 mutations inhibit or enhance these processes. Additionally, ABCA7 expression is regulated by intracellular cholesterol levels through the SREBP2 pathway, whereby its expression is upregulated by cholesterol depletion and downregulated by higher cellular cholesterol levels (Iwamoto et al. 2006). A series of experiments focusing on this pathway in the ABCA7 KO iPSC lines were planned, with cholesterol depletion to be mimicked using the cholesterol-lowering drug mevastatin, an inhibitor of the HMG-CoA reductase enzyme (Bamji-Mirza et al. 2016). Preliminary results with Kolf2 WT microglia stimulated with 10  $\mu$ M mevastatin (ML-236B, Sigma Aldrich) for 4 hours showed that mevastatin treatment significantly increased expression of SREBF2 and the cholesterol-synthesis enzymes fatty acid synthase (FASN), low density lipoprotein receptor (LDLR) and HMG-CoA synthase 1 (HMGCS1) (see appendix 5). Likewise, experiments assessing the effects of C1q stimulation on gene expression of cholesterol pathway genes should be carried out, and comparisons made between WT and ABCA7-deficient microglia.

Phagocytosis and clearance of debris is a quintessential and defining function of microglia (Gordon & Martinez 2010). Indeed, a growing research area within the field revolves around their involvement in synaptic pruning, whereby microglia engulf and eliminate synapses during development (Paolicelli et al. 2011; Schafer et al. 2012). Though there is very little

evidence for microglial-mediated synaptic pruning after development, proper microglia function is critical for the correcting wiring of embryonic brain circuits (Squarzoni et al. 2014). Furthermore, microglia have been shown to mediate synaptic loss in AD mouse models through the CR3 pathway, a process that precedes plaque deposition and is dependent on C1q expression (Hong et al. 2016). Fluorescence imaging of synaptic membrane dynamics has been reported using the pH-sensitive pHluorin (Miesenböck et al. 1998; Royle et al. 2008) and thus can be adapted for in vitro live imaging assays, by co-culturing microglia with synapto-pHluorin-expressing iPSC-derived neurons. This would allow to investigate synaptic pruning in vitro as well as the effects of ABCA7 mutations on this microglial activity.

# 7. GENERAL DISCUSSION

## 7.1 General discussion and future perspectives

### 7.1.1 Characterisation of the phenotype of HD109 iPSC-derived microglia

The accumulation of reactive microglia is a key feature of the HD brain (Sapp et al. 2001), with imaging studies going on to demonstrate that this extensive microglial activation is apparent long before age of onset in HD gene carriers (Tai et al. 2007) and that it correlates with neuronal loss in symptomatic patients (Pavese et al. 2006). Moreover, studies in mouse models and post-mortem human brains have shown that HD microglia acquire an inflammatory phenotype, resulting in elevated levels of proinflammatory cytokines (Dalrymple et al. 2007; Silvestroni et al. 2009). Though microglial activation in the HD brain has been relatively well reported, it remains unclear whether this phenomenon is a secondary response to neuronal degeneration or mainly down to the cell-autonomous effects of mutant HTT expression in immune cells.

The first aim of this thesis was to investigate the phenotype of microglia derived from a Huntington's disease human iPSC cell line containing 109 CAG repeats in the HTT gene. The transcriptome of HD109 iPSC-derived microglia was compared to that of WT cells derived from a different genetic background by RNA sequencing. The transcriptional hallmarks of mutant HTT-associated immune dysfunction, which include NF $\kappa$ B dysregulation and higher expression of pro-inflammatory SPI1-target genes, were not detected in the HD109 microglia. In fact, the findings presented in chapter 4 point towards the notion that the pathogenic hallmarks of mutant HTT-expressing microglia, as described in the literature, may not be innate to their basal transcriptome.

The study's focus then turned to assessing whether the pro-inflammatory properties of HD microglia would manifest following exogenous stimulation. Surprisingly, results showed that the *in vitro* HD microglia did not exhibit a hyper-reactive activation profile when challenged with LPS. When paying close attention to genes belonging to the two HD affected pathways of NF $\kappa$ B and LPS, no evidence of dysregulation in gene expression were found in those pathways, contrary to findings reported elsewhere (Crotti et al. 2014).

These results therefore indicate that the transcriptome of human HD microglia may not be primed; instead, evidence points towards a distinct neuroprotective signature with several pathways highlighted as activated in patient-isolated monocytes predicted to be inhibited. As already mentioned, one attractive explanation is that this is down to the impact of the neuronal environment, particularly the neuron-derived cytokine IL-34 on the microglial phenotype, which illustrates the transcriptional alterations that microglia undergo as they populate the embryonic brain. This could be viewed as an adaptation of the HD microglial transcriptome to its surrounding neuronal environment, shown to be susceptible to degeneration early in neurodevelopment (Molero et al. 2009; Ring et al. 2015). Indeed, the fragile HD brain may initially potentiate the phenotype of microglia in HD, potentially dampening the priming effects of mutant HTT expression.

Another possibility is that this inhibitory transcriptomic signal represents a human microglial-specific effect, given that microglia from HD mouse models exhibit activated inflammatory pathways. A crucial point of difference between the findings outlined in chapter 4 and those of patient-derived monocytes resides in the age of the patient-derived cells from Miller et al. 2016, where the mean age of participants at the early or moderate stage of the disease was 48 years old. In contrast, a feature of differentiation protocols is that they seldom give rise to adult differentiated cells. Indeed, this remains a great challenge for the iPSC modelling field. Given this caveat, it is plausible that differences in transcriptome-wide pathway activation from the respective studies reflect different stages of the choreography of inflammation in Huntington's disease. Furthermore, these findings imply that the basal transcriptome of microglia in HD may be non-pathogenic and/or neuroprotective, with gradual changes in phenotype towards those reported in mouse models and HD patients with characteristics such as increased pro-inflammation, as a likely consequence of exposure to the HD brain environment and degeneration in the striatum. One way to test this hypothesis would be to use human iPSC-derived microglia from HD and isogenic control lines in combination with xenotransplantation compatible WT mice (e.g. MITRG) (Rongvaux et al. 2014) and corresponding HD mouse models, along with single cell transcriptomic approaches to investigate the effects of both ageing and exposure to the HD brain microenvironment on the immune phenotype of human microglia. Such an experiment would answer pertinent

questions about the effect of ageing on the phenotype of HD microglia. In addition, this would shed a light on the contribution of diseased and non-diseased microglia on inflammatory processes in the HD brain, and subsequently on neural degeneration in the striatum.

### 7.1.2 The effects of correcting the HD CAG mutation on the microglial phenotype

Comparing iPSC-derived neural stem cells, Xu et al. 2017 recently found that transcriptome differences between HD and non-isogenic lines were not detected when comparing HD with isogenic corrected line samples, suggesting that those differences resulted from non-HD-specific effects, a consequence of genetic background variations. The second aim of this thesis was therefore to determine the effects of correcting the HD CAG expansion mutation on the phenotype of HD109 iPSC-derived microglia. Given the predictions of potential impairments in several immune pathways in the HD109 microglia (when compared to WT Kolf2 iPSC-derived microglia), experiments were carried out to ascertain the HD-specific nature of these HD109 transcriptome changes, with comparisons against microglia differentiated from HD isogenic corrected iPSC lines. When assayed, the HD109 cells displayed no functional deficits in phagocytosis or chemotaxis compared to HD corrected and Kolf2 cells. Similarly, an investigation into the immune response of the corrected HD microglia failed to pinpoint mutant HTT-specific phenotypic differences in the LPS response of HD109 microglia. Taken together, the data point towards genetic background, rather than HD-specific, differences between the transcriptome of HD109 and Kolf2 microglia. This is best illustrated by the fact that while RNA-seq data showed lower levels of chemokines expressed in HD109 cells implying a dysregulation in chemokine signalling, validation by Fluidigm qRT-PCR confirmed that these differences were most likely due to genetic background, as the LPS chemokine profile of the HD109 microglia post LPS was found to match that of the LPS-stimulated HD corrected cells.

The absence of any predicted transcriptome-associated functional dysfunctions in the HD109 microglia, allied with the lack of manifestation of phenotypic differences with the HD corrected cells, could be explained by an absence of mutant HTT expression in the in vitro derived HD109 microglia. One way to confirm this hypothesis would be to measure mutant

HTT expression by Western blotting, which, due to time constraints, was not undertaken and remains a significant limitation of this study.

Mutant HTT detection has been reported in new-born mice microglia (Crotti et al. 2014), but not human microglia, although it was found to be expressed in other immune cells isolated from symptomatic HD patients such monocytes, T cells and B cells (Weiss et al. 2012). However, it should be pointed out that the characteristics and reactivity of microglia in rodent models of Huntington's disease vary greatly across species. In a recent study, Harrison et al. 2018 used quinolinic acid lesion models of HD to evaluate differences in survival of engrafted tissues in mice and rats and demonstrated that mice models exhibited a lower engraftment survival than equivalent rat grafts, and substantially higher microglia activation and recruitment to the site of transplantation (Harrison et al. 2018). The outcome of higher mouse microglia reactivity has many implications that are important to consider, not just for mouse transplantation studies (since mouse models comprise the majority of transgenic HD models) but also for the fields of microglial research in general and in neurodegenerative diseases such HD and AD. Additionally, it emphasises a particular disparity in the immune response between rodent models that is under-reported in the neuroinflammation field and is highly likely to translate into differences with human cells. In turn, it could be argued that this could be reflected in the human iPSC models used in this work.

No matter whether mutant HTT expression can be detected in HD iPSC-derived microglia in future experiments, the absence of a HD phenotype in these embryonic-like cells demonstrates that the cell autonomous effects of mutant HTT on the microglial phenotype must be triggered by either intrinsic cellular events (e.g. mutant HTT aggregation or ageing) or by extrinsic factors, such as interactions between microglia and the HD brain microenvironment. This entails that the presence of the CAG expansion track in the HTT gene on its own is insufficient to trigger the manifestation of the pathogenic effects characteristic of HD microglia, an observation compatible with reports of increased microglial activation with age in HD patients (Pavese et al. 2006; Tai et al. 2007). It also suggests that, rather than a causal disease mechanism, microglial activation in HD should be considered as a disease biomarker. Nonetheless, this does not preclude from microglia contributing to striatal degeneration.

This is the first study to evaluate the effects of reversing the HD mutation on immune dysfunction in human microglia. Given the extensive evidence for the involvement of microglia and other immune cells in HD neuropathology, it is imperative to investigate the effects of mutant HTT lowering on HD human immune cells. In addition, this area of research is of greater importance in the light of current encouraging developments in human clinical trials of the mutant HTT-lowering antisense oligonucleotide-based IONIS-HTTRx (RG6042) (Østergaard et al. 2013; Skotte et al. 2014). Preliminary phase 1/2 trials have assessed safety of this treatment and confirmed a dose-dependent reduction of mutant HTT in the CSF of HD patients, using a single-molecule counting mHTT immunoassay (Wild et al. 2015). Studies in HD mouse models had earlier demonstrated that human mutant HTT-targeting antisense oligonucleotides produced long-lasting reductions in HTT brain mRNA and protein levels, which correlated with improved motor function and survival (Kordasiewicz et al. 2012).

### 7.1.3 Modelling neuroinflammation with iPSC-derived microglia

As well as helping to elucidate the pathogenic mechanisms underlying microglial involvement in HD, iPSC-based models hold great potential for Alzheimer's disease. Firstly, they provide a good alternative to animal models for drug screening. In vitro microglia can certainly be used to develop assays that probe the effects of immunomodulatory therapies on immune activation. One aspect of microglial function that can certainly be exploited in this manner, using Seahorse assays, is the link between metabolism and inflammatory processes, which work in this thesis attempted to investigate. This is especially relevant to AD, with evidence for the influence of metabolic processes on microglial function coming from mouse model studies by Ulland et al. 2017, where the authors demonstrated that TREM2 deletion disrupts microglial function by impairing other metabolic pathways including glycolysis, the TCA cycle and the pentose phosphate pathway (Ulland et al. 2017). Indeed, TREM2-deficient mouse microglia exhibit mitochondrial impairments including reduced mitochondrial mass and increased autophagy.

Secondly, iPSC-derived microglia can and are being used to understand the role of microglia-enriched disease-associated risk genes in microglial biology, enabling researchers to look at both rare and common disease variants. While the former offer an insight into pathological mechanisms, the latter allows us to model predisposition to disease, increasing the likelihood

of discovering preventative therapies. The advent of CRISPR/Cas9 genome editing, along with the progress made in generating patient-specific iPSCs, have opened the door for in vitro functional studies in these two contexts.

One important challenge of this microglial differentiation protocol remains that there are doubts surrounding the suitability of monocultured in vitro microglia. Reasons for this include the lack of elaborate ramifications in the in vitro microglia and the relatively high expression of inflammatory genes in the IL-34 and GM-CSF treated iPSC-derived microglia. The first observation is partly reflective of the neuronal-free culture conditions, while the second is a reported feature of ex vivo microglial culture (Bohlen et al. 2017). Another possibility, currently being investigated in our lab, is that the absence of a dampened immune signature in the in vitro monocultured microglia cells could represent an artefact of in vitro differentiation with GM-CSF, which has been shown to regulate cell proliferation and enhance several inflammatory functions (Shiomi & Usui 2015).

Given our rapidly evolving understanding of how the transcriptome, phenotype and functions of microglia is modulated by the CNS microenvironment, the findings described in this thesis underline the importance of using the appropriate culture conditions that more faithfully recapitulate microglia origins, maturation and homeostasis. Therefore, the use of more complex model systems such as co-cultures that better mimic the natural microglial habitat should be greatly encouraged, where possible. These systems would ideally integrate neuronal and astrocytic cell types in order to more faithfully study the effects of the functional interactions between the relevant cell types on the phenotypes and functionality of the individual cell types.

## 7.2 Concluding remarks

Immune activation within the CNS is now accepted as a key feature of Alzheimer's disease, Huntington's disease and many other neurodegenerative diseases. In AD, recent GWAS findings highlighting several microglia-enriched genes as disease-associated risk loci have focused current research on the role of microglia-mediated inflammation. Using iPSC-derived microglia, loss-of-function mutations in ABCA7 have been found to impair phagocytosis and regulate microglial inflammatory responses in preliminary studies. Although limited, the ABCA7 work in this thesis provides the starting point for more in-depth mechanistic studies to explore the role of ABCA7 in microglial biology.

Data from human imaging studies in Huntington's disease point towards the detrimental influence of microglia-mediated neuroinflammatory processes to disease progression. In addition, studies in HD mouse models have established that mutant HTT induces pathogenic cell-autonomous effects on the phenotype of microglia. Using microglia derived from HD iPSCs, this study demonstrates that the pathogenic and inflammatory phenotype of diseased HD microglia is not innate to their transcriptome, suggesting that it may therefore be a consequence of intrinsic factors or extrinsic interactions with the degenerative HD brain microenvironment. In particular, the lack of manifestation of the phenotypic abnormalities characteristic of diseased HD microglia in the embryonic-like in vitro microglia suggests that the HD microglial phenotype may not be accurately reflected outside of the diseased HD brain environment. These findings provide an insight into the limitations of in vitro models of microglia, whilst emphasising the need for iPSC-based models that better recapitulate disease pathology and subsequently better enable dissecting the contribution of microglia to pathogenesis.

## 8. REFERENCES

- Abe-dohmae, S. et al., 2004. Human ABCA7 Supports Apolipoprotein-mediated Release of Cellular Cholesterol and Phospholipid to Generate High Density Lipoprotein. *Journal of Biological Chemistry*, 279(1), pp.604–611.
- Abe-Dohmae, S., Ueda, K. & Yokoyama, S., 2006. ABCA7, a molecule with unknown function. *FEBS Letters*, 580(4), pp.1178–1182.
- Abud, E.M. et al., 2017. iPSC-Derived Human Microglia-like Cells to Study Neurological Disease. *Neuron*, 94(2), pp.278–293. Available at: <http://dx.doi.org/10.1016/j.neuron.2017.03.042>.
- Abutbul, S. et al., 2012. TGF- $\beta$  signaling through SMAD2/3 induces the quiescent microglial phenotype within the CNS environment. *Glia*, 60(7), pp.1160–1171.
- Aderem, A., 2002. How to eat something bigger than your head. *Cell*, 110(1), pp.5–8.
- Aguzzi, A. et al., 2013. Microglia: Scapegoat, Saboteur, or Something Else ? *Science*, 156(January), pp.156–162.
- Aikawa, T., Holm, M. & Kanekiyo, T., 2018. ABCA7 and Pathogenic Pathways of Alzheimer's Disease. *Brain Sciences*, 1, pp.1–13.
- Akiyama, H. & McGeer, P.L., 1990. Brain microglia constitutively express beta-2 integrins. *Journal of neuroimmunology*, 30(1), pp.81–93.
- Allen, M. et al., 2017. ABCA7 loss-of-function variants, expression, and neurologic disease risk. *Neurology Genetics*, 0, pp.1–7.
- An, M.C. et al., 2012. Genetic Correction of Huntington's Disease Phenotypes in Induced Pluripotent Stem Cells. *Cell Stem Cell*, 11, pp.253–263.
- An, M.C. et al., 2014. Polyglutamine Disease Modeling: Epitope Based Screen for Homologous Recombination using CRISPR/Cas9 System. *PLoS currents*, 6.
- Andrew, S.E. et al., 1993. The relationship between trinucleotide (CAG) repeat length and clinical features of Huntington's disease. *Nature genetics*, 4(4), pp.398–403.
- Angelopoulos, P. et al., 2008. Cytokines in Alzheimer's disease and vascular dementia. *The International journal of neuroscience*, 118(12), pp.1659–1672.
- Ard, M.D. et al., 1996. Scavenging of Alzheimer's amyloid beta-protein by microglia in culture. *Journal of neuroscience research*, 43(2), pp.190–202.
- Armulik, A. et al., 2010. Pericytes regulate the blood-brain barrier. *Nature*, 468(7323), pp.557–561.
- Asai, H. et al., 2015. Depletion of microglia and inhibition of exosome synthesis halt tau propagation. *Nature Neuroscience*, 18(11), pp.1584–1593. Available at: <http://www.nature.com/doi/10.1038/nn.4132>.
- Ashburner, M. et al., 2000. Gene ontology: tool for the unification of biology. The Gene Ontology Consortium. *Nature genetics*, 25(1), pp.25–29.
- Askew, K. et al., 2017. Coupled Proliferation and Apoptosis Maintain the Rapid Turnover of Microglia in the Adult Brain. *Cell Reports*, 18(2), pp.391–405.
- Aung, H.T. et al., 2006. LPS regulates proinflammatory gene expression in macrophages by altering histone deacetylase expression. *The FASEB journal*, 20(9), pp.1315–1327.
- Avramopoulos, D., 2009. Genetics of Alzheimer's disease: recent advances. *Genome Medicine*, 1(3), pp.1–7.
- Bae, S., Park, J. & Kim, J.S., 2014. Cas-OFFinder: A fast and versatile algorithm that searches

- for potential off-target sites of Cas9 RNA-guided endonucleases. *Bioinformatics*, 30(10), pp.1473–1475.
- Bailey, C.C. et al., 2014. IFITM-Family Proteins: The Cell's First Line of Antiviral Defense. *Annual review of virology*, 1, pp.261–283. Available at: <http://www.ncbi.nlm.nih.gov/pmc/articles/PMC4295558/>.
- Bamji-Mirza, M. et al., 2016. Genetic Variations in ABCA7 Can Increase Secreted Levels of Amyloid-40 and Amyloid-42 Peptides and ABCA7 Transcription in Cell Culture Models. *Journal of Alzheimer's disease : JAD*, 53, pp.875–892.
- Banati, R.B., 2002. Visualising microglial activation in vivo. *Glia*, 40(2), pp.206–217.
- Baxter, A.W. et al., 2011. Role of P2X4 receptors in synaptic strengthening in mouse CA1 hippocampal neurons. *European Journal of Neuroscience*, 34(2), pp.213–220.
- Beach, T.G., Walker, R. & McGeer, E.G., 1989. Patterns of gliosis in Alzheimer's disease and aging cerebrum. *Glia*, 2(6), pp.420–436.
- Beek, J., Guskov, A. & Slotboom, D.J., 2014. Structural diversity of ABC transporters. *The Journal of General Physiology*, pp.419–435.
- Bellenguez, C. et al., 2017. Contribution to Alzheimer's disease risk of rare variants in TREM2, SORL1, and ABCA7 in 1779 cases and 1273 controls. *Neurobiology of Aging*, 59, p.220.e1-220.e9.
- Bennett, F.C. et al., 2018. A Combination of Ontogeny and CNS Environment Establishes Microglial Identity. *Neuron*, 98(6), p.1170–1183.e8. Available at: <https://doi.org/10.1016/j.neuron.2018.05.014>.
- Berry, B.J. et al., 2018. Physiological A $\beta$  Concentrations Produce a More Biomimetic Representation of the Alzheimer's Disease Phenotype in iPSC Derived Human Neurons. *ACS Chemical Neuroscience*, pp.1–9.
- Bertrand, J.Y. et al., 2005. Three pathways to mature macrophages in the early mouse yolk sac Three pathways to mature macrophages in the early mouse yolk sac. *Blood*, 106(9), pp.3004–3011.
- Bhaskar, K. et al., 2010. Regulation of tau pathology by the microglial fractalkine receptor. *Neuron*, 68(1), pp.19–31. Available at: <http://dx.doi.org/10.1016/j.neuron.2010.08.023>.
- Biber, K. et al., 2007. Neuronal 'On' and 'Off' signals control microglia. *Trends in Neurosciences*, 30(11), pp.596–602.
- Biswas, S.K. & Mantovani, A., 2010. Macrophage plasticity and interaction with lymphocyte subsets: Cancer as a paradigm. *Nature Immunology*, 11(10), pp.889–896. Available at: <http://dx.doi.org/10.1038/ni.1937>.
- Biswas, S.K. & Mantovani, A., 2012. Orchestration of metabolism by macrophages. *Cell Metabolism*, 15(4), pp.432–437. Available at: <http://dx.doi.org/10.1016/j.cmet.2011.11.013>.
- Björkqvist, M. et al., 2008. A novel pathogenic pathway of immune activation detectable before clinical onset in Huntington's disease. *The Journal of experimental medicine*, 205(8), pp.1869–77. Available at: <http://jem.rupress.org/content/205/8/1869>.
- Block, M.L., Zecca, L. & Hong, J.-S., 2007. Microglia-mediated neurotoxicity: uncovering the molecular mechanisms. *Nature reviews. Neuroscience*, 8(1), pp.57–69. Available at: <http://www.nature.com/nrn/journal/v8/n1/pdf/nrn2038.pdf>.
- Bodzioch, M. et al., 1999. The gene encoding ATP-binding cassette transporter 1 is mutated in Tangier disease. *Nature genetics*, 22(4), pp.347–351.
- Bohlen, C.J. et al., 2017. Diverse Requirements for Microglial Survival, Specification, and Function Revealed by Defined-Medium Cultures. *Neuron*, 94(4), p.759–773.e8.

- Available at: <http://dx.doi.org/10.1016/j.neuron.2017.04.043>.
- Bolger, A.M., Lohse, M. & Usadel, B., 2014. Trimmomatic: a flexible trimmer for Illumina sequence data. *Bioinformatics*, 30(15), pp.2114–2120.
- Bouchard, J. et al., 2012. Cannabinoid Receptor 2 Signaling in Peripheral Immune Cells Modulates Disease Onset and Severity in Mouse Models of Huntington's Disease. *Journal of Neuroscience*, 32(50), pp.18259–18268. Available at: <http://www.jneurosci.org/cgi/doi/10.1523/JNEUROSCI.4008-12.2012>.
- Bradford, J. et al., 2009. Expression of mutant huntingtin in mouse brain astrocytes causes age-dependent neurological symptoms. *Proceedings of the National Academy of Sciences*, 106(52), pp.22480–22485. Available at: <http://www.pnas.org/lookup/doi/10.1073/pnas.0911503106>.
- Breteler, M.M.B., 2000. Vascular risk factors for Alzheimer's disease: An epidemiologic perspective. *Neurobiology of Aging*, 21(2), pp.153–160. Available at: <http://www.sciencedirect.com/science/article/pii/S0197458099001104?via%3Dihub> [Accessed October 9, 2017].
- Broccardo, C. et al., 2001. Comparative analysis of the promoter structure and genomic organization of the human and mouse ABCA7 gene encoding a novel ABCA transporter. *Cytogenetics and cell genetics*, 92(3–4), pp.264–270.
- Brooke, G. et al., 2004. Human lymphocytes interact directly with CD47 through a novel member of the signal regulatory protein (SIRP) family. *Journal of immunology*, 173(4), pp.2562–2570.
- Brown, G.C. & Neher, J.J., 2014. Microglial phagocytosis of live neurons. *Nature Reviews Neuroscience*, 15(4), pp.209–216. Available at: <http://dx.doi.org/10.1038/nrn3710%5Cnpapers2://publication/doi/10.1038/nrn3710>.
- Brownjohn, P.W. et al., 2018. Functional Studies of Missense TREM2 Mutations in Human Stem Cell-Derived Microglia. *Stem Cell Reports*, 10, pp.1–14. Available at: <https://doi.org/10.1016/j.stemcr.2018.03.003>.
- Buchrieser, J., James, W. & Moore, M.D., 2017. Human Induced Pluripotent Stem Cell-Derived Macrophages Share Ontogeny with MYB-Independent Tissue-Resident Macrophages. *Stem Cell Reports*, 8(2), pp.334–345. Available at: <http://dx.doi.org/10.1016/j.stemcr.2016.12.020>.
- Budka, H. et al., 1995. Neuropathological diagnostic criteria for Creutzfeldt-Jakob disease (CJD) and other human spongiform encephalopathies (prion diseases). *Brain pathology*, 5(4), pp.459–466.
- Butovsky, O. et al., 2014. Identification of a unique TGF- $\beta$ -dependent molecular and functional signature in microglia. *Nature neuroscience*, 17(1), pp.131–43. Available at: <http://www.pubmedcentral.nih.gov/articlerender.fcgi?artid=4066672&tool=pmcentrez&rendertype=abstract>.
- Buttgereit, A. et al., 2016. Sall1 is a transcriptional regulator defining microglia identity and function. *Nature Immunology*, 17(12), pp.1397–1406. Available at: <http://www.nature.com/doi/10.1038/ni.3585>.
- Cagnin, A. et al., 2001. In-vivo measurement of activated microglia in dementia. *Lancet*, 358(9280), pp.461–467.
- Cajal, 1913 (*Contribución al conocimiento de la neuroglia del cerebro humano. Trab. Lab. Invest. Biol.* 11, 255–345
- Canton, J., 2014. Phagosome maturation in polarized macrophages. *Journal of Leukocyte Biology*, 96(5), pp.729–738. Available at:

- <http://www.jleukbio.org/cgi/doi/10.1189/jlb.1MR0114-021R>.
- Cardona, A.E. et al., 2006. Control of microglial neurotoxicity by the fractalkine receptor. *Nature Neuroscience*, 9(7), pp.917–924.
- Carter, S.F. et al., 2012. Evidence for Astrocytosis in Prodromal Alzheimer Disease Provided by 11C-Deuterium-L-Deprenyl: A Multitracer PET Paradigm Combining 11C-Pittsburgh Compound B and 18F-FDG. *Journal of Nuclear Medicine*, 53(1), pp.37–46. Available at: <http://jnm.snmjournals.org/cgi/doi/10.2967/jnumed.110.087031>.
- Castellano, J.M. et al., 2011. Human apoE Isoforms Differentially Regulate Brain Amyloid- $\beta$  Peptide Clearance. *Science Translational Medicine*, 3(89).
- Castoreno, A.B. et al., 2005. Transcriptional regulation of phagocytosis-induced membrane biogenesis by sterol regulatory element binding proteins. *Proceedings of the National Academy of Sciences of the United States of America*, 102(37), pp.13129–13134.
- Cattaneo, E., Zuccato, C. & Tartari, M., 2005. Normal huntingtin function: An alternative approach to Huntington's disease. *Nature Reviews Neuroscience*, 6(12), pp.919–930.
- Cervantes, J.L. et al., 2012. TLR8: the forgotten relative revindicated. *Cellular And Molecular Immunology*, 9, p.434. Available at: <http://dx.doi.org/10.1038/cmi.2012.38>.
- Chakrabarty, P. et al., 2015. IL-10 Alters Immunoproteostasis in APP Mice, Increasing Plaque Burden and Worsening Cognitive Behavior. *Neuron*, 85(3), pp.519–533. Available at: <http://dx.doi.org/10.1016/j.neuron.2014.11.020>.
- Chan, S.L. et al., 2008. ATP-binding cassette transporter A7 regulates processing of amyloid precursor protein in vitro. *Journal of Neurochemistry*, 106(2), pp.793–804.
- Chen, H. et al., 2003. Nonsteroidal anti-inflammatory drugs and the risk of Parkinson disease. *Archives of neurology*, 60(8), pp.1059–1064.
- Cherry, J.D., Olschowka, J.A. & O'Banion, M.K., 2014. Are 'resting' microglia more 'M2'? *Frontiers in Immunology*, 5(NOV), pp.2–5.
- Chiu, I.M. et al., 2013. A neurodegeneration-specific gene-expression signature of acutely isolated microglia from an amyotrophic lateral sclerosis mouse model. *Cell Reports*, 4(2), pp.385–401. Available at: <http://dx.doi.org/10.1016/j.celrep.2013.06.018>.
- Choi, S.H. et al., 2012. Inhibition of NADPH oxidase promotes alternative and anti-inflammatory microglial activation during neuroinflammation. *Journal of Neurochemistry*, 120(2), pp.292–301.
- Choo, I.L.H. et al., 2014. Astrocytosis measured by (1)(1)C-deprenyl PET correlates with decrease in gray matter density in the parahippocampus of prodromal Alzheimer's patients. *European journal of nuclear medicine and molecular imaging*, 41(11), pp.2120–2126.
- Clark, R.B., 2002. The role of PPARs in inflammation and immunity. *Journal of leukocyte biology*, 71(3), pp.388–400.
- Colantuoni, C. et al., 2011. Temporal dynamics and genetic control of transcription in the human prefrontal cortex. *Nature*, 478(7370), pp.519–523.
- Colonna, M., 2003. Tremors in the immune system and beyond. *Nature Reviews Immunology*, 3(6), pp.445–453.
- Corder, E.H. et al., 1993. Gene Dose of Apolipoprotein E Type 4 Allele and the Risk of Alzheimer's Disease in Late Onset Families. *Science*, 261(14), pp.921–923.
- Costa, V. & Scorrano, L., 2012. Shaping the role of mitochondria in the pathogenesis of Huntington's disease. *EMBO Journal*, 31(8), pp.1853–1864. Available at: <http://dx.doi.org/10.1038/emboj.2012.65>.
- Croft, D. et al., 2014. The Reactome pathway knowledgebase. *Nucleic acids research*,

- 42(Database issue), pp.D472-7.
- Cronk, J.C. et al., 2018. Peripherally derived macrophages can engraft the brain independent of irradiation and maintain an identity distinct from microglia. *The Journal of Experimental Medicine*, 215(6), pp.1627–1647. Available at: <http://www.jem.org/lookup/doi/10.1084/jem.20180247>.
- Crotti, A. et al., 2014. Mutant Huntingtin promotes autonomous microglia activation via myeloid lineage-determining factors. *Nature Neuroscience*, 17(4), pp.513–521.
- Crotti, A. & Glass, C.K., 2015. The choreography of neuroinflammation in Huntington's disease. *Trends in Immunology*, 36(6), pp.364–373. Available at: <http://dx.doi.org/10.1016/j.it.2015.04.007>.
- Cummings, J.L., Morstorf, T. & Zhong, K., 2014. Alzheimer's disease drug-development pipeline : few candidates , frequent failures. *Alzheimer's research & therapy*, pp.1–7.
- Cuyvers, E. et al., 2015. Mutations in ABCA7 in a Belgian cohort of Alzheimer's disease patients: A targeted resequencing study. *The Lancet Neurology*, 14(8), pp.814–822. Available at: [http://dx.doi.org/10.1016/S1474-4422\(15\)00133-7](http://dx.doi.org/10.1016/S1474-4422(15)00133-7).
- D'Andrea, M.R., Cole, G.M. & Ard, M.D., 2004. The microglial phagocytic role with specific plaque types in the Alzheimer disease brain. *Neurobiology of Aging*, 25, pp.675–683.
- Dagher, N.N. et al., 2015. Colony-stimulating factor 1 receptor inhibition prevents microglial plaque association and improves cognition in 3xTg-AD mice. *Journal of Neuroinflammation*, 12(1), pp.1–14. Available at: <http://dx.doi.org/10.1186/s12974-015-0366-9>.
- Dahlgren, K.N. et al., 2002. Oligomeric and fibrillar species of amyloid- $\beta$  peptides differentially affect neuronal viability. *Journal of Biological Chemistry*, 277(35), pp.32046–32053.
- Dalrymple, A. et al., 2007. Proteomic profiling of plasma in Huntington's disease reveals neuroinflammatory activation and biomarker candidates. *Journal of Proteome Research*, 6(7), pp.2833–2840.
- Damiano, M. et al., 2010. Mitochondria in Huntington's disease. *Biochimica et Biophysica Acta - Molecular Basis of Disease*, 1802(1), pp.52–61. Available at: <http://dx.doi.org/10.1016/j.bbadis.2009.07.012>.
- Danbolt, N.C., 2001. Glutamate uptake. *Progress in neurobiology*, 65(1), pp.1–105.
- Davalos, D. et al., 2005. ATP mediates rapid microglial response to local brain injury in vivo. *Nature Neuroscience*, 8(6), pp.752–758.
- Davis, E.J., Foster, T.D. & Thomas, W.E., 1994. Cellular forms and functions of brain microglia. *Brain research bulletin*, 34(1), pp.73–78.
- Dawe, H.R. et al., 2003. ADF/cofilin controls cell polarity during fibroblast migration. *Current Biology*, 13(3), pp.252–257.
- Dean, M. & Annilo, T., 2005. Evolution of the ATP-binding cassette (ABC) transporter superfamily in vertebrates. *Annual review of genomics and human genetics*, 6, pp.123–142.
- Dehairs, J. et al., 2016. CRISP-ID: Decoding CRISPR mediated indels by Sanger sequencing. *Scientific Reports*, 6(July), pp.1–5. Available at: <http://dx.doi.org/10.1038/srep28973>.
- Dobin, A. et al., 2013. STAR: ultrafast universal RNA-seq aligner. *Bioinformatics*, 29(1), pp.15–21.
- Donato, M. et al., 2013. Analysis and correction of crosstalk effects in pathway analysis. *Genome Research*, 23, pp.1885–1893.
- Draghici, S. et al., 2007. A systems biology approach for pathway level analysis. *Genome*

- Research*, 17, pp.1537–1545.
- Drouin-ouellet, J. et al., 2015. Cerebrovascular and Blood – Brain Barrier Impairments in Huntington’s Disease : Potential Implications for Its Pathophysiology. *Annals of Neurology*, 78, pp.160–177.
- Durafour, B.A. et al., 2012. Comparison of Polarization Properties of Human Adult Microglia and Blood-Derived Macrophages. *Glia*, 727(August 2011), pp.717–727.
- Dursun, E. et al., 2015. The interleukin 1 alpha, interleukin 1 beta, interleukin 6 and alpha-2-macroglobulin serum levels in patients with early or late onset Alzheimer’s disease, mild cognitive impairment or Parkinson’s disease. *Journal of neuroimmunology*, 283, pp.50–57.
- Edison, P. et al., 2008. Microglia, amyloid, and cognition in Alzheimer’s disease: An [11C](R)PK11195-PET and [11C]PIB-PET study. *Neurobiology of disease*, 32(3), pp.412–419.
- Ellrichmann, G. et al., 2013. The Role of the Immune System in Huntington’s Disease. *Clinical and Developmental Immunology*, 2013(541259), pp.1–11. Available at: <http://dx.doi.org/10.1155/2013/541259%0AReview>.
- Erblich, B. et al., 2011. Absence of colony stimulation factor-1 receptor results in loss of microglia, disrupted brain development and olfactory deficits. *PLoS ONE*, 6(10), p.e26317.
- Erdman, L.K. et al., 2009. CD36 and TLR interactions in inflammation and phagocytosis: implications for malaria. *Journal of immunology (Baltimore, Md. : 1950)*, 183(10), pp.6452–6459.
- Esiri, M.M., Al Izz, M.S. & Reading, M.C., 1991. Macrophages, microglial cells, and HLA-DR antigens in fetal and infant brain. *Journal of Clinical Pathology*, 44, pp.102–106.
- Estrada-Sánchez, A.M. & Rebec, G. V., 2012. Corticostriatal dysfunction and glutamate transporter 1 (GLT1) in Huntington’s disease: Interactions between neurons and astrocytes. *Basal Ganglia*, 2(2), pp.57–66.
- Etminan, M., Gill, S. & Samii, A., 2003. Effect of non-steroidal anti-inflammatory drugs on risk of Alzheimer’s disease: systematic review and meta-analysis of observational studies. *BMJ*, 327, pp.1–5.
- Everts, B. et al., 2012. Commitment to glycolysis sustains survival of NO-producing inflammatory dendritic cells. *Blood*, 120(7), pp.1422–1431.
- Everts, B. et al., 2014. TLR-driven early glycolytic reprogramming via the kinases TBK1- IKKvarepsilon supports the anabolic demands of dendritic cell activation. *Nature immunology*, 15(4), pp.323–332.
- Fabelo, N. et al., 2014. Altered lipid composition in cortical lipid rafts occurs at early stages of sporadic Alzheimer’s disease and facilitates APP/BACE1 interactions. *Neurobiology of Aging*, 35(8), pp.1801–1812. Available at: <http://dx.doi.org/10.1016/j.neurobiolaging.2014.02.005>.
- Fan, R. et al., 2007. Minocycline Reduces Microglial Activation and Improves Behavioral Deficits in a Transgenic Model of Cerebral Microvascular Amyloid. *Journal of Neuroscience*, 27(12), pp.3057–3063. Available at: <http://www.jneurosci.org/cgi/doi/10.1523/JNEUROSCI.4371-06.2007>.
- Farkas, E. & Luiten, P.G.M., 2001. *Cerebral microvascular pathology in aging and Alzheimer’s disease*,
- Fedoroff, S., Zhai, R. & Novak, J.P., 1997. Microglia and Astroglia Have a Common Progenitor Cell. *Journal of Neuroscience Research*, 50, pp.477–486.

- Forlenza, O.V. et al., 2009. Increased serum IL-1beta level in Alzheimer's disease and mild cognitive impairment. *Dementia and geriatric cognitive disorders*, 28(6), pp.507–512.
- Fowler, J.S. et al., 2005. Translational neuroimaging: positron emission tomography studies of monoamine oxidase. *Molecular imaging and biology : MIB : the official publication of the Academy of Molecular Imaging*, 7(6), pp.377–387.
- Franciosi, S. et al., 2012. Age-dependent neurovascular abnormalities and altered microglial morphology in the YAC128 mouse model of Huntington disease. *Neurobiology of Disease*, 45(1), pp.438–449. Available at: <http://dx.doi.org/10.1016/j.nbd.2011.09.003>.
- Francis, G.A., Knopp, R.H. & Oram, J.F., 1995. Defective removal of cellular cholesterol and phospholipids by apolipoprotein A-I in Tangier Disease. *The Journal of clinical investigation*, 96(1), pp.78–87.
- Fraser, D.A., Pisalyaput, K. & Tenner, A.J., 2010. C1q enhances microglial clearance of apoptotic neurons and neuronal blebs, and modulates subsequent inflammatory cytokine production. *Journal of Neurochemistry*, 112(3), pp.733–743.
- Fu, Y. et al., 2016. ABCA7 Mediates Phagocytic Clearance of Amyloid- $\beta$  in the Brain. *Journal of Alzheimer's disease : JAD*, 54, pp.569–584.
- Galatro, T.F. et al., 2017. Transcriptomic analysis of purified human cortical microglia reveals age-associated changes. *Nature Neuroscience*, 20(8), pp.1162–1174.
- Galea, I., Bechmann, I. & Perry, V.H., 2007. What is immune privilege (not)? *Trends in Immunology*, 28(1), pp.12–18.
- Galimberti, D. et al., 2006. Serum MCP-1 levels are increased in mild cognitive impairment and mild Alzheimer's disease. *Neurobiology of aging*, 27(12), pp.1763–1768.
- Galván-peña, S. & O'Neill, L.A.J., 2014. Metabolic reprogramming in macrophage polarization. *Frontiers in Immunology*, 5(September), pp.1–6.
- Gatz, M. et al., 2006. Role of Genes and Environments for Explaining Alzheimer Disease. *Archives in Genetic Psychiatry*, 63(2), pp.168–174.
- GeM-HD Consortium, 2015. Identification of Genetic Factors that Modify Clinical Onset of Huntington's Disease. *Cell*, 162, pp.516–526.
- Ginhoux, F. et al., 2010. Hematopoietic Waves of Microglial Recruitment and Differentiation Occur in the Central Nervous. *Science*, 330(2009).
- Ginhoux, F. et al., 2013. Origin and differentiation of microglia. *Frontiers in cellular neuroscience*, 7(April), p.45. Available at: <http://www.pubmedcentral.nih.gov/articlerender.fcgi?artid=3627983&tool=pmcentrez&rendertype=abstract>.
- Goate, A.M. et al., 1991. Segregation of a missense mutation in the amyloid precursor protein gene with familial Alzheimer's disease. *Nature*, 349.
- Gomez-Nicola, D. & Perry, V.H., 2015. Microglial Dynamics and Role in the Healthy and Diseased Brain: A Paradigm of Functional Plasticity. *The Neuroscientist*, 21(1), pp.169–184.
- Gomez Perdiguero, E. et al., 2014. Tissue-resident macrophages originate from yolk-sac-derived erythro-myeloid progenitors. *Nature*, 518(7540), pp.547–551. Available at: <http://www.nature.com/doi/10.1038/nature13989>.
- Gordon, S. & Martinez, F.O., 2010. Alternative activation of macrophages: Mechanism and functions. *Immunity*, 32(5), pp.593–604. Available at: <http://dx.doi.org/10.1016/j.immuni.2010.05.007>.
- Gosselin, D. et al., 2014. Environment drives selection and function of enhancers controlling tissue-specific macrophage identities. *Cell*, 159(6), pp.1327–1340. Available at:

- <http://dx.doi.org/10.1016/j.cell.2014.11.023>.
- Götz, J. & Ittner, L.M., 2008. Animal models of Alzheimer's disease and frontotemporal dementia. *Nature Neuroscience*, 9(july).
- Grabert, K. et al., 2016. Microglial brain region-dependent diversity and selective regional sensitivities to aging. *Nature Neuroscience*, (January). Available at: <http://www.nature.com/doi/10.1038/nn.4222>.
- Graeber, M.B., Li, W. & Rodriguez, M.L., 2011. Role of microglia in CNS inflammation. *FEBS Letters*, 585(23), pp.3798–3805. Available at: <http://dx.doi.org/10.1016/j.febslet.2011.08.033>.
- Gray, M. et al., 2008. Full-Length Human Mutant Huntingtin with a Stable Polyglutamine Repeat Can Elicit Progressive and Selective Neuropathogenesis in BACHD Mice. *Journal of Neuroscience*, 28(24), pp.6182–6195. Available at: <http://www.jneurosci.org/cgi/doi/10.1523/JNEUROSCI.0857-08.2008>.
- Greter, M. et al., 2012. Stroma-Derived Interleukin-34 Controls the Development and Maintenance of Langerhans Cells and the Maintenance of Microglia. *Immunity*, 37, pp.1050–1060.
- Griciuc, A. et al., 2013. Alzheimer's Disease Risk Gene CD33 Inhibits Microglial Uptake of Amyloid Beta. *Neuron*, 78(4), pp.631–643. Available at: <http://dx.doi.org/10.1016/j.neuron.2013.04.014>.
- Le Guennec, K. et al., 2016. ABCA7 rare variants and Alzheimer disease risk. *Neurology*, 86(23), pp.2134–2137.
- Guerreiro, R. et al., 2013. TREM2 Variants in Alzheimer's Disease. *New England Journal of Medicine*, 368(2), pp.117–127.
- Gulyas, B. et al., 2011. Activated MAO-B in the brain of Alzheimer patients, demonstrated by [11C]-L-deprenyl using whole hemisphere autoradiography. *Neurochemistry international*, 58(1), pp.60–68.
- Ha, S.-D. et al., 2008. Cathepsin B Is Involved in the Trafficking of TNF- $\alpha$ -Containing Vesicles to the Plasma Membrane in Macrophages. *The Journal of Immunology*, 181(1), pp.690–697. Available at: <http://www.jimmunol.org/cgi/doi/10.4049/jimmunol.181.1.690>.
- van de Haar, H.J. et al., 2016. Blood-Brain Barrier Leakage in Patients with Early Alzheimer Disease. *Radiology*, 281(2), pp.527–535. Available at: <https://doi.org/10.1148/radiol.2016152244>.
- van de Haar, H.J. et al., 2016. Neurovascular unit impairment in early Alzheimer's disease measured with magnetic resonance imaging. *Neurobiology of Aging*, 45, pp.190–196. Available at: <http://dx.doi.org/10.1016/j.neurobiolaging.2016.06.006>.
- de Haas, A.H., Boddeke, H.W.G.M. & Biber, K., 2008. Region-specific expression of immunoregulatory proteins on microglia in the healthy CNS. *Glia*, 56(8), pp.888–894.
- Haenseler, W. et al., 2017. Excess  $\alpha$ -synuclein compromises phagocytosis in iPSC-derived macrophages. *Scientific Reports*, (July), pp.1–11. Available at: <http://dx.doi.org/10.1038/s41598-017-09362-3>.
- Halliday, G.M. et al., 1998. Regional specificity of brain atrophy in Huntington's disease. *Experimental neurology*, 154(2), pp.663–672.
- Hamelin, L. et al., 2016. Early and protective microglial activation in Alzheimer's disease: a prospective study using  $^{18}$ F-DPA-714 PET imaging. *Brain*, 139(4), pp.1252–1264. Available at: <https://academic.oup.com/brain/article-lookup/doi/10.1093/brain/aww017>.
- Hammond, T.R. et al., 2018. Complex cell-state changes revealed by single cell RNA

- sequencing of 76 , 149 microglia throughout the mouse lifespan and in the injured brain. *Biorxiv*, pp.1–22.
- Hanisch, U.-K.K. & Kettenmann, H., 2007. Microglia: active sensor and versatile effector cells in the normal and pathologic brain. *Nature Neuroscience*, 10(11), pp.1387–1394. Available at: <http://www.ncbi.nlm.nih.gov/pubmed/17965659>.
- Hanisch, U.K., Johnson, T. V. & Kipnis, J., 2008. Toll-like receptors: roles in neuroprotection? *Trends in Neurosciences*, 31(4), pp.176–182.
- Hao, C., Richardson, A. & Fedoroff, S., 1991. Macrophage-like cells originate from neuroepithelium in culture: characterization and properties of the macrophage-like cells. *International journal of developmental neuroscience*, 9(1), pp.1–14.
- Hardy, J. & Selkoe, D.J., 2002. The amyloid hypothesis of Alzheimer’s disease: progress and problems on the road to therapeutics. *Science (New York, N.Y.)*, 297(5580), pp.353–356. Available at: <http://www.ncbi.nlm.nih.gov/pubmed/12130773>.
- Hardy, J.A. & Higgins, G.A., 1992. Alzheimer’s disease: the amyloid cascade hypothesis. *Science (New York, N.Y.)*, 256(5054), pp.184–185.
- Harold, D. et al., 2009. Genome-wide association study identifies variants at CLU and PICALM associated with Alzheimer ’ s disease. *Nature genetics*, 41(10).
- Harris, M.A. et al., 2004. The Gene Ontology (GO) database and informatics resource. *Nucleic acids research*, 32(Database issue), pp.D258-61.
- Harrison, D.J. et al., 2018. The Effect of Tissue Preparation and Donor Age on Striatal Graft Morphology in the Mouse. *Cell Transplantation*, 27(2), pp.230–244.
- Haynes, S.E. et al., 2006. The P2Y12 receptor regulates microglial activation by extracellular nucleotides. *Nature neuroscience*, 9(12), pp.1512–1519.
- HD iPSC Consortium, 2012. Induced Pluripotent Stem Cells from Patients with Huntington’s Disease Show CAG-Repeat-Extension Associated Phenotypes. *Cell Stem Cell*, 11, pp.264–278.
- Heneka, M.T. et al., 2013. NLRP3 is activated in Alzheimer’s disease and contributes to pathology in APP/PS1 mice. *Nature*, 493(7434), pp.674–678. Available at: <http://www.ncbi.nlm.nih.gov/pubmed/23254930><http://www.nature.com/nature/journal/v493/n7434/pdf/nature11729.pdf>.
- Herrup, K., 2015. The case for rejecting the amyloid cascade hypothesis. *Nature Neuroscience*, 18(6), pp.794–799. Available at: <http://www.nature.com/doi/10.1038/nn.4017><http://www.ncbi.nlm.nih.gov/pubmed/26007212><http://www.nature.com/neuro/journal/v18/n6/pdf/nn.4017.pdf>.
- Hickman, S.E. et al., 2013. The microglial sensome revealed by direct RNA sequencing. *Nature neuroscience*, 16(12), pp.1896–905. Available at: <http://www.pubmedcentral.nih.gov/articlerender.fcgi?artid=3840123&tool=pmcentrez&rendertype=abstract>.
- Higgins, C.F., 1992. ABC transporters: from microorganisms to man. *Annual review of cell biology*, 8, pp.67–113.
- Higgins, C.F. & Linton, K.J., 2004. The ATP switch model for ABC transporters. *Nature reviews. Structural & molecular biology*, 11(10), pp.918–926.
- Hirschhorn, J.N. & Daly, M.J., 2005. genome-wide association studies for common diseases and complex traits. *Nature reviews. Genetics*, 6(February), pp.95–108.
- Hoek, R.M. et al., 2000. Down-regulation of the macrophage lineage through interaction

- with OX2 (CD200). *Science (New York, N.Y.)*, 290(5497), pp.1768–1771.
- Hollingworth, P. et al., 2011. Common variants at ABCA7, MS4A6A/MS4A4E, EPHA1, CD33 and CD2AP are associated with Alzheimer's disease. *Nature genetics*, 43(5), pp.429–436.
- Holtzman, D.M., Morris, J.C. & Goate, A.M., 2011. Alzheimer's Disease : The Challenge of the Second Century. *Science Translational Medicine*, 3(77), pp.1–18.
- Hong, S. et al., 2016. Complement and microglia mediate early synapse loss in Alzheimer mouse models. *Science*, 8373, pp.1–9. Available at: <http://www.sciencemag.org/cgi/doi/10.1126/science.aad8373>.
- Hoozemans, J.J.M. et al., 2011. Soothing the inflamed brain: effect of non-steroidal anti-inflammatory drugs on Alzheimer's disease pathology. *CNS & neurological disorders drug targets*, 10(1), pp.57–67.
- Hsiao, H.-Y. et al., 2014. Inhibition of soluble tumor necrosis factor is therapeutic in Huntington's disease. *Human Molecular Genetics*, 23(16), pp.4328–4344. Available at: <https://academic.oup.com/hmg/article-lookup/doi/10.1093/hmg/ddu151>.
- Huang, D.W., Sherman, B.T. & Lempicki, R.A., 2008. Systematic and integrative analysis of large gene lists using DAVID bioinformatics resources. *Nature Protocols*, 4, p.44. Available at: <http://dx.doi.org/10.1038/nprot.2008.211>.
- Huyhn, a et al., 1995. Characterization of hematopoietic progenitors from human yolk sacs and embryos. *Blood*, 86(12), pp.4474–85. Available at: <http://www.ncbi.nlm.nih.gov/pubmed/8541536>.
- Ikeda, Y. et al., 2003. Posttranscriptional regulation of human ABCA7 and its function for the apoA-I-dependent lipid release. *Biochemical and Biophysical Research Communications*, 311(2), pp.313–318.
- Imai, F. et al., 2007. Neuroprotective effect of exogenous microglia in global brain ischemia. *Journal of cerebral blood flow and metabolism*, 27(3), pp.488–500.
- Ishii, K. et al., 1997. Increased A $\beta$ 42(43)-plaque deposition in early-onset familial Alzheimer's disease brains with the deletion of exon 9 and the missense point mutation ( H163R ) in the PS-1 gene. *Neuroscience Letters*, 228, pp.17–20.
- Itagaki, S. et al., 1989. Relationship of microglia and astrocytes to amyloid deposits of Alzheimer disease. *Journal of neuroimmunology*, 24(3), pp.173–182.
- Iwamoto, N. et al., 2006. ABCA7 expression is regulated by cellular cholesterol through the SREBP2 pathway and associated with phagocytosis. *Journal of lipid research*, 47(9), pp.1915–1927.
- Jankowsky, J.L. et al., 2004. Mutant presenilins specifically elevate the levels of the 42 residue beta-amyloid peptide in vivo: evidence for augmentation of a 42-specific gamma secretase. *Human molecular genetics*, 13(2), pp.159–170.
- Jehle, A.W. et al., 2006. ATP-binding cassette transporter A7 enhances phagocytosis of apoptotic cells and associated ERK signaling in macrophages. *The Journal of cell biology*, 174(4), pp.547–556.
- Jones, L. et al., 2015. Convergent genetic and expression data implicate immunity in Alzheimer's disease. *Alzheimer's and Dementia*, 11(6), pp.658–671.
- Jonsson, T. et al., 2013. Variant of TREM2 Associated with the Risk of Alzheimer's Disease. *New England Journal of Medicine*, 368(2), pp.107–116.
- Jossan, S.S. et al., 1991. Monoamine oxidase B in brains from patients with Alzheimer's disease: a biochemical and autoradiographical study. *Neuroscience*, 45(1), pp.1–12.
- Kajiwara, M. et al., 2012. Donor-dependent variations in hepatic differentiation from

- human-induced pluripotent stem cells. *Proceedings of the National Academy of Sciences*, 109(36), pp.14716–14716. Available at: <http://www.pnas.org/cgi/doi/10.1073/pnas.1212710109>.
- Kalonia, H. et al., 2010. Protective effect of rofecoxib and nimesulide against intra-striatal quinolinic acid-induced behavioral, oxidative stress and mitochondrial dysfunctions in rats. *Neurotoxicology*, 31(2), pp.195–203.
- Kalonia, H. & Kumar, A., 2011. Suppressing inflammatory cascade by cyclo-oxygenase inhibitors attenuates quinolinic acid induced Huntington's disease-like alterations in rats. *Life sciences*, 88(17–18), pp.784–791.
- Kaminski, W.E. et al., 2000. Identification of a novel human sterol-sensitive ATP-binding cassette transporter (ABCA7). *Biochemical and biophysical research communications*, 273, pp.532–538.
- Kanehisa, M. et al., 2012. KEGG for integration and interpretation of large-scale molecular data sets. *Nucleic acids research*, 40(Database issue), pp.D109–14.
- Kapellos, T.S. et al., 2016. A novel real time imaging platform to quantify macrophage phagocytosis. *Biochemical Pharmacology*, 116, pp.107–119. Available at: <http://dx.doi.org/10.1016/j.bcp.2016.07.011>.
- Karch, C.M. et al., 2012. Expression of Novel Alzheimer's Disease Risk Genes in Control and Alzheimer's Disease Brains. *PLoS ONE*, 7(11), p.e50976.
- Karch, C.M. & Goate, A.M., 2015. Alzheimer's Disease Risk Genes and Mechanisms of Disease Pathogenesis. *Biological Psychiatry*, 77(1), pp.43–51. Available at: <http://linkinghub.elsevier.com/retrieve/pii/S0006322314003394>.
- Karlsson, K.R. et al., 2008. Homogeneous monocytes and macrophages from human embryonic stem cells following coculture-free differentiation in M-CSF and IL-3. *Experimental Hematology*, 36(9), pp.1167–1175.
- Kashon, M.L. et al., 2004. Associations of cortical astrogliosis with cognitive performance and dementia status. *Journal of Alzheimer's disease : JAD*, 6(6), pp.581–595.
- Katakura, T. et al., 2004. CCL17 and IL-10 as effectors that enable alternatively activated macrophages to inhibit the generation of classically activated macrophages. *Journal of immunology (Baltimore, Md. : 1950)*, 172(3), pp.1407–1413.
- Kerschbamer, E. & Biagioli, M., 2016. Huntington's disease as neurodevelopmental disorder: Altered chromatin regulation, coding, and non-coding RNA transcription. *Frontiers in Neuroscience*, 9(JAN), pp.1–5.
- Kettenmann, H. et al., 2011. Physiology of microglia. *Physiological reviews*, 91(2), pp.461–553. Available at: <http://physrev.physiology.org/content/91/2/461.abstract>.
- Khoshnan, A. et al., 2017. IKK $\beta$  and mutant huntingtin interactions regulate the expression of IL-34: implications for microglial-mediated neurodegeneration in HD. *Human Molecular Genetics*, 0(0), pp.1–11.
- El Khoury, J. et al., 2007. Ccr2 deficiency impairs microglial accumulation and accelerates progression of Alzheimer-like disease. *Nature Medicine*, 13(4), pp.432–438.
- Kierdorf, K. et al., 2013. Microglia emerge from erythromyeloid precursors via Pu.1- and Irf8-dependent pathways. *Nature Neuroscience*, 16(3), pp.273–280. Available at: <http://dx.doi.org/10.1038/nn.3318>.
- Kim, S. et al., 2014. Highly efficient RNA-guided genome editing in human cells via delivery of purified Cas9 ribonucleoproteins. *Genome Research*, 24, pp.1012–1019.
- Kim, T.-S. et al., 2008. Changes in the levels of plasma soluble fractalkine in patients with mild cognitive impairment and Alzheimer's disease. *Neuroscience letters*, 436(2),

pp.196–200.

- Kim, W.S. et al., 2005. Abca7 null mice retain normal macrophage phosphatidylcholine and cholesterol efflux activity despite alterations in adipose mass and serum cholesterol levels. *Journal of Biological Chemistry*, 280(5), pp.3989–3995.
- Kim, W.S. et al., 2013. Deletion of Abca7 increases cerebral amyloid- $\beta$  accumulation in the J20 mouse model of Alzheimer's disease. *Journal of Neuroscience*, 33(10), pp.4387–94. Available at: <http://www.ncbi.nlm.nih.gov/pubmed/23467355>.
- Kim, W.S. et al., 2006. Quantitation of ATP-binding cassette subfamily-A transporter gene expression in primary human brain cells. *Neuroreport*, 17(9), pp.891–6. Available at: <http://www.ncbi.nlm.nih.gov/pubmed/16738483>.
- Kinchen, J.M. et al., 2005. Two pathways converge at CED-10 to mediate actin rearrangement and corpse removal in *C. elegans*. *Nature*, 434(649), pp.93–100.
- Kitamura, T., Miyake, T. & Fujita, S., 1984. Genesis of Resting Microglia in the Gray Matter of Mouse Hippocampus. *Journal of Comparative Neurology*, 226, pp.421–433.
- Kiyota, T. et al., 2009. CCL2 accelerates microglia-mediated Abeta oligomer formation and progression of neurocognitive dysfunction. *PLoS one*, 4(7), p.e6197.
- Kleinberger, G. et al., 2014. TREM2 mutations implicated in neurodegeneration impair cell surface transport and phagocytosis. *Science Translational Medicine*, 6(243).
- Koldamova, R., Staufenbiel, M. & Lefterov, I., 2005. Lack of ABCA1 Considerably Decreases Brain ApoE Level and Increases Amyloid Deposition in APP23 Mice. *Journal of Biological Chemistry*, 280(52), pp.43224–43235.
- Kordasiewicz, H.B. et al., 2012. Sustained Therapeutic Reversal of Huntington's Disease by Transient Repression of Huntingtin Synthesis. *Neuron*, 74(6), pp.1031–1044. Available at: <http://dx.doi.org/10.1016/j.neuron.2012.05.009>.
- Krabbe, G. et al., 2013. Functional Impairment of Microglia Coincides with Beta-Amyloid Deposition in Mice with Alzheimer-Like Pathology. *PLoS ONE*, 8(4).
- Krasemann, S. et al., 2017. The TREM2-APOE Pathway Drives the Transcriptional Phenotype of Dysfunctional Microglia in Neurodegenerative Diseases. *Immunity*, 47(3), pp.566–581. Available at: <http://dx.doi.org/10.1016/j.immuni.2017.08.008>.
- Kreisl, W.C. et al., 2013. In vivo radioligand binding to translocator protein correlates with severity of Alzheimer's disease. *Brain*, 136(7), pp.2228–2238.
- Krencik, R. et al., 2011. Specification of transplantable astroglial subtypes from human pluripotent stem cells. *Nature Biotechnology*, 29(6), pp.528–534. Available at: <http://www.nature.com/doi/10.1038/nbt.1877>.
- Kreutzberg, G.W., 1996. Microglia: a sensor for pathological events in the CNS. *Trends in neurosciences*, 19(8), pp.312–318.
- Kumaravelu, P. et al., 2002. Quantitative developmental anatomy of definitive haematopoietic stem cells/long-term repopulating units (HSC/RUs): role of the aorta-gonad-mesonephros (AGM) region and the yolk sac in colonisation of the mouse embryonic liver. *Development (Cambridge, England)*, 129(21), pp.4891–4899.
- Kunkle, B.W. et al., 2017. Targeted sequencing of ABCA7 identifies splicing, stop-gain and intronic risk variants for Alzheimer disease. *Neuroscience Letters*, 649, pp.124–129. Available at: <http://dx.doi.org/10.1016/j.neulet.2017.04.014>.
- Kwan, W. et al., 2012. Bone Marrow Transplantation Confers Modest Benefits in Mouse Models of Huntington's Disease. *Journal of Neuroscience*, 32(1), pp.133–142. Available at: <http://www.jneurosci.org/cgi/doi/10.1523/JNEUROSCI.4846-11.2012>.
- Kwan, W. et al., 2012. Mutant huntingtin impairs immune cell migration in Huntington

- disease. *J Clin Invest.*, 122(12), pp.4737–4747.
- Labadorf, A. et al., 2015. RNA Sequence Analysis of Human Huntington Disease Brain Reveals an Extensive Increase in Inflammatory and Developmental Gene Expression. *Plos One*, 10(12), p.e0143563. Available at: <http://dx.plos.org/10.1371/journal.pone.0143563>.
- Lacy, P. & Stow, J.L., 2011. Cytokine release from innate immune cells : association with diverse membrane trafficking pathways. *Blood*, 118(1), pp.9–19.
- Laferla, F.M. & Green, K.N., 2012. Animal Models of Alzheimer Disease. *Cold Spring Harbour Perspectives in Medicine*, pp.1–14.
- Lambert, J. et al., 2009. Genome-wide association study identifies variants at CLU and CR1 associated with Alzheimer’s disease. *Nature Genetics*, 41(10), pp.1094–1099. Available at: <http://dx.doi.org/10.1038/ng.439>.
- Lambert, J.C. et al., 2013. Meta-analysis of 74,046 individuals identifies 11 new susceptibility loci for Alzheimer’s disease. *Nature genetics*, 45(12), pp.1452–8. Available at: <http://www.pubmedcentral.nih.gov/articlerender.fcgi?artid=3896259&tool=pmcentrez&rendertype=abstract>.
- Langfelder, P. & Horvath, S., 2008. WGCNA: An R package for weighted correlation network analysis. *BMC Bioinformatics*, 9.
- Langmann, T. et al., 2003. Real-Time Reverse Transcription-PCR Expression Profiling of the Complete Human ATP-Binding Cassette Transporter Superfamily in Various Tissues. *Clinical Chemistry*, 238, pp.230–238.
- Lapchak, P.A. et al., 2001. Neuroprotection by the selective cyclooxygenase-2 inhibitor SC-236 results in improvements in behavioral deficits induced by reversible spinal cord ischemia. *Stroke*, 32(5), pp.1220–1225.
- Lauber, K. et al., 2004. Clearance of Apoptotic Cells : Getting Rid of the Corpses. *Molecular Cell*, 14, pp.277–287.
- Lavin, Y. et al., 2014. Tissue-Resident Macrophage Enhancer Landscapes Are Shaped by the Local Microenvironment. *Cell*, 159(6), pp.1312–1326. Available at: <http://dx.doi.org/10.1016/j.cell.2014.11.018>.
- Lawson, L.J. et al., 1990. Heterogeneity in the distribution and morphology of microglia in the normal adult mouse brain. *Neuroscience*, 39(1), pp.151–170.
- Lawson, L.J., Perry, V.H. & Gordon, S., 1992. Turnover of resident microglia in the normal adult mouse brain. *Neuroscience*, 48(2), pp.405–415.
- Li, H., Karl, T. & Garner, B., 2015. Understanding the function of ABCA7 in Alzheimer’s disease. *Biochemical Society Transactions*, 43(5), pp.920–923. Available at: <http://biochemsoctrans.org/cgi/doi/10.1042/BST20150105>.
- Li, S. et al., 1997. Glutamate transporter alterations in Alzheimer disease are possibly associated with abnormal APP expression. *Journal of neuropathology and experimental neurology*, 56(8), pp.901–911.
- Liao, Y., Smyth, G.K. & Shi, W., 2014. featureCounts: an efficient general purpose program for assigning sequence reads to genomic features. *Bioinformatics*, 30(7), pp.923–930.
- Liévens, J.C. et al., 2001. Impaired glutamate uptake in the R6 Huntington’s disease transgenic mice. *Neurobiology of Disease*, 8(5), pp.807–821.
- Lim, R.G. et al., 2017. Huntington’s Disease iPSC-Derived Brain Microvascular Endothelial Cells Reveal WNT-Mediated Angiogenic and Blood-Brain Barrier Deficits. *Cell Reports*, 19(7), pp.1365–1377. Available at: <http://dx.doi.org/10.1016/j.celrep.2017.04.021>.
- Linsel-nitschke, P. et al., 2005. Potential role of ABCA7 in cellular lipid efflux to apoA-I.

- Journal of lipid research*, 46, pp.86–93.
- Liu, D. & Niu, Z.-X., 2009. The structure, genetic polymorphisms, expression and biological functions of complement receptor type 1 (CR1/CD35). *Immunopharmacology and Immunotoxicology*, 31(4), pp.524–535. Available at: <http://www.tandfonline.com/doi/full/10.3109/08923970902845768>.
- Livak, K.J. et al., 2013. Methods for qPCR gene expression profiling applied to 1440 lymphoblastoid single cells. *Methods (San Diego, Calif.)*, 59(1), pp.71–79.
- López-Lázaro, M., 2008. The warburg effect: why and how do cancer cells activate glycolysis in the presence of oxygen? *Anti-cancer agents in medicinal chemistry*, 8(3), pp.305–312.
- Lotze, M.T. et al., 2007. The grateful dead: Damage-associated molecular pattern molecules and reduction/oxidation regulate immunity. *Immunological Reviews*, 220(1), pp.60–81.
- Love, M.I., Huber, W. & Anders, S., 2014. Moderated estimation of fold change and dispersion for RNA-seq data with DESeq2. *Genome Biology*, 15(12), p.550. Available at: <https://doi.org/10.1186/s13059-014-0550-8>.
- Lucin, K.M. & Wyss-Coray, T., 2009. Immune Activation in Brain Aging and Neurodegeneration: Too Much or Too Little? *Neuron*, 64(1), pp.110–122. Available at: <http://dx.doi.org/10.1016/j.neuron.2009.08.039>.
- Van Der Maaten, L.J.P. & Hinton, G.E., 2008. Visualizing high-dimensional data using t-sne. *Journal of Machine Learning Research*, 9, pp.2579–2605. Available at: [https://lvdmaaten.github.io/publications/papers/JMLR\\_2008.pdf](https://lvdmaaten.github.io/publications/papers/JMLR_2008.pdf) [http://www.ncbi.nlm.nih.gov/entrez/query.fcgi?db=pubmed&cmd=Retrieve&dopt=AbstractPlus&list\\_uids=7911431479148734548related:VOiAgwMNY20J](http://www.ncbi.nlm.nih.gov/entrez/query.fcgi?db=pubmed&cmd=Retrieve&dopt=AbstractPlus&list_uids=7911431479148734548related:VOiAgwMNY20J).
- MacAuley, M.S., Crocker, P.R. & Paulson, J.C., 2014. Siglec-mediated regulation of immune cell function in disease. *Nature Reviews Immunology*, 14(10), pp.653–666.
- MacDonald, M.E. et al., 1993. A novel gene containing a trinucleotide repeat that is expanded and unstable on Huntington's disease chromosomes. *Cell*, 72(6), pp.971–983.
- Magno, L. et al., 2018. Alzheimer's disease Phospholipase C-gamma-2 (PLCG2) protective variant is a functional hypermorph. *Biorxiv*, 2, pp.1–21.
- Mahley, R.W. & Rall, S.C., 2000. APOLIPOPROTEIN E : Far More Than a Lipid Transport Protein. *Annual Review of Genomics and Human Genetics*, 1(59), pp.507–537.
- Mann, D.M.A. & Pickering-brown, S.M., 2001. Amyloid Angiopathy and Variability in Amyloid  $\beta$  Deposition Is Determined by Mutation Position in Presenilin-1-Linked Alzheimer's Disease. *The American Journal of Pathology*, 158(6), pp.2165–2175. Available at: [http://dx.doi.org/10.1016/S0002-9440\(10\)64688-3](http://dx.doi.org/10.1016/S0002-9440(10)64688-3).
- Mantovani, A. et al., 2004. The chemokine system in diverse forms of macrophage activation and polarization. *Trends in Immunology*, 25(12), pp.677–686.
- Maphis, N. et al., 2015. Reactive microglia drive tau pathology and contribute to the spreading of pathological tau in the brain. *Brain*, 138(6), pp.1738–1755.
- Maragakis, N.J. & Rothstein, J.D., 2006. Mechanisms of Disease: astrocytes in neurodegenerative disease. *Nature clinical practice. Neurology*, 2(12), pp.679–689.
- Martinez, F.O. & Gordon, S., 2014. The M1 and M2 paradigm of macrophage activation: time for reassessment. *F1000prime reports*, 6(March), p.13. Available at: <http://www.pubmedcentral.nih.gov/articlerender.fcgi?artid=3944738&tool=pmcentrez&rendertype=abstract>.
- Masliah, E. et al., 1996. Deficient glutamate transport is associated with neurodegeneration

- in Alzheimer's disease. *Annals of neurology*, 40(5), pp.759–766.
- Mass, E. et al., 2016. Specification of tissue-resident macrophages during organogenesis. *Science*, 4238(August).
- Mastrolakos, A. et al., 2015. Huntington's disease biomarker progression profile identified by transcriptome sequencing in peripheral blood. *European Journal of Human Genetics*, 23(10), pp.1349–1356.
- Mattis, V.B. et al., 2015. HD iPSC-derived neural progenitors accumulate in culture and are susceptible to BDNF withdrawal due to glutamate toxicity. *Human molecular genetics*, 24(11), pp.3257–3271.
- Mattis, V.B. & Svendsen, C.N., 2017. Modeling Huntington's disease with patient-derived neurons. *Brain Research*, 1656, pp.76–87. Available at: <http://dx.doi.org/10.1016/j.brainres.2015.10.001>.
- May, P., Bock, H.H. & Nofer, J., 2013. Low density receptor-related protein 1 (LRP1) promotes anti-inflammatory phenotype in murine macrophages. *Cell Tissue Research*, 354, pp.887–889.
- May, P., Herz, J. & Bock, H.H., 2005. Molecular mechanisms of lipoprotein receptor signalling. *Cellular and Molecular Life Science*, 62, pp.2325–2338.
- McGeer, P.L. et al., 1988. Reactive microglia are positive for HLA-DR in the substantia nigra of Parkinson's and Alzheimer's disease brains. *Neurology*, 38(8), pp.1285–1291.
- McGrath, K.E. et al., 2003. Circulation is established in a stepwise pattern in the mammalian embryo. *Blood*, 101(5), pp.1669–1676.
- McKercher, S.R. et al., 1996. Targeted disruption of the PU.1 gene results in multiple hematopoietic abnormalities. *The EMBO journal*, 15(20), pp.5647–5658.
- McMahon, H.T., Wigge, P. & Smith, C., 1997. Clathrin interacts specifically with amphiphysin and is displaced by dynamin. *FEBS letters*, 413(2), pp.319–322.
- Meissner, T.B. et al., 2010. NLR family member NLRC5 is a transcriptional regulator of MHC class I genes. *Proceedings of the National Academy of Sciences of the United States of America*, 107(31), pp.13794–13799.
- Menalled, L.B. et al., 2012. Comprehensive Behavioral and Molecular Characterization of a New Knock-In Mouse Model of Huntington's Disease: ZQ175. *PLoS ONE*, 7(12).
- Meyerholz, A. et al., 2005. Effect of Clathrin Assembly Lymphoid Myeloid Leukemia Protein Depletion on Clathrin Coat Formation. *Traffic*, 6(13), pp.1225–1234.
- Miesenböck, G., De Angelis, D.A. & Rothman, J.E., 1998. Visualizing secretion and synaptic transmission with pH-sensitive green fluorescent proteins. *Nature*, 394(6689), pp.192–195.
- Migliaccio, G. et al., 1986. Human Embryonic Hemopoiesis. *J Clin Invest*, 78, pp.51–60.
- Miller, J.R. et al., 2016. RNA-Seq of Huntington's Disease Patient Myeloid Cells Reveals Innate Transcriptional Dysregulation Associated With Proinflammatory Pathway Activation. *Human Molecular Genetics*, 0(0), p.ddw142. Available at: <http://www.hmg.oxfordjournals.org/lookup/doi/10.1093/hmg/ddw142>.
- Miller, J.R.C. et al., 2015. Mutant Huntingtin Does Not Affect the Intrinsic Phenotype of Human Huntington's Disease T Lymphocytes. *Plos One*, 10(11), pp.1–16. Available at: <http://dx.plos.org/10.1371/journal.pone.0141793>.
- Mittelbronn, M. et al., 2001. Local distribution of microglia in the normal adult human central nervous system differs by up to one order of magnitude. *Acta neuropathologica*, 101(3), pp.249–255.
- Molero, A.E. et al., 2009. Impairment of developmental stem cell-mediated striatal

- neurogenesis and pluripotency genes in a knock-in model of Huntington's disease. *Proceedings of the National Academy of Sciences of the United States of America*, 106(51), pp.21900–5. Available at: <http://www.pubmedcentral.nih.gov/articlerender.fcgi?artid=2799796&tool=pmcentrez&rendertype=abstract>.
- Monier, A. et al., 2007. Entry and distribution of microglial cells in human embryonic and fetal cerebral cortex. *Journal of Neuropathology and Experimental Neurology*, 66(5), pp.372–382. Available at: <http://www.embase.com/search/results?subaction=viewrecord&from=export&id=L46701319%5Cnhttp://dx.doi.org/10.1097/nen.0b013e3180517b46>.
- Montagne, A., Zhao, Z. & Zlokovic, B. V., 2017. Alzheimer's disease : A matter of blood – brain barrier dysfunction ? The Journal of Experimental Medicine. *Journal of Experimental Medicine*, 214(11), pp.3151–3169.
- Moore, M.A. & Metcalf, D., 1970. Ontogeny of the haemopoietic system: yolk sac origin of in vivo and in vitro colony forming cells in the developing mouse embryo. *British journal of haematology*, 18(3), pp.279–296. Available at: <http://www.ncbi.nlm.nih.gov/pubmed/5491581>.
- Morris, J.C. et al., 2010. APOE Predicts Amyloid-Beta but Not Tau Alzheimer Pathology in Cognitively Normal Aging. *Annals of Neurology*, 67, pp.122–131.
- Mosher, K.I. & Wyss-Coray, T., 2014. Microglial dysfunction in brain aging and Alzheimer's disease. *Biochemical Pharmacology*, 88(4), pp.594–604. Available at: <http://dx.doi.org/10.1016/j.bcp.2014.01.008>.
- Mucke, L. et al., 2000. High-level neuronal expression of abeta 1-42 in wild-type human amyloid protein precursor transgenic mice: synaptotoxicity without plaque formation. *Journal of Neuroscience*, 20(11), pp.4050–4058.
- Muffat, J. et al., 2016. Derivation of microglia-like cells from human pluripotent stem cells. *Nature Medicine*, (September). Available at: <http://dx.doi.org/10.1038/nm.4189>.
- Munsie, L. et al., 2011. Mutant huntingtin causes defective actin remodeling during stress: Defining a new role for transglutaminase 2 in neurodegenerative disease. *Human Molecular Genetics*, 20(10), pp.1937–1951.
- Murabe, Y. & Sano, Y., 1982. Morphological studies on neuroglia. VI. Postnatal development of microglial cells. *Cell and tissue research*, 225(3), pp.469–485.
- Murabe, Y. & Sano, Y., 1983. Morphological studies on neuroglia. VII. Distribution of 'brain macrophages' in brains of neonatal and adult rats, as determined by means of immunohistochemistry. *Cell and tissue research*, 229(1), pp.85–95.
- Myers, R.H. et al., 1991. Decreased neuronal and increased oligodendroglial densities in Huntington's disease caudate nucleus. *Journal of neuropathology and experimental neurology*, 50(6), pp.729–742.
- Nagele, R.G. et al., 2003. Astrocytes accumulate A beta 42 and give rise to astrocytic amyloid plaques in Alzheimer disease brains. *Brain research*, 971, pp.197–209.
- Naj, A.C. et al., 2011. Common variants at MS4A4/MS4A6E, CD2AP, CD33 and EPHA1 are associated with late-onset Alzheimer's disease. *Nature genetics*, 43(5).
- Nakamura, Y., 2000. Regulating factors for microglial activation. *Biological and Pharmaceutical Bulletin*, 72(6), pp.465–468.
- Nash, K.R. et al., 2013. Fractalkine overexpression suppresses tau pathology in a mouse model of tauopathy. *Neurobiology of Aging*, 34(6), pp.1540–1548. Available at: <http://dx.doi.org/10.1016/j.neurobiolaging.2012.12.011>.

- Nicolle, R., Radvanyi, F. & Elati, M., 2015. CoRegNet: Reconstruction and integrated analysis of co-regulatory networks. *Bioinformatics*, 31(18), pp.3066–3068.
- Nimmerjahn, A., Kirchhoff, F. & Helmchen, F., 2005. Resting Microglial Cells Are Highly Dynamic Surveillants of Brain Parenchyma in Vivo. *Science*, 308(May), pp.1314–1319. Available at: <http://www.sciencemag.org/content/suppl/2005/05/26/1110647.DC1>.
- Nioi, P. et al., 2007. In vitro detection of drug-induced phospholipidosis using gene expression and fluorescent phospholipid-based methodologies. *Toxicological Sciences*, 99(1), pp.162–173.
- Norflus, F. et al., 2004. Anti-inflammatory treatment with acetylsalicylate or rofecoxib is not neuroprotective in Huntington's disease transgenic mice. *Neurobiology of disease*, 17(2), pp.319–325.
- O'Neill, L.A.J., Kishton, R.J. & Rathmell, J., 2016. A guide to immunometabolism for immunologists. *Nature reviews. Immunology*, 16(9), pp.553–65. Available at: <http://www.ncbi.nlm.nih.gov/pubmed/27396447><http://www.pubmedcentral.nih.gov/articlerender.fcgi?artid=PMC5001910>.
- Ogden, C.A. et al., 2001. C1q and Mannose Binding Lectin Engagement of Cell Surface Calreticulin and CD91 Initiates Macropinocytosis and Uptake of Apoptotic Cells. *Journal of Experimental Medicine*, 194(6).
- Ohgidani, M. et al., 2014. Direct induction of ramified microglia-like cells from human monocytes: Dynamic microglial dysfunction in Nasu-Hakola disease. *Scientific Reports*, 4(4957), pp.1–7. Available at: <http://www.nature.com/doi/10.1038/srep04957>.
- Okello, A. et al., 2009. Microglial activation and amyloid deposition in mild cognitive impairment: a PET study. *Neurology*, 72(1), pp.56–62.
- Okita, K., Ichisaka, T. & Yamanaka, S., 2007. Generation of germline-competent induced pluripotent stem cells. *Nature*, 448(July), pp.313–318.
- Olmos-Alonso, A. et al., 2016. Pharmacological targeting of CSF1R inhibits microglial proliferation and prevents the progression of Alzheimer's-like pathology. *Brain*, 139(3), pp.891–907.
- Olson, J.K. & Miller, S.D., 2004. Microglia Initiate Central Nervous System Innate and Adaptive Immune Responses through Multiple TLRs. *The Journal of Immunology*, 173(6), pp.3916–3924. Available at: <http://www.jimmunol.org/cgi/doi/10.4049/jimmunol.173.6.3916>.
- Orihuela, R., Mcpherson, C.A. & Harry, G.J., 2016. Microglial M1/M2 polarization and metabolic states. *British Journal of Pharmacology*, 173, pp.649–665.
- Orkin, S.H. & Zon, L.I., 2008. Hematopoiesis: An Evolving Paradigm for Stem Cell Biology. *Cell*, 132(4), pp.631–644.
- Orre, M. et al., 2014. Isolation of glia from Alzheimer's mice reveals inflammation and dysfunction. *Neurobiology of Aging*, 35(12), pp.2746–2760.
- Østergaard, M.E. et al., 2013. Rational design of antisense oligonucleotides targeting single nucleotide polymorphisms for potent and allele selective suppression of mutant Huntingtin in the CNS. *Nucleic Acids Research*, 41(21), pp.9634–9650.
- Palazuelos, J. et al., 2009. Microglial CB2 cannabinoid receptors are neuroprotective in Huntington's disease excitotoxicity. *Brain*, 132(11), pp.3152–3164.
- Palis, J. et al., 1999. Development of erythroid and myeloid progenitors in the yolk sac and embryo proper of the mouse. *Development (Cambridge, England)*, 126(22), pp.5073–5084. Available at: <http://www.ncbi.nlm.nih.gov/pubmed/10529424>.
- Pandya, H. et al., 2017. Differentiation of human and murine induced pluripotent stem cells

- to microglia-like cells. *Nature Neuroscience*, (March), pp.2–11. Available at: <http://www.nature.com/neuro/journal/vaop/ncurrent/full/nn.4534.html>.
- Paolicelli, R.C. et al., 2011. Synaptic Pruning by Microglia Is Necessary for Normal Brain Development. *Science*, 333(September), pp.1456–1459.
- Park, J. et al., 2013. Mitochondrial dynamics modulate the expression of pro-inflammatory mediators in microglial cells. *Journal of Neurochemistry*, 127(2), pp.221–232. Available at: <http://doi.wiley.com/10.1111/jnc.12361>.
- Park, J. et al., 2015. Mitochondrial ROS govern the LPS-induced pro-inflammatory response in microglia cells by regulating MAPK and NF- $\kappa$ B pathways. *Neuroscience letters*, 584, pp.191–6. Available at: <http://www.ncbi.nlm.nih.gov/pubmed/25459294>.
- Pavese, N. et al., 2006. Microglial activation correlates with severity in Huntington disease: a clinical and PET study. *Neurology*, 66(11), pp.1638–1643.
- Perry, V.H., 1998. A revised view of the central nervous system microenvironment and major histocompatibility complex class II antigen presentation. *Journal of neuroimmunology*, 90(2), pp.113–121.
- Perry, V.H., Hume, D.A. & Gordon, S., 1985. Immunohistochemical localization of macrophages and microglia in the adult and developing mouse brain. *Neuroscience*, 15(2), pp.313–326.
- Pike, L.J., Han, X. & Gross, R.W., 2005. Epidermal growth factor receptors are localized to lipid rafts that contain a balance of inner and outer leaflet lipids: a shotgun lipidomics study. *The Journal of biological chemistry*, 280(29), pp.26796–26804.
- Pocock, J.M. & Kettenmann, H., 2007. Neurotransmitter receptors on microglia. *Trends in Neurosciences*, 30(10), pp.527–535.
- Politis, M. et al., 2015. Increased central microglial activation associated with peripheral cytokine levels in premanifest Huntington’s disease gene carriers. *Neurobiology of Disease*, 83, pp.115–121. Available at: <http://dx.doi.org/10.1016/j.nbd.2015.08.011>.
- Politz, O. et al., 2000. Pseudoxons and regulatory elements in the genomic sequence of the beta-chemokine, alternative macrophage activation-associated CC-chemokine (AMAC)-1. *Cytokine*, 12(2), pp.120–126.
- Polyzos, A.A. & McMurray, C.T., 2017. The chicken or the egg: mitochondrial dysfunction as a cause or consequence of toxicity in Huntington’s disease. *Mechanisms of Ageing and Development*, 161, pp.181–197. Available at: <http://dx.doi.org/10.1016/j.mad.2016.09.003>.
- Prinz, M. et al., 2011. Heterogeneity of CNS myeloid cells and their roles in neurodegeneration. *Nature neuroscience*, 14(10), pp.1227–1235.
- Prokop, S., Miller, K.R. & Heppner, F.L., 2013. Microglia actions in Alzheimer’s disease. *Acta neuropathologica*, 126(4), pp.461–477.
- Quazi, F. & Molday, R.S., 2013. Differential phospholipid substrates and directional transport by ATP-binding cassette proteins ABCA1, ABCA7, and ABCA4 and disease-causing mutants. *Journal of Biological Chemistry*, 288(48), pp.34414–34426.
- Querfurth, H.W. & Laferla, F.M., 2010. Alzheimer’s Disease. *The New England Journal of Medicine*, 362(4), pp.329–344.
- Rabinovitch, M., 1995. Professional and non-professional phagocytes: an introduction. *Trends in cell biology*, 5(3), pp.85–87.
- Rajagopalan P, Hibar DP, T.P., 2013. TREM2 and Neurodegenerative Disease. *New England Journal of Medicine*, 369(16), pp.1565–1567. Available at: <http://www.nejm.org/doi/10.1056/NEJMc1306509>.

- Ramjaun, A.R. & Mcpherson, P.S., 1998. Multiple Amphiphysin II Splice Variants Display Differential Clathrin Binding : Identification of Two Distinct. *Journal of Neurochemistry*, 70(6), pp.2369–2376.
- Ransohoff, R.M., 2016. How neuroinflammation contributes to neurodegeneration. *Science*, 353(6301), pp.168–175.
- Ransohoff, R.M. & Perry, V.H., 2009. Microglial physiology: unique stimuli, specialized responses. *Annual review of immunology*, 27, pp.119–45. Available at: <http://www.ncbi.nlm.nih.gov/pubmed/19302036>.
- Rebeck, C.W. et al., 1993. Apolipoprotein E in Sporadic Alzheimer's Disease : Allelic Variation and Receptor Interactions. *Neuron*, 11, pp.575–580.
- Rees, D.C., Johnson, E. & Lewinson, O., 2009. ABC transporters: the power to change. *Nature reviews. Molecular cell biology*, 10(3), pp.218–27. Available at: <http://dx.doi.org/10.1038/nrm2646>.
- Reich, D.E. et al., 2001. Linkage disequilibrium in the human genome. *Nature*, 411, pp.199–204.
- Reitz, C. et al., 2013. Variants in the ATP-Binding Cassette and the Risk of Late-Onset Alzheimer Disease. *JAMA*, 309(14), pp.1483–1493.
- Remaley, A.T. et al., 1997. Decreased reverse cholesterol transport from Tangier disease fibroblasts. Acceptor specificity and effect of brefeldin on lipid efflux. *Arteriosclerosis, thrombosis, and vascular biology*, 17(9), pp.1813–1821.
- Ren, G. et al., 2006. The BAR Domain Proteins : Molding Membranes in Fission, Fusion, and Phagy. *Microbiology and Molecular Biology Reviews*, 70(1), pp.37–120.
- Rezaie, P. & Male, D., 1999. Colonisation of the developing human brain and spinal cord by microglia: a review. *Microscopy research and technique*, 45(6), pp.359–382.
- Ring, K.L. et al., 2015. Genomic Analysis Reveals Disruption of Striatal Neuronal Development and Therapeutic Targets in Human Huntington's Disease Neural Stem Cells. *Stem Cell Reports*, 5(6), pp.1023–1038. Available at: <http://dx.doi.org/10.1016/j.stemcr.2015.11.005>.
- del Rio-Hortega, P. (1919) El tercer elemento de los centros nerviosos. *Biol. Soc. Esp. Biol.* 9, 69–120.
- del Rio-Hortega, D. (1932). "Microglia," in *Cytology and Cellular Pathology of the Nervous System*, Vol. 2, ed W. Penfield, (New York, NY: P. B. Hoeber, Inc.), 482–534.
- de Rivero Vaccari, J.P. et al., 2012. P2X4 Receptors Influence Inflammasome Activation after Spinal Cord Injury. *Journal of Neuroscience*, 32(9), pp.3058–3066. Available at: <http://www.jneurosci.org/cgi/doi/10.1523/JNEUROSCI.4930-11.2012>.
- Robinson, M., Lee, B.Y. & Hane, F.T., 2017. Recent Progress in Alzheimer's Disease Research, Part 2: Genetics and Epidemiology. *Journal of Alzheimer's disease : JAD*, 57(2), pp.317–330.
- Rocha, N.P. et al., 2016. Neuroimmunology of Huntington's Disease : Revisiting Evidence from Human Studies. *Mediators of Inflammation*, 2016, pp.1–10. Available at: <http://dx.doi.org/10.1155/2016/8653132>.
- Rodriguez-Vieitez, E. et al., 2016. Diverging longitudinal changes in astrocytosis and amyloid PET in autosomal dominant Alzheimer's disease. *Brain*, 139(Pt 3), pp.922–936.
- Roeck, A. De et al., 2017. Deleterious ABCA7 mutations and transcript rescue mechanisms in early onset Alzheimer's disease. *Acta Neuropathologica*.
- Rogers, J. et al., 1996. Inflammation and Alzheimer's disease pathogenesis. *Neurobiology of aging*, 17(5), pp.681–686.

- Rogers, J. et al., 2002. Microglia and Inflammatory Mechanisms in the Clearance of Amyloid- $\beta$  Peptide. *Glia*, 269(July), pp.260–269.
- Rogers, J. et al., 2006. Peripheral clearance of amyloid  $\beta$  peptide by complement C3-dependent adherence to erythrocytes. *Neurobiology of Aging*, 27(12), pp.1733–1739.
- Rongvaux, A. et al., 2014. Development and function of human innate immune cells in a humanized mouse model. *Nature Biotechnology*, 32(4), pp.364–372.
- Ross, C.A. et al., 2014. Huntington disease: Natural history, biomarkers and prospects for therapeutics. *Nature Reviews Neurology*, 10(4), pp.204–216. Available at: <http://dx.doi.org/10.1038/nrneurol.2014.24>.
- Ross, C.A. & Tabrizi, S.J., 2011. Huntington's disease: From molecular pathogenesis to clinical treatment. *The Lancet Neurology*, 10(1), pp.83–98. Available at: [http://dx.doi.org/10.1016/S1474-4422\(10\)70245-3](http://dx.doi.org/10.1016/S1474-4422(10)70245-3).
- Royle, S.J. et al., 2008. Imaging pHluorin-based probes at hippocampal synapses. *Methods in Molecular Biology*, 457(8), pp.293–303.
- Runne, H. et al., 2007. Analysis of potential transcriptomic biomarkers for Huntington's disease in peripheral blood. *Proceedings of the National Academy of Sciences of the United States of America*, 104(36), pp.14424–14429.
- Rupprecht, R. et al., 2010. Translocator protein (18 kDa) (TSPO) as a therapeutic target for neurological and psychiatric disorders. *Nature Reviews Drug Discovery*, 9(12), pp.971–988. Available at: <http://dx.doi.org/10.1038/nrd3295>.
- Sagare, A.P. et al., 2013. Pericyte loss influences Alzheimer-like neurodegeneration in mice. *Nature Communications*, 4, pp.1–14. Available at: <http://dx.doi.org/10.1038/ncomms3932>.
- Sakae, N. et al., 2016. ABCA7 Deficiency Accelerates Amyloid-beta Generation and Alzheimer's Neuronal Pathology. *Journal of Neuroscience*, 36(13), pp.3848–3859.
- Santillo, A.F. et al., 2011. In vivo imaging of astrocytosis in Alzheimer's disease: an (1)(1)C-L-deuteriodeprenyl and PIB PET study. *European journal of nuclear medicine and molecular imaging*, 38(12), pp.2202–2208.
- Sapp, E. et al., 2001. Early and progressive accumulation of reactive microglia in the Huntington disease brain. *Journal of neuropathology and experimental neurology*, 60(2), pp.161–172.
- Sato, K. et al., 2015. ATP-binding cassette transporter A7 (ABCA7) loss of function alters Alzheimer amyloid processing. *Journal of Biological Chemistry*, 290(40), pp.24152–24165.
- Saura, J. et al., 1994. Increased monoamine oxidase B activity in plaque-associated astrocytes of Alzheimer brains revealed by quantitative enzyme radioautography. *Neuroscience*, 62(1), pp.15–30.
- Saura, J. et al., 1996. Molecular neuroanatomy of human monoamine oxidases A and B revealed by quantitative enzyme radioautography and in situ hybridization histochemistry. *Neuroscience*, 70(3), pp.755–774.
- Schaefer, C.F. et al., 2009. PID: the Pathway Interaction Database. *Nucleic acids research*, 37(Database issue), pp.D674-9.
- Schafer, D.P. et al., 2012. Microglia Sculpt Postnatal Neural Circuits in an Activity and Complement-Dependent Manner. *Neuron*, 74(4), pp.691–705. Available at: <http://dx.doi.org/10.1016/j.neuron.2012.03.026>.
- Schellenberg, G.D. & Montine, T.J., 2012. The genetics and neuropathology of Alzheimer's disease. *Acta Neuropathologica*, 124, pp.305–323.

- Schilling, T. et al., 2001. Astrocyte-released cytokines induce ramification and outward K<sup>+</sup>channel expression in microglia via distinct signalling pathways. *European Journal of Neuroscience*, 14(3), pp.463–473.
- Schmid, C.D. et al., 2002. Heterogeneous expression of the triggering receptor expressed on myeloid cells-2 on adult murine microglia. *Journal of neurochemistry*, 83(6), pp.1309–1320.
- Schulz, C. et al., 2012. A Lineage of Myeloid Cells Independent of Myb and Hematopoietic Stem Cells. *Science*, 336(86), pp.2–7.
- Serio, A. et al., 2013. Astrocyte pathology and the absence of non-cell autonomy in an induced pluripotent stem cell model of TDP-43 proteinopathy. *Proceedings of the National Academy of Sciences of the United States of America*, 110(12), pp.4697–702. Available at: <http://www.pubmedcentral.nih.gov/articlerender.fcgi?artid=3607024&tool=pmcentrez&rendertype=abstract>.
- Shaltouki, A. et al., 2013. Efficient generation of astrocytes from human pluripotent stem cells in defined conditions. *Stem Cells*, 31(5), pp.941–952.
- Sheng, J.G., Mrak, R.E. & Griffin, W.S.T., 1997. Neuritic plaque evolution in Alzheimer's disease is accompanied by transition of activated microglia from primed to enlarged to phagocytic forms. *Acta Neuropathologica*, 94(1), pp.1–5.
- Shi, Q. et al., 2017. Complement C3 deficiency protects against neurodegeneration in aged plaque-rich APP/PS1 mice. *Science Translational Medicine*, 6295(May).
- Shin, J.-Y. et al., 2005. Expression of mutant huntingtin in glial cells contributes to neuronal excitotoxicity. *The Journal of Cell Biology*, 171(6), pp.1001–1012. Available at: <http://www.jcb.org/lookup/doi/10.1083/jcb.200508072>.
- Shin, J.W. et al., 2016. Permanent inactivation of Huntington's disease mutation by personalized allele-specific CRISPR/Cas9. *Human molecular genetics*, 25(20), pp.4566–4576. Available at: <http://www.ncbi.nlm.nih.gov/pubmed/27634650>.
- Shiomi, A. & Usui, T., 2015. Pivotal roles of GM-CSF in autoimmunity and inflammation. *Mediators of Inflammation*, 2015.
- Shulman, J. et al., 2013. Genetic Susceptibility for Alzheimer Disease Neuritic Plaque Pathology. *JAMA Neurology*, 70(9), pp.1150–1157.
- Sierra, A. et al., 2013. Janus-faced microglia: beneficial and detrimental consequences of microglial phagocytosis. *Frontiers in Cellular Neuroscience*, 7(January), pp.1–22. Available at: <http://journal.frontiersin.org/article/10.3389/fncel.2013.00006/abstract>.
- Silvestroni, A. et al., 2009. Distinct neuroinflammatory profile in post-mortem human Huntington's disease. *NeuroReport*, 20(12), pp.1098–1103.
- Simard, A.R. et al., 2006. Bone marrow-derived microglia play a critical role in restricting senile plaque formation in Alzheimer's disease. *Neuron*, 49(4), pp.489–502.
- Simmons, D.A. et al., 2007. Ferritin accumulation in dystrophic microglia is an early event in the development of Huntington's disease. *Glia*, 55(10), pp.1074–1084.
- Simpson, J.E. et al., 2010. Astrocyte phenotype in relation to Alzheimer-type pathology in the ageing brain. *Neurobiology of Aging*, 31(4), pp.578–590. Available at: <http://dx.doi.org/10.1016/j.neurobiolaging.2008.05.015>.
- Sims, R. et al., 2017. Rare coding variants in PLCG2, ABI3, and TREM2 implicate microglial-mediated innate immunity in Alzheimer's disease. *Nature genetics*, (June), pp.1–15.
- Singhrao, S.K. et al., 1999. Increased complement biosynthesis by microglia and complement activation on neurons in Huntington's disease. *Experimental Neurology*,

- 159(2), pp.362–376.
- Skotte, N.H. et al., 2014. Allele-specific suppression of mutant huntingtin using antisense oligonucleotides: Providing a therapeutic option for all Huntington disease patients. *PLoS ONE*, 9(9).
- Slow, E.J. et al., 2003. Selective striatal neuronal loss in a YAC128 mouse model of Huntington disease. *Human molecular genetics*, 12(13), pp.1555–1567.
- Smith, J.D. et al., 2004. ABCA1 mediates concurrent cholesterol and phospholipid efflux to apolipoprotein A-I. *Journal of lipid research*, 45(4), pp.635–644.
- Soreq, L. et al., 2017. Major Shifts in Glial Regional Identity Are a Transcriptional Hallmark of Human Brain Aging. *Cell Reports*, 18(2), pp.557–570. Available at: <http://dx.doi.org/10.1016/j.celrep.2016.12.011>.
- Spangenberg, E.E. et al., 2016. Eliminating microglia in Alzheimer's mice prevents neuronal loss without modulating amyloid- $\beta$  pathology. *Brain*, 139(4), pp.1265–1281.
- Spurgeon, S.L., Jones, R.C. & Ramakrishnan, R., 2008. High throughput gene expression measurement with real time PCR in a microfluidic dynamic array. *PLoS ONE*, 3(2).
- Squarzone, P. et al., 2014. Microglia Modulate Wiring of the Embryonic Forebrain. *Cell Reports*, 8(5), pp.1271–1279. Available at: <http://dx.doi.org/10.1016/j.celrep.2014.07.042>.
- Stanley, A.C. & Lacy, P., 2010. Pathways for Cytokine Secretion. *Physiology*, 25(4), pp.218–229. Available at: <http://physiologyonline.physiology.org/cgi/doi/10.1152/physiol.00017.2010>.
- Steinberg, S. et al., 2015. Loss-of-function variants in ABCA7 confer risk of Alzheimer's disease. *Nature Genetics*, 47(5), pp.445–447. Available at: <http://www.nature.com/doi/10.1038/ng.3246>.
- Stolzing, A. & Grune, T., 2004. Neuronal apoptotic bodies: phagocytosis and degradation by primary microglial cells. *FASEB Journal*, 18(6).
- Strittmatter, W.J. et al., 1993. Apolipoprotein E : High-avidity binding to  $\beta$ -amyloid and increased frequency of type 4 allele in late-onset familial Alzheimer disease. *Proceedings of the National Academy of Sciences of the United States of America*, 90(March), pp.1977–1981.
- Stuart, L.M. et al., 2007. CD36 signals to the actin cytoskeleton and regulates microglial migration via a p130Cas complex. *Journal of Biological Chemistry*, 282(37), pp.27392–27401.
- Subramanian, A. et al., 2005. Gene set enrichment analysis: a knowledge-based approach for interpreting genome-wide expression profiles. *Proceedings of the National Academy of Sciences of the United States of America*, 102(43), pp.15545–15550.
- Tai, F. et al., 2007. Microglial activation in presymptomatic Huntington's disease gene carriers. *Brain*, 130, pp.1759–1766.
- Takahashi, K. et al., 2007. Induction of Pluripotent Stem Cells from Adult Human Fibroblasts by Defined Factors. *Cell*, pp.861–872.
- Takahashi, K., Rochford, C.D.P. & Neumann, H., 2005. Clearance of apoptotic neurons without inflammation by microglial triggering receptor expressed on myeloid cells-2. *The Journal of Experimental Medicine*, 201(4), pp.647–657. Available at: <http://www.jem.org/lookup/doi/10.1084/jem.20041611>.
- Takahashi, K. & Yamanaka, S., 2006. Induction of Pluripotent Stem Cells from Mouse Embryonic and Adult Fibroblast Cultures by Defined Factors. *Cell*, 2, pp.663–676.
- Tanaka, N. et al., 2011. HMG-CoA reductase inhibitors enhance phagocytosis by

- upregulating ATP-binding cassette transporter A7. *Atherosclerosis*, 217(2), pp.407–414. Available at: <http://dx.doi.org/10.1016/j.atherosclerosis.2011.06.031>.
- Tannahill, G.M. et al., 2013. Succinate is an inflammatory signal that induces IL-1 $\beta$  through HIF-1 $\alpha$ . *Nature*, 496(7444), pp.238–242. Available at: <http://dx.doi.org/10.1038/nature11986>.
- Tavian, M. & Péault, B., 2005. Embryonic development of the human hematopoietic system. *International Journal of Developmental Biology*, 49, pp.243–250.
- Tay, T.L. et al., 2017. A new fate mapping system reveals context-dependent random or clonal expansion of microglia. *Nature Neuroscience*, 20(6), pp.793–805.
- Thinakaran, G. & Koo, E.H., 2008. Amyloid precursor protein trafficking, processing, and function. *Journal of Biological Chemistry*, 283(44), pp.29615–29619.
- Tian, Y. et al., 2013. Adaptor complex AP2/PICALM, through interaction with LC3, targets Alzheimer's APP-CTF for terminal degradation via autophagy. *Proceedings of the National Academy of Sciences of the United States of America*, 110(42), pp.17071–17076.
- Tomioka, M. et al., 2017. Lysophosphatidylcholine export by human ABCA7. *BBA - Molecular and Cell Biology of Lipids*, 1862(7), pp.658–665. Available at: <http://dx.doi.org/10.1016/j.bbalip.2017.03.012>.
- Trager, U. et al., 2015. Characterisation of immune cell function in fragment and full-length Huntington's disease mouse models. *Neurobiology of Disease*, 73, pp.388–398.
- Träger, U. et al., 2014. HTT-lowering reverses Huntington's disease immune dysfunction caused by NF $\kappa$ B pathway dysregulation. *Brain*, 137(3), pp.819–833.
- Trapp, B.D. et al., 2007. Evidence for synaptic stripping by cortical microglia. *Glia*, 55(4), pp.360–368.
- Tsuchiya, S. et al., 1980. Establishment and characterization of a human acute monocytic leukemia cell line (THP-1). *International journal of cancer*, 26(2), pp.171–176.
- Ulland, T.K. et al., 2017. TREM2 Maintains Microglial Metabolic Fitness in Alzheimer's Disease. *Cell*, 170(4), p.649–656.e13. Available at: <http://dx.doi.org/10.1016/j.cell.2017.07.023>.
- Vasquez, J.B., Fardo, D.W. & Estus, S., 2013. ABCA7 expression is associated with Alzheimer's disease polymorphism and disease status. *Neuroscience Letters*, 556, pp.58–62. Available at: <http://dx.doi.org/10.1016/j.neulet.2013.09.058>.
- Vatine, G.D. et al., 2017. Modeling Psychomotor Retardation using iPSCs from MCT8-Deficient Patients Indicates a Prominent Role for the Blood-Brain Barrier. *Cell Stem Cell*, 20(6), p.831–843.e5. Available at: <http://dx.doi.org/10.1016/j.stem.2017.04.002>.
- Velazquez, P. et al., 1997. Aspartate residue 7 in amyloid beta-protein is critical for classical complement pathway activation: implications for Alzheimer's disease pathogenesis. *Nature medicine*, 3, pp.77–79.
- Verghese, P.B. et al., 2013. ApoE influences amyloid- $\beta$  (A $\beta$ ) clearance despite minimal apoE/A $\beta$  association in physiological conditions. *Proceedings of the National Academy of Sciences of the United States of America*, 110(19), pp.E1807–E1816.
- Verney, C. et al., 2010. Early microglial colonization of the human forebrain and possible involvement in periventricular white-matter injury of preterm infants. *Journal of Anatomy*, 217(4), pp.436–448.
- Vetrivel, K.S. & Thinakaran, G., 2010. Membrane rafts in Alzheimer's disease beta-amyloid production. *Biochimica et Biophysica Acta*, 1801(8), pp.860–867. Available at: <http://dx.doi.org/10.1016/j.bbalip.2010.03.007>.

- Vonsattel, J.P. et al., 1985. Neuropathological classification of Huntington's disease. *Journal of neuropathology and experimental neurology*, 44(6), pp.559–577.
- Te Vrugte, D. et al., 2004. Accumulation of glycosphingolipids in Niemann-Pick C disease disrupts endosomal transport. *Journal of Biological Chemistry*, 279(25), pp.26167–26175.
- van der Wal, E.A., Gomez-Pinilla, F. & Cotman, C.W., 1993. Transforming growth factor-beta 1 is in plaques in Alzheimer and Down pathologies. *Neuroreport*, 4(1), pp.69–72.
- Walker, D.G. et al., 2009. Decreased expression of CD200 and CD200 receptor in Alzheimer's disease: A potential mechanism leading to chronic inflammation. *Experimental Neurology*, 215(1), pp.5–19. Available at: <http://dx.doi.org/10.1016/j.expneurol.2008.09.003>.
- Wang, C.C., Wen, C.Y. & Medical, T., 1996. Immunohistochemical study of amoeboid microglial cells. *Journal of Anatomy*, 189, pp.567–574.
- Wang, N. et al., 2003. ATP-binding Cassette Transporter A7 (ABCA7) Binds Apolipoprotein A-I and Mediates Cellular Phospholipid but Not Cholesterol Efflux. *Journal of Biological Chemistry*, 278(44), pp.42906–42912.
- Wang, N. et al., 2000. Specific Binding of ApoA-I, Enhanced Cholesterol Efflux, and Altered Plasma Membrane Morphology in Cells Expressing ABCA1. *Journal of Biological Chemistry*, 275(42), pp.33053–33058.
- Wang, Y. et al., 2012. IL-34 is a tissue-restricted ligand of CSF1R required for the development of Langerhans cells and microglia. *Nature immunology*, 13(8), pp.753–60. Available at: <http://dx.doi.org/10.1038/ni.2360>.
- Weiss, A. et al., 2012. Mutant huntingtin fragmentation in immune cells tracks Huntington's disease progression. *Journal of Clinical Investigation*, 122(10), pp.3731–3736.
- Westin, K. et al., 2012. CCL2 is associated with a faster rate of cognitive decline during early stages of Alzheimer's disease. *PLoS one*, 7(1), p.e30525.
- Wild, E. et al., 2011. Abnormal peripheral chemokine profile in Huntington's disease. *PLoS currents*, 3, p.RRN1231.
- Wild, E.J. et al., 2015. Quantification of mutant huntingtin protein in cerebrospinal fluid from Huntington's disease patients. *The Journal of clinical investigation*, 125(5), pp.1–8.
- van Wilgenburg, B. et al., 2013. Efficient, long term production of monocyte-derived macrophages from human pluripotent stem cells under partly-defined and fully-defined conditions. *PLoS one*, 8(8), p.e71098. Available at: <http://www.pubmedcentral.nih.gov/articlerender.fcgi?artid=3741356&tool=pmcentrez&rendertype=abstract>.
- Wright, G.J. et al., 2000. Lymphoid/neuronal cell surface OX2 glycoprotein recognizes a novel receptor on macrophages implicated in the control of their function. *Immunity*, 13(2), pp.233–242.
- Wright, G.J. et al., 2001. The unusual distribution of the neuronal/lymphoid cell surface CD200 (OX2) glycoprotein is conserved in humans. *Immunology*, 102(2), pp.173–179.
- Wynn, T.A., Chawla, A. & Pollard, J.W., 2013. Macrophage biology in development, homeostasis and disease. *Nature*, 496(7446), pp.445–455.
- Wyss-Coray, T. et al., 2003. Adult mouse astrocytes degrade amyloid-beta in vitro and in situ. *Nature medicine*, 9(4), pp.453–457.
- Wyss-Coray, T. et al., 2001. TGF-beta1 promotes microglial amyloid-beta clearance and reduces plaque burden in transgenic mice. *Nature medicine*, 7(5), pp.612–618.
- Xian, X. et al., 2017. LRP1 integrates murine macrophage cholesterol homeostasis and

- inflammatory responses in atherosclerosis. *eLife*, 6(e29292), pp.1–31.
- Xiao, Q. et al., 2012. Role of Phosphatidylinositol Clathrin Assembly Lymphoid-Myeloid Leukemia ( PICALM ) in Intracellular Amyloid Precursor Protein ( APP ) Processing and Amyloid Plaque Pathogenesis \*. *Journal of Biological Chemistry*, 287(25), pp.21279–21289.
- Xu, J. et al., 2016. Microglia Colonization of Developing Zebrafish Midbrain Is Promoted by Apoptotic Neuron and Lysophosphatidylcholine. *Developmental Cell*, 38, pp.214–222.
- Xu, X. et al., 2017. Reversal of Phenotypic Abnormalities by CRISPR/Cas9-Mediated Gene Correction in Huntington Disease Patient-Derived Induced Pluripotent Stem Cells. *Stem Cell Reports*, 8(3), pp.619–633.
- Yamamoto, M. et al., 2005. Overexpression of monocyte chemotactic protein-1/CCL2 in beta-amyloid precursor protein transgenic mice show accelerated diffuse beta-amyloid deposition. *The American journal of pathology*, 166(5), pp.1475–1485.
- Yamamoto, M. et al., 2004. Regulation of Toll/IL-1-receptor-mediated gene expression by the inducible nuclear protein I $\kappa$ B $\zeta$ . *Nature*, 430, p.218. Available at: <http://dx.doi.org/10.1038/nature02738>.
- Yang, L. et al., 2016. LRP1 modulates the microglial immune response via regulation of JNK and NF- $\kappa$ B signaling pathways. *Journal of Neuroinflammation*, 13(304), pp.1–13. Available at: <http://dx.doi.org/10.1186/s12974-016-0772-7>.
- Yusa, K., 2013. Seamless genome editing in human pluripotent stem cells using custom endonuclease-based gene targeting and the piggyBac transposon. *Nature Protocols*, 8(10), pp.2061–2078.
- Zetterberg, H., Andreasen, N. & Blennow, K., 2004. Increased cerebrospinal fluid levels of transforming growth factor-beta1 in Alzheimer's disease. *Neuroscience letters*, 367(2), pp.194–196.
- Zhang, B. et al., 2013. Integrated Systems Approach Identifies Genetic Nodes and Networks in Late-Onset Alzheimer's Disease. *Cell*, 153(3), pp.707–720. Available at: <http://linkinghub.elsevier.com/retrieve/pii/S0092867413003875>.
- Zhang, Y. et al., 2016. Purification and Characterization of Progenitor and Mature Human Astrocytes Reveals Transcriptional and Functional Differences with Mouse. *Neuron*, 89(1), pp.37–53. Available at: <http://dx.doi.org/10.1016/j.neuron.2015.11.013>.
- Zhou, Q. et al., 2012. A hypermorphic missense mutation in PLCG2, encoding phospholipase C $\gamma$ 2, causes a dominantly inherited autoinflammatory disease with immunodeficiency. *American Journal of Human Genetics*, 91(4), pp.713–720.
- Zipser, B.D. et al., 2007. Microvascular injury and blood-brain barrier leakage in Alzheimer's disease. *Neurobiology of aging*, 28(7), pp.977–986.
- Zlokovic, B. V., 2011. Neurovascular pathways to neurodegeneration in Alzheimer's disease and other disorders. *Nature Reviews Neuroscience*, 12(12), pp.723–738. Available at: <http://dx.doi.org/10.1038/nrn3114>.
- Zurhove, K. et al., 2008.  $\gamma$ -Secretase Limits the Inflammatory Response Through the Processing of LRP1. *Science Signalling*, 1(47), pp.1–13.
- Zuris, J.A. et al., 2015. Cationic lipid-mediated delivery of proteins enables efficient protein-based genome editing in vitro and in vivo. *Nature Biotechnology*, 33(1), pp.73–80.
- Zwilling, D. et al., 2011. Kynurenine 3-monooxygenase inhibition in blood ameliorates neurodegeneration. *Cell*, 145(6), pp.863–874.

# 9. APPENDICES

Appendix 1. Top 50 differentially expressed genes in HD109 iPSC-derived microglia.

Genes were ranked by p-value correction with

<b>Symbol</b>	<b>LogFC</b>	<b>p-value</b>
LRRC61	-4.101	1.00E-06
BDKRB1	-5.42	1.00E-06
CALR	-1.127	1.00E-06
CD151	-1.339	1.00E-06
CTSB	-1.108	1.00E-06
CX3CR1	9.412	1.00E-06
DGKG	-2.242	1.00E-06
EVI2A	1.026	1.00E-06
F3	-2.066	1.00E-06
F10	-3.127	1.00E-06
GABRA3	5.026	1.00E-06
GALNT2	-1.083	1.00E-06
CXCL1	-2.356	1.00E-06
GSTM1	8.009	1.00E-06
HLA-A	-1.878	1.00E-06
HLA-B	-1.728	1.00E-06
HLA-H	-2.147	1.00E-06
ID2	1.159	1.00E-06
IL15RA	-2.306	1.00E-06
ITGA2	-4.622	1.00E-06
JARID2	1.027	1.00E-06
CD82	-1.989	1.00E-06
MFGE8	-2.753	1.00E-06
MELTF	-3.198	1.00E-06
MYO10	-2.137	1.00E-06
P4HB	-1.314	1.00E-06
PRKY	-10	1.00E-06
MASP1	-5.793	1.00E-06
RPA1	1.079	1.00E-06
RPS4Y1	-10	1.00E-06
RRAD	-4.167	1.00E-06

CCL7	<b>-4.399</b>	<b>1.00E-06</b>
SLC22A3	<b>-4.6</b>	<b>1.00E-06</b>
SMPD1	<b>-1.023</b>	<b>1.00E-06</b>
TAP1	<b>-1.182</b>	<b>1.00E-06</b>
TCN2	<b>-2.424</b>	<b>1.00E-06</b>
MEG9	<b>-3.74</b>	<b>1.00E-06</b>
TIMP1	<b>-3.057</b>	<b>1.00E-06</b>
FAM155A	<b>-2.434</b>	<b>1.00E-06</b>
UTY	<b>-10</b>	<b>1.00E-06</b>
VTN	<b>-4.171</b>	<b>1.00E-06</b>
ZFX	<b>1.171</b>	<b>1.00E-06</b>
MIR4458HG	<b>-9.571</b>	<b>1.00E-06</b>
ZFY	<b>-10</b>	<b>1.00E-06</b>
ZNF232	<b>-1.438</b>	<b>1.00E-06</b>
TFPI2	<b>-6.756</b>	<b>1.00E-06</b>
KDM5D	<b>-10</b>	<b>1.00E-06</b>
USP9Y	<b>-10</b>	<b>1.00E-06</b>
DDX3Y	<b>-10</b>	<b>1.00E-06</b>
PLOD3	<b>-1.182</b>	<b>1.00E-06</b>

Appendix 2. IPA output of upstream transcriptional regulators inhibited in HD109 iPSC-derived microglia.

This table contains the rest of the transcriptional regulators identified as inhibited in HD109 via IPA.

Upstream regulator	Activation z-score	P value of overlap
IL6	-3.348	0.000811
IFNL1	-3.286	0.000048
ERK1/2	-3.236	0.000124
SMARCA4	-3.168	0.0000153
IRF1	-3.16	0.00513
P38 MAPK	-2.728	0.00112
Interferon alpha	-2.66	0.00000881
IRF3	-2.655	0.00357
IL4	-2.591	0.00000563
IL1B	-2.576	1.1E-09
JAK	-2.433	0.000599
STAT1	-2.374	0.00928
SREBF1	-2.301	0.00284
PRL	-2.184	7.86E-08
CCL11	-2.084	0.00000379

forskolin	-2.082	0.0000173
VEGFA	-2.012	0.0000252

Appendix 3. IPA output of upstream transcriptional regulators activated in HD109 iPSC-derived microglia.

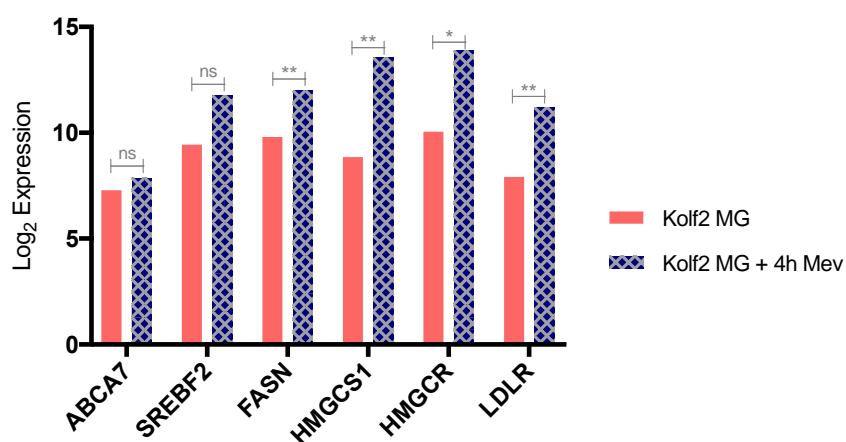
Upstream regulator	Activation z-score	P value of overlap
SB203580	3.885	1.33E-08
calphostin C	2.42	2.16E-07
RARA	3.414	5.49E-07
NKX2-3	2.103	6.63E-06
Go 6976	2.97	1.30E-05
miR-199a-5p	2.72	2.48E-05
tyrphostin AG 1478	2.397	1.32E-04
PD98059	2.746	1.86E-04
DKK1	2.005	1.94E-04
UDP-D-glucose	2.449	1.61E-09
MYCN	2.671	7.85E-04
2-aminopurine	2.165	9.46E-04
IL1RN	2.279	1.64E-03

Appendix 4. IPA output of inhibited upstream transcriptional regulators specific to HD109 iPSC-derived macrophage precursors.

Upstream regulator	Activation z-score	P value of overlap
3-deazaneplanocin	-2.561	2.48E-05
OSM	-2.709	1.07E-04
lipopolysaccharide	-3.881	4.60E-04
enterotoxin B	-2.414	1.27E-03
pyrrolidine dithiocarbamate	2.584	1.35E-03
TGFB1	-2.206	1.37E-03
IRF7	-2.18	5.04E-03
TP53	-2.251	5.38E-03

## Appendix 5. Microglia response to cholesterol depletion

Kolf2 WT microglia were stimulated with 10  $\mu$ M mevastatin for 4 hours.



## Appendix 6. List of qRT-PCR primers used in this project (continued)

Gene	Forward	Reverse
MERTK	TCC ATC CGT CCG GAG AGA AA	CCC TTG CCT CAG TGA TAG CTC
C1QA	TGG AGT TGA CAA CAG GAG GC	ATA TGG CCA GCA CAC AGA GC
PROS1	ATGACCCGGAACCGGATTATT	AGCATTAGTTGACTGACGTGC
GPR34	CCCAGCTGACACAACCAAGA	TGCATTAAGTTCAGGTTTCGCC
CR1	ATAGCAGGGTCTTCCTTGAC	TTTAGCACGAGGCAGAAGGG
CR2	AATCGGATCACCAATGGAACCC	CTGCAGCAATACCACAAAGGACAG
SDHA	TGG GAA CAA GAG GGC ATC TG	CCA CCA CTG CAT CAA ATT CAT G
HPRT1	TGA CAC TGG CAA AAC AAT GCA	GGT CCT TTT CAC CAG CAA GCT
UBC	CGG TGA ACG CCG ATG ATT AT	ATC TGC ATT GTC AAG TGA CGA
HMBS	TGC AAC GGC GGA AGA AAA	ACG AGG CTT TCA ATG TTG CC
GAPDH	TGC ACC ACC AAC TGC TTA GC	GGC ATG GAC TGT GGT CAT GAG
CD33	TCAACGTCACCTATGTTCCAC	CACTCCTGCTCTGGTCTCTTG
TYROBP	CTGCGGAGGCAGCGA	GGCCTCTGTGTGTTGAGGTC
SYK	GGGAAAGAAGTTCGACACGC	ACATTTCCCTGTGTGCCGATT
APOE	CAGGTCACCCAGGAAGTGGAG	CGGGGTCAGTTGTTCTCTCC
$\beta$ -actin	CCC AGC ACA ATG AAG ATC AA	ACA TCT GCT GGA AGG TGG AC
PICALM	TGGAGTCAACCAGGTGAAAAG	GGGTGCGTATTGTGGAAAATG
CD36	GCCAGGTATTGCAGTTCTTTTC	TGTCTGGGTTTTCAACTGGAG
IL8	ATACTCCAAACCTTCCACCC	TCTGCACCCAGTTTTCTTG
IRF1	CAACAGATGAGGATGAGGAAGG	GGTTCATTGAGTAGGTACCCC
ADORA3	CTTATCTTTACCCACGCCTCC	CAGGAATGACACCAGCCA
CLEC7A	TGTCATAAATTCCTGGGATGG	ATCAGGTTGGGAAGACACTTG
SIGLEC12	TCCCTGCAAAACGAGTACAC	GGACCTCACTACAACGAAGATG
CD22	TGTAATAGTTGGTGCTCGTGG	AGAAGTCACATTGGAGGCTG

CLU	ATTCAAAATGCTGTCAACGGG	CTTTGTCTCTGATTCCCTGGTC
ICAM1	CAATGTGCTATTCAAAGTCCC	CAGCGTAGGGTAAGGTTCTTG
FCER1G	TCGACTGAAGATCCAAGTGC	ACCGCATCTATTCTAAAGCTACTG
NR1H2	GATGTCCCAGGCACTGATG	ACAGACACGGCAAAGCTC
TLR4	TGCGTGAGACCAGAAAGC	TTAAAGCTCAGGTCCAGGTTC
CD40	AAGCTGTGAGACCAAAGACC	ATAAAGACCAGCACCAAGAGG
CABLES1	TCATTGGTCTGGAAGGTGTG	GTTACGGAACTGGGAGAAAGAG
STAT1	TGAACTTACCCAGAATGCC	CAGACTCTCCGCAACTATAGTG
MRC1	CACCTTAACAACTGGATTTGCCA	TGGTGGATTGTCTTGAGGAGC
CCL18	CTTGTCTCTGCTGCACCAT	TTGTGGAATCTGCCAGGAGG
CCL17	CTTCAAGGGAGCCATTCCCC	CCTGCCCTGCACAGTTACA
CCL2	AATCAATGCCCCAGTCACCT	CTTCTTTGGGACACTTGCTGC
CD163	TATTTCTGGAATGAAAAGGAGGC	ATCTTAAAGGCTGAACTCACTGGG
CCR2	GGTTCAGTTGCTGAGAAGCC	GTAAGGGGAAATGCGTCCT
CYBB	GGAATGCCCAATCCCTCAGT	AAAACCGCACCAACCTCTCA
NLRP3	GCGATCAACAGGAGAGACCT	TTCAATGCTGTCTTCTGGCA
NR1H3	TTCTGGACAGGAACTGCACC	TGGTCATTACCAAGGCACTGT
SOCS3	GGAGACTTCGATTCGGGACC	GGAGCCAGCGTGGATCTG
CCR7	CTTCTGTGTGGTTTTACCGC	CACAGGCATACCTGGAAAATGA
CCL22	TACTGGACCTCAGACTCCTGC	GAATCATCTTACCCAGGGCA
CD68	ATCCCCACCTGCTTCTCTCA	CCGAGAATGTCCACTGTGCT
SPI1	GATCTGACCGACTCGGAGC	GTCTTCTGATGGCTGAGGGG
HLA-DR	TTCAGGAATCAGAAAGGACTC	TCTGCATTCAGCTCAGGAA